Contourite development:

Analysing the interaction between bottom currents and sedimentary systems

DISSERTATION

at the Faculty of Geosciences

University of Bremen

by

Henriette Wilckens

Bremen, 2023

University of Bremen

marum

Contourite development:

Analysing the interaction between bottom currents and sedimentary systems

Dissertation

zur Erlangung des Doktorgrades der Naturwissenschaften

am Fachbereich Geowissenschaften

der Universität Bremen

vorgelegt von

Henriette Wilckens

Eingereicht: 22.02.2023

Promotionskolloquium: 12.05.2023

Examiners

Prof. Dr. Elda Miramontes
Universität Bremen
Faculty of Geosciences
Klagenfurter Straße 2-4
28359 Bremen - Germany

Dr. Michele Rebesco
Istituto Nazionale di Oceanografia e di Geofisica Sperimentale - OGS
Borgo Grotta Gigante n. 42/c
34010 Sgonico (Trieste) - Italia

Abstract

Oceanic currents flowing near the seafloor erode, transport and deposit sediments, organic carbon, nutrients, and pollutants in deep-water sedimentary systems. Sediment deposits, which have mainly formed under the influence of these bottom currents (contourites) are high-resolution archives for reconstructing past ocean conditions. However, the interaction of sedimentary systems with oceanographic processes in deep-water environments is not well understood. The main objective of this thesis is to better understand the connection between contourites and the hydrodynamics that generate them in order to improve reconstructions of paleocurrents and sediment transport pathways. To achieve this objective a multidisciplinary study combining multibeam bathymetry, seismo-acoustic data, sediment samples, vessel-mounted Acoustic Doppler Current Profiler data, numerical modelling of ocean currents and three-dimensional flume tank experiments has been conducted.

Elongated depressions (moats) and their associated drifts form at the northern Argentine margin on top of relatively flat seafloor surfaces (terraces) next to a steep slope. The main current direction is along-slope, and the speed is higher near the slope and decreases on the terrace basinwards. Flume tank experiments show that a moat-drift system forms if there is a secondary basinward flow near the seafloor. The secondary flow increases with higher speeds and steeper slopes, leading to steeper adjacent drifts. Once the moat-drift system has developed, the secondary circulation is confined by the drift into a helix structure. Simultaneously, the primary along-slope velocity is increased. The measured current speed over the moats from the Argentine continental margin and the Bahamas area is high (up to 63 cm/s at 150–200 m) and decreases by 5-48% over the associated drift. Measurements from 185 cross-sections of moat-drift systems distributed at 39 different locations worldwide show that moats at steeper slopes have a steeper drift and that the angle of the slope side is on average 1.6 times higher than the angle of the drift side. However, no statistical relation is found between latitude and moat-drift morphology or stratigraphy. The flume tank experiments show that moat-drift systems can form solely because of along-slope currents without any additional oceanographic processes as eddies, internal waves or ocean current surface fronts. However, Acoustic Doppler Current Profiler data and the hydrodynamic model from the Argentine continental margin show that eddies near the seafloor can form on a contourite terrace. These eddies might lead to the small erosion surfaces on the Ewing Terrace, even though it is mainly a depositional environment and currents are relatively weak (below 30 cm/s). Experiments show that the migration of the moat-drift system and the formation of internal stratigraphic architecture is a function of current strength in combination with sediment supply. The different stratigraphic types of more erosive and more depositional moat-drift systems have been observed in seismic data. A new sub-classification of moat-drift systems based on their stratigraphy is proposed.

In summary, this study provides new insights into the interaction between ocean currents and sedimentary systems. It shows the importance of current strength, current variability (in time and space) and sediment supply for the formation of contourite systems. The combined data suggest that higher speeds and steeper slopes intensify the secondary flow, leading to steeper adjacent drifts. Thus, the morphology and internal architecture of the moat-drift systems can be used as a paleo-velocimeter. Furthermore, this study identifies the need for more *in situ* measurements near the seafloor.

Zusammenfassung

Meeresströmungen in der Nähe des Meeresbodens erodieren, transportieren und lagern Sedimente, organischen Kohlenstoff, Nährstoffe und Schadstoffe in Tiefseesedimentsystemen ab. Sedimentablagerungen, die sich im Wesentlichen unter dem Einfluss dieser Bodenströmungen gebildet haben (Konturite), sind hochauflösende Archive zur Rekonstruktion vergangener Meeresströmungen. Allerdings ist die Wechselwirkung zwischen Sedimentsystemen und ozeanographischen Prozessen in der Tiefsee noch nicht hinreichend erforscht. Ziel dieser Arbeit ist es, den Zusammenhang zwischen Konturiten und den hydrodynamischen Prozessen, die sie erzeugen, besser zu verstehen, um eine genauere Rekonstruktion von Paläoströmungen und Sedimenttransportwegen zu ermöglichen. Um dieses Ziel zu erreichen, wurde eine multidisziplinäre Studie durchgeführt, die Fächerecholot-Bathymetrie, seismo-akustische Daten, Sedimentproben, schiffsgestützte Akustik-Doppler-Profil-Strömungsmesser Daten, numerische Modellierung von Meeresströmungen und dreidimensionale Laborexperimente (Strömungstank) miteinander kombiniert.

Am nördlichen Kontinentalhang Argentiniens entstehen auf relativ flachen Meeresbodenflächen (Terrassen) neben steilen Hangen langgestreckte Vertiefungen (Gräben) sowie die dazugehörigen Drifts. Die Hauptströmungsrichtung führt entlang des Hangs und die Geschwindigkeit ist in der Nähe des Hangs höher und nimmt auf der Terrasse in Richtung Becken ab. Strömungstankexperimente belegen, dass sich ein Graben-Drift-System bildet, wenn in der Nähe des Meeresbodens eine sekundäre, beckenwärts gerichtete Strömung vorhanden ist. Die sekundäre Strömung nimmt mit höheren Geschwindigkeiten und steileren Hängen zu und bewirkt steilere angrenzende Drifts. Sobald sich das Graben-Drift-System entwickelt hat, wird die sekundäre Zirkulation durch den Drift in einer Helixstruktur im Graben eingegrenzt. Gleichzeitig erhöht sich die primäre Geschwindigkeit entlang des Hangs. Die gemessene Strömungsgeschwindigkeit über den Gräben am Argentinischen Kontinentalhang und im Bahamas-Gebiet ist hoch (bis zu 63 cm/s in 150-200 m) und nimmt über dem zugehörigen Drift um 5-48% ab. Messungen von 185 Querschnitten von Graben-Drift-Systemen an 39 verschiedenen Orten weltweit zeigen, dass Gräben an steileren Hängen einen steileren Drift aufweisen und dass der Winkel der Hangseite im Durchschnitt 1,6-mal größer ist als der Winkel der Driftseite. Es wurde jedoch kein statistischer Zusammenhang zwischen der geografischen Breite und der Morphologie oder Stratigraphie des Graben-Drift-Systems festgestellt. Die Experimente im Strömungstank zeigen, dass sich Graben-Drift-Systeme allein aufgrund von Strömungen entlang des Hangs bilden können, ohne dass zusätzliche ozeanographische Prozesse wie Wirbel, interne Wellen oder Meeresströmungsfronten eine Rolle spielen. Die Daten des Akustik-Doppler-Profil-Strömungsmessers sowie das hydrodynamische Modell vom Argentinischen Kontinentalrand zeigen jedoch, dass sich Wirbel in der Nähe des Meeresbodens auf einer Terrasse bilden. Diese Wirbel könnten zu den kleinen Erosionsflächen auf der Ewing-Terrasse führen, obwohl es sich primär um eine Ablagerungsumgebung handelt und die Strömungen relativ schwach sind (unter 30 cm/s). Experimente zeigen, dass die Verschiebung des Graben-Drift-Systems und die Bildung der internen stratigraphischen Architektur von der Strömungsstärke in Kombination mit der Verfügbarkeit von Sedimenten abhängen. Die unterschiedlichen stratigraphischen Typen von eher erosiven und eher ablagerungsdominierten Graben-Drift-Systemen wurden mittels seismischer Daten beobachtet. Es wird eine neue Unterteilung von Graben-Drift-Systemen auf Grundlage ihrer Stratigraphie vorgeschlagen.

Zusammenfassend lässt sich sagen, dass diese Studie neue Erkenntnisse über die Wechselwirkung zwischen Meeresströmungen und sedimentären Systemen liefert. Sie zeigt die Bedeutung von Strömungsstärke, Strömungsvariabilität (zeitlich und räumlich) und Sedimentangebot für die Bildung von Konturit-Systemen. Die kombinierten Daten deuten darauf hin, dass höhere Geschwindigkeiten und steilere Hänge die Sekundärströmung verstärken, was zu steileren angrenzenden Drifts führt. Somit können die Morphologie und die innere Architektur der Graben-Drift-Systeme als Paläo-Geschwindigkeitsmesser verwendet werden. Darüber hinaus macht diese Studie deutlich, dass weitere *in situ* Messungen in der Nähe des Meeresbodens erforderlich sind.

Contents

List of Tables

List of Figures

List of Abbreviations

AABW	Antarctic Bottom Water
AAIW	Antarctic Intermediate Water
ADCP	Acoustic Doppler Current Profiler
BP	Before Present
CDS	Contourite Depositional System
CDW	Circumpolar Deep Water
CSB Moat	Cay Sal Bank Moat
CTD	Conductivity, Temperature and Depth
ET Moat 1	Ewing Terrace Moat 1
ET Moat 2	Ewing Terrace Moat 2
GBB Moat	Great Bahamas Bank Moat
GBC	Giant Box Corer
GC	Gravity Corer
GoC	Gulf of Cadiz
GS	Grab Sampler
LCDW	Lower Circumpolar Deep Water
LGM	Last Glacial Maximum
MBES	Multibeam Echosounder
MdP Canyon	Mar del Plata Canyon
MUC	Multicorer
NADW	North Atlantic Deep Water
SACW	South Atlantic Central Water
SASW	Subantarctic Surface Water
TW	Tropical Water
UCDW	Upper Circumpolar Deep Water
UDOP	Ultrasonic Doppler velocimeter
VE	Vertical Exaggeration
VM	Vessel-Mounted

Chapter 1

Introduction

1.1 Thesis outline and authors contribution

This cumulative thesis is divided into 6 chapters. Chapter 1 gives a general introduction to contourites and outlines the existing knowledge and knowledge gaps. At the end, the aim of the study and the hypotheses are summarised. One key objective is to determine if it is possible to reconstruct bottom current speeds based on contourite morphology and stratigraphy. Chapter 2 explains the methods used in the multidisciplinary approach which combines the fields of marine geophysics, marine sedimentology, physical oceanography, and physical modelling. The data acquisition and methods are also described in each manuscript and additional information about the data can be found in the cruise reports. The focus here is to explain how these methods work in principle and why these methods are chosen to be jointly interpreted in the presented thesis.

Chapters 3-5 present the individual manuscripts that all establish a clearer link between contourite features and the oceanographic processes that form them. Chapter 3 shows the contouritic setting along the northern Argentine margin and combines oceanographic measurements and numerical models with geophysical and sedimentological data. The identified contouritic features include large contourite terraces (La Plata Terrace, Ewing Terrace) and an abraded surface connecting the terraces, as well as smaller erosional and depositional features like moats, erosion surfaces on the Ewing Terrace, sediment waves and contourite drifts. Among other results, we found that the bottom current is intensified over two elongated depressions which are classified as moats (Fig. 1.1). Possibly, the intensification is at least partly due to the focusing effect of the current related to the underlying morphology. Knowing if a moat has a particular characteristic that is different from other moats (e.g particularly wide or long) is difficult since these features are rarely measured and there is no review paper about moats. Chapter 4 shows the analyses of over 100 cross-sections from moats and their associated contourite drifts at different locations to understand similarities and differences in morphology and stratigraphy. This allowed us to subclassify three types of moats (Fig. 1.2). Our statistical analyses indicate that

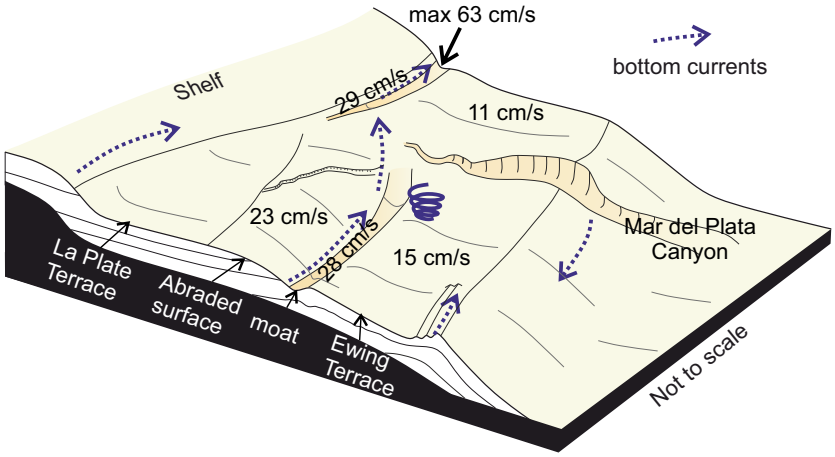

Figure 1.1: Conceptual model of bottom currents and sedimentary features at the contourite depositional system on the north Argentine margin. (Graphical abstract Chapter 3)

at steeper slopes, the drift that forms alongside the moat is also steeper. Additionally, current measurements from four moat-drift systems are used to better understand the hydrodynamics of this kind of contourite system. The current speed above the moats is higher compared to the associated drift. However, due to the limitation in data availability of velocity measurements from bottom currents, it became necessary to further test our hypothesis by physical modelling in a flume tank. Furthermore, it remained unknown if the intensification of the current above the moat initially started to create this specific morphology or if the flow was intensified due to the pre-existing morphology. This is a common problem in the study of natural systems because the evolution of sedimentary features can take several thousands to millions of years. One way to overcome this issue is physical modelling in a flume tank.

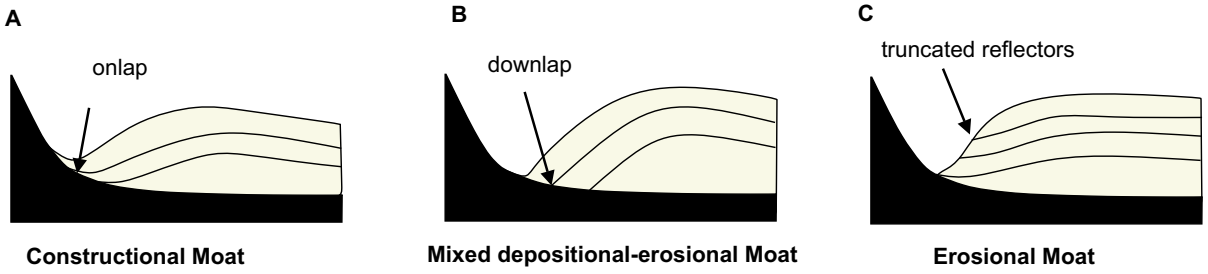

Figure 1.2: Nomenclature of moats based on seismic or sub-bottom profiler data. Three different stratigraphic types of moats: (A) Constructional Moat: Reflections onlap at the slope side; (B) Mixed Moat: reflections downlap at the bottom of the moat; (C) Erosional Moat: reflections are truncated at the drift side (Graphical abstract Chapter 4).

Chapter 5 demonstrates how a moat can self-emerge in a flume tank. For this study, detailed analyses of moats in the natural environment were necessary to show that the flume tank experiments are realistic. The experiments show that faster currents and

steeper slopes lead to steeper drifts. This is linked to the strength of a secondary flow that depends on the steepness of the slope and the current speed (Fig. 1.3). After the moat has formed, the secondary flow is confined within the moat and has a helix structure. Furthermore, the experiments confirm the hypothesis from chapter 3 that the current becomes more focused due to the existence of the moat. Chapter 6 presents the conclusions and points out the gained knowledge by combining the manuscripts. In summary, the results indicate that reconstruction of past ocean-current speeds based on stratigraphy is possible when the steepness of the slope is considered.

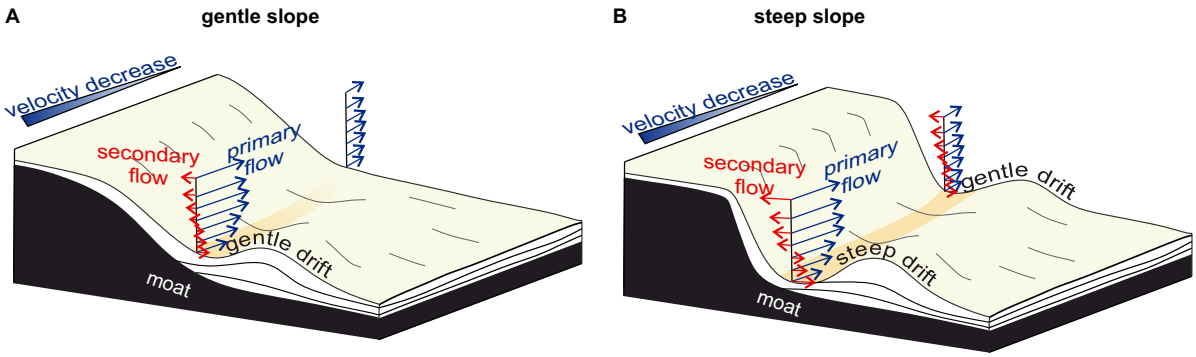

Figure 1.3: Conceptual model of current dynamics over the moat-drift system. The moat-drift system forms if there is a secondary flow near the seafloor that transports sediment from the slope toward the drift. The secondary flow decreases with lower speeds and more gentle slopes (Graphical abstract Chapter 5).

The contributions of all authors to each manuscript are described below:

Chapter 3: *'The erosive power of the Malvinas Current: Influence of bottom currents on morpho-sedimentary features along the northern Argentine margin (SW Atlantic Ocean)'*
Published in 2021 in Marine Geology

1. Henriette Wilckens: conception of the study, processing of ADCP data, data analysis and interpretation, manuscript writing and figures preparation
2. Elda Miramontes: help with the conception of the study and interpretation of the data
3. Tilmann Schwenk: data acquisition and support during the analysis and interpretation of multibeam bathymetry and seismo-acoustic data
4. Camila Artana: analysis and interpretation of hydrodynamic modelling
5. Wenyan Zhang: conceptual discussion of hydrodynamics at the seafloor
6. Alberto Piola: interpretation of oceanographic data
7. Michele Baques: acquisition of ADCP data and interpretation of oceanographic data
8. Christine Provost: interpretation of hydrodynamic modelling
9. F. Javier Hernandez-Molina: conceptual discussion of the formation of sediment features

10. Meret Felgendreher: analysis and interpretation of sediment grain size in connection to bottom currents
11. Volkhard Spieß: general discussion of geological setting and scope of the study
12. Sabine Kasten: cruise coordination, data acquisition, placing this study in interdisciplinary contexts

Chapter 4: *'Factors controlling the morphology and internal sediment architecture of moats and their associated contourite drifts'* Accepted in 2023 by Sedimentology

1. Henriette Wilckens: conception of the study, processing of ADCP data, data analysis and interpretation, manuscript writing and figures preparation
2. Tilmann Schwenk: acquisition of data from Argentina and Galicia, discussion of classification and concept of formation of moat-drift systems
3. Thomas Lüdmann: acquisition of data from Bahamas, discussion of factors that influence moat formation
4. Christian Betzler: acquisition of data from Bahamas, discussion of factors that influence moat formation
5. Wenyan Zhang: discussion of hydrodynamics above moats
6. Jiayue Chen: discussion of hydrodynamics above moats
7. F. Javier Hernández-Molina: discussion of moat development in time and space, and support with data from Spain
8. Alice Lefebvre: analysis and interpretation of statistics
9. Antonio Cattaneo: acquisition of data from Corsica and placing this study in interdisciplinary contexts
10. Volkhard Spieß: acquisition of data from Argentina and Galicia and general discussion of geological settings and scope of the study
11. Elda Miramontes: support with the conception of the study, the data compilation and the interpretation of the results

Chapter 5: *'Flume tank experiments demonstrate the hydrodynamic conditions necessary to form contourite systems'* Submitted in 2023 to Communications Earth & Environment

1. Henriette Wilckens: conception of the study, running the experiments, data processing, analysis and interpretation of data, manuscript writing and figures preparation
2. Joris T. Eggenhuisen: help with the setup of experiments and data interpretation
3. Pelle H. Adema: help with the setup of experiments
4. F. Javier Hernández-Molina: general discussion and comparison with natural systems
5. Ricardo Silva Jacinto: general discussion and support with the interpretation of physical processes
6. Elda Miramontes: support with the conception of the study and interpretation, and help with the setup of experiments

1.2 General background and purpose of the PhD thesis

Oceanic currents impact climate and deep sea ecosystems. They are often strong enough to erode and deposit sediment at large scales and thereby shape continental margins (Heezen, 1959; Heezen and Hollister, 1964; Stow et al., 2009). Sediment deposits formed mainly under the influence of currents related to oceanographic processes flowing near the seafloor (bottom currents) are classified as contourites (Rebesco and Camerlenghi, 2008; Rebesco et al., 2014). On a long time scale, the development of contourites is related to climate-induced change in thermohaline circulation and isostatic movements (e.g. tectonics). But also smaller physical oceanographic processes like sub-inertial oscillations, tides and internal waves potentially shape the evolution of contourites. However, until today, it is not clear how these multi-scale processes interact with each other and control the evolution of contourites.

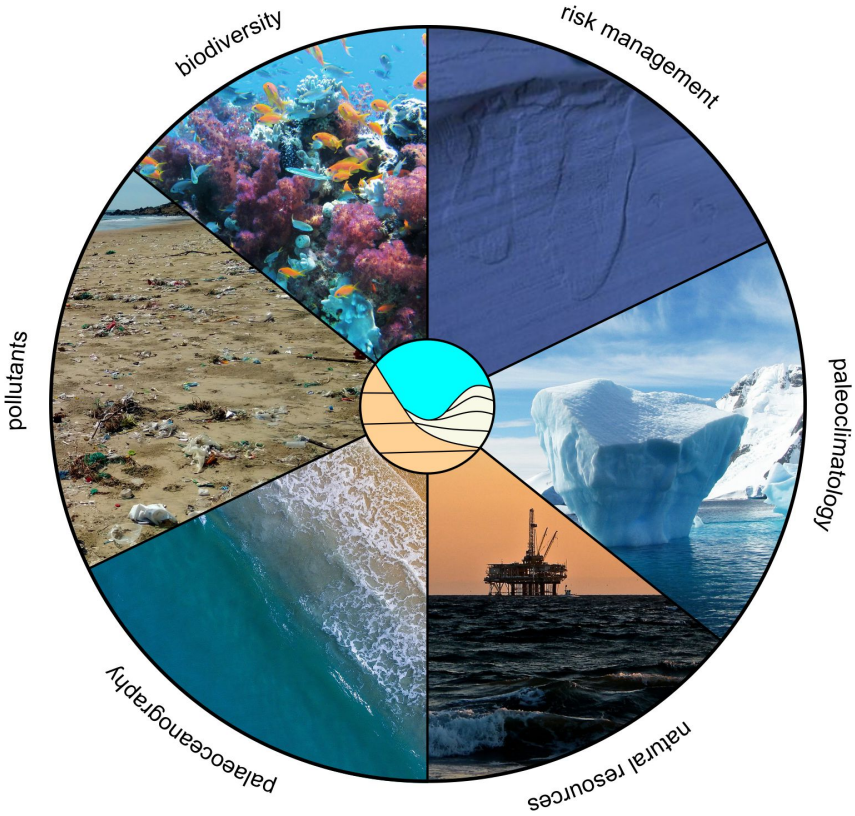

Figure 1.4: Contourite research is important for palaeoclimatology, palaeoceanography, risk management, marine ecology threatened by pollutants, and natural resources.

A better understanding of contourite development is relevant for several fields (Fig. 1.4) that include palaeoclimatology and palaeoceanography, risk management regarding slope instabilities, marine ecology and hydrocarbon exploration (Rebesco et al., 2014; Hebbeln et al., 2016; Hernández-Molina et al., 2018; Miramontes et al., 2018; Kane et al., 2020). Ocean currents transport oxygen and nutrients to the seafloor and thereby facilitate the

development of deep-sea ecosystems with high biodiversity, for instance, cold-water corals (Hebbeln et al., 2016; Steinmann et al., 2020). Thus, the biodiversity in contourite systems is often high. Bottom currents also transport microplastics and thereby creating hotspots in the same areas where biodiversity is high, which is a potential threat to marine ecosystems (Kane et al., 2020). Palaeocurrent conditions can be reconstructed from grain size analyses of sediment cores and from the internal sediment architecture using seismic data (Hernández-Molina et al., 2014; Uenzelmann-Neben et al., 2017; McCave et al., 1995; 2017). However, the reconstruction of past ocean conditions based on the geological record can be improved by understanding the present deposition mechanisms better (Surlyk and Lykke-Andersen, 2007; Preu et al., 2012; Betzler et al., 2013; Miramontes et al., 2021). Today, the grain size of samples from sediment cores are mainly used for current speed reconstructions, which only provide very localized information (McCave et al., 1995; 2017; Wu et al., 2021). However, using seismic data for quantitative palaeoceanographic reconstructions is limited due to our poor understanding of linking hydrodynamic processes with sedimentary features (Miramontes et al., 2021).

There are many studies about the evolution of the different water masses, as described in Chapter 1.3. Water masses can be characterised by their chemical properties like oxygen or salinity. These water masses can be analysed with Conductivity, Temperature and Depth (CTD) measurements. In contrast, currents are a physical process that can erode, transport and deposit sediment and can consist of one water mass or several water masses flowing together. Surface currents are well known, but currents flowing near the bottom (bottom currents) are often not well known, due to only few existing measurements. Here, we attempt to study these bottom currents and how they affect contourite depositional systems by focusing on the recent deposits, which can be linked with velocity measurements and existing current models. This research aims at improving our understanding of hydrodynamics processes that shape the morphology of contourites which then ultimately lead to improve the reconstruction of past ocean currents.

1.3 Contourites and oceanographic processes

Distinguishing contourite features

Contourites are, together with (hemi)pelagic settling of particles, turbidites and mass transport deposits, the main sediment types in the deep sea (Rebesco et al., 2014). The different contourites have been classified mainly by considering the differences in morphology and seismic stratigraphy (Faugères et al., 1999; Stow et al., 2002b; Rebesco et al., 2014; Miramontes et al., 2021). The nomenclature of contourite features can slightly differ between authors (e.g. the infill drift is not always included in the definition), but the commonly observed contourites and the features on which we focus are the same (Fig. 1.5). Moats are elongated depressions that form at the foot of a slope and are associ-

ated with sediment drifts. Alongside the moat forms a mounded sediment drift, which is usually called a separated mounded drift (Rebesco et al., 2014). When the separated mounded drift is imaged with seismic reflection data, the reflections in the drift are bent toward the moat (Fig. 1.5). Moats and separated mounded drifts are here considered as one system and thus referred to as a moat-drift system. The deepest point inside the moat is the trough and the shallowest point of the contourite drift is the drift crest. The width of the moat is here defined as the horizontal distance between the drift crest and the slope. The relief is defined as the vertical distance between the moat trough and the drift crest. There are other possibilities to define the width, but this definition is the most practical one to apply to different data sets, as finding the minimum and maximum in a system is usually possible. Alternatively, to the separated mounded drift, there is also a detached mounded drift. This has a similarly mounded morphology, but it is not located next to a slope. Another elongated depression that forms next to a slope is the contourite channel, where the seismic reflections are truncated at the basinwards contourite channel side (Fig. 1.5). Some channels are also found without any connection to a slope (Miramontes et al., 2020; 2021).

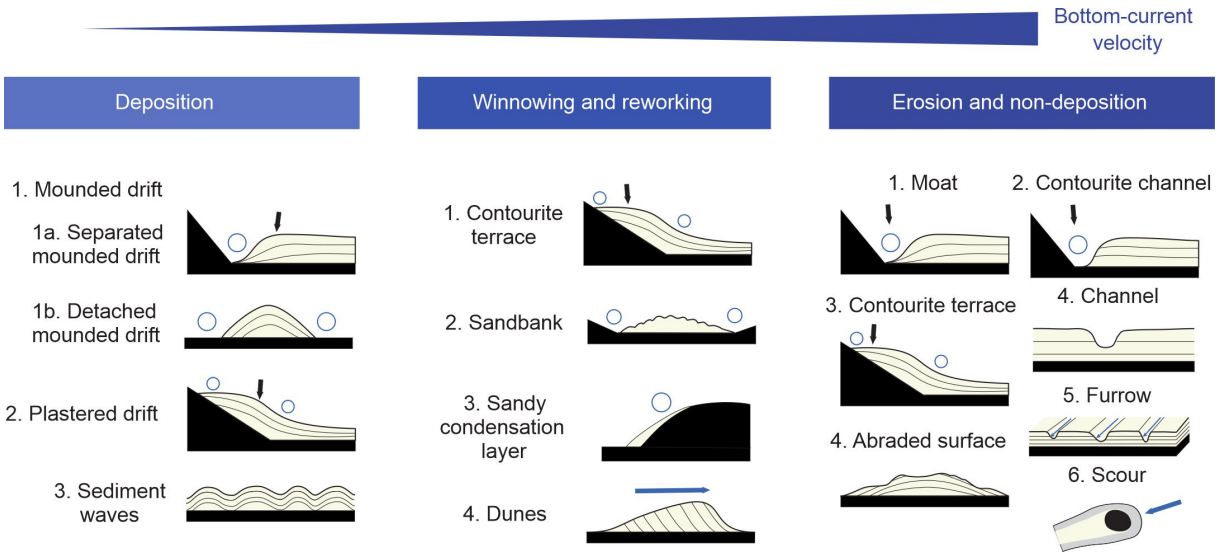

Figure 1.5: Different types of contourites are classified based on their morphology and internal architecture. Different features are associated with different current speeds (adapted from Miramontes et al., 2021).

Plastered drifts are large (1-10s of km) features and are characterised by slightly mounded and convex geometry. Usually, plastered drifts are located on a gentle slope and are less mounded than mounded drifts (Faugères et al., 1999; Rebesco et al., 2014). Contourite terraces are relatively flat surfaces developed by hydrodynamic processes and not due to tectonic events. They are often associated with plastered drifts on the landward side (Miramontes et al., 2021). In the thesis, we consider the limits of the contouritic terraces a significant increase in the slope gradient over a distance of several kilometres or in the seis-

mic/subbottom profiler data; the limits are further identified as either an abraded/erosion surface or a transition to a plastered drift. An abraded/erosion surface is identified in seismic/subbottom profiler data by truncated reflections. In some areas, sediment waves cover large areas ($> 1000\,km^2$) on the seafloor showing the influence of bottom currents (Wynn and Masson, 2008). They are generally tens of metres to a few kilometres in wavelength and several metres high (Wynn and Stow, 2002). These waves can migrate upstream or downstream and/or aggregate. Some authors also defined abyssal sheeted drifts, which have slightly wavy reflections or can be covered by sediment waves. They can cover large areas, but unlike all other drifts, they do not have a mounded morphology (Wynn and Stow, 2002; Rebseco et al., 2014). This makes it difficult to distinguish them from turbidites or hemipelagic sediment deposits.

In addition to the large drifts ($> 1\,km$), there are smaller secondary features ($< 1\,km$) that can be superimposed on top of the contourite, like ripples, small sediment waves, dunes, small drifts, furrows, scours or small abraded surfaces (Miramontes et al., 2021). Some authors have also further subclassified the smaller drifts like a patch drift that can be found, for example, inside of a contourite channel or a moat (Stow et al., 2002) and infill drifts that infill a previously existing depression (Laberg et al., 2001; Rebesco et al., 2014). However, with all the different names for drifts, it becomes more difficult to communicate with researchers from different disciplines. Here we focus on a better understanding of the hydrodynamics that formed the drift rather than describing a specific area in detail. Thus, we do not further distinguish between any of the smaller drifts and the drift types where the name is specific for the environment in which it forms like channel-related and confined drifts. Channel-related and confined drifts can be found on flat surfaces constrained by a slope on the side (Faugères et al., 1999). They have a mounded morphology and thin out near the slope of the channel or another type of topographic boundary. Here, we classify them as two separated mounded drifts that have grown into each other, leading to one mounded geometry. But the two separated mounded drifts are still associated with two moats at the channel slope.

Processes in contourite formation

The evolution of contourites is influenced by bottom currents and vice versa; the fluid dynamics is influenced by the morphology of the contourites. This makes understanding contourite evolution difficult. Nonetheless, different contourite elements are associated with more or less vigorous bottom currents (Fig. 1.5). Constructional contouritic elements are associated with low current speeds. Erosional features or non-depositional features are connected to high bottom current speeds that allow only bypassing of the sediment. It is not well understood yet if contourite features mainly react to the mean current speed or to the minimum or maximum. The variability is relevant for contourite

development as the simulated bottom eddy kinetic energy is three times higher in contourite systems (Thran et al., 2018). Plastered drifts develop between two faster bottom currents that are in the upper and in the distal part of the plastered drift. Thus, the highest sediment accumulation of the plastered drift is in the middle with an energy minimum or where bottom currents are weak (Miramontes et al., 2019). This might be at first somewhat counterintuitive since contourites form because of bottom currents. However, more sediment can be transported with higher current speeds and deposited when the current speed changes. Thus, the highest amount of sediment accumulation in a plastered drift might be the area with the highest rate of change in current speed.
Terraces are mixed systems, meaning there can be erosion and deposition. Some particularly flat and large terraces, like the terraces at the Argentine margin, have been suggested to be formed due to internal waves (Preu et al., 2013; Hernández-Molina et al., 2016a). These internal waves are gravity waves and can propagate similarly to surface waves at density contrasts within the water column. This density contrast exists between water masses that differ in salinity or temperature. When the internal wave increases the bottom shear stress, the sediment might be easier to erode (Cacchione et al., 2002). The internal waves are also suggested to initiate the development of sediment waves and dunes (Droghei et al., 2016; Ribó et al., 2016; Reiche et al., 2018).

Contourite channels are associated with the core of the currents meaning the bottom currents are strong along the slope allowing erosion of sediment, which creates an elongated depression. Sometimes channels do not form alongside a slope break or an escarpment,

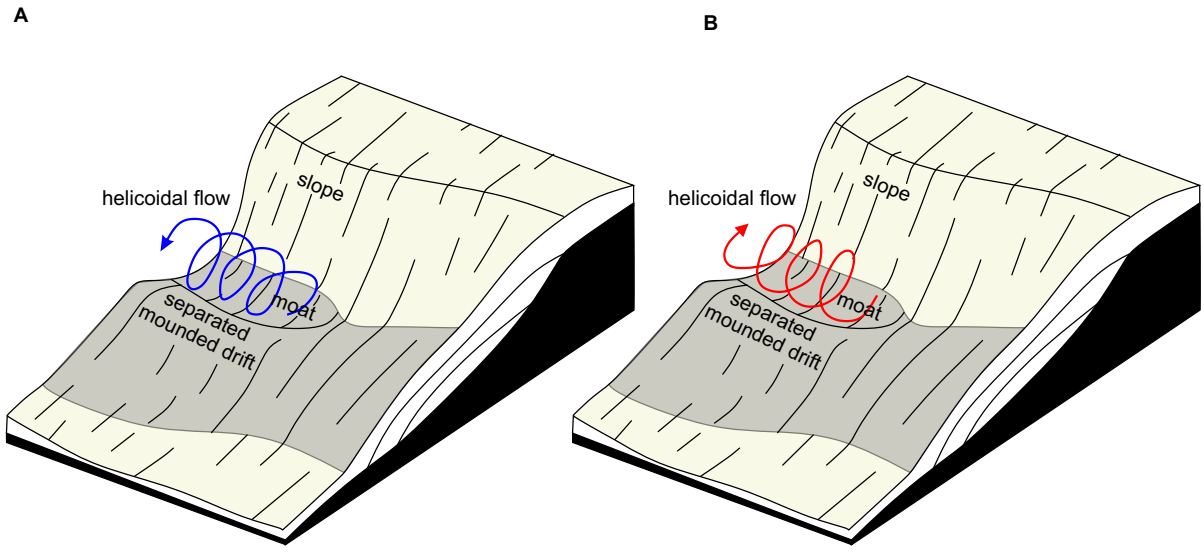

Figure 1.6: Suggested helicoidal flow over moats (adapted from Hernández-Molina et al., 2008). The spinning direction differs between authors. (A) The spinning direction near the seafloor is towards the slope (Hernández-Molina et al., 2008; Gong et al., 2017). (B) The spinning direction near the floor is towards the basin (Rebesco et al., 2014).

but occur on the slope without any topographic constraints. These channels are formed by other oceanic processes than contourite currents. This includes, for example, internal waves that propagate at density boundaries within the water column (Miramontes et al., 2020); or several pockmarks that were formed by fluid seepage and then got eroded and elongated by bottom currents (Yu et al., 2021). Similarly to contourite channels, moats are also associated with strong bottom currents along the slope, but the current speeds are suggested to become weaker basinwards, which allows the formation of a drift (Hanebuth et al., 2015). It was speculated that a helicoidal flow could develop in moats (e.g. Roden, 1987; Allen 1982; 1994; Hernández-Molina et al., 2006; Preu et al. 2013). This idea was proposed more than 30 years ago, but it has not been modelled or measured and the possible effect for separated mounded drifts has not been discussed in detail. Moreover, the suggested spinning direction differs between authors (Fig. 1.6). For turbidity flows and river flows, a helicoidal flow was previously measured (Corney et al. 2006; Keevil et al., 2011; Wells and Cossu, 2013).

1.4 Argentine margin and the Brazil-Malvinas Confluence Zone

The Modern system

The Argentine continental margin is a passive volcanic-rifted continental margin formed during the Cretaceous period (Hinz et al., 1999; Franke et al., 2007). It is strongly impacted by vigorous (bottom) currents making it a natural laboratory to study its impact on sedimentation processes. The resulting Contourite Depositional System (CDS) at the Argentine continental margin is characterized by moats and channels, contouritic terraces, abraded surfaces and sediment drift deposits like plastered and separated mounded drifts (Urien and Ewing, 1974; Hernández-Molina et al., 2009; 2016b; Krastel et al., 2011; Preu et al., 2012, Preu et al., 2013; Voigt et al., 2016; Warratz et al., 2017, Warratz et al., 2019). The slope of the continental margin is interrupted by contouritic terraces (Fig. 1.7). At the southern Argentine margin, these are named: Nágera Terrace at ∼500 m depth, the Perito Moreno Terrace at ∼1000 m depth, the Piedra Buena Terrace at ∼2500 m depth and the Valentin Feilberg Terrace at ∼3500 m depth (Hernández-Molina et al., 2009). At the northern part, they are named: La Plata Terrace at ∼500 m depth, the Ewing Terrace at ∼1200 m depth and the Necochea Terrace at ∼3500 m depth (Urien and Ewing, 1974; Preu et al., 2013).

At the continental margin, two currents interact with each other. From the South, the cold and oxygen-rich Malvinas current is flowing northwards and from the North, the warm and salty Brazil current is flowing southwards (Fig. 1.8). At the northern Argentine margin near the Mar del Plata Canyon (MdP), the currents meet, forming the Brazil-Malvinas Confluence Zone, detach from the slope and continue flowing into the deep

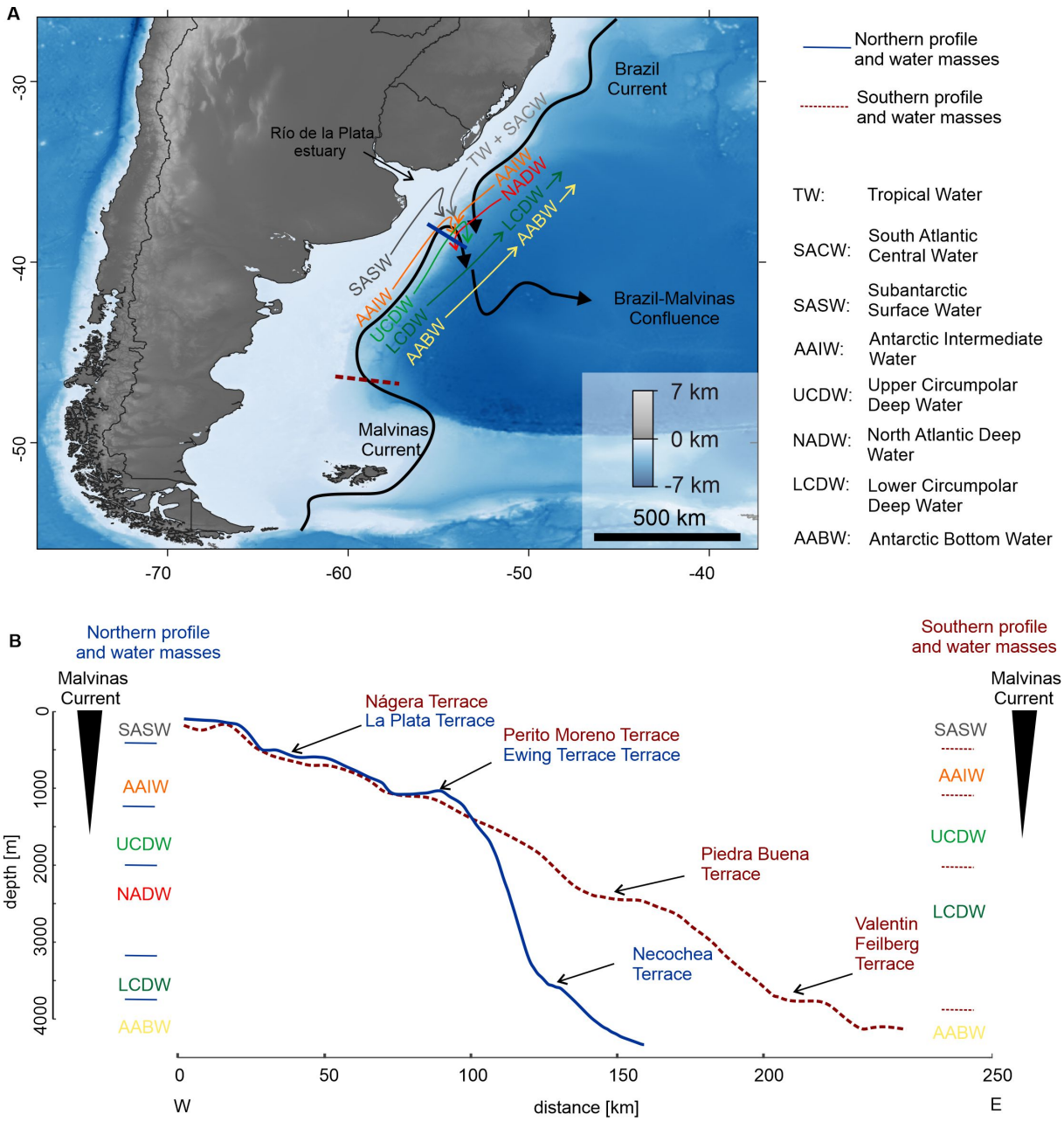

Figure 1.7: (A) Regional bathymetric map (GEBCO 2020) showing the SE American margin. The black arrows indicate the circulation pattern of the Malvinas Current, the Brazil Current and their confluence. The smaller, coloured arrows indicate the flow patterns of the different water masses. (B) Two cross-sections illustrate the morphology of the SE American margin that includes large terraces.

Argentine basin (Fig. 1.8). On average, the axis of the confluence zone is situated at an approximate latitude of ∼38°S (Gordon and Greengrove, 1986; Artana et al., 2019; Piola and Matano, 2019). Different water masses can be distinguished based on salinity, oxygen concentration and temperature. The northward flowing water masses from sea surface to bottom are: Subantarctic Surface Water (SASW), Antarctic Intermediate Water (AAIW), Circumpolar Deep Water (CDW) and the Antarctic Bottom Water (AABW) (Preu et al., 2013; Piola and Matano, 2019). The southward flowing water masses are Tropical Water

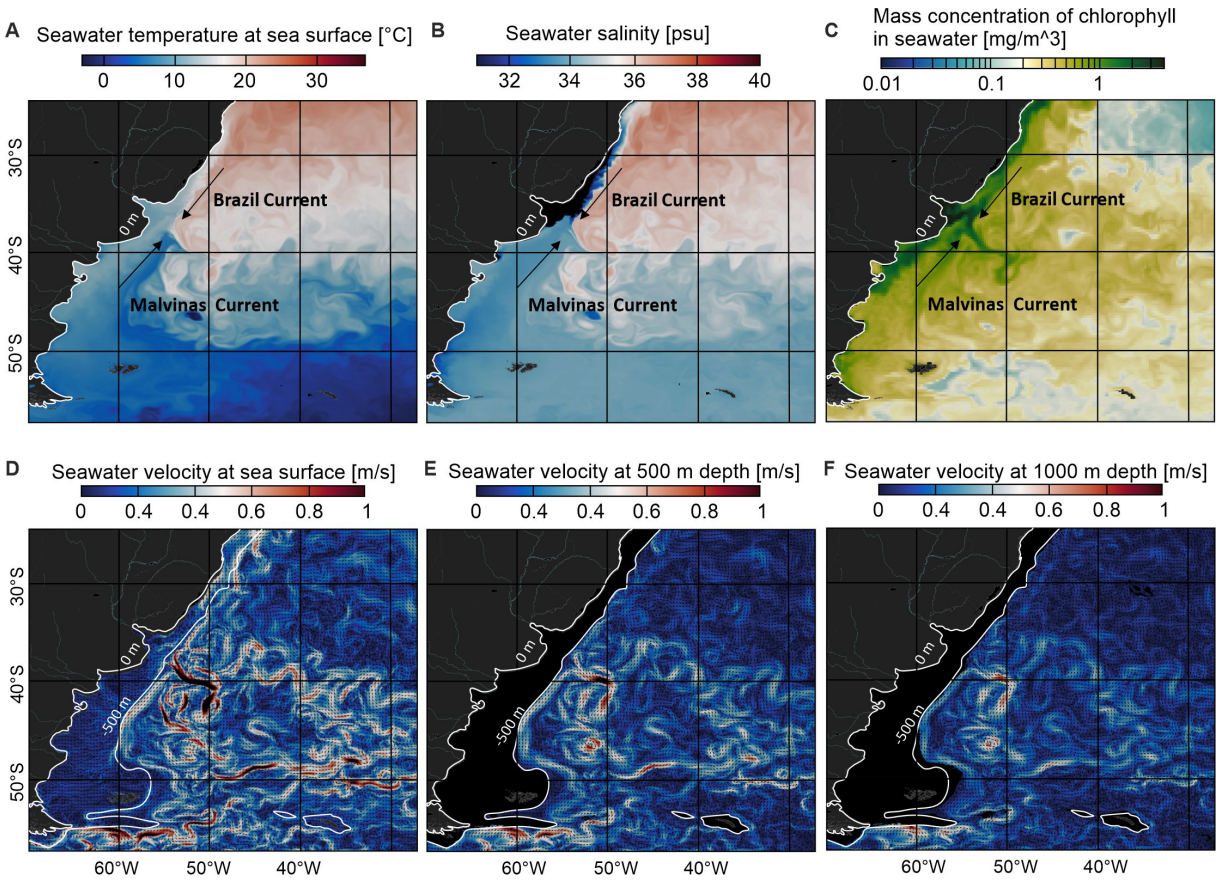

Figure 1.8: Confluence zone at the SE American margin. (A) Seawater temperature at the sea surface shows the confluence zone. (B) Sea water salinity at the sea surface shows confluence and the outflow from the rivers throw the Río de la Plata estuary. (C) Chlorophyll in seawater shows the confluence zone. (D-F) Sea water velocity at different water depths. The data is an example from 10 Jul. 2019 at 02:00 UTC. (MyOceanViewer: Copernicus Marine Service `https://doi.org/10.48670/moi-00021`

(TW), South Atlantic Central Water (SACW), AAIW that was recirculated around the South Atlantic subtropical gyre and North Atlantic Deep Water (NADW) (Preu et al., 2013; Valla et al., 2018; Valla et al., 2018; Piola and Matano, 2019). Near 38°S the NADW flows southward between Upper Circumpolar Deep Water (UCDW) and Lower Circumpolar Deep Water (LCDW) (Reid et al., 1977; Piola and Matano, 2019). The depth of the interfaces between the water masses varies with time and between locations (Preu et al., 2013; Piola and Matano, 2019). Some of these water masses have different chemical signatures but flow together.

Reconstructed past system

During the mid-Miocene (15 Ma Before Present (BP)), the NADW gradually strengthened because the central American seaway started to close (Newkirk and Martin, 2009; Preu et al., 2012). This led to a significant upwards shift in AAIW/UCDW interface until the early Pliocene (Hermann, 1990; Preu et al., 2012). In this calmer environment,

large plastered drifts accumulated at the lower slope (Gruetzner et al., 2011; Preu et al., 2012; Ercilla et al., 2019). NADW production increased significantly in the late Pliocene (Burton et al., 1997; Nisancioglu et al., 2003; Butzin et al., 2011), leading to a shift in the interface of UCDW/NADW further upwards. The Brazil-Malvinas Confluence Zone must have been located at its modern position or further to the South (Preu et al., 2012). At 14 Ma BP, an erosion surface on the Piedra Buena Terrace indicates a strong current regime (today at 2500 m) (Gruetzner et al., 2011). However, during the same time, the Valentin Feiberg Terrace (today at 3500 m) started to grow, which indicates that the AABW became weaker or changed position after 14 Ma BP (Gruetzner et al., 2011). The change could be related to the deepening of the Vema Channel that connects the Argentine and the Brazil basins (Kennett, 1982). During the late Miocene (9-6 Ma BP) well stratified homogeneous deposits suggest moderate bottom water flow over the Valentin Feilberg Terrace (Gruetzner et al., 2011).

When the climate started to cool, and sea level dropped during the last glacial maximum (LGM) the AAIW is interpreted to become stronger (Pahnke et al. 2005; Voigt et al., 2013; 2016). Waelbroeck et al. (2002) suggested that the AAIW was ∼100 – 150 m deeper in the past, which may be linked to a lowering of the sea level during glacial times. A glacial downshift of the recirculated AAIW was also postulated in studies from the Brazilian margin (Viana et al., 1998; Makou et al., 2010). In agreement with Waelbroeck et al. (2002) also Steinmann et al. (2020) suggested that the lower boundary of the oxygen-rich AAIW was deeper compared to its modern position, making coral growth on the Ewing terrace possible during the LGM. However, the start of the growth of corals is not clear due to a lack of dating. During the glacial period, turbidity currents became more frequent and started to flow from the MdP head area downwards (Fig. 1.8; Warratz et al., 2019). These turbidites have the same composition as the sediments from the Ewing Terrace (Warratz et al., 2019). A strengthened glacial AAIW could have increased the nepheloid layer located at the AAIW/UCDW interphase and, thereby, the sediment supply to the MdP Canyon (Voigt et al., 2013; Warratz et al., 2019). However, this explains the observed increased sedimentation in the MdP canyon but not the particular increase at the canyon head area that led to more turbidites. On the other hand, Warratz at al. (2019) further concluded that a shallower glacial AAIW could have shifted the position of the responsible nepheloid layer close to the uppermost canyon head. In agreement with that, modelling results suggest that the AAIW/UCDW boundary was shallower during glacial times (Li et al., 2021). Ronge et al. (2015) suggested a shallower AAIW by using carbon and oxygen isotope records.

Benthic foraminiferal Cadmium/Calcium ratios indicate a shallower glacial NADW (Marchitto et al., 2006). A shallower and less dominant glacial NADW in the Atlantic Ocean was also suggested based on calcium carbonate corrosion in sediment cores (Volbers and

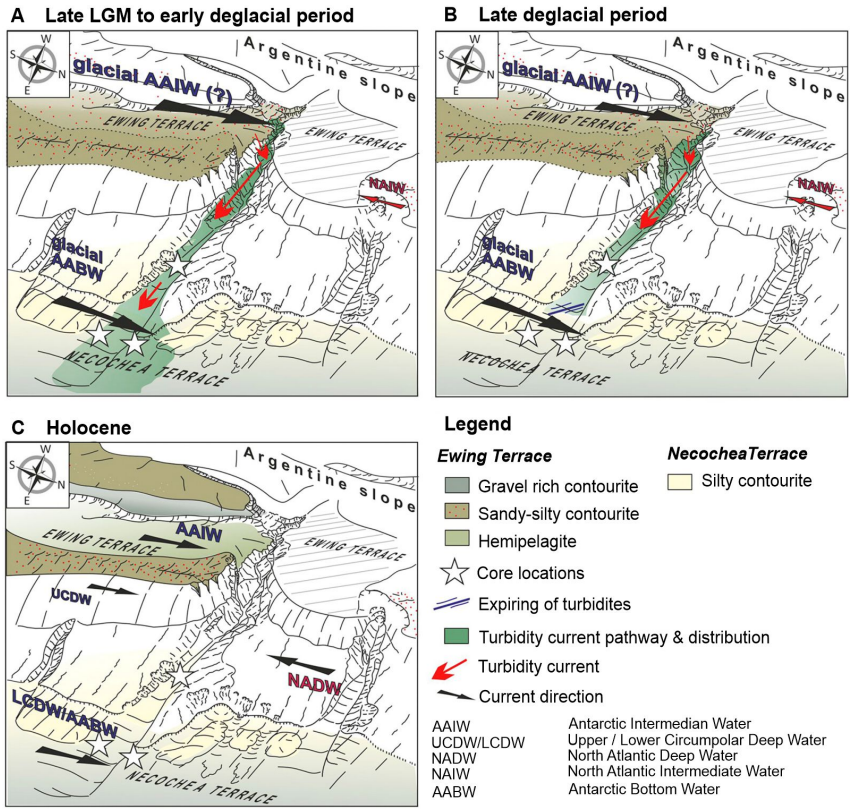

Figure 1.9: Sketch showing the change in water masses location and strength from Last Glacial Maximum to Holocene (adapted from Warratz et al., 2019).

Henrich, 2004). In the confluence zone, a change in corrosion can be related to a change in the position of water masses, either due to a vertical shift in water masses or a shift in the Brazil-Malvinas Confluence Zone. Water masses with high oxygen content, like the AAIW, lead to more oxygenation and, thereby, to low preservation of carbonates. Water masses with low oxygen content, like the NADW, lead to less oxidation and preserve carbonates better. Warratz et al. (2016) reported on low carbonate in the MdP Canyon due to corrosion and/or low productivity during late LGM and early deglacial. Warratz et al. (2016) interpreted that there was an enhanced LCDW and AABW flow strength from 14 to 10 ka BP (late deglacial). Due to the absence of carbon from 20-13 ka BP. the NADW was interpreted to be weaker and deeper. NADW then became shallower at 13 ka BP (Warratz et al., 2019).

After the LGM, the climate started to warm again, the sea level rose and the Malvinas Current became weaker on average (Preu et al., 2013; Voigt et al., 2013; Warratz et al., 2019). During the Holocene, the AAIW was weaker compared to the late glacial, which led to less turbidity currents in the MdP Canyon (Fig. 1.9; Voigt et al., 2016; Warratz et al., 2019). Voigt et al. (2016) suggested, based on sortable silt measurements from GeoB13862 (located inside MdP Canyon at 3588 m), that the AAIW was stronger during early/mid Holocene than during the late Holocene. Furthermore, the sedimentation rate

decreased and grain size became finer (Riedinger et al., 2005). The AAIW/UCDW interface is suggested to shift upwards, which caused deeper cold-water corals on the southern Ewing Terrace to die (Steinmann et al., 2020). At the lower slope and part of the MdP Canyon, an increase in carbonates is observed, which might be linked to an increase in preservation caused by a stronger NADW (Fig. 1.9; Warratz et al., 2019). The suggested stronger NADW possibly shifted the LCDW and AABW downwards during the Holocene (compared to during the late deglacial and early deglacial) (Warratz et al., 2019). Carbonate content is also related to productivity. Razik et al. (2013) argued that during the late deglacial and early Holocene, the Brazil-Malvinas Confluence Zone was located more to the South compared to today. This interpretation was derived from low carbonate concentration in the core that might reflect low productivity proposedly linked to the salty subtropical waters during the glacial period. However, these results could also be linked to bad preservation instead of low productivity. Furthermore, calcite solubility increases with depth because of an increase in pressure (Volbers and Henrich, 2004). Thus, water depth and the CO_3^{2-} of the surrounding water mass can be dominant controls on calcium carbonate preservation (Volbers and Henrich, 2004). Porewater undersaturation due to the oxidation of organic matter within the sediment is also a significant driver of calcite dissolution (Hales and Emerson, 1997). Thus, linking carbonate content with the preservation or productivity related to different water masses might be able to show general trends on larger scales, like the entire Argentine margin. However, its use to reconstruct water masses in the confluence zone needs to be further tested. Contradicting to Razik et al. (2013), Preu et al. (2013) suggested a northward shift of the Brazil-Malvinas Confluence Zone during glacial times compared to today. In modern times, a southward trend of the Brazil-Malvinas Confluence Zone is recorded (e.g. Lumpkin and Garzoli, 2011) which was linked to global warming (de Souza et al., 2019). In agreement with the reconstructions from Preu et al. (2013), this might indicate that the Brazil-Malvinas Confluence Zone is located in the South during warm periods and moves to the North in cold periods.

1.5 Aim of the study and hypotheses

The driving processes of Contourite Depositional Systems (CDS) are not entirely understood. This study aims to establish a clearer link between contourite features and the oceanographic processes that form them. This could increase the knowledge about past ocean currents that we can derive from the morphology and stratigraphy of contourites. We consider moats and their associated separated mounded drifts a promising type of contourite to derive current direction and speed from the morphology and stratigraphy because it is associated with high current speeds.

Hypotheses

1. The current speed over a large abraded surface connecting La Plata and Ewing Terrace is higher than on these terraces.
2. The current speed is higher over the moat than over the drift.
3. Eddies on a terrace can lead to small erosion surfaces.
4. Moats can initially start to develop with no special oceanographic settings. This means that no internal waves or small obstacles are necessary to start moat formation.
5. Moats and drifts migrate upslope due to high sediment availability.
6. The morphology of moats and drifts depends on the current speed. Higher current speeds lead to larger moats than low current speeds considering the same period. Higher current speeds also lead to higher slope angles of the drift on the side of the moat.
7. A steeper slope can focus the current and intensify it, which leads to higher slope angles of the drift on the side of the moat.
8. The Coriolis force steers the current towards the slope in areas where moats are developing. Coriolis force depends on the Coriolis parameter, which depends on the latitude. Thus, at higher latitudes, the aspect ratio and the slope angles of the drift on the side of the moat increase.
9. There is a secondary across-slope flow of the moat-drift system that depends on the along-slope velocity and the steepness of the continental slope.
10. Speed increases due to the morphology of the moat because it focuses the current.

Chapter 2

Materials and methods

2.1 Oceanographic dataset

2.1.1 Current measurements

To understand oceanographic processes we use ocean current velocity measurements. This data is used for resolving local hydrodynamic processes like small eddies and local intensification of current speed. The data was acquired with a vessel-mounted Acoustic Doppler Current Profiler (VM-ADCP) during cruise SO260 in January–February 2018 offshore Argentine (Kasten et al., 2019) and during cruise M95 in March-April 2013 in the Bahamas (Betzler et al., 2014b). Please see the individual manuscripts for the instrument settings during the cruise.

The ADCP transmits an acoustic wave that is scattered back to the transducer due to small particles in the water column. The small particles move with the current. Due to the relative velocity of the particles to the transmitter, the backscattered signal has a different phase than the transmitted signal. This phase shift is known as the doppler shift. No data is collected near the transducer. The ADCP blanking is caused by the electronics and transducer recovery time (Simpson, 2002; Müller et al., 2009). Near the

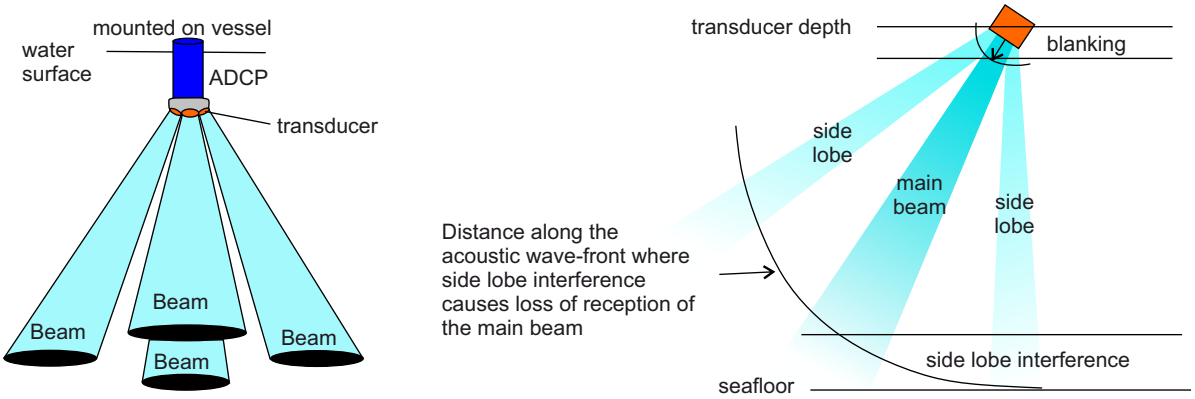

Figure 2.1: Acoustic Doppler current profiler beam pattern and locations of unmeasured areas in each profile (adapted from Simpson, 2002; Müller et al., 2009).

seafloor, the data quality is too poor to use due to the side lobe interference caused by the reflection (from the seafloor) of the downward pointing side lobe (Fig. 2.1).

For the processing of the VM-ADCP with Cascade V7.2 software, the STA files with the same instrument settings are combined into one STA file. Cascade works with raster data. The ADCP data from SO260 has 120 bins with 16 m vertical resolution and the ADCP data from M94 has 128 bins with 8 m vertical resolution. Based on the high amplitude signal from the seafloor, it is possible to detect the seafloor. The data is cleaned with a linear filter. Cascade can estimate and correct the misalignment, amplitude, and pitch based on the tracked seafloor. For the ADCP data from SO260 the misalignment is 0.29 ± 0.01 deg and the amplitude correction is 0.996 ± 0.00 and for the ADCP data from M94 the misalignment is 0.31 ± 0.01 deg and amplitude correction is 0.999 ± 0.00. Often the pitch variability is smaller than the accuracy of the correction method and cannot be corrected then. In the data presented here, the weather conditions were good during the data acquisition. Thus, the pitch variability was smaller than the error and could therefore not be corrected. Modelled tides can be calculated and subtracted from the data, but in this case we did not delete them as they are also part of the current structure which is relevant for sediment transport. However, the modelled tides are much smaller than the currents and make only a very small difference (Fig. 2.2). The data can be exported either as a cross-section (we used a horizontal grid cell size of 1 km) or from each measurement point in a specific water depth range.

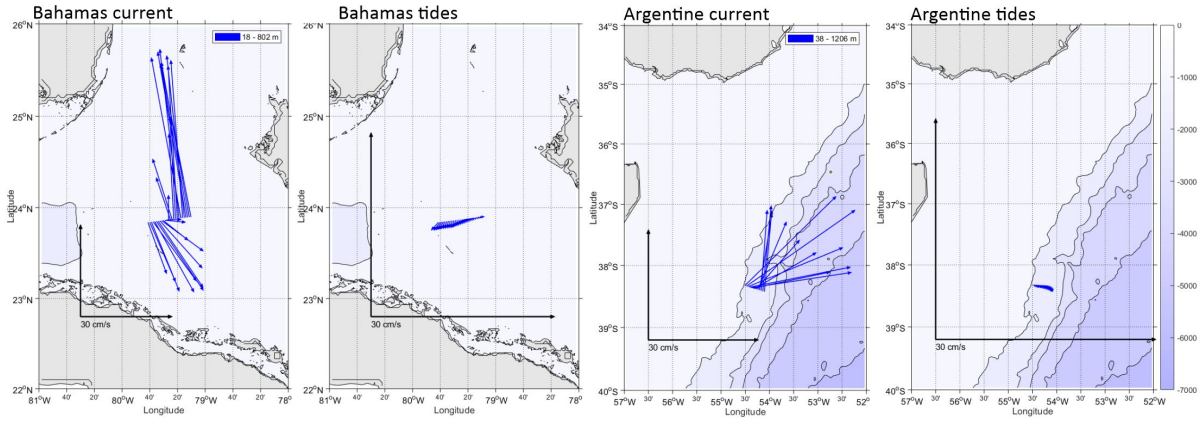

Figure 2.2: ADCP current measurements and modelled tidal currents from the Argentine margin and the Bahamas.

In the flume tank, the velocity was measured with an Ultrasonic Doppler velocimeter developed by Signal Processing SA (UDOP 4000 velocimeter). The UDOP, is similar to the ADCP, based on the doppler current shift but has a higher resolution due to a higher emitter frequency. The UDOP consists of four probes (Fig. 2.3). One TR0110 1 MHz probe is used as the emitter and three are used as receivers to record the velocity in 3D.

The UDOP was located ∼15 cm above the sediment surface at the start of the experiment. The first 10 cm near the emitter could not be used do to the poor data quality in this zone.

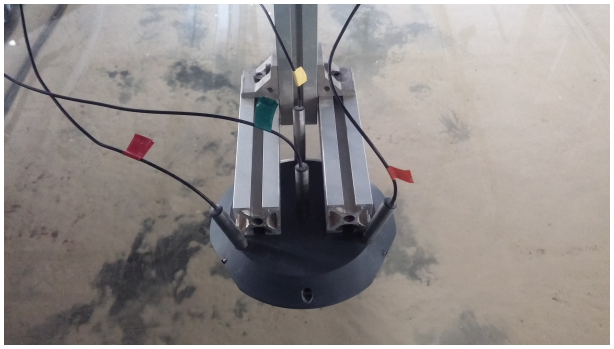

Figure 2.3: Picture of the Ultrasonic Doppler velocimeter (UDOP 4000) installed on a frame inside the flume tank.

2.1.2 Conductivity, Temperature and Depth (CTD)

Conductivity, Temperature, and Depth (CTD) data were used to identify the different water masses. CTD data were acquired during Cruise SO260 with the CTD Seabird 9.11plus (Kasten et al. 2019). The Seabird 9.11plus instrument measures temperature, depth, oxygen concentration, and conductivity, which is a measure of the salinity. At the end of the processing, we used one temperature, salinity, and oxygen value for every meter. In total, we used six CTD profiles which were collected down to approximately 50 m above the ocean floor with the deepest measurements located at 1357 m below sea level.

2.1.3 Ocean current reanalysis modelling

Current velocity measurements have a higher resolution than the used hydrodynamic model. However, the current measurements lack large-scale coverage and continuity over long periods of time. Thus, in addition to current velocity measurements, we use a numerical model, which improves our understanding of long-term mean current direction and speed as well as short-term variability.

In this study, we use the Mercator Ocean reanalysis (GLORYS12) Operational Model. This model calculates daily mean values (temperature, salinity, currents, sea-ice, and sea level) over the period 1993-2017 based on the current real-time global high-resolution forecasting Copernicus Marine Environment Monitoring Service (CMEMS) system PSY4V3 (Lellouche et al., 2018, Artana et al., 2019). The model assimilates satellite and *in situ* observations to present realistic circulation and water mass patterns (Lellouche et al., 2018). The horizontal resolution of the model is 1/12° and it has 50 vertical levels. The

vertical resolution of the model depends on the depth (Fig. 2.4). Near the sea surface the vertical resolution is 1 m and increases down to 450 m for the deepest layers.

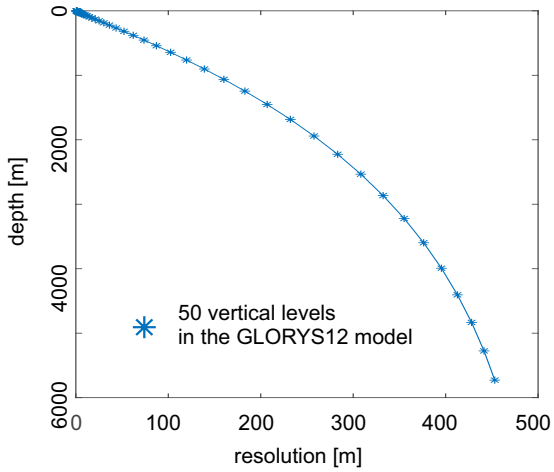

Figure 2.4: Vertical resolution of the Mercator Ocean reanalysis (GLORYS12).

In this study, we use the mean velocity, the standard deviation, potential temperature and salinity over 25 years from the reanalyses performed by Artana et al. (2021a). Potential temperature and salinity are used to calculate the potential density (Fig. 2.5). Based on the potential density, the different water masses can be identified as defined by Maamaatuaiahutapu et al. (1994). Maamaatuaiahutapu et al. (1994) defined the boundary between South Atlantic Central Water and Upper Antarctic Intermediate Water at 27.00 kg/m^3, between Upper and Central Antarctic Intermediate Water at 27.14 kg/m^3, between Central and Lower Antarctic Intermediate Water at 27.28 kg/m^3, and between Lower Antarctic Intermediate Water and Upper Circumpolar Deep Water at 27.35 kg/m^3.

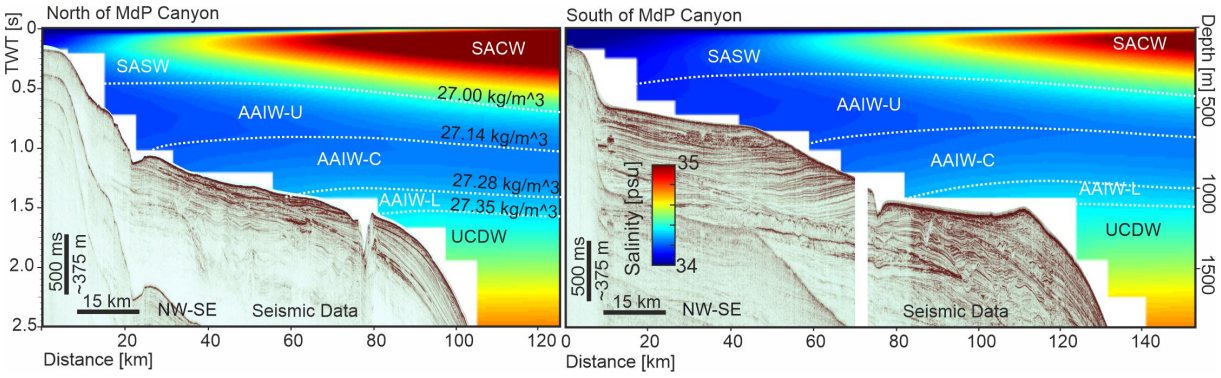

Figure 2.5: Salinity values from the Mercator Ocean reanalysis (GLORYS12). SASW: Subantarctic Surface Water, SACW: South Atlantic Central Water, AAIW-U: Upper Antarctic Intermediate Water, AAIW-C: Central Antarctic Intermediate Water, AAIW-L: Lower Antarctic Intermediate Water, UCDW: Upper Circumpolar Deep Water. The location of the cross-sections is shown in Fig. 3.2.

2.2 Geological and geophysical dataset

2.2.1 Bathymetry

Multibeam echosounder (MBES) data is used to understand the morphology of the deep sea. The transmitter (oriented along the vessel) and receiver (oriented across the vessel) of a multibeam system are mounted beneath the vessel (Renard and Allenou, 1979). The transmitter transmits multiple sound waves. At the seafloor, the sound waves are scattered back to the vessel where they are recorded by the receiver (Fig. 2.6). Based on the

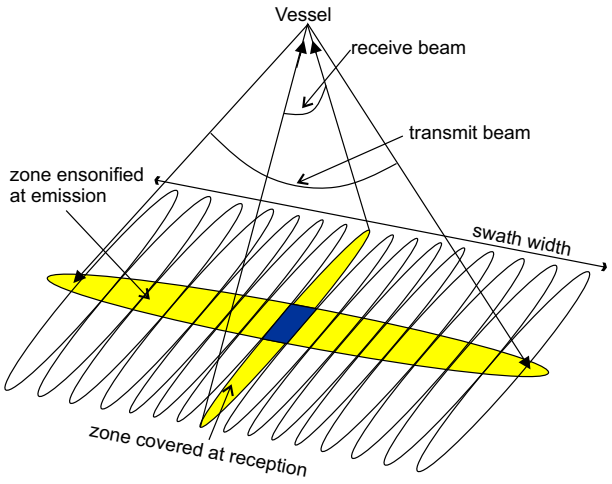

Figure 2.6: Schematic drawing of data acquisition of a multibeam sonar system. The yellow area symbolizes the total area that is ensonified by the emitter and the total area that is covered by the receiving hydrophones. As a result, the blue area shows the usable ensonified area (adapted from Hughs Clarke, 2018 and Bikonis and Demkowicz, 2018).

time between emitted and recorded signal the sea surface depth can be calculated. For calculating the depth of the seafloor in meters, the sound wave speed must be known. This information can be extracted from the CTD measurements. The uncertainty of the location of the resolved bathymetry depends on the accuracy of the position and orientation of the sensors, the bottom detection algorithm, and the accuracy of the sound speed in the water column (Hughs Clarke, 2018; Bikonis and Demkowicz, 2018). The footprint of each beam is determined by the opening angle of the transmitter array and the receiver array as well as the water depth. Furthermore, due to geometry, the footprint at the outer edges of the swath is larger. Thus, the size of the footprint also depends on the swath width. The footprint of each beam gives an idea of the possible resolution at a given depth. However, the resolution depends on the sounding density and the along-track resolution also depends on the vessel speed.

In the thesis, we use MBES data from offshore North Argentina (SW Atlantic Ocean), the

Table 2.1: Overview of the bathymetry data.

Area	**Acquisition**	**Reference**	**Grid cell size**	**Chapter**
North Argentina (SW Atlantic Ocean)	cruise SO260 onboard the R/V SONNE in 2018	Kasten et al., 2019; Steinmann et al., 2021	25 m	3 and 4
North Argentina (SW Atlantic Ocean)	cruise SO260 onboard the R/V SONNE in 2018	Kasten et al., 2019	100 m	3
Mozambique Basin (SW Indian Ocean)	cruise PAMELA-MOZ2 onboard the R/V L'Atalante in 2014	Robin and Laurence, 2014; Miramontes et al., 2021	30 m	4
Corsica Trough (northern Tyrrhenian Sea, NW Mediterranean Sea)	cruise PRISME2 onboard the R/V L'Atalante and cruise PRISME3 onboard the R/V Pourquoi pas? survey in 2013	Cattaneo 2013a,b; Miramontes et al., 2016	15 m	4
Offshore Galicia (NW Spain, NE Atlantic Ocean)	cruise M84/4 onboard the R/V Meteor in 2011	Hanebuth et al., 2011; 2015	75 m	4
Santaren Channel in the Bahamas	cruise M95 onboard the R/V Meteor in 2013	Betzler et al. 2014a;b; Lüdmann et al. 2016	200 m	4
Gulf of Cadiz	cruise CADIPOR 1+2 onboard the R/V Belgica in 2002 and 2005	Van Rensbergen et al., 2005; Vandorpe et al., 2017	30 m	4
Offshore Lanzarote and offshore north Ireland	-	EMODnet bathymetry	115 m	4
Offshore Patagonia (Drake Passage)	-	GEBCO 2021 bathymetry	460 m	4
Flume Tank	Laserscan	Chapter 5	0.005 m	5

Mozambique Basin (SW Indian Ocean), the Corsica Trough (NW Mediterranean Sea), offshore Galicia (NE Atlantic Ocean), the Santaren Channel in the Bahamas and the Gulf of Cadiz (NE Atlantic Ocean). All data were already processed before my thesis project started. Table 2.1 gives an overview where the data was previously published and what cell size the provided grid has. I used QGIS3.12 to visualize and measure topographic features.

Additionally, the General Bathymetric Chart of the Oceans (GEBCO; GEBCO Compilation Group (2020)) is used to understand large-scale features. GEBCO is an open access terrain model for land and ocean, and combines available bathymetric data into a global gridded model. In areas where no or very limited multibeam data is available, GEBCO

relies on depth values derived from the satellite altimetry method (Watherall et al., 2015). EMODnet (European Marine Observation and Data Network) aims at understanding the European seas better but also provides bathymetric data from the entire world. EMODnet uses multibeam and single beam data and combines them with the GEBCO grid resulting in a merged grid of the world as well as higher resolution grids covering smaller areas.

For the flume tank experiments, a laser was used to measure the morphology. Since the laser cannot penetrate through water, the water must be removed from the tank for every laser scan. The laser scanner measures every 2 mm at pre-defined across-slope profiles that are 50 cm spaced. The data were gridded with MATLAB. I applied no filters with MATLAB, but small artefacts were removed by gridding the data with a cell size of 5 mm.

2.2.2 High-resolution multi-channel seismic reflection and sub-bottom profiler data

Seismic reflection data and sub-bottom profiler data are used for understanding the internal architecture of sedimentary features. Furthermore, in chapter 4, we use the figures from scientific publications to measure the size of moats and their associated drift. For seismic reflection data acquisition in the marine environment, a seismic source that produces sound waves, also named seismic waves or pressure waves (p-wave), is usually towed behind a vessel. The seismic source can for example be an airgun that shoots air bubbles which generates seismic waves. After each shot, the gun is silent until it is triggered again. The emitted seismic waves travel through the water column and are reflected at the seafloor and geological boundaries (Crutchley and Kopp, 2018). Seismic waves are reflected at boundaries that have an impedance contrast. The impedance is calculated by the product of density and acoustic wave velocity. Usually, the highest impedance contrast is found at the seafloor and thus the strongest reflection. The reflected acoustic waves travel back to the sea surface where they are recorded by hydrophones that are installed inside a streamer that is towed behind the vessel (Fig. 2.7). High-resolution surveys use a high frequency source where the high-frequency seismic waves cannot penetrate as deep as low-frequency waves. Based on the time between the emitted and received signal it can be calculated where the wave was reflected. If the speed of the seismic wave is known for each layer, the exact depth in meters below the sea surface can be calculated. However, the speed is usually not accurately known and thus, seismic data is often not converted into depth. Because the seismic waves travel down to the reflector and back to the surface, the vertical axis from seismic data is usually given in Two-Way travel Time (TWT). All used seismic data was processed before this thesis project started.

Sub-bottom profiler data (sometimes also referred to as a Sediment echosounder) can

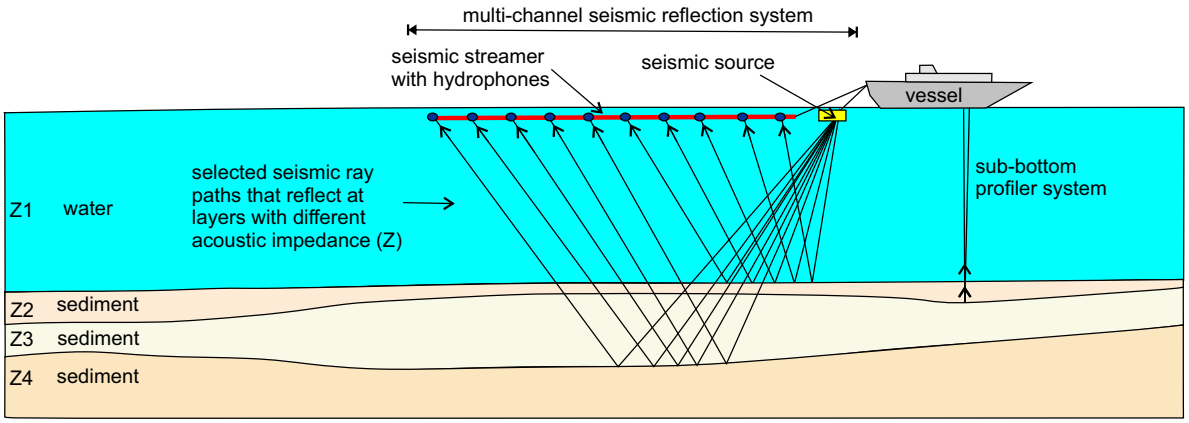

Figure 2.7: Schematic drawing of data acquisition of a 2D marine seismic reflection and sub-bottom profiler system (adapted from Crutchley and Kopp, 2018).

show the internal architecture of sedimentary features in higher resolution than seismic reflection data because it uses a higher source frequency. The method relies on the same reflection principle as multi-channel seismic reflection data but has only a single channel (Dondurer, 2018). Sub-bottom profilers are mounted beneath or at the side of the vessel (Fig. 2.7). The sub-bottom profiler data was converted from PS3 to SEGY format before this thesis project started and I visualised it with IHS KINGDOM.

2.2.3 Sediment samples

Sediment samples are used in this thesis for grain size analyses. In a system that is mainly controlled by bottom currents, we expect coarse material in areas with high bottom current speeds and fine material in areas with low bottom current speeds. Where available, we used sediment samples that were taken by a Multicorer (MUC) or a Giant Box Corer (GBC) because it is most suitable for surface sediment sampling in the deep sea. The Grab Sampler (GS) works well for sand, but it bears the risk that finer material might fall out. In areas where no other sediment samples were available, we used samples taken by a Gravity Corer (GC) and a sea floor drill rig (MeBo). Both methods have the risk of over-penetrating the ground and thus not correctly showing the undisturbed seafloor surface. However, we did not see any differences in sediment grain size distribution when we compared sediment samples that were taken in close proximity to each other, regardless of the method they were derived from.

The grain size analyses were performed by Meret Felgendreher on bulk sediment samples with a Beckman Coulter Laser LS 13320 at MARUM laboratories (Fig. 2.8) as part of her Bachelor's Thesis (Felgendreher, 2020). During the preparation for the measurements, the sediment is heated together with water and Sodium hexametaphosphate as a dispersant.

Figure 2.8: Beckman Coulter Laser LS 13320 at MARUM laboratories for grain size measurements.

2.3 Flume tank experiments

2.3.1 Setup

With the flume tank experiments, we aim at understanding the conditions necessary to create a moat-drift system. Thus, the structure must self-emerge in the tank while we closely monitor the morphology and current dynamics. As starting condition for the experiment, we used a morphology similar to the north Argentinian continental margin (Preu et al., 2012). The morphology in the tank consisted of a gentle lower slope (not part of the study area), a terrace and an upper slope of 18° or 26°. These slopes are steeper than the slope at which the moats at the Ewing Terrace form but such slopes can also exist in nature, for instance typically around topographic obstacles (O'Grady et al., 2000; Hanebuth et al., 2015). The morphology in the tank is built out of sand (Fig. 2.9A) and then covered by artificial grass (Fig. 2.9B). The artificial grass stabilizes the morphology

Figure 2.9: Photos showing the setup of the experimental site in the flume tank. (A) Morphology built with sediment. (B) Morphology covered with artificial grass. (C) A thin layer of crushed walnut shell on top of artificial grass.

and makes it possible to repeat experiments with the same starting conditions. The artificial grass is 4 m wide, and 10 m long, it weighs 1260 g/m^2, it is made of polypropylene and the fibre height is 5 mm. Since the artificial grass floats in water, it is pushed down by sand, which sinks between the blades of the grass. The top of the artificial grass is covered by a thin layer of crushed walnut shells which we used as an analogue for deep

sea sediments throughout our experiments (Fig. 2.9C). After each experiment finished, the added walnut shells were removed. In this setup, three self-priming centrifugal pumps (Calpeda AM 50-125CE) were used to create a current that runs clockwise in the tank. These pumps were attached to the wall of the tank at the opposite side of the slope (where the experiments were conducted) (Fig. 2.10A). The motor of the pump was placed outside

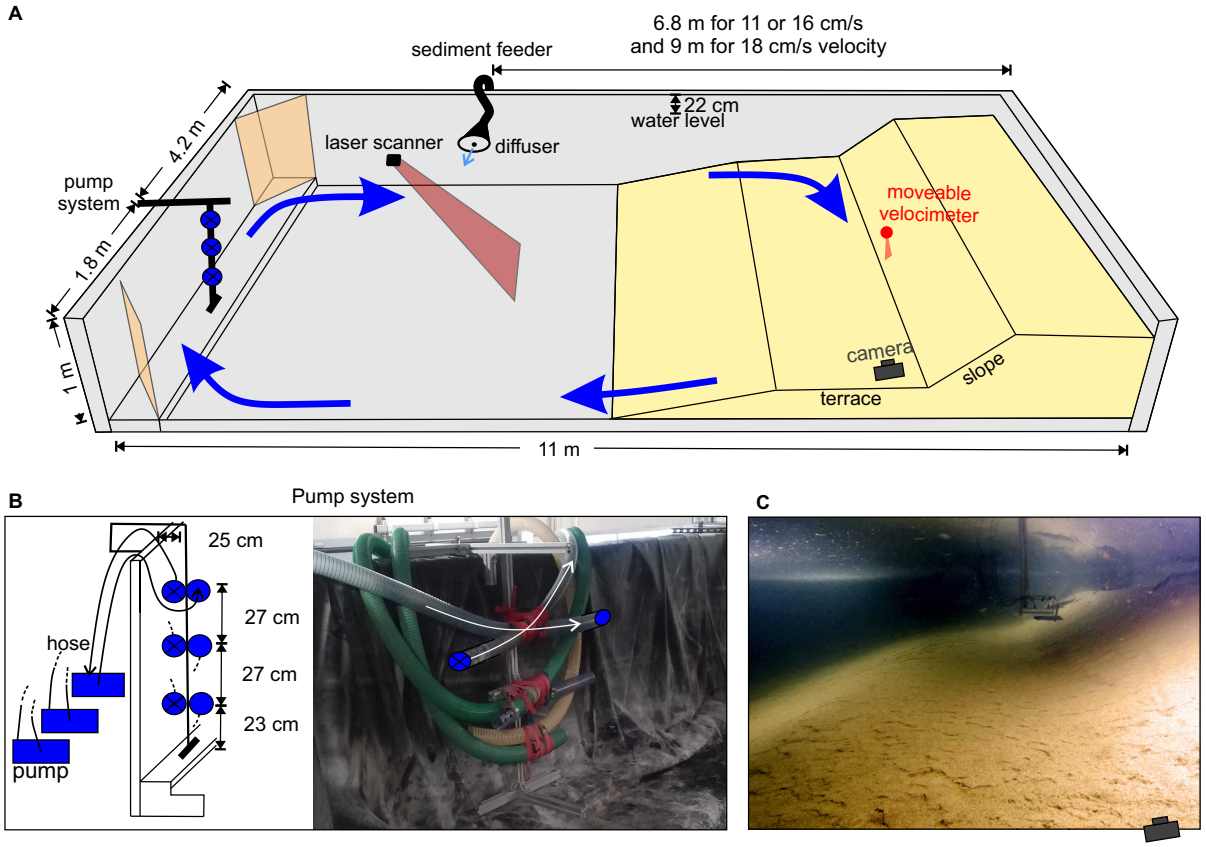

Figure 2.10: (A) Schematic drawing of the instruments used during the experiments. (B) Schematic drawing and photo of the pump system. (C) Photo of the study site taken during one experiment.

the tank and two hoses were attached to it. One was used to suck the water out of the tank whereas the other was used to pump the water back into the tank (Fig. 2.10B). The pumps always operated at the same pump speed. With all three pumps switched on, the maximum velocity we were able to reach at the study site was 18 cm/s.

The experiments were conducted using walnut shells with a grain size range of 200−450 μm and a density of 1350 kg/m^3. We used walnut shells due to their lower density compared to siliciclastic sediment. This allows the transport of walnut shells at lower velocities than siliciclastic sediment with the same grain size. The bottom shear stress (τ) to erode sediment depends on the velocity (Soulsby and Whitehouse, 1997):

$$\tau = p_f \; u_*^2 \quad , \tag{2.1}$$

with seawater density is $p_f = 1000\,\mathrm{kg/m^3}$ and friction velocity is u_*. The friction velocity can be calculated assuming a logarithmic relation between the friction velocity and the variation of velocity with height, a von Kármán constant $\kappa = 0.4$ and bottom roughness length $z_0 = 0.0035\,\mathrm{m}$ (Schlichting, 1962):

$$u_* = \frac{\kappa u(z)}{ln\frac{z}{z_0}}\,, \tag{2.2}$$

where z is the distance from the bottom where the current velocity u(z) is measured. Sediment motion can be initiated when the maximum shield parameter is higher than the critical bottom shear stresses (Soulsby and Whitehouse, 1997):

$$\frac{\tau}{g(p_s - p_f)}d > \frac{0.3}{1 + (1.2 \cdot D_*)} + 0.055(1 - e^{-0.02D_*})\,, \tag{2.3}$$

with sediment density $p_s = 2650\,\mathrm{kg/m^3}$ for silt and $1350\,\mathrm{kg/m^3}$ for walnut shells, diameter d, dimensionless grain size D_* and gravitational acceleration of $g = 9.81\,\mathrm{m/s}$. Dimensionless grain size D_* is calculated with:

$$D_* = \left(\frac{\frac{p_s}{p_f} - 1}{\frac{g}{\eta^2}}\right)^{\frac{1}{3}} d\,, \tag{2.4}$$

where $\eta = 1.052610^{-6}\,\frac{\mathrm{m}^2}{\mathrm{s}}$ is the kinematic viscosity of water at a temperature of 18°C. According to the critical shield parameter for motion initiation (Soulsby and Whitehouse, 1997), the bottom shear stresses reach critical shear stresses ($0.19\,\mathrm{N/m^2}$ for silt and $0.05\,\mathrm{N/m^2}$ for walnut shell) for silt (sediment grain sizes $d = 20\,\mu\mathrm{m}$) and walnut shells (sediment grain sizes $d = 325\,\mu\mathrm{m}$) at a current velocity of 8 cm/s (measured at 20 cm above the seafloor). Thus, we used the walnut shells as an analogue for silt because they are transported as bedload with similar speeds. The advantage of the coarse walnut shells over the fine silt is that it settles faster because, according to Stoke's Law, the grain size factors into the settling velocity quadratic and the density only linear. This allows us to run the experiments in a smaller setup. The settling velocity is calculated with Stoke's Law:

$$v_{settl} = \frac{p_s - p_f}{18\eta}d^2 g\,. \tag{2.5}$$

For silt with a diameter $d = 20\,\mu\mathrm{m}$ and a density $p_s = 2650\,\mathrm{kg/m^3}$, the settling velocity is only 0.034 cm/s. For walnut shells with a diameter $d = 325\,\mu\mathrm{m}$ and a density $p_s = 1350\,\mathrm{kg/m^3}$ the settling velocity is 1.914 cm/s. However, Stoke's Law assumes spherical particles and the walnut shells are probably not very spherical. Thus, the calculation only gives a very rough estimate of the settling velocity.

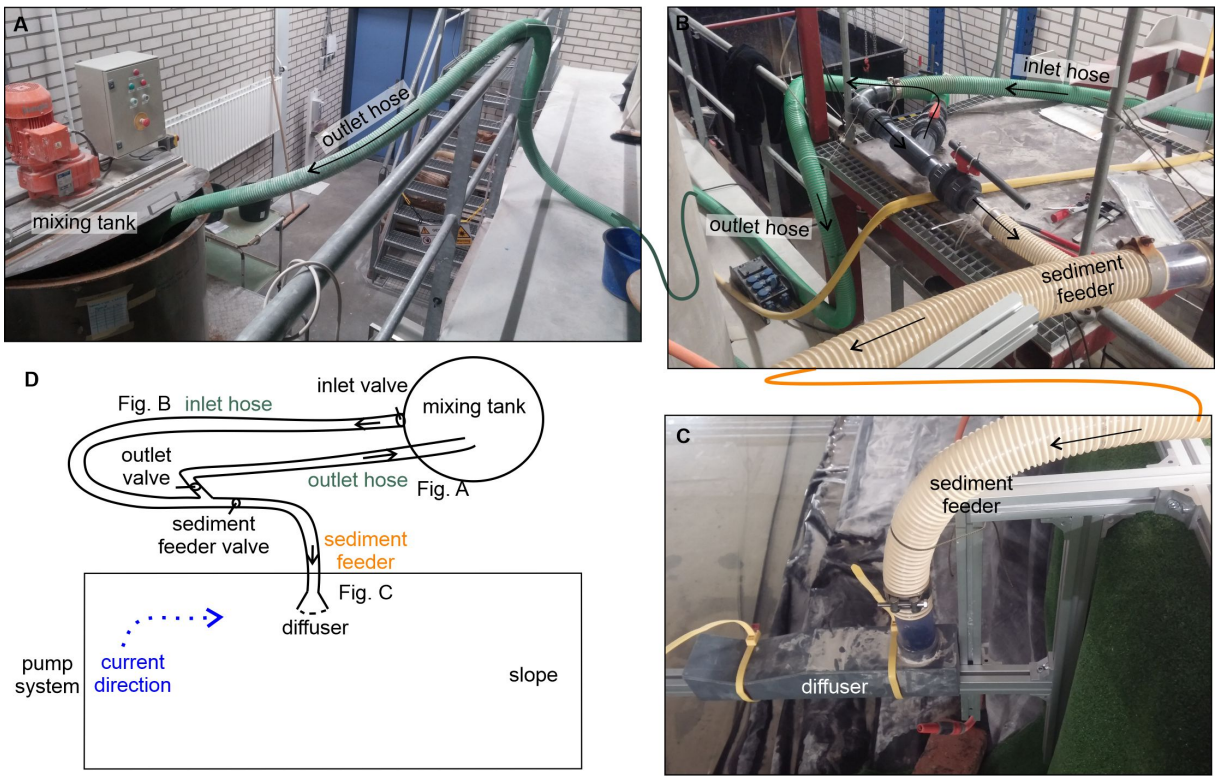

Figure 2.11: (A) Photo of the outlet pump that brings the sediment back to the mixing tank that is not fed into the flume tank. (B) Photo of the inlet hose that transports sediment out of the mixing tank. From this hose part of the sediment can be let into the recirculation hose and part of it can be let into the sediment feeder. (C) Photo of the sediment feeder that feeds the sediment into the flume tank. (D) Schematic drawing in plain view of the sediment feeding system used for the experiments.

The walnut shells are mixed with water in the mixing tank before entering the flume tank to avoid surface tension, which hinders the particles from settling (2.11A). The particles are not supposed to settle inside the hoses on their way to the tank. Thus, the current velocity in the hoses must be high enough to prevent settling. On the other side, the velocity of the water-walnut shell mixture should not be too high when it enters the flume tank, to not influence the circular current structure in the flume tank. Thus, we set up a recirculation loop in which the sediment is pumped out (of the mixing tank) and then back into the mixing tank (Fig. 2.11). From this recirculation loop, part of the mixture can be let into the flume tank with the sediment feeder (Fig. 2.11C). Depending on the used current speed, the sediment feeder must be positioned closer or further away from the slope (Fig. 2.10) so that the particles settle on the slope and can then be further transported by contour currents as bedload. To run each experiment and to ensure comparability of the results, we established the following workflow:

1. The inlet valve is closed while the particles are mixed in the mixing tank, the outlet valve is opened, and the sediment feeder valve is closed.

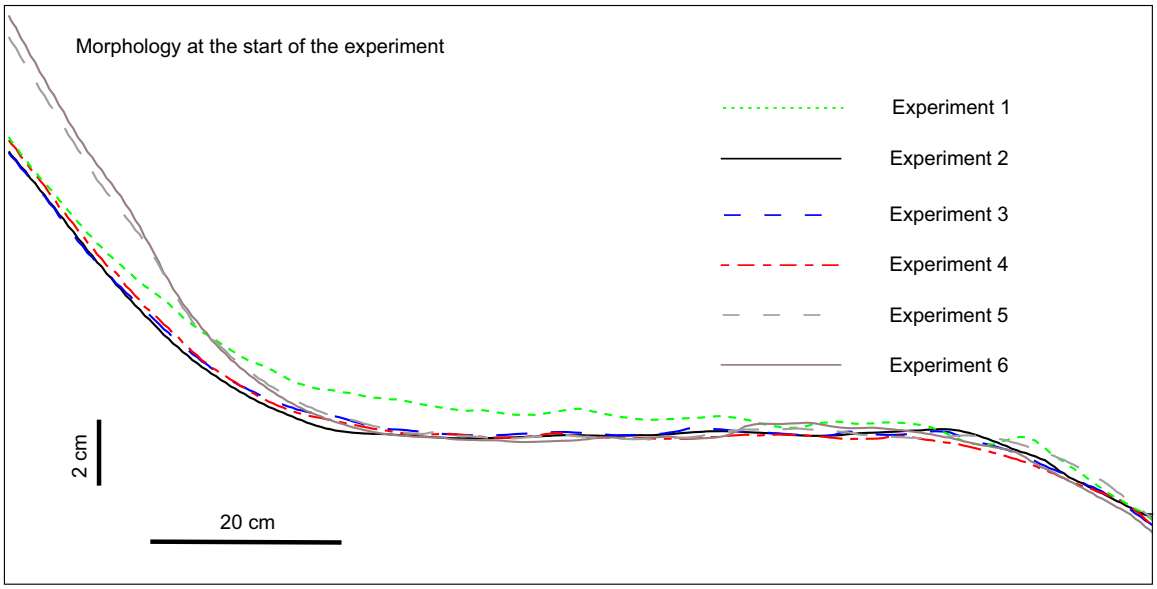

Figure 2.12: Starting morphology of the six experiments. Experiment 1 has 1.5 cm of sediment covering the green grass. Experiments 2-6 only have 0.5 cm of sediment cover.

2. The air is removed from the inlet hose with an isostatic pump, while a tap that is connected to the inlet hose is open.
3. When the inlet hose is filled with water, the isostatic pump and the tap are turned off and the pump that pumps the water through the hose is turned on.
4. Immediately after that, the inlet valve is opened. Now the mixture runs through the recirculation loop.
5. While the current in the flume tank is flowing clockwise, the water-walnut shell mixture enters the flume tank by opening the sediment feeder valve.

2.3.2 Repeatability

In the flume tank experiments, we distinguish between the sediment input phase, where 80 cm^3 sediment is pumped into the tank, and the sediment reworking phase, where no sediment is pumped into the tank. The sediment is pumped in over a period of 2 h, which allows to keep the sediment concentration (volume) below 2%. The low concentration avoids that the particles interact with each other. In total, we conducted 6 experiments with 2 different slopes and 3 different velocities (Table 2.2). Experiment 1 aimed at understanding how sediment availability influences the evolution of the moat-drift system. Here, we wanted to have an erodable substrate already at the beginning of the experiment (Fig. 2.12). This allowed us to measure the across-slope velocity structure, which takes 40 min, while sediment is already reworked. The measurement at each location only takes 2 minutes, however, since the UDOP is moved manually, it takes longer. Experiments 2-6 aimed at studying the influence of slope angle and current speed on the developing

Table 2.2: Summary of the conducted experiments

Experiment	**1**	**2**	**3**	**4**	**5**	**6**
Velocity [cm/s]	18	11	16	18	11	16
Slope [°]	18	18	18	18	26	26

morphology. Thus, we always started with the same morphology (Fig. 2.12). During these experiments, the velocity is only measured at one location. The sediment is always pumped in after 15 minutes.

For the flume tank experiments to be repeatable, it is necessary not only to always have the same starting morphology, but also to always pump in the sediment in the same way. This is critical because the process is not fully automated. Thus, we analysed the morphology of the slope before and after 80 cm^3 of the walnut shells were added during the sediment input phase. We compared the difference between two experiments that were conducted with the same current speed. Both cases led to the same amount of aggradation on the terrace (Fig. 2.13), which confirms that the sediment input phase is repeatable.

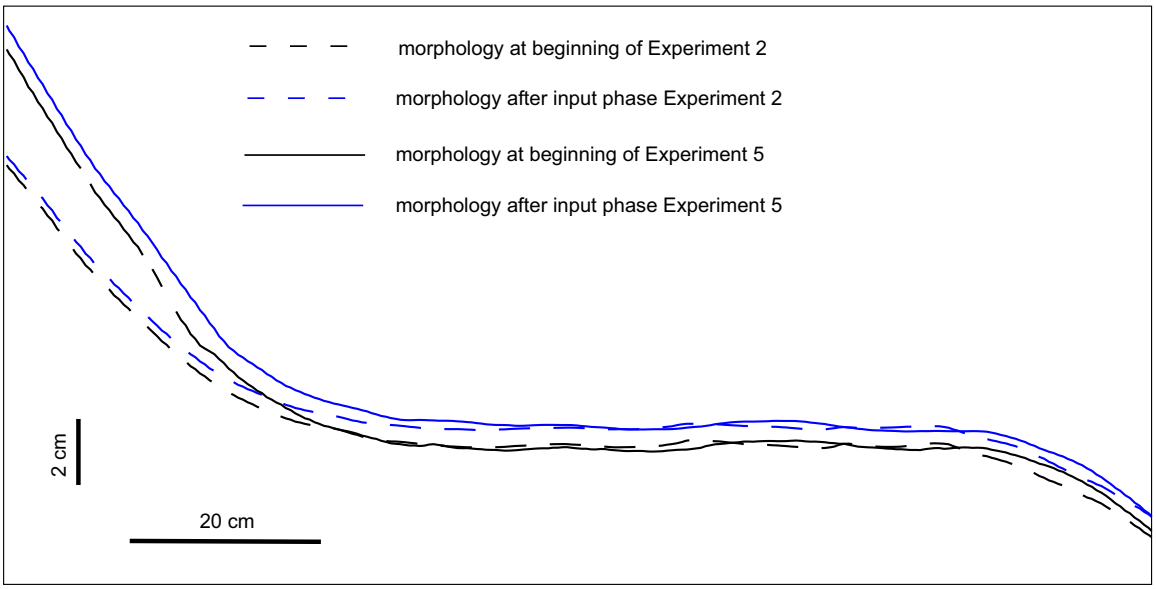

Figure 2.13: Morphology before and after the sediment input phase of experiments 2 and 5, which were run with the same current speed. In both experiments, the same amount of sediment is accumulated on the terrace.

Chapter 3

The erosive power of the Malvinas Current: Influence of bottom currents on morpho-sedimentary features along the northern Argentine margin (SW Atlantic Ocean)

Published in: Marine Geology in 2021
https://doi.org/10.1016/j.margeo.2021.106539

Henriette Wilckens [a,b], Elda Miramontes [a,b], Tilmann Schwenk [a], Camila Artana [c], Wenyan Zhang [d], Alberto R. Piola [e,f], Michele Baques [e,g], Christine Provost [h], F. Javier Hernández-Molina [i], Meret Felgendreher [j], Volkhard Spieß [a], Sabine Kasten [a,b,k]*

a Faculty of Geosciences, University of Bremen, Bremen, Germany.
b MARUM - Center for Marine Environmental Sciences, University of Bremen, Germany
c MERCATOR-OCÉAN, Parc Technologique du Canal, Ramonville Saint Agne, France
d Institute of Coastal Systems, Helmholtz-Zentrum Hereon, Geesthacht, Germany
e Departamento Oceanografía, Servicio de Hidrografía Naval, Buenos Aires, Argentina
f Instituto Franco-Argentino para el Estudio del Clima y sus Impactos (UMI-IFAECI/CNRS-CONICET-UBA), Buenos Aires, Argentina
g Acoustic Propagation Department, Argentinian Navy Research Office and UNIDEF (National Council of Scientific and Technical Research - Ministry of Defense), Buenos Aires, Argentina
h Laboratoire LOCEAN-IPSL, Sorbonne Universit´es (UPMC, Univ. Paris 6) CNRS-IRD-MNHN, Paris, France
i Department of Earth Sciences, Royal Holloway University of London, Egham, Surrey, UK
j Institute of Geosciences, Kiel University, Kiel, Germany
k Alfred Wegener Institute Helmholtz Centre for Polar and Marine Research, Bremerhaven, Germany
* Corresponding author: Henriette Wilckens: cwilcken@uni-bremen.de

Keywords: Contour current; Deep-water environment; Sediment drift; Contourite Depositional Systems; Sediment transport; Argentine Margin

3.1 Abstract

Sediment deposits formed mainly under the influence of bottom currents (contourites) are widely used as high-resolution archives for reconstructing past ocean conditions. However, the driving processes of Contourite Depositional Systems (CDS) are not entirely understood. The aim of this study is to establish a clearer link between contourite features and the oceanographic processes that form them. The morphosedimentary characteristics of a large CDS were analysed together with the current dynamics along the northern Argentine continental margin. This study combines multibeam bathymetry, seismo-acoustic data, sediment samples, vessel-mounted Acoustic Doppler Current Profiler (VM-ADCP) data and numerical modelling of ocean currents. The contouritic features include large contourite terraces (La Plata Terrace, Ewing Terrace) and an abraded surface connecting the terraces, as well as smaller erosional and depositional features like moats, erosion surfaces on the Ewing Terrace, sediment waves and contourite drifts. Measured and modelled near-bottom currents are vigorous (up to 63 cm/s at 150–200 m above the seafloor) where abraded surfaces and moats are present, and relatively weak (below 30 cm/s) on the La Plata Terrace and the Ewing Terrace. Generally, bottom currents follow the upper and middle slope morphology. Decreasing velocity of water masses flowing northward leads to less erosion and finer sediment deposits. ADCP data and the hydrodynamic model show the formation of eddies near the seafloor which probably lead to the small erosion surfaces on the Ewing Terrace, even though it is mainly a depositional environment. Overall, this study contributes to a better understanding of the formation of CDS and can help future reconstructions of past ocean conditions based on sedimentary structures.

3.2 Introduction

Continental margins can be shaped by ocean currents, which influence sediment erosion and deposition even at large scales (Heezen, 1959; Heezen and Hollister, 1964; Stow et al., 2009). Sediment deposits formed mainly under the influence of bottom currents (i.e. currents related to oceanographic processes flowing near the seafloor) are classified as contourites (Rebesco and Camerlenghi, 2008; Rebesco et al., 2014). These currents often supply oxygen and nutrients favouring the development of deep-sea ecosystems with high biodiversity, for instance cold-water corals are often found in contourite depositional systems (Hebbeln et al., 2016; Steinmann et al., 2020). Bottom currents that lead to large sediment deposits can also control the distribution of microplastics and lead to hotspots in the same area where biodiversity is high, which is a potential threat for marine ecosystems (Kane et al., 2020). Furthermore, contourites are important for several fields including paleoclimatology and palaeoceanography, risk management regarding slope instabilities and hydrocarbon exploration (Rebesco et al., 2014; Hernández-Molina et al., 2018; Miramontes et al., 2018). Many physical oceanographic processes, ranging from quasi-steady

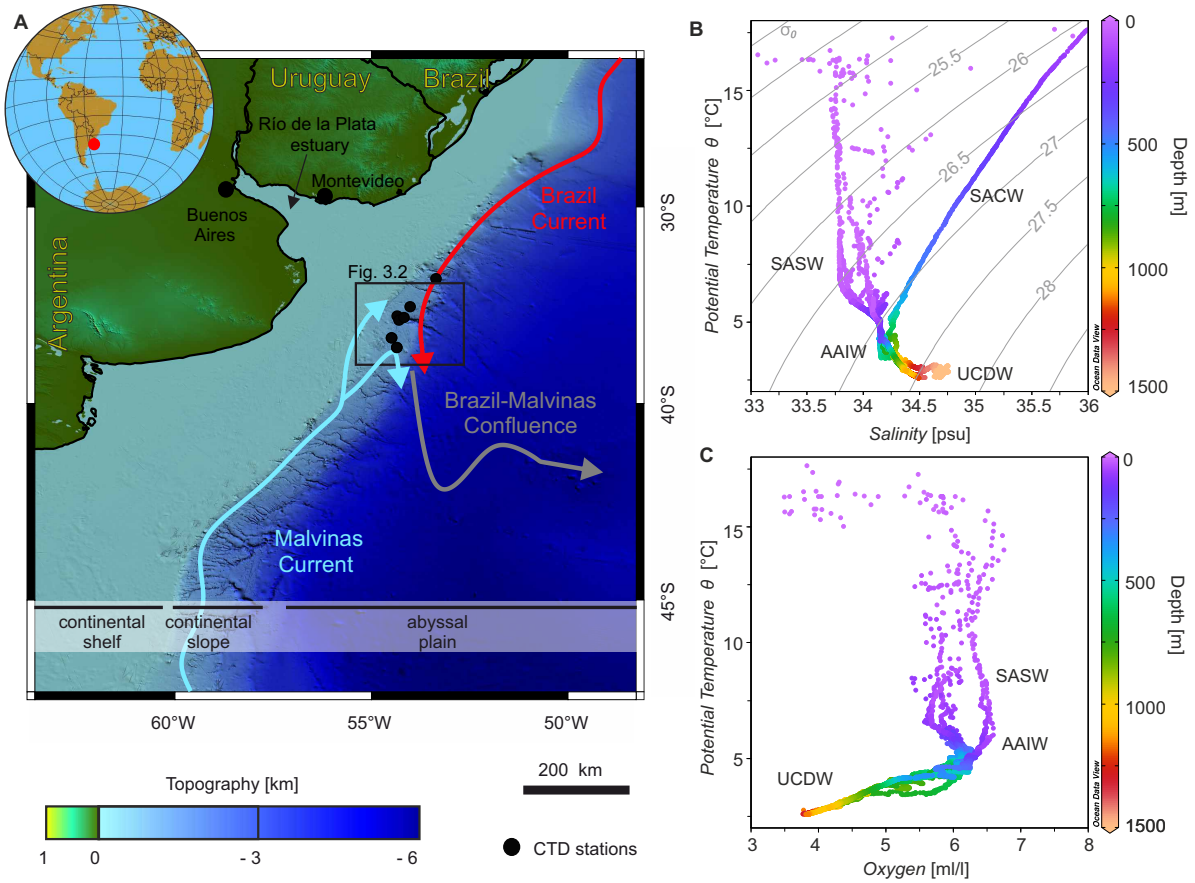

Figure 3.1: (A) Regional bathymetric map showing the SE American margin. The arrows indicate the general circulation pattern of the cold Malvinas Current, the warm Brazil Current and their confluence. (B/C) Potential temperature versus salinity/oxygen based on CTD data collected during cruise SO260 that allowed the identification of different water masses: SASW: Subantarctic Surface Water, SACW: South Atlantic Central Water, AAIW: Antarctic Intermediate Water, UCDW: Upper Circumpolar Deep Water. σ_0: potential density anomaly.

geostrophic currents, sub-inertial oscillations, tides to internal waves, have potentially significant impact on the morphogenesis and evolution of contourites. On a long time scale, the development of contourites is subject to climate-induced change in thermohaline circulation and isostatic movements (e.g. tectonics). However, it is still not clear how these multi-scale processes interact and control the formation and evolution of contourites. Understanding the present deposition mechanisms is necessary for the reconstruction of past ocean conditions based on the geological record (Surlyk and Lykke-Andersen, 2007; Preu et al., 2012; Betzler et al., 2013).

A large Contourite Depositional System (CDS) has been recognised along the northern Argentine and Uruguayan margin (Hernández-Molina et al., 2009; 2016b; Preu et al., 2012; 2013). The CDS includes three large contourite terraces that have been documented along the continental margin off the Río de la Plata Estuary (northern Argentina) in close proximity to the Mar del Plata (MdP) submarine Canyon (Preu et al., 2012, Preu et al.,

2013). The study area is located in the confluence zone of the northward flowing Malvinas Current and the southward flowing Brazil Current (Fig. 3.1; Artana et al., 2019; Piola and Matano, 2019). This complex oceanographic setting makes it an interesting study area for analysing the influence of currents on contourite formation. In this study we use a multidisciplinary approach based on multibeam bathymetry, hydroacoustic data, sediment samples, vessel-mounted Acoustic Doppler Current Profiler (VM-ADCP) data, Conductivity, Temperature and Depth (CTD) data and 25 years of high-resolution ocean reanalysis. The main aim of the study is to derive further insights into basic physical oceanographic mechanisms that control the formation of large-scale contourites in such a complex and unique oceanographic configuration. More specifically, this multidisciplinary study has the following three main goals: 1) to report on the characteristics of near-bottom currents in the Brazil-Malvinas Confluence Zone; 2) to discuss differences within the contourite system regarding seafloor morphology, sediment architecture and grain size; 3) to interpret and discuss the oceanographic processes that may contribute to the formation of the observed contouritic features.

3.3 Regional setting

3.3.1 Oceanographic framework

Strong ocean currents are present along the Argentine and Uruguayan continental margin from the surface down to 2000 m water depth (Piola and Matano, 2019). The Malvinas Current (MC) transports cold and nutrient rich waters northwards. The Brazil Current flows southwards along the continental slope and is shallower than the Malvinas Current (Piola and Matano, 2019). The study area is located in the region where these two boundary currents encounter, forming the Brazil-Malvinas Confluence Zone. On average, the axis of the confluence zone is situated at an approximate latitude of 38°S (Gordon and Greengrove, 1986; Artana et al., 2019; Piola and Matano, 2019). The confluence shows large migrations at synoptic (800 km) and interannual (300 km) scales compared to rather small seasonal changes (<150 km) (Artana et al., 2019; 2021a). Numerical simulations suggest that at the confluence the Malvinas Current splits into two branches (Provost et al., 1995; Artana et al., 2019). The offshore branch joins the Brazil Current and detaches from the continental slope while the inner branch subducts and continues flowing northward along the upper continental slope (Provost et al., 1995; Artana et al., 2019). Currents flowing on the wide Argentine shelf continue flowing northward beyond the Brazil-Malvinas Confluence (Piola et al., 2018).

The Malvinas and the Brazil Current both carry several different water masses which are defined by their different thermohaline, nutrient and dissolved oxygen characteristics (Maamaatuaiahutapu et al., 1994). The northward flowing water masses at the continental slope from sea surface to bottom are: Subantarctic Surface Water (SASW), Antarctic

Intermediate Water (AAIW), Circumpolar Deep Water (CDW) and the Antarctic Bottom Water (AABW) (Preu et al., 2013; Piola and Matano, 2019). The southward flowing water masses are: Tropical Water, South Atlantic Central Water (SACW), AAIW and North Atlantic Deep Water (NADW) (Preu et al., 2013; Valla et al., 2018; Piola and Matano, 2019). Southward flowing AAIW is an older (saltier and less oxygenated) variety of the AAIW recirculated around the South Atlantic subtropical gyre (Valla et al., 2018). The NADW flows southward between Upper Circumpolar Deep Water (UCDW) and Lower Circumpolar Deep Water (LCDW) (Reid et al., 1977; Piola and Matano, 2019). The depth of the interfaces between the water masses varies with time and between locations. In close proximity to the MdP Canyon the interfaces between AAIW, UCDW, NADW, LCDW and AABW are located at 1200, 2000, 3200, 3800 m, respectively (Preu et al., 2013). The zone of interest in this study (located at 450–1400 m water depth) is mainly under the influence of the AAIW (identified by a salinity minimum and a dissolved oxygen maximum) and the UCDW (identified by a dissolved oxygen minimum) (Fig. 3.1B,C; Preu et al., 2013). The interface between the AAIW and the UCDW is characterised by an increase of salinity and dissolved oxygen decrease with depth (Fig. 3.1B,C). This modern ocean circulation and stratification pattern was established during the Middle Miocene after the onset of the (paleo-) NADW circulation in the southern hemisphere, which significantly influenced the formation of the CDS (Preu et al., 2012).

3.3.2 Geological setting

The study area is located at the passive volcanic-rifted northern Argentine continental margin, offshore the Río de la Plata estuary formed during the Cretaceous period (Fig. 3.1A; Hinz et al., 1999; Franke et al., 2007). The rivers flowing into the Río de la Plata, together with the Colorado and Negro rivers, that are located further south, are the main sources of sediments to the continental margin (Giberto et al., 2004; Voigt et al., 2013; Razik et al., 2015a; Franco-Fraguas et al., 2016). Frenz et al. (2003a) and Razik et al. (2015a) analysed the sediment grain size of surface sediments from the SE South American margin and suggested that sedimentation and grain size distribution on the Argentine and Uruguayan margin are strongly controlled by the oceanic circulation. The continental slope is composed of contourites, forming a large Contourite Depositional System (CDS) composed of moats/channels, contouritic terraces, abraded surfaces and sediment drift deposits (Urien and Ewing, 1974; Hernández-Molina et al., 2009; 2016b; Krastel et al., 2011; Preu et al., 2012, Preu et al., 2013; Voigt et al., 2016; Warratz et al., 2017; 2019). At the southern Argentine margin four terraces (i.e. relatively flat surfaces) are present: Nágera Terrace at ∼500 m depth, the Perito Moreno Terrace at ∼1000 m depth, the Piedra Buena Terrace at ∼2500 m depth and the Valentin Feilberg Terrace at ∼3500 m depth (Hernández-Molina et al., 2009). The Nágera Terrace, the Perito Moreno and the Valentin Feilberg Terrace can be followed further to the north but in the northern part

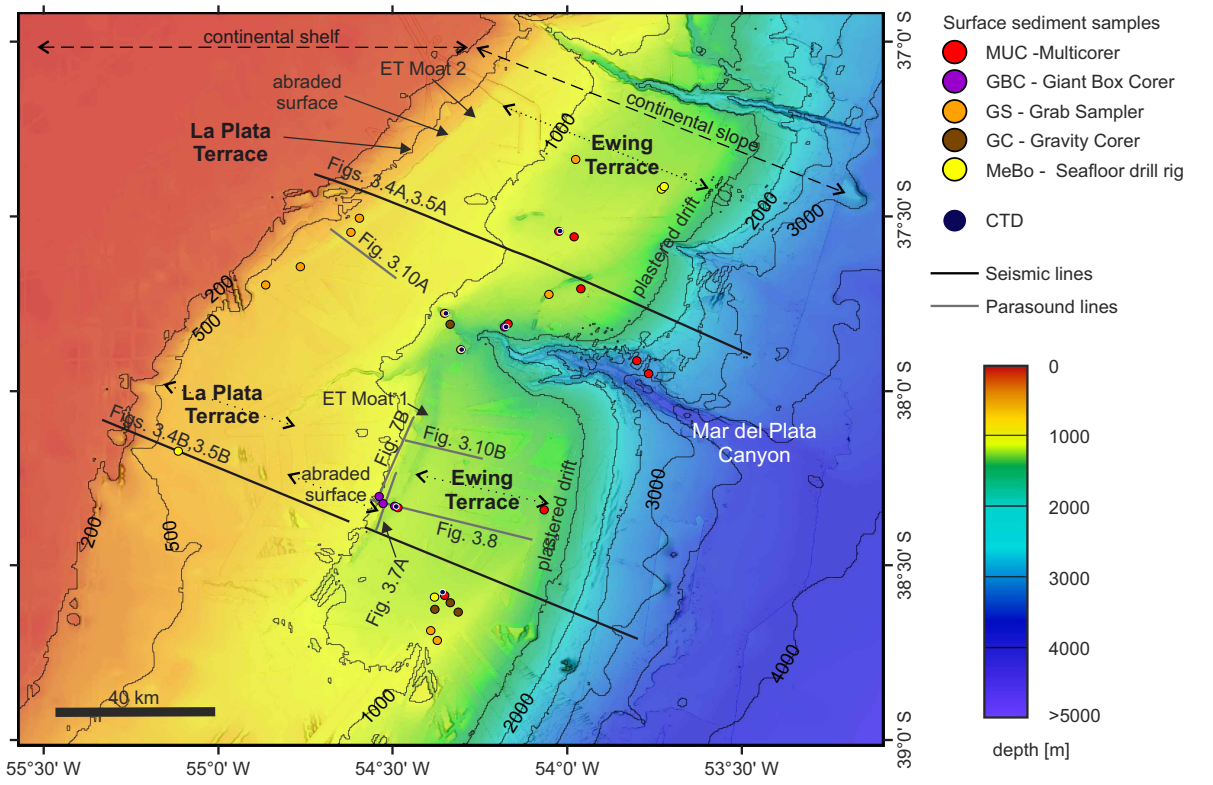

Figure 3.2: Bathymetric map of the study area showing the location of the main morphological and contouritic features, surface sediment samples, CTD stations, seismic and Parasound profiles. The first contour line at 200 m indicates the approximate location of the continental shelf break. The deeper contour lines are every 500 m. See Fig. 3.1 for location.

of the margin they are known as La Plata Terrace at ∼500 m depth, the Ewing Terrace at ∼1200 m depth and the Necochea Terrace at ∼3500 m depth (Urien and Ewing, 1974; Preu et al., 2013). Seismic data shows that the La Plata Terrace is much wider south of the MdP Canyon compared to the north (Preu et al., 2013). The La Plata Terrace is deeper (∼500 m) south of the MdP Canyon compared to the north where it is located at shallower depth (∼400 m) (Preu et al., 2013). Contourite terraces can show depositional and erosional features and often correspond to the landward upper part of plastered drifts (Hernández-Molina et al., 2016b; Thiéblemont et al., 2019; Miramontes et al., 2021). The Ewing Terrace is associated with plastered drifts at the basinward side, but at the La Plata Terrace no plastered drifts could be recognised (Hernández-Molina et al., 2009; Preu et al., 2013). Two channels where found in the landward side of the Ewing Terrace that were recently reclassified as moats due to the evidence of sedimentation and its association with a separated mounded drift (Fig. 3.2; Bozzano et al., 2011; 2021; Preu et al., 2012; 2013; Voigt et al., 2013; Steinmann et al., 2020). Steinmann et al. (2020) described the southern moat for the purpose of analysing cold-water corals in close proximity to this moat. In the moat, Steinmann et al. (2020) reported current speeds decreasing from south to north and oscillating between 3 and 52 cm/s. Bozzano et al. (2021) described

several morphological depressions hosting dropstones of an Antarctic Peninsula and Subantarctic islands origin.

The prominent MdP Canyon crosses the Ewing Terrace between 1000 and 4000 m water depth (Krastel et al., 2011). The canyon is disconnected from the continental shelf and it has been excluded that it ever had a direct connection (Krastel et al., 2011). Turbidity currents in the canyon were active from the Last Glacial Maximum to the late deglacial (Warratz et al., 2019). During sea-level highstands, most of the sediments from the Río de la Plata plume were transported northwards and did not directly reach the zone around the MdP Canyon (Razik et al., 2015a). The MdP Canyon acts in part as a sediment trap for sediments transported along the Ewing Terrace by bottom currents (Voigt et al., 2013; Warratz et al., 2019).

3.4 Materials and methods

3.4.1 Oceanographic dataset

Ocean current velocities were measured with a 38 kHz vessel-mounted Acoustic Doppler Current Profiler (VM-ADCP) during the R/V SONNE cruise SO260 in January–February 2018 (Kasten et al., 2019). These short-term measurements are used to understand small-scale oceanographic phenomena (e.g. eddies and local acceleration) and changes in bottom currents that can be linked to the underlying morphology. The 38 kHz VM-ADCP system was configured to operate in a long range narrow band mode with a 16 m depth cell which leads to a depth range of over 1000 m. The exact maximum range depends on the area. During SO260 the ADCP reached a maximum of 1600 m. Thus, in some areas, e.g. inside the MdP Canyon, no analysis of near-bottom currents is possible. The data were processed with the Cascade V7.2 software, using a horizontal grid cell size of 1 km and vertical grid cell size of 16 m. For analyses of the currents near the sea-surface, the average velocity between 50 and 150 m depth below sea surface was calculated. For analyses of the near-bottom current the average velocity between 150 and 200 m above seafloor was calculated. In the lower 150 m above the seafloor the data quality is too poor to be used with confidence (similar to Steinmann et al. (2020)). To check that the data quality between 150 and 200 m is good we also calculated the average between 150 and 350 m above the seafloor. Since the results are very similar and the interpretation does not change we will only show the data between 150 and 200 m above the seafloor. Furthermore, Steinmann et al. (2020) showed that the selection of this level is a reasonable approximation of bottom currents since, in this particular area, the vertical shear of the along-slope velocity between these depths is low.
The Conductivity, Temperature and Depth (CTD) data were acquired using a Sea-Bird 911 plus and were used to identify the different water masses in the study area at the

time of the R/V SONNE cruise SO260 (Fig. 3.1) (Kasten et al., 2019). Typically, the CTD profiles were collected down to 50 m above the ocean floor.

As the direct current observations are only useful to depict the circulation over a limited region at the time of the cruise, we use high-resolution ocean reanalysis to better understand the large-scale and long-term circulation. The Mercator Ocean reanalysis (GLORYS12) delivers daily mean values (temperature, salinity, currents, sea-ice, and sea level) over the period 1993–2017 as part of the Copernicus Marine Environment Monitoring Service (CMEMS, `http://marine.copernicus.eu/`) and assimilates satellite and *in situ* observations to present realistic circulation and water mass patterns (Lellouche et al., 2018). The model uses the ETOPO bathymetry (Fig. 3.15 of the supplementary material). The reanalysis in the study region was validated with direct observations including current measurements at depth (Artana et al., 2018). The resolution of the model is 1/12° in horizontal and it has 50 vertical levels with variable spacing. The vertical resolution is 1 m near the sea surface and increases downward to 450 m in the deepest layers. In the 450 and 1400 m water depth range, the model vertical resolution varies between 80 and 200 m.

3.4.2 Geological and geophysical dataset

Multibeam bathymetry was acquired during cruise SO260 in 2018 with a hull-mounted Kongsberg Simrad system EM122 operating at a nominal frequency of 12 kHz (swath opening angle across track up to 150°, the opening angle of each beam is 0.5°x1°, equidistant mode) (Kasten et al., 2019). Processing and gridding were carried out using the open-source software MB-Systems. This data set was used to construct a grid with a 25 m cell size for detailed analysis of two moats in the study area. A combined grid with a 100 m resolution was computed with MB-Systems (Fig. 3.2) using previously collected multibeam data acquired during R/V Meteor cruise M78/3 in 2009 (Kongsberg Simrad system EM120) and R/V Meteor cruise M49/2 in 2001 (Atlas Hydrosweep system DS2) for the analysis of the larger area. Data from the GEBCO grid (General Bathymetric Chart of the Oceans; GEBCO Compilation Group (2020); `https://www.gebco.net/`) at 15 arc-second intervals are used in areas where no multibeam bathymetry is available. The resulting bathymetric grid has been visualised with the open-source software QGIS (QGIS 3.12).

For detailed analyses of sub-bottom morpho-sedimentary features, we used sediment echosounder data collected with a hull-mounted narrow-beam parametric PARASOUND P70 system during cruise SO260 (Kasten et al., 2019). The PARASOUND system makes use of the parametric effect to produce a secondary low frequency based on two primary high frequencies (for details, see Grant and Schreiber, 1990)). For the analyses of the subseafloor, the secondary low frequency, which was set to 4 kHz, was used. This results in a vertical resolution of a few decimetres. A despike algorithm was applied to re-

move noise bursts from crosstalk with other sounding systems using the software package VISTA Desktop Seismic Data Processing Software (Schlumberger). To enhance reflector coherency, the envelope was calculated and visualised with 'The Kingdom Software' (IHS Markit).

The high-resolution multi-channel reflection seismic data set was acquired during R/V Meteor cruise M49/2 in 2001 (Spieß et al., 2002). The seismic data were previously processed and analysed in Preu et al. (2012) and Preu et al. (2013). In this study, the two longest available seismic profiles on both sides of the MdP Canyon were used for a joint interpretation of the seafloor sedimentary structures together with oceanographic results from model outputs. These profiles are the most representative ones because they cover the entire La Plata and Ewing Terraces and are perpendicular to the flow direction making it easier to understand the geology and oceanography together. Seismic profiles were acquired with an analogue streamer from the University of Bremen. The streamer has 96 channels over a length of 600 m. As an acoustic source, a 1.7 L GI-Gun (TMSODERA) with a main frequency of 100–500 Hz was used. This results in a vertical resolution of a few metres. The data set was processed with the software package 'VISTA Desktop Seismic Data Processing Software' (Schlumberger) following standard seismic procedures including bandpass filtering and common mid-point (CMP) binning. CMP bin size varies among profiles between 5 and 10 m depending on data quality and coverage. After the CMP stacking a residual static correction and finite-difference time migration was calculated (Preu et al., 2012; 2013). For interpretation of the data, the software package 'The Kingdom Software' (IHS Markit) was used.

Sediment samples were collected during the R/V SONNE cruise SO260 and the R/V Meteor cruise M78/3 using different sampling methods: giant box corer, multicorer, grab sampler, seafloor drill rig and gravity corer (Krastel and Wefer, 2012; Kasten et al., 2019). When available we used sediment samples that where derived with a multicorer or a giant box corer because it is most suitable for surface sediment sampling. Grain size analyses for particles between 0.04 and 2000 μm were performed on bulk sediment samples with a Beckman Coulter Laser LS 13320 at MARUM laboratories using Sodium hexametaphosphate as a dispersant. We also used grain size measurements from previous studies to get a better understanding of the overall sediment dynamics, which are available on PANGAEA (Frenz et al. (2003b) `https://doi.pangaea.de/10.1594/PANGAEA.95396`; and Razik et al. (2015b) `https://doi.pangaea.de/10.1594/PANGAEA.843433`).

3.4.3 Nomenclature

For classifying the different observed contouritic features, we follow the nomenclature of Faugères et al. (1999), Stow et al. (2002b) and Rebesco et al. (2014). Plastered drifts

are usually located on a gentle slope and are characterised by a broad, slightly mounded and convex geometry. They are associated with contourite terraces on the landward side, which are relatively flat surfaces (Miramontes et al., 2021). The limits of the contouritic terraces are marked by a significant increase in the slope gradient over a distance of several kilometres. In the seismic and Parasound data the limits are further identified as either an abraded/erosion surface or a transition to a plastered drift. Separated mounded drifts are more mounded than plastered drifts and often associated with steeper slopes, from which they are detached by a distinct erosional contourite channel or a non-depositional moat (Rebesco et al., 2014).

For the names of the different features in this region (e.g. terraces and canyons), we follow the widely accepted nomenclature of previous papers that described these structures to some extent (Urien and Ewing, 1974; Hernández-Molina et al., 2009; 2016b; Krastel et al., 2011; Preu et al., 2012; 2013; Voigt et al., 2016; Warratz et al., 2017; 2019). The southern moat in the study area was named Ewing Terrace Moat by Steinmann et al. (2020) and is here referred to as Ewing Terrace Moat 1 (ET Moat 1). As our study area extends further north and includes a second moat located north of the MdP Canyon that is also up-slope the Ewing Terrace, we named it Ewing Terrace Moat 2 (ET Moat 2). The ET Moat 2 was previously named La Plata Terrace Moat (Bozzano et al., 2021). Since this moat is disconnected from the La Plata Terrace by an erosional surface visible in seismic and Parasound data we find it more accurate to name it ET Moat 2. The term 'bottom current' is used in a general way for all currents related to oceanographic processes flowing near the seafloor and does not refer to any specific origin, flow direction or velocity (Rebesco and Camerlenghi, 2008).

3.5 Results

3.5.1 Modelled bottom currents

Simulated bottom currents averaged over 25 years show that the dominant flow direction is towards the N-NE (Figs. 3.3A and 3.4). The Malvinas Current affects most of the upper and middle slope down to depths of about 1600 m south of the MdP Canyon and about 1300 m north of the canyon (Figs. 3.3A and 3.5). Following the model, the Malvinas Current splits near the seafloor (SW part of study area) into three branches, here referred to as MC 1, MC 2 and MC 3 (Figs. 3.3A and 3.5). The strongest mean bottom currents in the study area, reaching up to 25 cm/s, are located at about 1000 m water depth in the zone where the Malvinas Current splits into three branches (Fig. 3.3A). MC 1 flows along the shelf edge and upper slope (at 200 m water depth), along the La Plata Terrace, with average near-bottom current speeds of 8 cm/s. MC 2 flows along the slope (abraded surface ∼700 m) between the La Plata Terrace and the Ewing Terrace with an average speed of 8 cm/s (Figs. 3.3A and 3.5). MC 1 and 2 remerge downstream

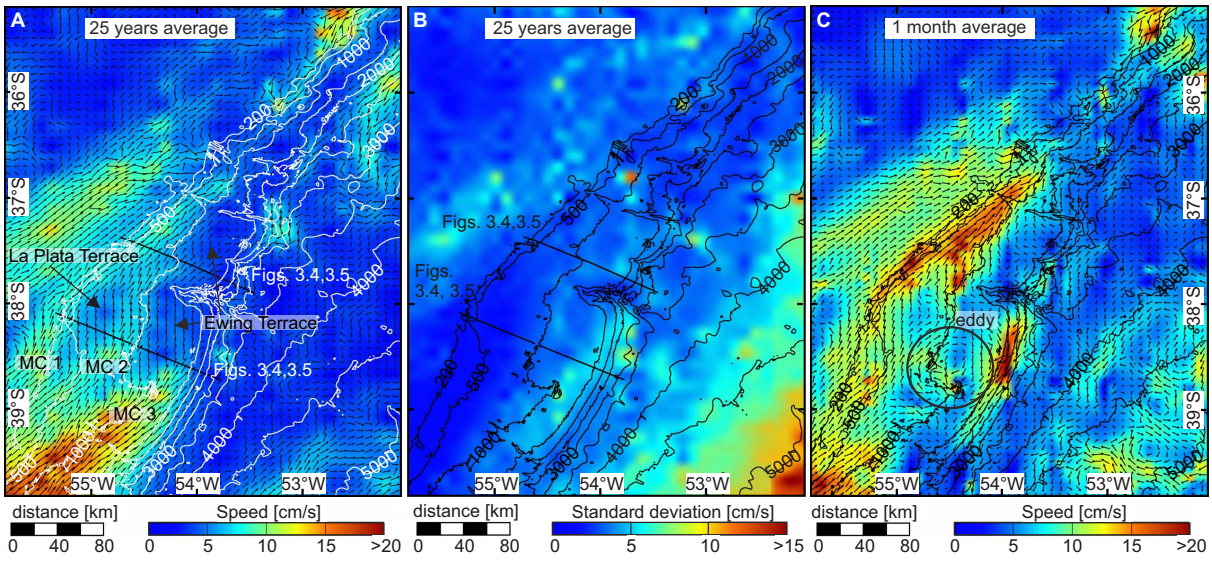

Figure 3.3: (A) Modelled mean bottom velocity over 25 years; (B) modelled standard deviation of the velocity $\sigma(=\sqrt{EKE})$ over 25 years; and (C) Modelled mean bottom velocity from 12/01/2012 to 14/02/2012. Note that the scale for the speed and the standard deviation is not the same. MC 1–3 refers to three branches of the Malvinas Current near the seafloor.

at the La Plata Terrace, west of MdP Canyon. These inner branches of the Malvinas Current (MC 1 + 2) flow in the NE direction to ∼36°S. North of this latitude bottom currents are mainly driven by the Brazil Current and flow south-eastwards at the shelf edge and upper slope (Fig. 3.3A). The deepest branch of the Malvinas Current (MC 3) flows northeastward along the Ewing Terrace (∼1200 m) and decreases in speed from 25 to 5 cm/s (over 60 km) as the terrace widens and the slope orientation changes to north-south (Fig. 3.3A). Even though the speed decreases, the mean near-bottom current at the middle slope (including Ewing Terrace) continues to flow northeastwards beyond 36°S (Fig. 3.3A). The two outer Malvinas Current branches, flowing over the abraded surface (MC2) and over the basinward limit of the Ewing Terrace (MC3), have their maximum mean northeastward velocity at about 500 and 1000 m water depth, respectively (Fig. 3.5).

The Malvinas Current carries different water masses in the study area, based on model potential density: the SASW from the surface down to ∼500 m water depth, the AAIW from ∼500 to ∼1100 m and the UCDW below ∼1100 m (Figs. 3.4 and 3.5). The shallowest branch of the Malvinas Current (MC 1) contains SASW, while the intermediate branch (MC 2) contains AAIW and the deepest branch (MC 3) is at the interface between the AAIW and the UCDW (Figs. 3.4 and 3.5). The interface between the AAIW and the UCDW is located at the Ewing Terrace (Fig. 3.4). On average all water masses (SASW and AAIW) over the La Plata Terrace flow towards the N-NE until ∼36°S (Fig. 3.4). Similarly, the mean bottom currents at the Ewing Terrace also flow towards the N-NE (Figs. 3.3A and 3.4). In the study area the influence of the Brazil Current, which

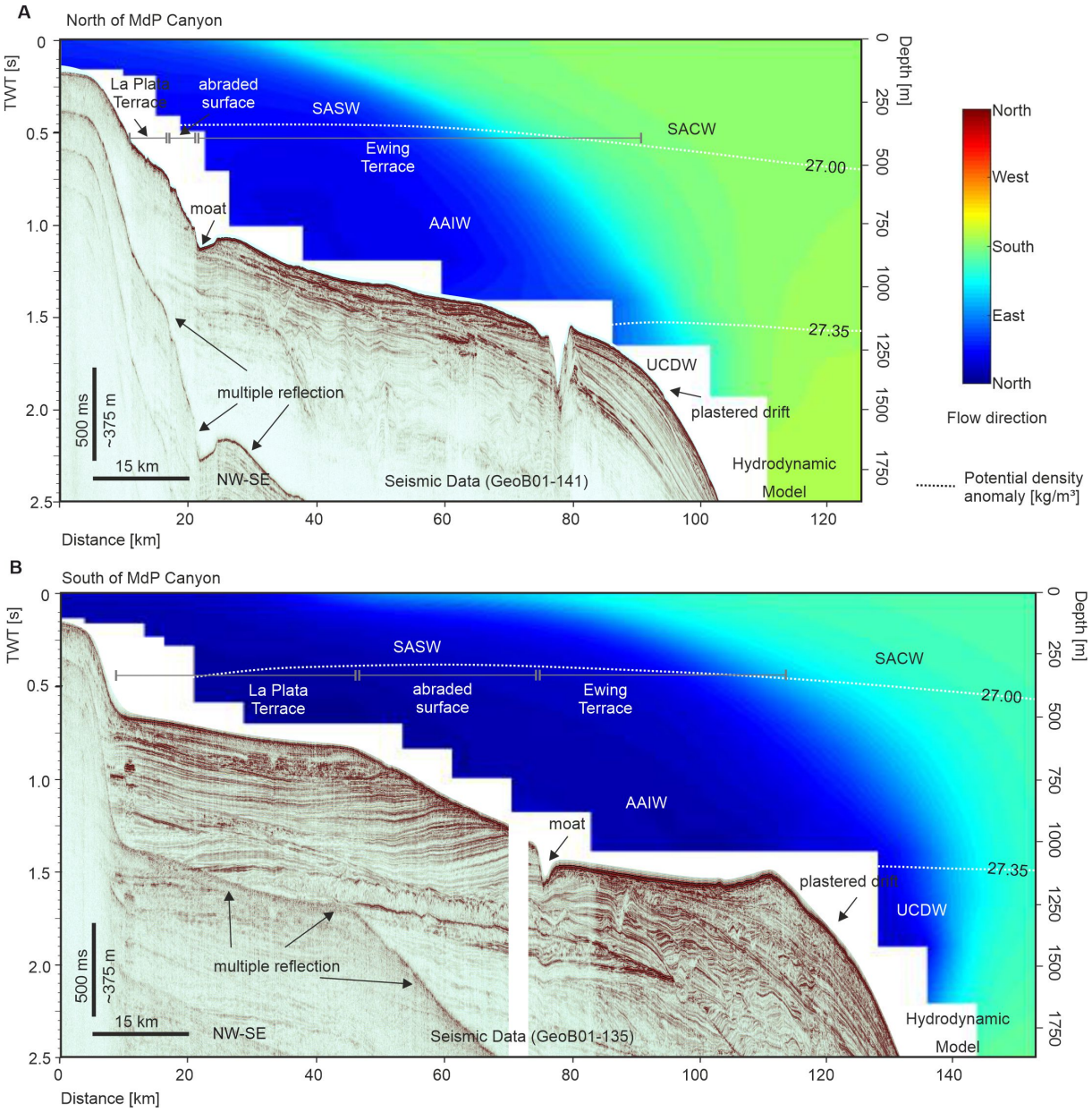

Figure 3.4: Cross-sections of the hydrodynamic model showing the 25-year mean flow direction in combination with seismic sections. The white dashed lines indicate the interface of water masses calculated based on the potential density anomaly (SASW: Subantarctic Surface Water, SACW: South Atlantic Central Water, AAIW: Antarctic Intermediate Water, UCDW: Upper Circumpolar Deep Water). The location of the cross-sections is shown in Fig. 3.2. (A) Seismic section GeoB01–141 located north of MdP Canyon and (B) GeoB01–135 located south of MdP Canyon (modified from Preu et al., 2012; 2013).

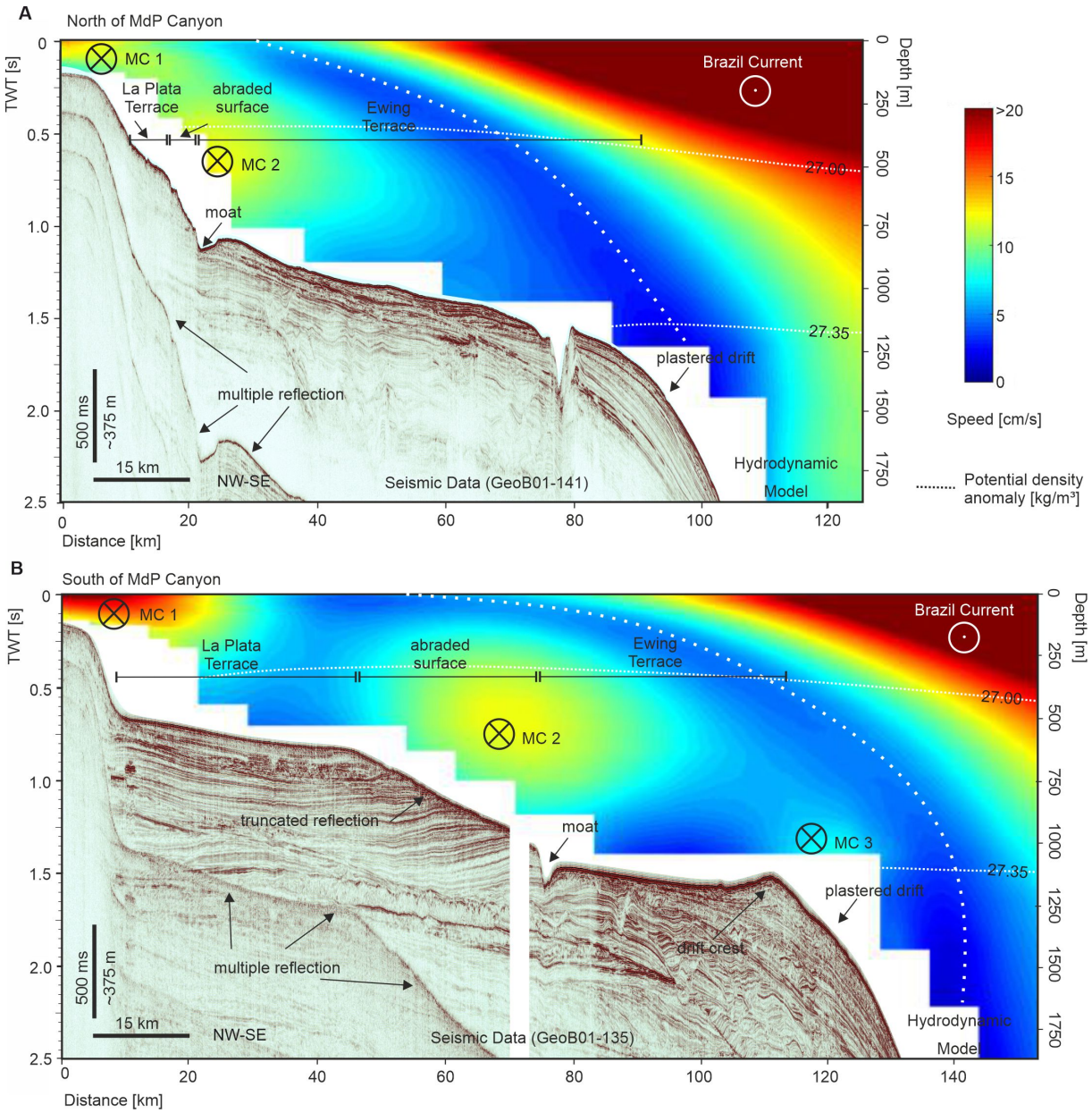

Figure 3.5: Cross-sections of the hydrodynamic model showing the 25-year mean speed in combination with seismic sections. The white dashed line indicates the border between southward and northward-flowing currents (see Fig. 3.4). The location of the cross-sections is shown in Fig. 3.2. (A) Seismic section GeoB01–141 located north of MdP Canyon and (B) GeoB01–135 located south of MdP Canyon (modified from Preu et al., 2012; 2013).

Table 3.1: Average mean near-bottom current speed for different areas: the Ewing Terrace south and north of the MdP Canyon, the slope connecting the La Plata Terrace with the Ewing Terrace (abraded surface) and the moats south and north of the MdP Canyon (ET Moat 1 and 2).

	Mean speed: ADCP measurement [cm/s]	**Standard deviation: ADCP measurement [cm/s]**
Ewing Terrace South	15	13
Ewing Terrace North	11	7
Abraded surface	23	12
ET Moat 1 (south)	28	11
ET Moat 2 (north)	29	17

flows towards the S-SE, is only noticeable close to the sea surface in the region above the Ewing Terrace (Fig. 3.4). The MdP Canyon influences the bottom current flow direction, leading to redirection of N-NE flowing water to the NE (Fig. 3.3A).

The standard deviation of modelled bottom currents over 25 years reaches 16 cm/s over the abyssal plain below 4000 m water depth and is lower over the shelf edge and continental slope, where it is mostly lower than 5 cm/s (Fig. 3.3B). The variability in flow speed on the La Plata Terrace is lower than 5 cm/s. In contrast, the variability in flow speed over the Ewing Terrace is up to 10 cm/s, being highest on the offshore part of the terrace near the MdP Canyon (Fig. 3.3A). High bottom-current variability in this part of the Ewing Terrace is related to changes in current direction and speed. Bottom currents modelled over 1 month (January–February 2012) indicate that the deep branch of the Malvinas Current does not extend north of 39°S. During that time the Ewing Terrace, and especially the offshore part at 1500–2000 m water depth, is affected by southward-flowing bottom currents that exceed 35 cm/s. In contrast, bottom currents over the La Plata Terrace show a similar pattern during January–February 2012 compared the 25-year average, although bottom current speeds are considerably higher during this short period of time, reaching 20 cm/s north of the MdP Canyon (Fig. 3.3C).

3.5.2 Direct current observations

The VM-ADCP data close to the sea surface show generally a strong (>40 cm/s) northward current in the region over the abraded surface between the La Plata Terrace and the Ewing Terrace south of the MdP Canyon, corresponding to the Malvinas Current (Fig. 3.6A). In the region above the deeper part of the MdP Canyon surface currents are strong

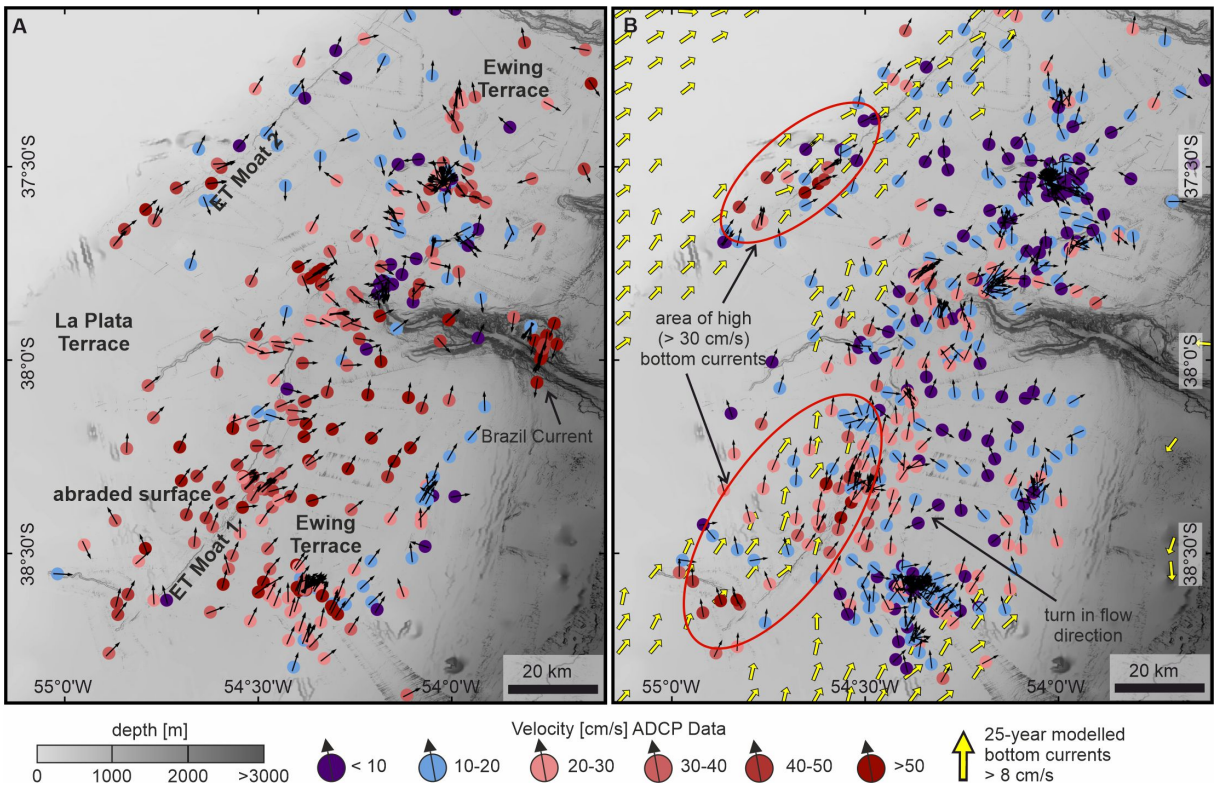

Figure 3.6: (A) Near-surface velocities from ADCP data average between 50 and 150 m below sea surface. (B) Near-bottom velocities from ADCP data average between 150 and 200 m above the seafloor. Yellow arrows indicate the modelled mean bottom current velocity over 8 cm/s.

(>50 cm/s) and flow in a southward direction, corresponding to the Brazil Current. Over the Ewing Terrace north of the MdP Canyon, the velocity is generally lower and the flow direction is more variable compared to the region south of the MdP Canyon because it corresponds to the confluence zone between the Malvinas and Brazil currents (Fig. 3.6A). Generally, near-bottom currents are lower than surface currents (Fig. 3.6A,B). Similar to the reanalysis, stronger near-bottom currents are measured at the abraded surface and slower currents over the contourite terraces (Fig. 3.6B). The speed over the Ewing Terrace south of the MdP Canyon is higher (15 cm/s) than north of the MdP Canyon (11 cm/s) (Table 3.1). The average speed over the abraded surface is 23 cm/s. Inside ET Moat 1 and ET Moat 2 bottom currents are even higher, reaching average speeds of 28 and 29 cm/s (Table 3.1). In all three locations, the velocity decreases northeastwards (Fig. 3.6B). The average measured near-bottom current over the moats is very similar but the standard deviation at ET Moat 2 is higher than at ET Moat 1 (Table 3.1). The velocity at the SW part of ET Moat 2 is higher than at the SW part of ET Moat 1. The velocity decreases faster in the northward direction along ET Moat 2 than it does along ET Moat 1 (Fig. 3.6B).

Over ET Moat 1 the velocity is higher close to the bottom (800–1000 m) than at mid-

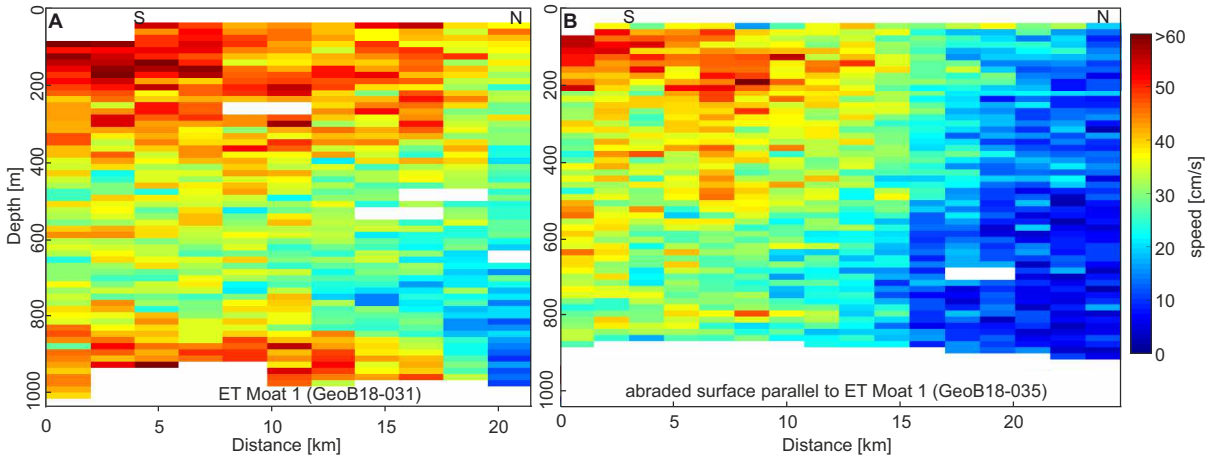

Figure 3.7: (A) ADCP cross-section showing the speed over and parallel to ET Moat 1 and (B) ADCP cross-section parallel to the slope connecting the La Plata Terrace with the Ewing Terrace. The sections are parallel to each other. See Fig. 3.2 for location.

depth (400–800 m) (Fig. 3.7A). In contrast, currents above the abraded surface generally decrease with increasing depth (Fig. 3.7B). The profile perpendicular to the ET Moat 1 confirms that the higher velocity at depth is only a local feature over the moat and does not affect the entire water column (Fig. 3.7A). Furthermore, this profile shows lower velocities over the Ewing Terrace (Fig. 3.8A). The near-bottom flow at 7–15 km distance along the profile turns 180° and thus flows southward. This flow reversal occurs only close to the seafloor and does not reach the sea surface (Fig. 3.8B). In this turn, the speed increases and reaches locally up to 20 cm/s near the seafloor (Fig. 3.8A).

3.5.3 Seafloor morphology and sediment architecture

The upper and middle slope of the northern Argentine continental margin are characterised by the presence of two contourite terraces separated by an abraded surface that shows truncated parallel reflections (Figs. 3.2 and 3.4; see also Preu et al., 2012, Preu et al., 2013). The deeper contourite terrace (Ewing Terrace) is associated with a plastered drift in basinward direction (Figs. 3.2 and 3.4). The La Plata Terrace is the shallowest contourite terrace. South of the MdP Canyon, it is located at 500–600 m water depth, has a width of ∼40 km and an average slope of 0.3°. North of the MdP Canyon the width of the La Plata Terrace decreases drastically (Fig. 3.5A). The abraded dipping basinward surface that separates both terraces has a width of 25 km, an average slope of 0.7° (Fig. 3.5B). The characteristics of the Ewing Terrace change north and south of the MdP Canyon. South of the MdP Canyon, it is located at 1000–1400 m, between the abraded surface and the plastered drift. The terrace deepens towards the MdP Canyon. It is ∼40 km wide and has a convex morphology due to the presence of a mounded deposit

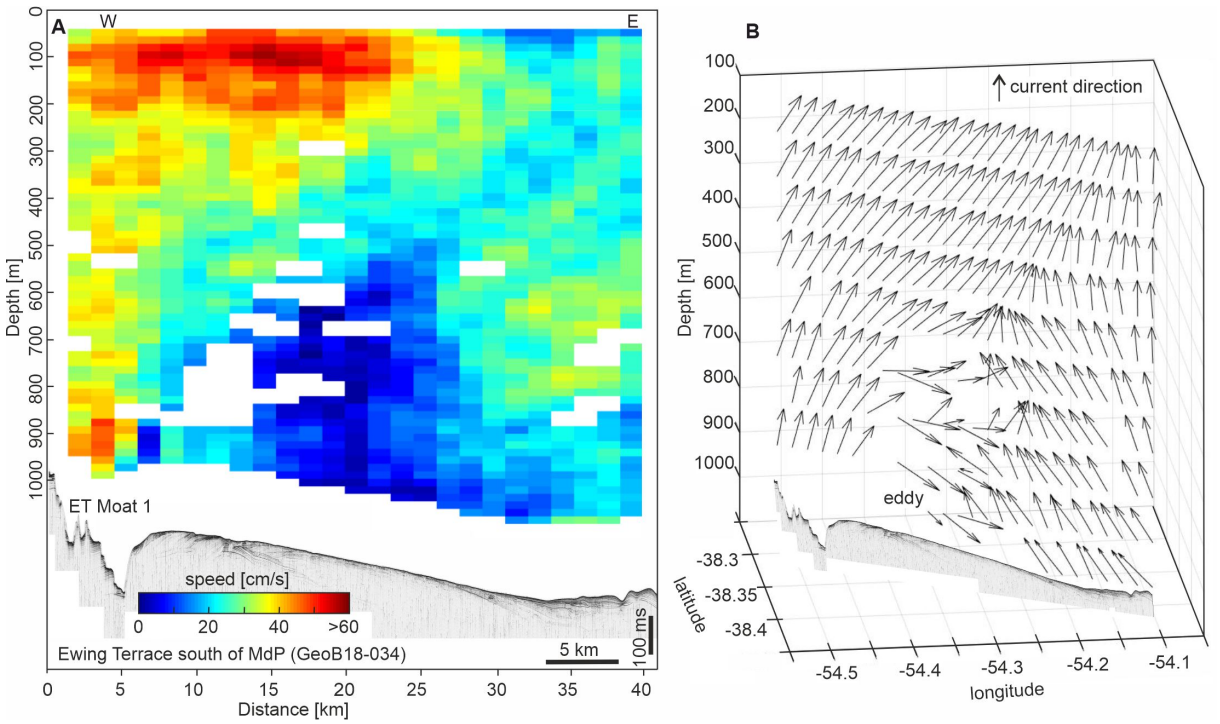

Figure 3.8: (A) ADCP cross-section showing the speed across the southern Ewing Terrace in combination with Parasound data. Note that ADCP data and Parasound data are not in the same vertical scale. (B) ADCP cross-section showing the current flow direction with arrows. An average mean velocity over 50 m is shown every 100 m below the sea surface. See Fig. 3.2 for location.

Table 3.2: Key parameters of ET Moat 1 (south of MdP Canyon) and ET Moat 2 (north of MdP Canyon).

	ET Moat 1	**ET Moat 2**
Length (SW-NE direction)	95 km	70 km
Max. width (NW-SE direction)	7 km	6 km
Water depth	1000 - 1300 m	700 - 850 m
Max. depth relative to basinward mounded drift	100 m (deeper in NE)	90 m (deeper in SW)

on top of the plastered drift that creates a topographic high (drift crest). North of the MdP Canyon, the Ewing Terrace is located at 800–1400 m between the abraded surface landwards and the plastered drifts basinwards (Fig. 3.5A). It is ∼70 km wide and has an average slope of 0.4°. The limit of the Ewing Terrace, is marked by an increase in slope, from 0.4° to >1° (Fig. 3.5).

Two moats and parallel separated mounded drifts are located at the landward side of the Ewing Terrace (Fig. 3.9). ET Moat 1 is located in a much deeper water depth (∼1150 m) than ET Moat 2 (∼775 m). Even though the moats are located in different water depths, they show several similarities regarding length (95 km in ET Moat 1 and 70 km in ET Moat 2), max. width (7 km in ET Moat 1 and 6 km in ET Moat 2 m) and max. depth relative to the basinward mounded drift (100 m in ET Moat 1 and 90 m in ET Moat 2)

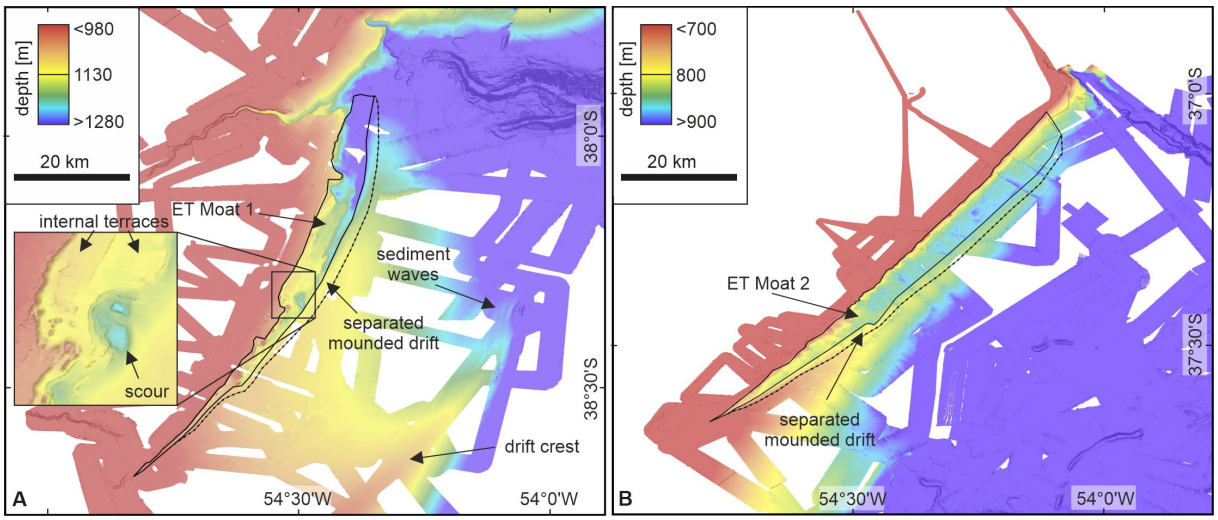

Figure 3.9: Bathymetric map of the Ewing Terrace showing the main small-scale features: moats, separated mounded drifts, sediment waves and drift crest (A) south and (B) north of the MdP Canyon.

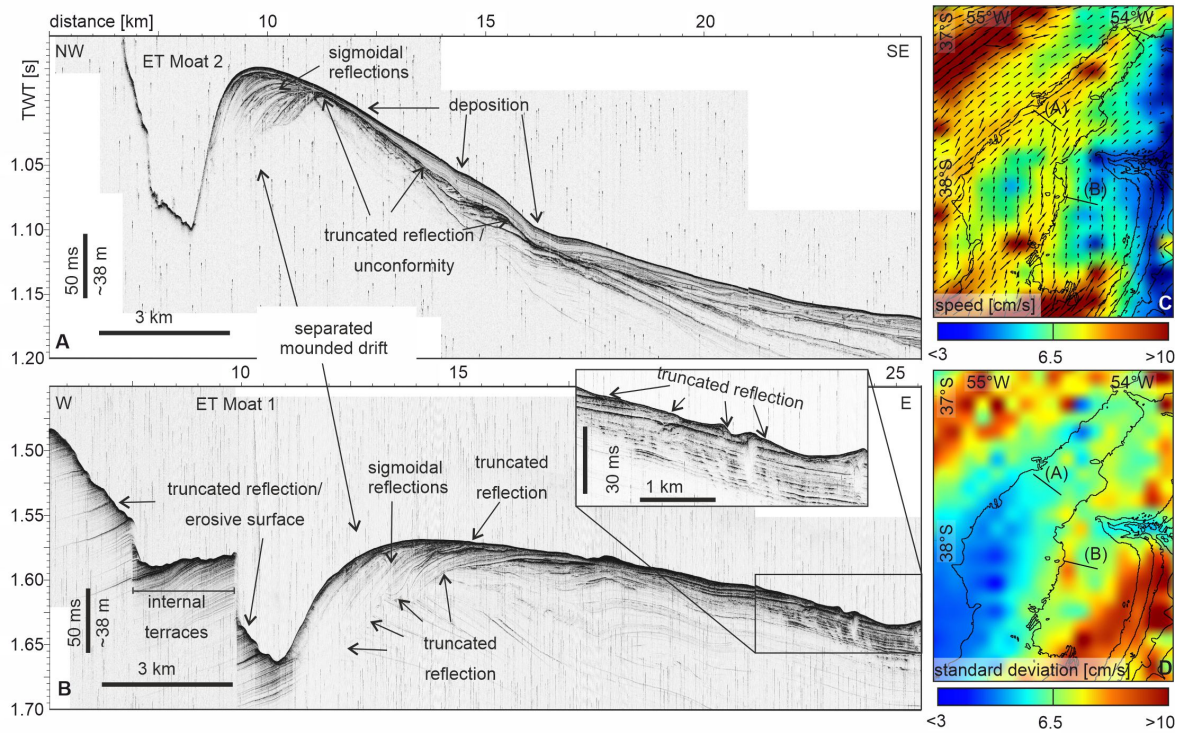

Figure 3.10: Parasound data showing (A) Ewing Terrace Moat 2 north of MdP Canyon and (B) Ewing Terrace Moat 1 south of MdP Canyon. See Fig. 3.10D for location. (C) Mean speed and (D) standard deviation of modelled bottom currents.

(Table 3.2). Both moats widen towards the N-NE. ET Moat 2 progressively widens, while ET Moat 1 shows an abrupt widening in its central zone towards the abraded surface (Fig. 3.9). The water depth increases in the same direction. Internal terraces and scours, at the edge where the moat suddenly widens are only visible inside ET Moat 1 (Figs. 3.9A and 3.10B). In the landward slope and in the deepest point of ET Moat 1 (south of

the MdP Canyon), truncated parallel reflections are visible in the Parasound data (Fig. 3.10B). In contrast, in ET Moat 2 (north of the MdP Canyon) and on its landward slope, Parasound penetration is very limited, and no reflections are recognised (Fig. 3.10A). Separated mounded drifts are identified associated with the moats and are located basinwards. These contourite drifts become thicker towards the N-NE (Figs. 3.9 and 3.10). The mounded drift related to ET Moat 1 shows continuous reflections with a sigmoidal to oblique, landward progradation pattern (Fig. 3.10B). The base of the separated mounded drifts is characterised by a widespread erosive surface. Truncations inside the separated mounded drift are abundant, suggesting frequent phases of erosion and drift construction. Adjacent to ET Moat 2 the reflections are continuous with a sigmoidal, landward progradation pattern (Fig. 3.10A). The sigmoidal reflections terminate at the basinward side at one point. The base of the separated mounded drifts is not imaged. Further basinward of the contourite drift, a thin unit with continuous, wavy, parallel basinward dipping reflections of low amplitudes is deposited on top of an erosional surface (Fig. 3.10A). Below this unconformity, the deposits are characterised by discontinuous reflections with variable amplitudes and basinwards there are transparent units. The reflections are also generally seaward dipping but towards the erosional reflection the dip angel is reduced. On the Ewing Terrace south of the MdP Canyon continuous reflections are imaged, sometimes interrupted by small erosional surfaces close to the seafloor (Fig. 3.10B).

Sediment waves are found at the seaward edge of the Ewing Terrace south of the MdP Canyon (Fig. 3.9A). The crests of the sediment waves are oriented parallel to the slope and migrate basinwards (up-slope of the above described drift crest that is located on top of the plastered drift). Towards the north, the drift crest becomes less distinct until the seafloor is more horizontal (Fig. 3.11A,B). The reflections of the sediment waves have good lateral continuity. The apparent sediment waves length and height decrease from south (∼2.2 km wide and ∼20 m high (Fig. 3.11C)) to north (∼1.1 km wide and ∼10 m high (Fig. 3.11A)). They are located on top of an unconformity (Fig. 3.11A,B). The reflectivity below the sediment waves is generally low. In the south the reflections below the sediment waves also show wavy structures, whereas towards the north they are generally dipping towards the basin.

3.5.4 Surface sediment samples

The grain size of surface sediments generally decreases northwards and basinwards. All analysed samples on the contourite terraces (excluding the moats) can be divided in three regions with similar sediment grain size: La Plata Terrace, Ewing Terrace south of the MdP Canyon and Ewing Terrace north of the MdP Canyon. The analyses show that the median grain size is coarsest on the Ewing Terrace south of the MdP Canyon (average median grain size of 103.2 μm), less coarse on the La Plata Terrace (average median grain

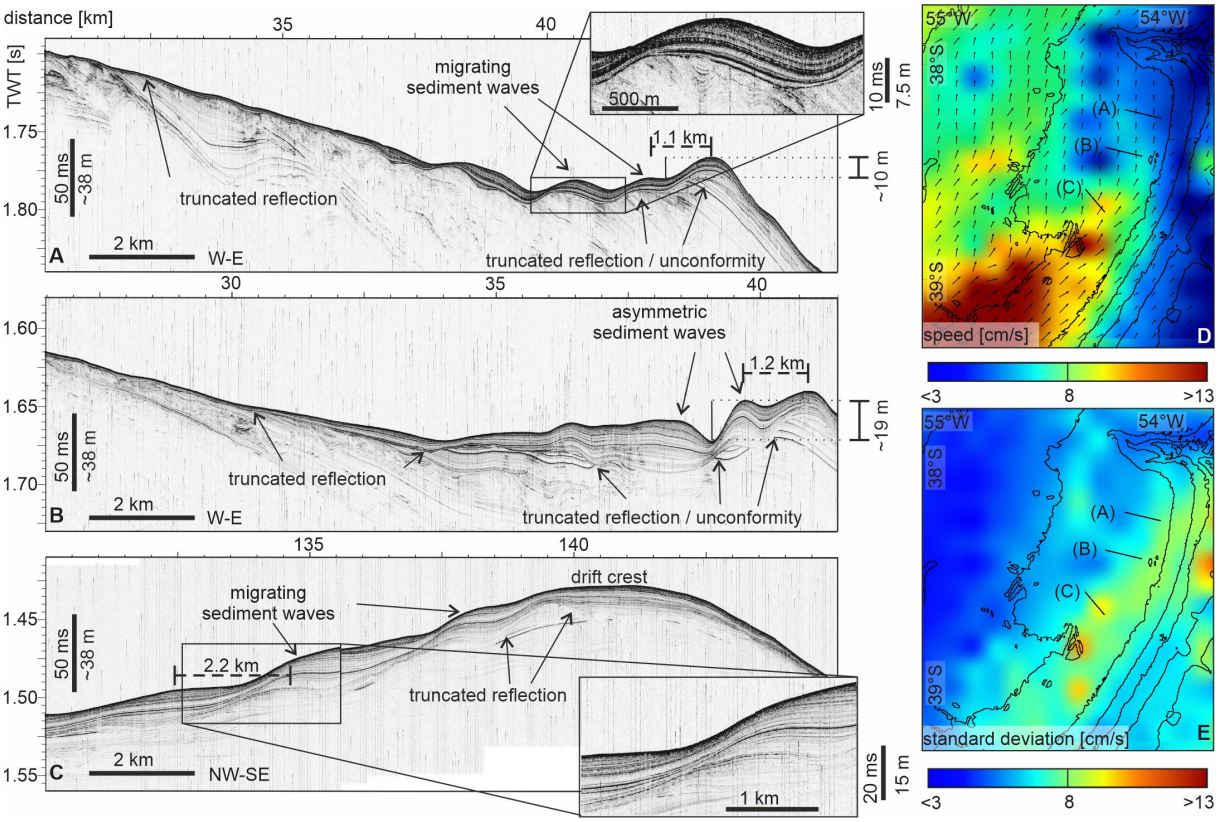

Figure 3.11: (A)(B)(C) Parasound data showing S-SE edge of southern Erwin Terrace (south of MdP Canyon). See Fig. 3.11E for location. (D) Mean speed and (E) standard deviation of modelled bottom currents.

size of 78 μm) and finest on the Ewing Terrace north of the MdP Canyon (average median grain size of 60.1 μm; Fig. 3.12A).

On the Ewing Terrace south of the MdP Canyon, the grain size distribution typically shows only one mode at 106 μm, and is poorly sorted with a standard deviation of 3.45 μm (Fig. 3.12B). In contrast, north of the MdP Canyon, the grain size distribution is typically bimodal with a main mode at 88 μm and a secondary mode at 20 μm, and it is poorly sorted with a standard deviation of 3.64 μm. The grain size distribution on the La Plata Terrace is also bimodal with a main mode at 106 μm and a second mode at 27 μm, and it is poorly sorted with a standard deviation of 3.67 μm. Sediment grain size in the moats is coarser then on the terraces and can reach median values of 173 μm, but its variability is very high (Fig. 3.12C). Sediment sample GeoB22712-3 (inside ET Moat 1), GeoB22732-1 (inside ET Moat 2) and GeoB22718-1 (inside MdP Canyon head area) also contain gravels and cobbles with sizes up to 10 cm (see Bozzano et al., 2021 for details). Several sediment samples are bioturbated and contain cold-water coral branches or fragments (Table 3.3, Fig. 3.16 of the supplementary material). Surface sediments on the small terrace inside the MdP Canyon and in the basin are much finer, with median grain sizes below 63 μm and percentages of sand below 60% (Fig. 3.12A).

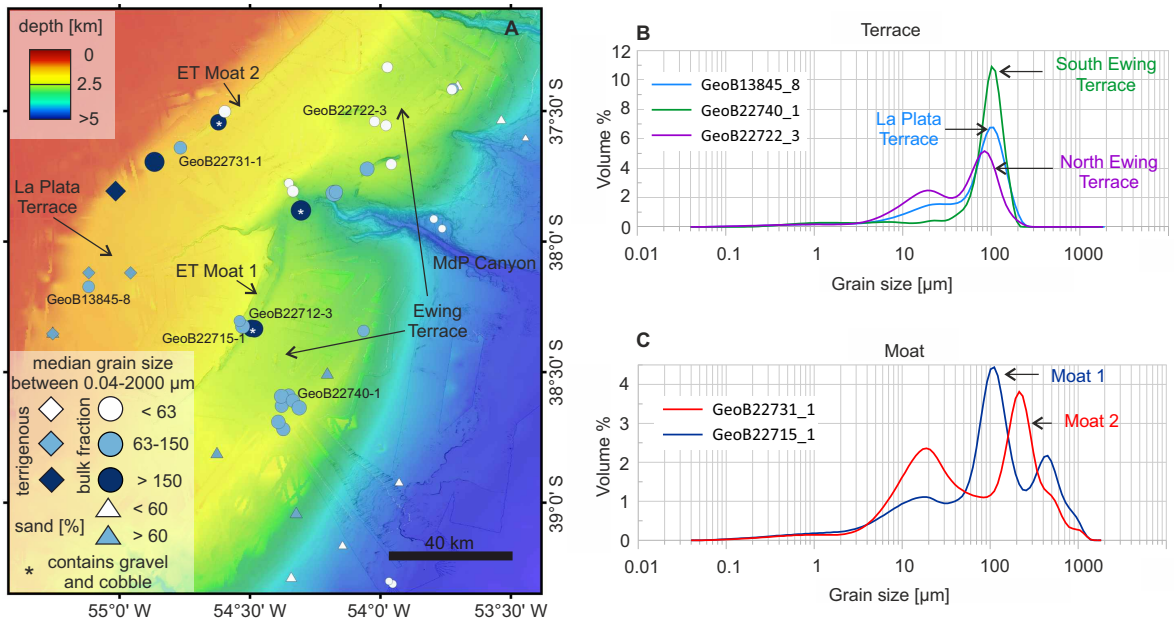

Figure 3.12: (A) Median grain size of all the bulk sediment samples collected in this study (circles), median grain size of the terrigenous fraction (diamonds, Razik et al., 2015a, Razik et al., 2015b) and percentage of sand of the bulk surface sediment (triangles, Frenz et al., 2003a, Frenz et al., 2003b). (B) Grain size distribution of three samples located on the contourite terraces. (C) Grain size distribution of two samples located inside of the two moats.

3.6 Discussion

3.6.1 Bottom current dynamics over the CDS

The Brazil-Malvinas Confluence Zone is a very dynamic area (Fig. 3.1), where southward flowing water from the Brazil Current encounters northward flowing water from the Malvinas Current (Piola et al., 2018; Artana et al., 2019; Piola and Matano, 2019). Current velocity measurements can resolve local intensification of speed from the current and small eddies. This is very important for linking oceanographic processes with sedimentary features. However, they lack large-scale coverage and continuity over long periods of time, which is especially important in a highly variable area like the confluence zone. This gap can be filled by numerical modelling that allows us to extend our observations in space and time, and can thus improve the understanding of long-term mean currents and short-term variability. This is especially important to drive sediment patterns (here the CDS) in geological time scales. The reanalysis covers a period of 25 years, however, contourites are developed over several thousands or millions of years. Still, the model is useful for understanding current dynamics since the modern ocean circulation and stratification pattern was already established during the Middle Miocene (Preu et al., 2012). Even though the ocean circulation has changed to some extent in terms of strength or position since the Middle Miocene, the patterns and processes that form the CDS are thought to have remained similar.

In the present study, we focus our analysis on the near-bottom currents and discuss the differences between currents near the seafloor and at the sea surface in the confluence zone. Former numerical simulations indicate that at the sea surface in the confluence zone, the Malvinas Current splits into two branches: the outer branch veers offshore and flows with the Brazil Current, while the inner branch subducts below the Brazil Current (Provost et al., 1995; Artana et al., 2019). Comparison of previous model results (Artana et al., 2019) with our model results (Fig. 3.3) show that on average the Brazil-Malvinas Confluence Zone between the northward flowing and the southward flowing currents is located further south near the surface. Our model results show additionally that the Malvinas Current at 39°S near the seafloor further splits into three branches that flow along the contourite terraces and over the abraded surface located between the terraces, respectively. Direct measurements at 40–41°S indicate that the mean Malvinas Current has an equivalent barotropic structure (Vivier and Provost, 1999). This usually indicates more homogeneous velocities throughout the water column. Thus, the described changes in velocity within the Malvinas Current might be connected to the interaction of the Malvinas Current with the Brazil Current at the confluence and to the interaction with the seafloor morphology.

Accelerated near bottom currents are important for deep-sea coral reefs because they need energetic currents to transport food particles and to inhibit burial (Roberts et al., 2006; Muñoz et al., 2012). Thus, corals are also an indicator of intense currents. Deep-sea coral reefs off Uruguay (Carranza et al., 2012) are in an energetic environment related to the Brazil Current (Franco-Fraguas et al., 2014). Cold water corals at the Argentine margin have been recognised in ET Moat 1 and on the abraded surface (Steinmann et al., 2020) and ET Moat 2 (Table 3.3 of the supplementary material) that are both controlled by high energetic cores of the Malvinas Current (Fig. 3.6B). The Malvinas Current carries different water masses (Fig. 3.4). Preu et al. (2013) identified different water masses at the seafloor based on all available historical hydrographic data. The extent of the NADW interaction with the seafloor based on the previous observations derived by Preu et al. (2013) is in good agreement with the southward near-bottom flow determined by the long-term average circulation derived from the ocean reanalysis (Fig. 3.13), suggesting that the model depicts a realistic near-bottom circulation.

The VM-ADCP measurements show similar flow patterns as the 25-year averaged model result, but generally the measured speed is higher (Figs. 3.3 and 3.6), which might be expected since it displays instantaneous measurements, in contrast the model shows the mean velocity. Artana et al. (2019) showed that especially the surface velocity variability in this zone is very high. Thus, the differences in speed probably reflect the strong flow variability in the confluence zone. The 1-month simulation result (12/01/2012 to

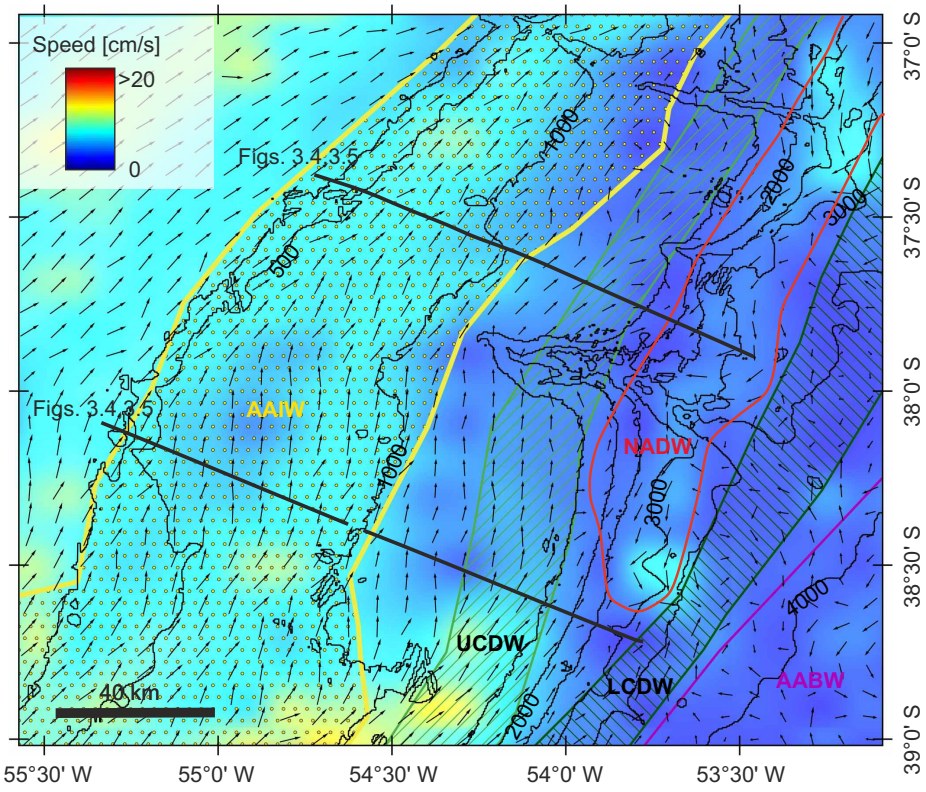

Figure 3.13: Modelled bottom current velocity (over 25 years) together with an illustration of the water masses (identified from CTD data) at the seafloor (adapted from Preu et al. 2013).

14/02/2012) also shows higher bottom current velocity than the 25-year averaged model result (Fig. 3.3). It highlights the variability not only in current speed but also in current direction.

3.6.2 Formation of sedimentary features

Sediment dynamics

Generally, for a constant seafloor depth a decrease in near-bottom current speed is observed from south to north in both modelled and measured currents (Figs. 3.3 and 3.6). This agrees well with the northward decrease in sediment grain size of surface sediments (Fig. 3.12). Erosional surfaces and coarse grain size are generally an indication for strong bottom currents, whereas fine grain size is rather a sign for weak bottom currents. In order to better understand whether the observed and modelled near-bottom currents would be capable of eroding and transporting sediment, we calculated the bottom shear stress ($\tau = \rho u_*^2$, with seawater density ρ and friction velocity u_*) from VM-ADCP measurements. Observed bottom shear stresses reach critical shear stresses (0.13 -0.17 N/m^2) for the observed sediment grain sizes (60-130 µm; according to critical shield parameter for motion initiation proposed by Soulsby and Whitehouse (1997)) along the slope between the La Plata Terrace and the Ewing Terrace, as well as along the moats (Fig. 3.6). This

shear stress corresponds to current velocities at 150 m above the seafloor over 30 cm/s, assuming a logarithmic relation between the friction velocity and the variation of velocity with height, a von Kármán constant equal to 0.4 and bottom roughness length equal to 0.0035 m (Schlichting, 1962). This prediction of sediment erosion based on the bottom shear stress agrees with the erosion visible in the Parasound data at the abraded surface between the La Plata Terrace and the Ewing Terrace as well as along the moats (Figs. 3.4, 3.5 and 3.10).

Some contouritic features are commonly related to mean flow velocity (Stow et al., 2009; Rebesco et al., 2014) or the corresponding mean bottom shear stress (Schlichting, 1962; Soulsby and Whitehouse, 1997). But for further understanding sediment dynamics, not only the mean velocity is relevant but also the flow variability and secondary (smaller scale) processes (e.g. eddies) that can increase bottom shear stress on the seafloor and control contouritic processes (Thran et al., 2018; Chen et al., 2019). On the Ewing Terrace south of the MdP Canyon, we observed erosional surfaces in the Parasound data even though the mean speed is low here (Fig. 3.10B). Internal acceleration due to a sloping morphology can lead to flow instabilities and finally to generation of waves and eddies (Rebesco et al., 2014; Zhang et al., 2016). This phenomenon possibly occurs at the Ewing Terrace south of the MdP Canyon that is tilted slightly towards the NE (Fig. 3.2). Furthermore, in this area the terrace width increases and thus the contour current has more space to flow over the flat terrace (Fig. 3.2). This divergence of isobaths may cause a decrease in the mean flow and also lead to the development of flow instabilities. We propose that this widening leads sometimes to turbulences and eddies at the seafloor, similar to water flowing out of a channel or a river mouth (Falcini and Jerolmack, 2010). This is also reflected by a slightly enhanced flow variability on the Ewing Terrace compared to the La Plata Terrace (Fig. 3.3B). Furthermore, as previously described, during times when the Malvinas Current is relatively weak, the flow direction over the Ewing Terrace can turn towards the south at the basinwards edge (Fig. 3.3C). On the other hand, one branch of the Malvinas Current (MC 2) flows northward along the abraded surface (landwards of the Ewing Terrace). The opposite flow direction makes the occurrence of clockwise rotating eddies likely. VM-ADCP measurements and the hydrodynamic modelling results averaged over one month confirm the presence of a cyclonic eddy on the Ewing Terrace (Figs. 3.3C and 3.8B). This suggest that these eddies can lead to local erosion because shear stress can be much higher in turbulent flow compared to laminar flow (Fig. 3.14; Schlichting and Gersten, 2016; Yin et al., 2019). However, this change in flow direction was not observed at all ADCP profiles and is not apparent in the model derived 25-year average bottom currents at the Ewing Terrace. Thus, these eddies may be transient features and there are energetic periods during which the sediment is eroded, alternating with calm periods during which sediment deposition is favoured. The non-

permanent character of the eddy is probably related to the large hydrodynamic changes in the confluence zone. This variability in bottom currents may also explain that the modern seafloor on the Ewing Terrace is patchy in terms of erosion and deposition (Fig. 3.11). These new observations refine our understanding of the sediment dynamics in the vicinity of the MdP Canyon. The depositional system located further south of this study area at ∼45°S might be different because of a more stable Malvinas Current with its main branch being located over the terrace (Piola et al., 2013).

Moats and separated mounded drifts

Moats and paleo-moats and the related separated mounded drifts are commonly used to reconstruct bottom currents because they provide a clear indication for strong bottom currents and their direction (Surlyk and Lykke-Andersen, 2007; Betzler et al., 2013). To make these reconstructions more reliable, it is necessary to study the geomorphology of active moats together with the characteristics of the flow regime. At the landward edge of the Ewing Terrace, two up-slope migrating moats are located, each with an associated separated mounded drift (Fig. 3.10). The morphology of the observed separated mounded drifts is not typical for a drift associated with a moat (Faugères et al., 1999; Stow et al., 2002a; Rebesco et al., 2014). Unlike here, typically, the units between the reflections become thinner leading to almost parallel, uniform reflections at the basinward side of the drift (Faugères et al., 1999; Stow et al., 2002a; Betzler et al., 2013; Rebesco et al., 2014). However, the drifts observed here clearly terminate just a few kilometres basinward of the moats. The unusual depositional character is possibly connected to the vigorous bottom currents and the intensification of near-bottom currents that was measured above ET Moat 1 (Fig. 3.7A). This makes it an erosive and very sandy and even gravelly moat, and a silty-sandy separated mounded drift (Bozzano et al., 2011), while separated mounded drifts related to moats are typically mud dominated (Rebesco et al., 2014; Miramontes et al., 2016). The initiation for developing a moat might be connected to local eddies, as discussed earlier. However, it is not clear yet how the development of moats initially starts and further investigation is needed. Possibly, turbulence and small eddies occurring in the moats leading to erosion, but these cannot be resolved by the present model because of the limited resolution. A detailed understanding of flow patterns inside the moat, will require very high-resolution numerical modelling of bottom currents and/or extensive (mooring-based) ADCP measurements to confirm the modelling results.

The available ADCP data show that bottom currents over the moat increase locally (Fig. 3.8). Along- and across-slope ADCP sections confirm that this increase in flow velocity is restricted to the near-bottom currents over the moat (Fig. 3.7). Thus, after the moat started to form, it affected the bottom currents, probably focusing bottom currents and leading to an increase in velocity. Current speed standard deviation in ET Moat 2 is

almost twice as high as in ET Moat 1 which could be due to a stronger decrease of speed in ET Moat 2. Taking velocity fluctuations in turbulent flow into account (Inman, 1949), this may explain why the sediment is less sorted. When a moat abruptly widens (like ET Moat 1), bottom currents interact with the edge of the slope possibly leading to the formation of vortices and eddies (Fig. 3.9). These eddies may have formed the observed scour inside the moat (Fig. 3.9A). This process of cutting back of the slope can be an important factor responsible for widening the contourite terrace (Preu et al., 2013). Furthermore, the ADCP data also show that as the moats widen northwards, the flow velocity decreases (Figs. 3.6 and 3.7). This has implications for the along-slope sediment transport. Sediment transported in close proximity to ET Moat 1 by the MC2 current branch can be deposited at the MdP Canyon head (see Section 5.3).

Drift crest

The modelled bottom currents averaged over 25 years show that the flow variability over the La Plata Terrace is lower than over the Ewing Terrace. The highest flow variability is at the basinward edge of the Ewing Terrace south of the MdP Canyon where MC3 drastically decreases in speed (from 25 to 5 cm over 60 km) (Figs. 3.3B, 3.5B and 3.11E). The maximum northward extent of MC3 fluctuates and is possibly dependent on the strength of the Malvinas Current, which can explain the higher variability in speed compared to the rest of the Ewing Terrace (Fig. 3.3B). In this area a drift crest or morphologic high developed on the upper part of the plastered drift (Figs. 3.9A, 3.11A and 3.14), possibly as a result of a weakening bottom current with reduced sediment transport capacity, allowing deposition. The decrease in bottom current speed towards the north may also inhibit the transport of coarse sediment, favouring its deposition and forming the observed drift crest, which is mainly composed of sand, with a median grain size of 103 μm.

Sediment waves

The drift crest on the basinward edge of the Ewing Terrace is partly covered by several sediment waves that migrate basinwards up-slope on the drift crest (Fig. 3.1). Sediment waves can be formed by downslope flowing turbidity currents and along-slope flowing bottom currents (McCave, 2017). The sediment waves discussed here are not associated with any downslope submarine channel and they are thus not formed by turbidity currents. Consequently they are contouritic sediment waves and part of the CDS. Flood (1988) proposed that the lee-wave mechanism can form sediment waves under bottom currents. Lee-waves can develop within a bottom current that flows over a wavy topography (Flood, 1988), but the sediment waves initiation process is not well understood. In agreement with this theory, the sediment waves discussed here are located at the lee side of the above-described drift crest. This drift crest could possibly lead to the development of

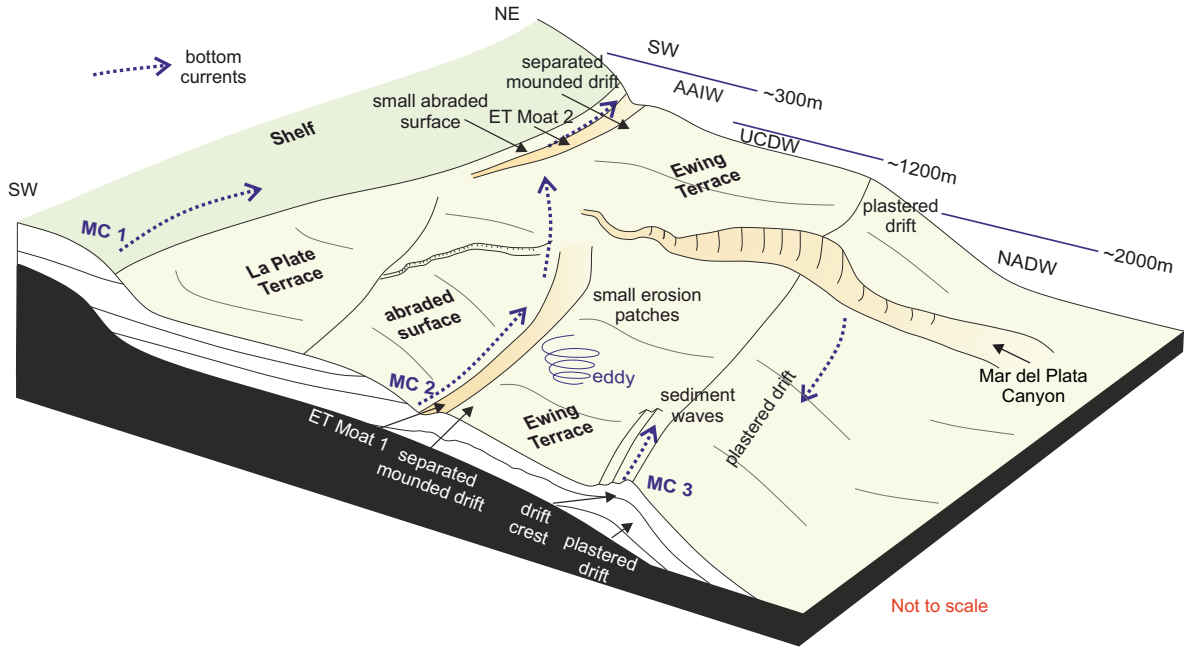

Figure 3.14: Conceptual model of the main bottom currents and associated contouritic features in the study area. The approximate water mass interfaces in this region are indicated (after Preu et al., 2013; Kasten et al., 2019; Piola and Matano, 2019). MC: Malvinas Current, SW: Surface Water, AAIW: Antarctic Intermediate Water, UCDW: Upper Circumpolar Deep Water, NADW: North Atlantic Deep Water.

the lee-waves. Flood (1988) assumed that the sediment waves are perpendicular to the current direction. However, further theoretical analyses taking the Coriolis force into account indicate that sediment waves under bottom currents can be oblique to the flow direction (Blumsack and Weatherly, 1989; Hopfauf and Spieß, 2001). Oblique sediment waves have been observed at several places (McCave, 2017). In this study we report on sediment waves that are parallel to the direction of currents (Figs. 3.9 and 3.11). This parallel orientation to the flow direction seems unlikely to be explained by lee-waves alone. Thus, other processes have to be taken into consideration. Previous research reported that internal waves can form sediment waves and dunes (Hand, 1974; Reeder et al., 2011; Droghei et al., 2016; Ribó et al., 2016; Reiche et al., 2018; Yin et al., 2019; Miramontes et al., 2020a). Internal waves can propagate at density discontinuities and have been previously proposed as a cause for the development of the Ewing Terrace and the La Plata Terrace (Hernández-Molina et al., 2009; Preu et al., 2013). The suggested mechanism is that the internal waves can propagate at the interface of AAIW, UCDW and NADW, respectively. The sediment waves discussed here are located slightly below the interface between the AAIW and the UCDW (Fig. 3.14). Internal waves with an amplitude of up to 250 m have been reported in deep-sea environments (Van Haren and Gostiaux, 2011). Possibly, part of the energy from the internal wave propagating at the

interface of AAIW/UCDW interacts with the northward bottom flow which influences the deposition of sediment waves. The formation of these sediment waves was initiated several thousands of years ago likely during times when the Malvinas Current was stronger, for example during glacial times (e.g. Voigt et al., 2013). Due to high bottom-currents, part of the top from the plastered drift was eroded forming part of the unconformity on which the sediment waves formed (Fig. 3.11A). In the south, sediment waves might have been already deposited below the unconformity but are not clearly visible because they are partly eroded. Their large variability in reflectivity could be related to the large glacial and interglacial changes in flow strength (e.g. Voigt et al., 2013). However, the processes leading to the formation of sediment waves are still not well understood.

Terrace formation

The initiation of the contouritic terraces formation was suggested by some authors to be related to internal waves propagating at water mass interfaces (Hernández-Molina et al., 2009, Hernández-Molina et al., 2016b; Preu et al., 2013; Ercilla et al., 2016; Yin et al., 2019; Llave et al., 2020). Other authors proposed that internal waves may be secondary processes that can form channels and dune fields on contourite terraces, but are not responsible for the original formation of the contourite terrace, which they argued is probably related to strong along-slope currents (Miramontes et al., 2019; 2020a). The model derived 25-year average bottom currents and the near-bottom water mass distribution derived from CTD measurements confirm that the contouritic terraces in the northern Argentine margin (Figs. 3.4 and 3.13) are roughly located at water-mass interfaces (Hernández-Molina et al., 2009; Preu et al., 2013). However, the modelled bottom currents averaged over 25 years indicate that the La Plata Terrace is not located at the interface of water masses carried by the Brazil Current and AAIW as suggested by Preu et al., 2013, but at the interface of SASW and AAIW (Fig. 3.4).
It has also been suggested that contourite terraces in the Mediterranean Sea are located in zones of relatively high geostrophic bottom currents, while plastered drifts are located in the adjacent zone of less intense bottom currents (Miramontes et al., 2019). Vigorous currents are observed and modelled only in the inner (landward) part of the contourite terraces, while the central and external (basinward) parts are affected by weaker bottom currents, although with a higher variability at the external (basinward) edge of the terrace (Figs. 3.3, 3.5 and 3.6). Modelled and observed bottom currents are the weakest over the plastered drifts (Figs. 3.3, 3.5 and 3.6). This current regime is also reflected in the general sediment stratigraphy of the Ewing Terrace (Preu et al., 2012). The landward part, where high currents are present, shows more evidence of erosion. As the flow weakens towards the basinward side, more deposition is possible and large plastered drifts form. On top of this general stratigraphy, secondary deposits like separated mounded drifts,

drift crests and sediment waves were deposited as discussed before. We suggest that contourite terraces may have been initiated by erosion on the slope generated by the action of two water masses and their interphase trough time, being the (paleo) Malvinas Current one of the key factors that progressively cut the slope landwards, widening the contourite terrace with time. The fact that the Argentine contourite terraces are much wider and flatter than other terraces observed for instance in the Mediterranean Sea (Ercilla et al., 2016; Miramontes et al., 2019), along the Mozambican margin (Thiéblemont et al., 2019; Miramontes et al., 2020a) and in the Makassar Strait (Brackenridge et al., 2020) could be related to the higher speed of near-bottom currents as part of the Malvinas Current and the long time period of erosion (since the opening of the Drake Passage). The particular flat morphology with an abrupt edge of the terraces along the Argentine margin may favour the formation of internal waves at the terrace edge, similar to those observed at the shelf break (Jackson et al., 2012), that could also favour sediment transport and erosion along the terrace. These processes are however expected to be weaker than on upper slopes and at the shelf break because of the weaker density gradient (Fig. 3.1B). Up to date, no internal waves could be directly identified near the seafloor in the study area. Magalhaes and da Silva (2017) analysed internal waves along the Malvinas Current with multispectral satellite imagery and found that most of the internal waves are located south of the study area in areas of submarine canyons. These internal waves propagate upstream of the Malvinas Current (Magalhaes and da Silva, 2017) and are thus not perpendicular to the slope. New *in situ* measurements close to the sea floor and modelling studies are necessary to determine the role of internal waves in the formation and the evolution of contourite terraces.

3.6.3 Sediment origin and submarine transport

The continental shelf and upper-middle slope of the northern Argentine margin are mainly dominated by sandy sediments (Fig. 3.12; Razik et al., 2015a and references therein). Loessoidal sands eroded from cliffs are one of the main sources for sandy deposits on the shelf, they are retransported by the Patagonian Current flowing northwards and are in part deposited on the outer shelf and upper slope offshore the Río de la Plata estuary (Gaiero et al., 2003; Razik et al., 2015a). Even though the aeolian dust supply from South America to the south Atlantic Ocean is very significant (Gaiero et al., 2003, Gaiero et al., 2007), aeolian dust (5-20 μm) is mainly deposited in the deep part of the Argentine Basin (Sachs and Ellwood, 1988). In several morphological depressions gravel to cobble sized rocks are found (Fig.3.12) and it was proposed that they have been transported by sea ice from the Antarctic Peninsula and Subantarctic islands (Bozzano et al., 2021). The primary origin of sediment deposits in the study area (upper and middle slope in the northern Argentine margin) was linked to a mountainous origin and igneous source rock lithology from the Andes, transported by the Colorado and Negro Rivers to the

ocean (Razik et al., 2015a; Bozzano et al., 2011). In the modern system sediment from the rivers is mainly deposited at their deltas (Gaiero et al., 2003). However, during sea-level lowstands sediment from the Patagonian rivers reached directly the continental slope (e.g. Zárate and Blasi, 1993). The sediment is then transported northward by along-slope bottom currents (Malvinas Current) and is finally deposited in the study area forming the observed contourite depositional system. The sediment derived from the Río de La Plata is at present mainly transported northwards by longshore currents and does not reach our study area (Razik et al., 2015a). Occasionally, when the Brazil Current is very strong (Fig. 3.3C), sediment may also enter the study area from the north. However, the area is primarily controlled by the northward flowing along-slope bottom currents and shows generally a northward grain size fining due to the decreasing current speed. This trend continues beyond the study area on the Uruguayan margin (Franco-Fraguas et al., 2014). Part of the sediment transported northwards along the Ewing Terrace may reach the head of the MdP Canyon. The general decrease in northward bottom current speed towards the MdP Canyon (Figs. 3.3 and 3.7) would favour the accumulation of sediments at the canyon head that could be transported down canyon by turbidity currents, in a similar way as longshore currents feeding shelf-incised submarine canyons like the Monterrey Canyon (Paull et al., 2005) and the Cap Breton Canyon (Mazières et al., 2014). Voigt et al. (2013) and Warratz et al. (2019) reported the absence of turbidites during the Holocene and the presence of turbidites during deglacial and glacial periods, which have the same composition as the sediments from the Ewing Terrace (Warratz et al., 2019). This was previously linked to variability in the nepheloid layer depending on the current strength (Voigt et al., 2013; 2016; Warratz et al., 2019). Since sandy sediment is transported mainly as bedload under the observed and modelled bottom-current velocities and is not part of the nepheloid layer, we propose that sediment transport associated with high velocity along-slope bottom current jets (here MC2) plays an important role in the sediment input to the MdP Canyon head and is then transported downslope by turbidity currents. The presence of only one major tributary to the MdP Canyon (Fig. 3.2; Krastel et al., 2011) and missing slope failure structures at the canyon walls (Warratz et al., 2019) also indicates a sediment input coming from the canyon head rather than from the southern lateral side of the canyon.

Some previous studies focused more on the variability of the latitude of the confluence zone and on the reconstruction of the strength of the Malvinas Current based on geological, geophysical data and oceanographic data (Lumpkin and Garzoli, 2011; Preu et al., 2012; 2013; Voigt et al., 2013; 2016; Razik et al., 2015a; Artana et al., 2018; 2021b). It is important to consider that the mean latitude of the confluence zone is not the same at the sea surface and near the seafloor (Fig. 3.6). The reanalyses from Artana et al. (2021b) showed that the strength of the Malvinas Current has not changed over the period of 1993–2017. The location of the confluence zone is a result of the strengths of Brazil

Current and Malvinas Current. Even though the strength of the Malvinas Current does not change (Artana et al., 2021a), a southward shift of the mean confluence zone of 0.6 to 0.9° per decade was observed in recent times (1992–2007) (Lumpkin and Garzoli, 2011). Thus, the shift in the confluence might be more controlled by the Brazil Current. This southward trend of the confluence zone is expected to continue with the present global warming due to anthropogenic climate change (de Souza et al., 2019). This shift could possibly threaten the cold-water coral ecosystem on the Ewing Terrace (Hebbeln et al., 2016; Steinmann et al., 2020) and other benthic and pelagic species (Franco et al., 2020). The frequency of turbidity currents in the MdP Canyon is linked to the strength of the Malvinas Current. After the last glacial maximum, when the climate became generally warmer and sea level rose, the Malvinas Current became weaker on average (Preu et al., 2013; Voigt et al., 2013; Warratz et al., 2019). These weaker currents can only transport finer sediment and thus probably transported less sediment into the study area leading to a lower sedimentation rate and fewer turbidites in the MdP Canyon (Voigt et al., 2013; 2016; Warratz et al., 2019). The described onset of sediment wave deposition on the Ewing Terrace possibly started in this less energetic environment (Fig. 3.11).

3.7 Conclusions

This study represents a step forward in understanding the sediment dynamics in proximity to the Mar del Plata (MdP) submarine Canyon at the northern Argentine margin by combining geophysical and sedimentological datasets (multibeam bathymetry, seismo-acoustic data and sediment cores) with oceanographic datasets and modelling (vessel-mounted ADCP measurements, CTD data and an ocean reanalysis). Overall, this study contributes to a better understanding of the formation of contourite depositional systems and can help future reconstructions of past ocean conditions based on sedimentary structures. The main conclusions can be summarized as follows:

- Measured and modelled current data show that in close proximity to the MdP Canyon the Malvinas Current dominates the sediment dynamics at the seafloor. We propose that sediment transport associated with high-velocity along-slope near-bottom current jets plays an important role in supplying sediments to the MdP Canyon head similarly to longshore currents feeding shelf-incised submarine canyons. The moat of the Ewing Terrace is possibly also a pathway for sediment transport to the MdP Canyon head.
- ADCP measurements together with the 25-year reanalysis of ocean currents show a northward velocity decrease of the northward-flowing waters. This decrease in speed leads to less erosion and the accumulation of finer sediment deposits north of the MdP Canyon, as observed in the surface sediment samples.

- Modelling results indicate that near the seafloor the Malvinas Current splits into 3 branches (at ∼39°S). The shallowest branch (MC1) flows along the upper slope of the La Plata Terrace and continues flowing below the Brazil Current reaching ∼36° S. MC2 flows along the abraded surface connecting the La Plata and Ewing Terrace. The offshore branch (MC3) flows at the basinward edge of the Ewing Terrace and drastically decreases in speed south of the MdP Canyon.
- The decrease in speed of branch MC3 reduces sediment transport capacity, which therefore allows deposition along its path and possibly leads to the formation of the observed drift crest. Downstream (northward) of the drift crest sediment waves with a parallel orientation to the flow direction are deposited.
- Instantaneous measured and modelled mean near-bottom currents are strong (up to 63 cm/s at 150–200 m above the seafloor) where abraded surfaces and moats are present, and weak (lower than 30 cm/s) on the La Plata Terrace and the Ewing Terrace. The strong bottom currents generate the moats located at the landward slope of the Ewing Terrace that are very sandy and even gravelly. In the moats, an intensification in flow velocity was measured and an up-slope migration observed. We suggest that contourite terraces may have been initiated by the action of two water masses and their interphase trough time, being the erosion on the slope generated by the (paleo) Malvinas Current that would progressively cut the slope landwards, widening the contourite terrace with time.
- The divergence of isobaths at the terraces possibly explains the measured and modelled weaker near-bottom currents on the La Plata Terrace and the Ewing Terrace. Together with the sloping morphology of the Ewing Terrace this can lead to flow instabilities near the seafloor. We suggest that this effect leads to local cyclonic eddies near the seafloor, which have also been measured and modelled. We propose that these eddies are transient and can cause local erosion only during energetic periods. The alternation between sediment deposition and erosion may also explain the absence of a clear large-scale erosional surface and the presence of several small erosional surfaces at the Ewing Terrace.

3.8 Data availability

The ADCP data, surface grain size analyses, Parasound Data and Seismic Data used in this article are available at PANGAEA database (Wilckens et al. (2021) `https://doi.org/10.1594/PANGAEA.931130`). Modelled data is freely available from the Copernicus Marine Environment Monitoring Service (CMEMS, `http://marine.copernicus.eu/`).

3.9 Acknowledgements

We thank the captains, crews and onboard scientific teams for their support during R/V SONNE cruise SO260 in 2018, R/V Meteor cruise M78/3 in 2009 and R/V Meteor cruise

M49/2 in 2001. We appreciate the help of K. Zonneveld and K.-H. Baumann for processing the CTD data during the SO260 cruise. We thank Brit Kockisch for her support during the collection and analysis of sediment samples. For funding of the cruise SO260 we acknowledge the DFG Research Centre/Cluster of Excellence 'The Ocean in the Earth System' (MARUM - Center for Marine Environmental Sciences at the University of Bremen). For additional funding we thank the Helmholtz Association (Alfred Wegener Institute Helmholtz Centre for Polar and Marine Research, Bremerhaven). The sediment sample material was provided by the GeoB Core Repository at the MARUM - Center for Marine Environmental Sciences, University of Bremen, Germany. The project was funded by the University of Bremen and supported by the GLOMAR - Bremen International Graduate School for Marine Sciences. This work has been done in collaboration with "The Drifters Research Group" at Royal Holloway University of London (RHUL). We thank the two anonymous reviewers and the guest editor A. Wåhlin for their comments that greatly improved our manuscript.

3.10 Supplementary material

For the analyses of model bottom currents, the underlying bathymetry plays a vital part because the currents interact with the seafloor morphology. There are generally no major differences between the ETOPO Bathymetry used for the Model (Fig. 3.15A) and the GEBCO Bathymetry combined with the 100-m grid measured with a Multibeam Echosounder (MBES) used for the geomorphological analysis (Fig. 3.15B). The comparison of the isobaths calculated from the different grids shows generally the same structure. On the shelf, both grids are similar, and in the study area (450 to 1400 m water depth), the differences are only minor. Because of the lower resolution of the ETOPO grid, the steep slopes cannot be resolved with the same details and the canyons are slightly wider (Fig. 3.15C).

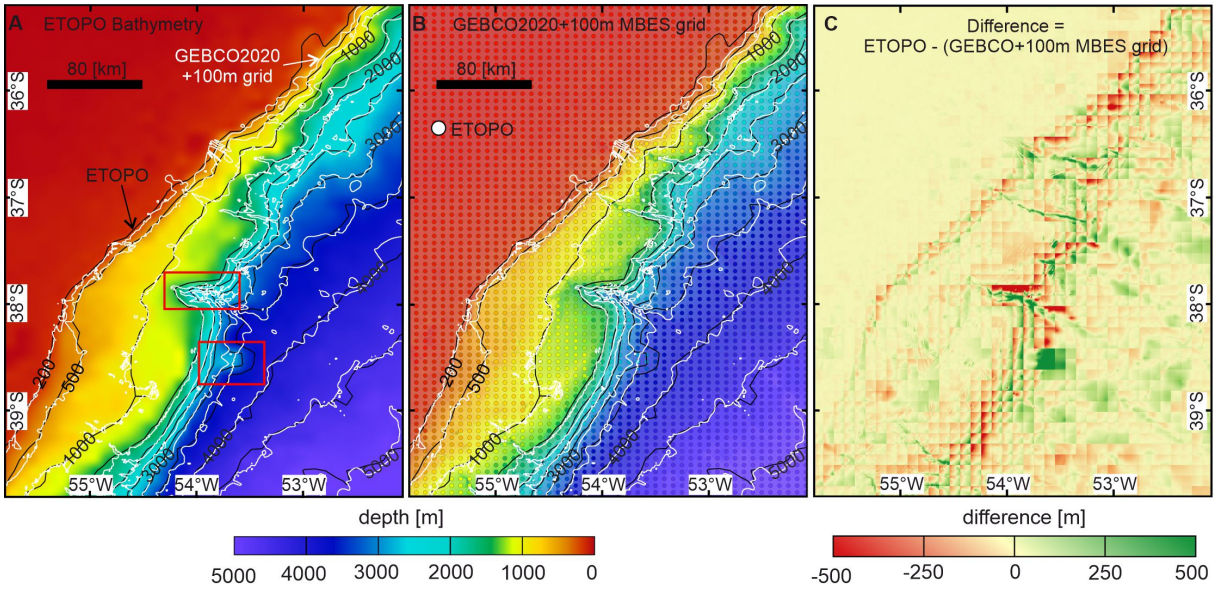

Figure 3.15: (A) ETOPO Bathymetry used for the Model. The red boxes indicate differences between isobaths calculated from ETOPO Bathymetry and of GEBCO Bathymetry combined with the 100-m grid measured with a Multibeam Echosounder (MBES). (B) Comparison between the GEBCO Bathymetry combined with the 100 m grid and ETOPO Bathymetry (coloured dots). (C) Difference between the ETOPO Bathymetry and the GEBCO Bathymetry combined with the 100-m grid.

Table 3.3: List and description of surface sediment samples used in this study: Multicorer (MUC), Giant Box Corer (GBC), Grab Sampler (GS), Gravity Corer (GC) and Sea floor drill rig (MeBo).

GeoB #	**Long**	**Lat**	**Device**	**Sediment description**
GeoB13868-1	-53.72	-37.41	MeBo	Very coarse silty very fine sand
GeoB13844-4	-53.73	-37.42	MeBo	Very fine sandy very coarse silt
GeoB13845-11	-55.12	-38.17	MeBo	Very fine sandy coarse silt, coral fragments
GeoB13845-8	-55.12	-38.17	MeBo	Very coarse silty very fine sand, coral fragments
GeoB22701-2	-54.18	-37.82	GBC	Very coarse silty very fine sand
GeoB22702-2	-54.17	-37.81	MUC	Coarse silty very fine sand
GeoB22706-1	-53.76	-37.95	MUC	Very fine sandy coarse silt
GeoB22707-2	-53.80	-37.91	MUC	Very fine sandy coarse silt
GeoB22708-3	-53.95	-39.31	MUC	Very fine sandy coarse silt
GeoB22709-1	-53.97	-39.30	GC	Very fine sandy coarse silt
GeoB22711-1	-54.48	-38.33	MUC	Coarse silty fine sand
GeoB22712-3	-54.49	-38.33	GBC	Coarse silty fine sand, cobbles, coral fragments
GeoB22713-1	-54.35	-38.59	MUC	Coarse silty very fine sand
GeoB22714-1	-54.38	-38.63	GC	Very coarse silty very fine sand
GeoB22715-1	-54.53	-38.32	GBC	Very coarse silty very fine sand, coral fragments
GeoB22718-1	-54.30	-37.88	GS	Very coarse silty medium sand
GeoB22720-1	-54.05	-37.72	GS	Very coarse silty very fine sand
GeoB22721-1	-53.98	-37.56	MUC	Very fine sandy very coarse silt
GeoB22722-3	-54.02	-37.54	MUC	Very fine sandy coarse silt
GeoB22723-2	-53.96	-37.70	MUC	Very coarse silty very fine sand
GeoB22725-1	-54.06	-38.34	MUC	Very coarse silty very fine sand
GeoB22726-2	-54.37	-38.72	GS	Very coarse silty very fine sand
GeoB22727-1	-54.39	-38.69	GS	Coarse silty fine sand
GeoB22728-3	-54.35	-37.78	GS	Very fine sandy medium silt
GeoB22729-1	-54.34	-37.81	GC	Very fine sandy very coarse silt, coral fragments
GeoB22730-1	-54.87	-37.69	GS	Very coarse silty medium sand
GeoB22731-1	-54.77	-37.64	GS	Coarse silty fine sand, coral fragments
GeoB22732-1	-54.62	-37.54	GS	Coarse silty medium sand
GeoB22733-1	-54.60	-37.50	GS	Fine sandy coarse silt, coral fragments
GeoB22738-1	-53.97	-37.33	GS	Very fine sandy very coarse silt
GeoB22739-2	-54.38	-38.59	MeBo	Coarse silty fine sand
GeoB22740-1	-54.34	-38.61	GC	Very coarse silty very fine sand
GeoB22741-1	-54.31	-38.64	GC	Very coarse silty fine sand
GeoB22744-2	-54.54	-38.30	GBC	Very coarse silty very fine sand, coral fragments

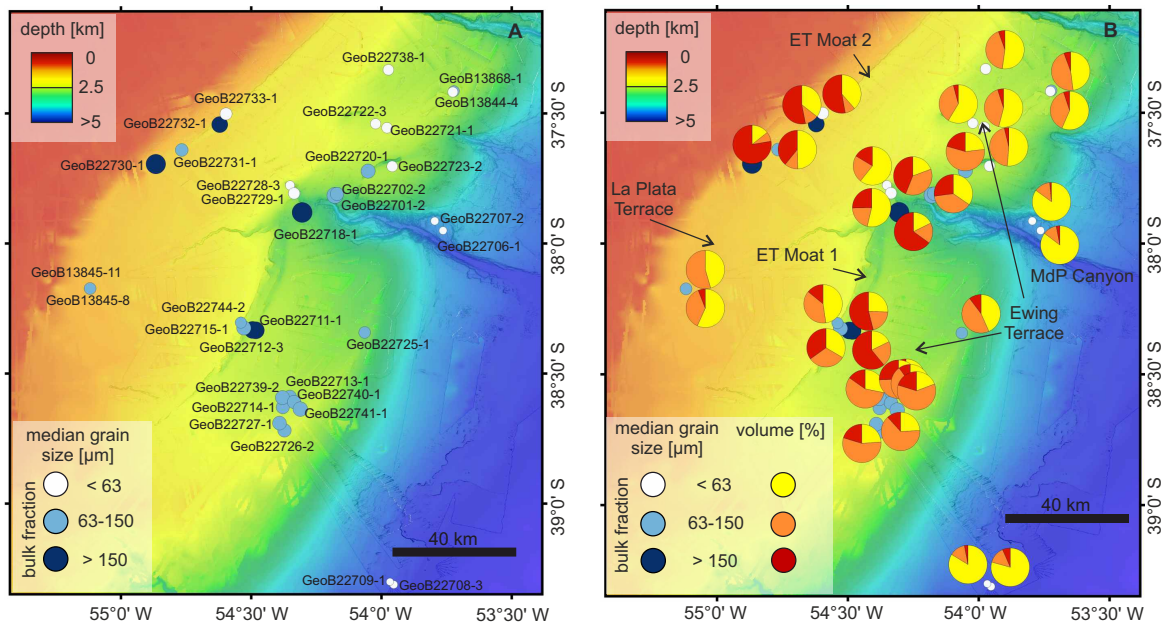

Figure 3.16: (A) Median grain size of all the bulk sediment samples ($< 2000\,\mu$m) analysed in this study and their names. (B) Pie chart showing the volume of sediments in three grainsize intervals of the mud and sand fraction.

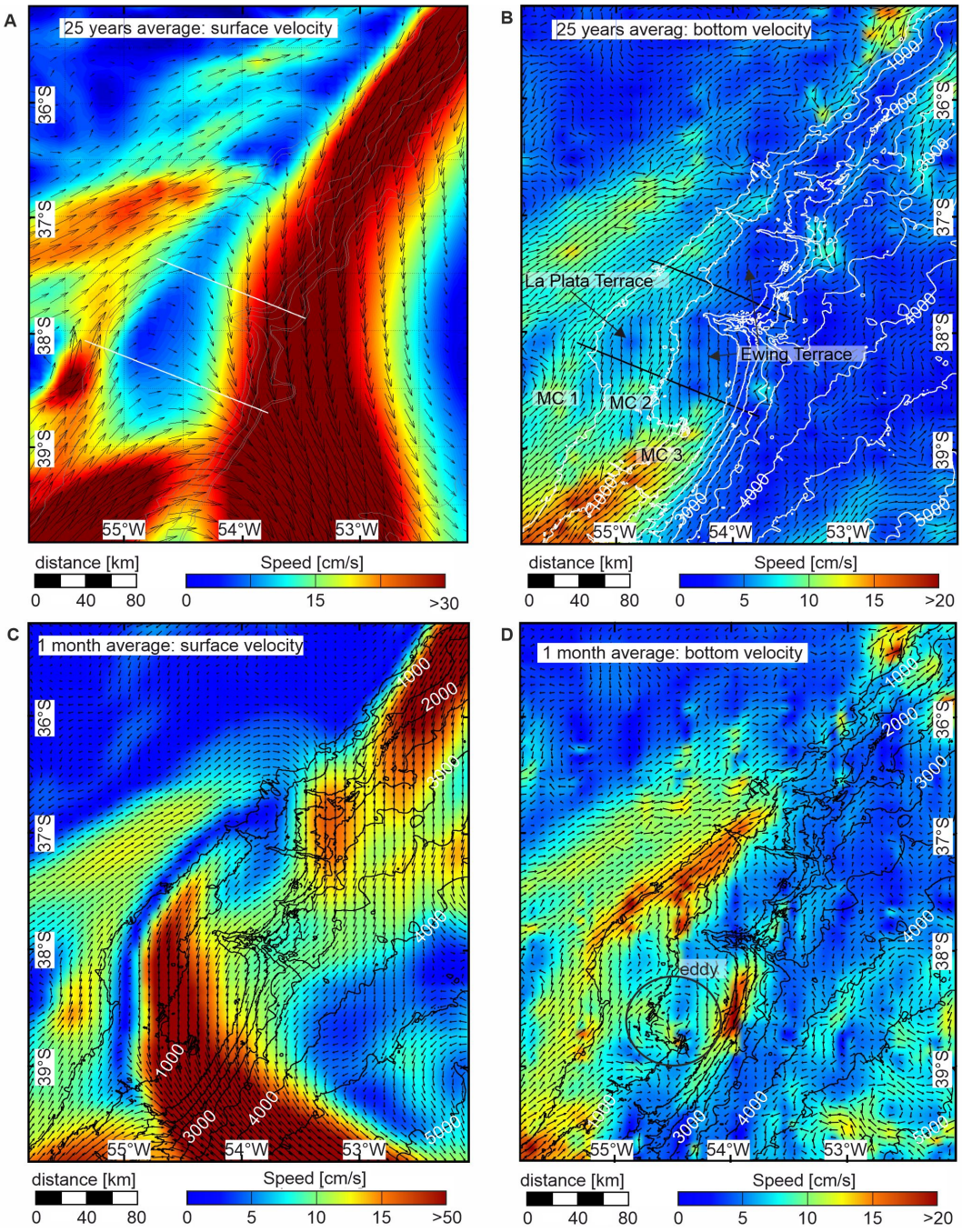

Figure 3.17: (A) Modelled mean sea surface velocity over 25 years (see Artana et al. 2021a). (B) Modelled mean bottom velocity over 25 years. (C) Modelled mean sea surface velocity from 12/01/2012 to 14/02/2012. (D) Modelled mean bottom velocity from 12/01/2012 to 14/02/2012. Note that the scale for the speed is not always the same.

Chapter 4

Factors controlling the morphology and internal sediment architecture of moats and their associated contourite drifts

Published in: Sedimentology in 2023
https://doi.org/10.1111/sed.13093

Henriette Wilckens [a,b], Tilmann Schwenk [a], Thomas Lüdmann [c], Christian Betzler [c], Wenyan Zhang [d], Jiayue Chen [d], F. Javier Hernández-Molina [e], Alice Lefebvre [b], Antonio Cattaneo [f], Volkhard Spieß [a], Elda Miramontes [a,b]*

a Faculty of Geosciences, University of Bremen, Bremen, Germany.

b MARUM - Center for Marine Environmental Sciences, University of Bremen, Germany

c Institute for Geology, University of Hamburg, 20146 Hamburg, Germany

d Institute of Coastal Systems, Helmholtz-Zentrum Hereon, 21502 Geesthacht, Germany

e Department of Earth Sciences, Royal Holloway University of London, Egham TW20 0EY, Surrey, UK

f UMR 6538 GEO-OCEAN, Ifremer, Univ Brest, CNRS, Univ. Bretagne-Sud, 29280 Plouzané, France

* Corresponding author: Henriette Wilckens: cwilcken@uni-bremen.de

Keywords: Geomorphology; Contourite drift; Bottom current; Sedimentary processes; Sediment transport; Moats

4.1 Abstract

The interaction of sedimentary systems with oceanographic processes in deep-water environments is not well understood yet, despite its importance for paleoenvironmental reconstructions, and for a full understanding of source-to-sink sediment transport. The aim of this study is to improve the understanding of how contourite moats, elongated depressions formed by bottom currents associated with contourite drifts, develop and of the link between moat-drift system morphology and bottom current dynamics. This study provides a systematic comparison of 185 cross-sections of moat-drift systems distributed at 39 different locations worldwide and a detailed analysis of the morphology of six moats that cover a wide range of typical geological and hydrodynamic settings. Additionally, *in situ* measured current data were analysed to better link hydrodynamics to moat morphology. The median of all profiles across all moat-drift systems reveals a 50 m relief, a width of 2.3 km, a relief to width ratio of 0.022, a slope angle of 6°, a drift angle of 3° and a concave-up shaped morphology. Moats can be over 100 km long. Some moats are driven by sediment erosion while others are depositional and primarily exist due to differential sedimentation inside the moat compared to the drift alongside the moat. A new sub-classification of moat-drift systems based on their stratigraphy is proposed. This classification distinguishes moats depending on the degree of erosion versus deposition. No relation is found between latitude and moat-drift morphology or stratigraphy in the analysed examples. The combined data indicate that a steeper slope focuses the current more than a gentle slope, resulting in an increase of the relief-width ratio and drift angle. Thus, this study provides new insides into the interaction of ocean currents with sedimentary morphology, which thereby affects the evolution of a poorly understood deep-water sedimentary system.

4.2 Introduction

Contourite moats are elongated depressions formed by ocean bottom currents and can be found parallel to the continental slope or other topographic obstacles (Rebesco et al., 2014; Miramontes et al., 2021). They are channel-like features, but in contrast to contourite channels that show erosion on both flanks, moats are not purely erosive. Moats are associated with separated mounded drifts forming parallel to one of the moats sides (Rebesco et al., 2014; Miramontes et al., 2021). Moats are common in a variety of geological settings like open continental slopes, around seamounts and carbonate mounds (Rebesco et al., 2014; Vandorpe et al., 2014; Hebbeln et al., 2016; Miramontes et al., 2021). As there is no moat without an associated drift, we consider them as one system that we refer to as a moat-drift system. Understanding the morphology of a moat also depends on the associated drift and thus moats and drifts cannot be studied independently. It has been proposed that moats are pathways for the transport of sediments and anthropogenic

particles (such as microplastic) due to vigorous bottom currents, while particle accumulation mainly occurs on their associated contourite drifts where bottom current speed is lower (Rebesco et al., 2014; Yin et al., 2019; Kane et al., 2020; Wilckens et al., 2021). Analysing how sediment is transported within moats is important for understanding the heterogeneity of sediment distribution on the seafloor and the final fate of sediments in source-to-sink systems.

Moats and cold-water coral mounds form due to bottom currents and are often found next to each other (Hebbeln et al., 2016). A better understanding of current behaviour over moats could also increase our understanding of how these ecosystems might develop in the future. We do not consider a link between moats and plastered drifts. They do occur in the same contourite depositional systems and thus there is a special link, but the current dynamics are different and thus there is no direct link in the formation process (Miramontes et al., 2021). Furthermore, moats and their associated separated mounded drifts provide records of past ocean conditions. The onset of contourite depositional systems, analysed based on morphological and seismic data, has been used in many different settings to identify large changes in global ocean circulation patterns, as well as the formation inside diferent water masses, and to understand relative changes in current speed over several thousands to millions of years (Hernández-Molina et al., 2014; Uenzelmann-Neben et al., 2017; Paulat et al., 2019; Yin et al., 2021). For quantitative reconstructions of speed mainly grain size analyses have been used (McCave et al., 1995; 2017; Wu et al., 2020), with calibrations for quantitative paleo-reconstructions for some areas (McCave et al., 2017). Taking several sediment cores is time-consuming and expensive, in particular in the deep sea. Efforts to link contourite morphology to the currents that formed them have progressed significantly in recent years due to more current measurements and high resolution modelling (Zhang et al., 2016; Miramontes et al., 2021; Wilckens et al., 2021; Rebesco et al., 2021). A better integration of the morphology in addition to sediment cores for the reconstruction of current speed could be faster, cheaper, applicable on larger scales and easier for reconstructing conditions over several million years.

There are different types of contourites, from which the morphology can be used for ocean current speed reconstructions, but so far the link between their morphology and the characteristics of currents is not very clear (McCave and Tucholke, 1986; Tucholke, 2002; Rebesco et al., 2014; Miramontes et al., 2019; 2021). It is hypothesized that moats are located under the main core of the current (Yin et al., 2019; Wilckens et al., 2021). This study intends to advance the understanding of the sedimentary processes that control moat formation and evolution. For decoding the sedimentary record of ocean currents, it is crucial to have a good understanding of the morphology and stratigraphy of the moat and the adjacent separated mounded drift, as well as the current conditions. Although

moats have been recognised all over the world, there has not yet been a detailed analysis and comparison of the similarities and differences between them.

The Coriolis force together with the water pressure gradient determines the flow direction of a geostrophic current. It has been proposed that moats can only form on a continental slope where the Coriolis force deflects the current against the slope (McCave and Tucholke, 1986; Faugères et al., 1999). The Coriolis force influences global ocean circulation by forcing the currents towards the right in the northern hemisphere and towards the left in the southern hemisphere. This can result in the formation of a contourite drift on the left side (looking downstream) of the moat in the northern hemisphere and on the right side in the southern hemisphere (Faugères et al., 1999; Llave et al., 2001; Rebesco et al., 2014). Thus, the Coriolis force is one parameter that influences where moats can form. However, it is unknown whether the Coriolis force also significantly influences the morphology of the moat. The Rossby number (Ro) is used to determine how important the Coriolis force is in a system (Davarpanah et al., 2020). The Rossby number is defined as Ro=U/fL, with mean velocity U, Coriolis frequency f and length scale L. The Coriolis frequency f is defined as $f = 2\omega sin(\phi)$, with angular velocity ω and latitude ϕ. While the influence of the Coriolis force on moats is still unknown, its influence on submarine channels that develop due to downslope flowing turbidity currents has been demonstrated (Cossu and Wells 2010; Wells and Cossu 2013; Allen et al., 2022). For submarine channels, field observations show a latitudinal dependence on sinuosity (Wells and Cossu 2013; Allen et al., 2022). Moats do not meander and thus sinuosity is not a relevant parameter, but possibly the latitudinal dependence is preserved in the aspect ratio.

Contourites not only form due to geostrophic currents, but also due to other oceanographic currents that flow near the seafloor (Rebesco et al., 2014). Around seamounts and other topographic obstacles moats can form not only on the side where the current is pushed against the slope, but also on the side where the Coriolis force deflects the current away from the slope (Hernández-Molina et al., 2006c; Hebbeln et al., 2016; Chen et al., 2022). It is suggested that the side where the Coriolis force is pushing the current towards the seamount is faster and leads to more erosion compared to the other side (Hernández-Molina et al., 2006c; Chen et al., 2022). It remains unclear if this concept is true for all sizes of seamounts. The pre-existing morphology could also affect the development of moats, and moat morphology is not only influenced by ocean currents but also by downslope movement of sediment, e.g. mud deposits from mud volcanos (Vandorpe et al., 2014). Therefore, understanding the dynamic feedback between the seafloor morphology and the bottom currents is of crucial importance in the study of contourite-moat systems.

In this study, we systematically investigate the morphology and stratigraphy of moats

and associated separated mounded drifts distributed worldwide. We then use the measurements from different morphologic parameters of the moats to test our hypotheses: 1) moat-drift systems have no specific aspect ratio because they are influenced by multiple processes; 2) moat morphology changes with latitude because the Rossby number and Coriolis force depend on it; 3) moat morphology correlates with water depth because of the influence of sediment availability and limited accommodation space; and 4) moat aspect ratio and the steepness of the drift depend on the steepness of the slope at which the moat forms because the slope influences the hydrodynamics. Where available, we also use current measurements from vessel-mounted Acoustic Doppler Current Profilers (VM-ADCP) to better understand the link between moat-drift system morphology and hydrodynamics.

4.3 Materials and methods

4.3.1 Measurements of moat parameters

We analysed moats from different locations around the world (Fig. 4.1) to provide a synthesis of their occurrence in the literature and identify common characteristics and genetic features. The location of all moats included in this study, and the key references of the previous studies in these areas, can be found together with the origin of the data sets used in the analysis in the supplementary material (Table 4.4). For the comparison of different morphologies of moat-drift systems around the world, we measured the following morphological parameters: width, relief, slope angle, drift angle and where possible, the length of moats (Fig. 4.2). The moat trough is the deepest point inside the moat and the drift crest the shallowest point of the contourite drift. The moat width is defined as the horizontal distance between the drift crest and the slope. The relief is defined as the vertical distance between moat trough and drift crest. The slope angle and the drift angle are the average gradient in both flanks of the moat: 1. between the moat trough and the slope and 2. between the moat trough and the drift crest (Fig. 4.2). In total, we analysed 45 different stratigraphic sections (using seismo-acoustic data) and measured 185 cross-sections (from bathymetric data) of moat-drift systems. For 59 moats, one cross-section was measured and for 19 moats multiple cross-sections were measured, that account in total for 126 cross-sections. For the statistics presented here, we used all datapoints, to also account for changes within one moat-drift system. To check if there is a bias in the statistics we calculated the median relief, width, ratio, slope angle and drift angle with all data points and with just one cross-section from each system. The relative deviation for all parameters is below 8%.

The size of previously published moats were measured from the seismic or sub-bottom profiler cross-sections that were published either in a journal or on the GeoMapApp

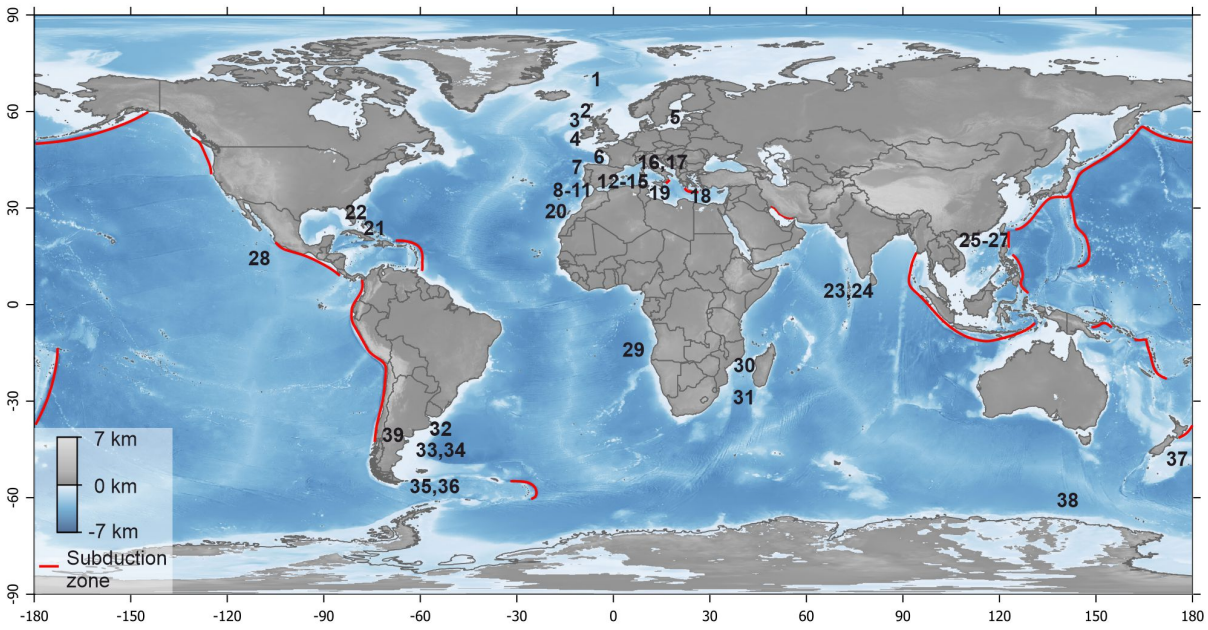

Figure 4.1: Location of moats considered in this study. 1 NW Barents Sea, 2 North Rockall Trough, 3 Rockall Trough (Seamount), 4 Ireland, 5 Baltic Sea, 6 Gulf of Biscay, 7 Galicia, 8-11 Gulf of Cadiz, 12-13 Adriatic Sea, 14 Balearic Sea, 15 Tyrrhenian Sea, 16-17 Alboran Sea, 18 Aegean Sea, 19 Malta, 20 Lanzarote, 21-22 Bahamas, 23-24 Maldives, 25-26 South China Sea, 28 Pacific Ocean (Clarion-Clipperton Zone), 29 Angola (Anna Ridge), 30 Mozambique, 31 Madagascar, 32-34 Argentina, 35-36 Patagonia, 37 New Zeeland, 38 Antarctica, 39 Lago Cardiel (Lake in Argentina). See Table 4.4 of the supplementary material for references. The subduction zones are adapted from van Keken et al. (2011).

(www.geomapapp.org) (supplementary material Table 4.4 and PANGAEA database). In cases in which multibeam data are available, we measured the parameters from the bathymetric map. We checked the consistency of the measurements using both methods (from the bathymetry and from the seismic profiles) on the Ewing Terrace Moat 2 (ET Moat 2) offshore North Argentina and we found the same results. We are therefore confident that all the measurements are comparable.

In the statistical analyses, the influence of one parameter on the morphologic moat parameters (relief, width, and aspect ratio) is tested. To understand which parameters are most relevant for shaping the moat-drift system, they are tested one at a time. However, this means that parameters that only have a small influence on the moat-drift system cannot be identified. One of the main interests is to determine how the strength of the Coriolis force influences the moat morphology, which is why we measure multiple morphologic parameters and correlate them with the latitude. The Coriolis frequency is higher at high latitudes and becomes zero at the equator. Since the hemisphere is relevant for the directions of the Coriolis force but not for its strength, we have not distinguished between the same latitudes on northern and southern hemisphere.

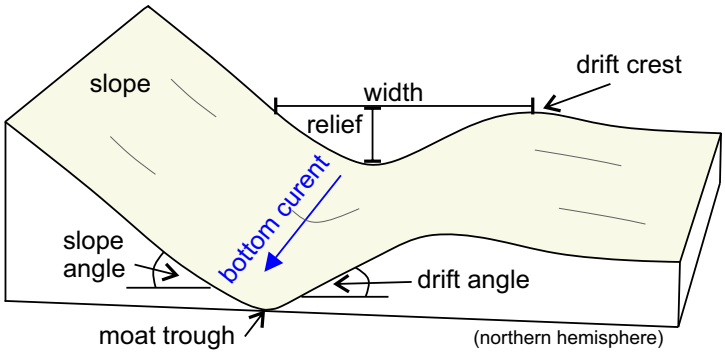

Figure 4.2: Cross-section of a moat-drift systems where the measured parameters (width, relief, slope angle and drift angle) are defined.

4.3.2 Bathymetric and Seismic Data

Bathymetric data was used from 9 different areas. Table 4.1 summarises the details of where the data comes from and the grid cell size.
The seismic data used in this study for the stratigraphic and morphological analysis of moats was obtained from previously published sources (Supplementary material Table 4.4). This study also shows unpublished seismic data collected during cruise SO260 onboard the R/V SONNE in 2018 (Kasten et al., 2019). Seismic data was acquired during the SO260 cruise with a 225 m (active length) long streamer with 96 channels from University of Bremen, and a SERCEL Mini-GI Gun with a chamber volume of 2 x 0.24 l as a seismic source. The data processing was conducted with the 'VISTA Desktop Seismic Data Processing Software' (Schlumberger) and included bandpass filtering, de-spiking, common mid-point (CMP) binning, Normal-Moveout (NMO) correction, CMP stacking, noise reduction and finite-difference time migration. 'The Kingdom Software' (IHS Markit) was used for interpretation. To convert the travel time of the seismic waves into depth, a constant velocity of 1500 m/s was used.

4.3.3 VM-ADCP Data

For four moats, ocean current velocities were measured with a vessel-mounted Acoustic Doppler Current Profiler (VM-ADCP). These quantitative measurements of the characteristics of ocean currents (strength and direction) at these locations in recent times, but not at times of the moat initiations. Two of the moats are carbonate moats located in the Santaren Channel in the Bahamas, and two are siliciclastic moats located at the open slope offshore north Argentina. The VM-ADCP data from the Argentine moats were partly described by Steinman et al. (2020) and Wilckens et al. (2021), and from the Bahamas moats were partly described in Lüdmann et al. (2016). The data from the Bahamas were reprocessed in a similar way as described in Wilckens et al. (2021). VM-ADCP data off Argentina were collected during cruise SO260 between January and

Table 4.1: Summary of the Bathymetry data. * Due to the relatively low resolution this grid was only used to measure structures above 10 km horizontal distance.

Area	**Cruise**	**Reference**	**Grid cell size**
North Argentina (SW Atlantic Ocean)	cruise SO260 onboard the R/V SONNE in 2018	Kasten et al., 2019; Wilckens et al., 2021	25 m
Mozambique Basin (SW Indian Ocean)	cruise PAMELA-MOZ2 onboard the R/V L'Atalante in 2014	Robin and Laurence, 2014; Miramontes et al., 2021	30 m
Corsica Trough (northern Tyrrhenian Sea, NW Mediterranean Sea)	cruise PRISME2 onbard the R/V L'Atalante and cruise PRISME3 onboard the R/V Pourquoi pas? survey in 2013	Cattaneo 2013a,b; Miramontes et al., 2016	15 m
Offshore Galicia (NW Spain, NE Atlantic Ocean)	cruise M84/4 onboard the R/V Meteor in 2011	Hanebuth et al., 2011; 2015	75 m
Offshore the Santaren Channel in the Bahamas	cruise M95 on board the R/V Meteor in 2013	Betzler et al. 2014a;b; Lüdmann et al. 2016	200 m
Gulf of Cadiz	cruise CADIPOR 1+2 onboard the R/V Belgica in 2002 and 2005	Van Rensbergen et al., 2005, Vandorpe et al., 2017	30 m
offshore Lanzarote and offshore north Ireland	-	EMODnet bathymetry	115 m
Offshore Patagonia (Drake Passage)	-	GEBCO 2021 bathymetry	460 m *

February 2018 (Kasten et al., 2019). The instrument parameters led to 16 m depth cells. VM-ADCP data off the Bahamas were collected during cruise M95 between March and April 2013 (Betzler et al., 2014b). The instrument parameters led to 8 m depth cells. Data processing was conducted with the Cascade V7.2 software. For analyses of near-bottom currents, the average speed between 150 and 200 m above the seafloor was calculated. Data within the deepest 150 m immediately above the seafloor were not used because of their poorer quality due to high scattering from the seafloor. The barotropic tides, obtained from the TPXO tidal model at the time and location of the ADCP acquisition, are below 4 cm/s in the study area and thus much lower than the total current speed. They are not removed from the dataset because they can also transport sediment and meanwhile contribute to total current strength.

4.3.4 Moat Names

Several moats are referred to by their previously used name. These names are: Great Bahamas Bank Moat (GBB Moat) and Cay Sal Bank Moat (CSB Moat) in the Bahamas (Betzler et al., 2014a), Ewing Terrace Moat 1 (ET Moat 1) and Ewing Terrace Moat 2 (ET Moat 2) offshore Argentina (Wilckens et al., 2021); Beira Moat offshore Mozambique (Miramontes et al., 2021); Álvarez Cabral Moat in the Gulf of Cadiz (Llave et al., 2001; García et al., 2009); Gijón Moat offshore northern Spain (Van Rooij et al., 2010; Liu et al., 2020). The moats that have not been previously named are a moat near Madagascar (Fig. 3A from Miramontes et al., 2021) that will be referred to here as the Madagascar Moat; a moat near Galicia (Fig. 1 from Hanebuth et al., 2015) that will be referred to as the Galicia Moat and a moat near Corsica (Fig. 8 from Miramontes et al., 2016) that will be referred to as the Corsica Moat.

4.4 Results

4.4.1 Fingerprint of a Moat

The moats included in this study are located between 60 m and 5000 m water depth and between latitude 75°N and 67°S. Moats size shows a large variability in terms of width, relief, relief-width ratio, slope angle, drift angle and length (Fig. 4.3). Relief ranges between 4 m and up to several hundreds of meters like the Madagascar Moat (505 m). Most of the measurements (90%) show a relief below 168 m and the median value is 50 m (Fig. 4.3; Table 4.2). Width is between 100 m, and up to tens of kilometres, like the Great Bahamas Bank Moat (26 km) or a moat off Patagonia (35 km). Of all measured moats, 90% are less than 13 km wide, the median width is 2.3 km, and only 10% are less than 0.5 km wide (Fig. 4.3; Table 4.2). Furthermore, the ratio between relief and width varies between 0.001 (e.g. Great Bahamas Bank Moat) and 0.1 (e.g. Galicia Moat). 90% of all measured relief-width ratios in this study are below 0.056 and the median is 0.022 (Fig. 4.3; Table 4.2). Only 10% of the measured moats have relief-width ratios below 0.004. The length of moats is rather difficult to compare since they are often unknown because there are not entirely covered by multibeam data. However, six examples are analysed in section 'Along-slope morphology and hydrodynamics of moat-drift systems'. The angle

Table 4.2: 10th percentile, 50th percentile (median), 90th percentile and maximum from the different measured properties of moats.

	Relief	**Width**	**Relief-Width Ratio**	**Slope angle**	**Drift angle**
Minimum	4 m	0.1 km	0.001	0.3°	0.2°
10th percentile	13 m	0.5 km	0.004	1°	0.4°
50th percentile	50 m	2.3 km	0.022	6°	3°
90th percentile	168 m	13 km	0.060	15°	8°
Maximum	505 m	35 km	0.1	25°	17°

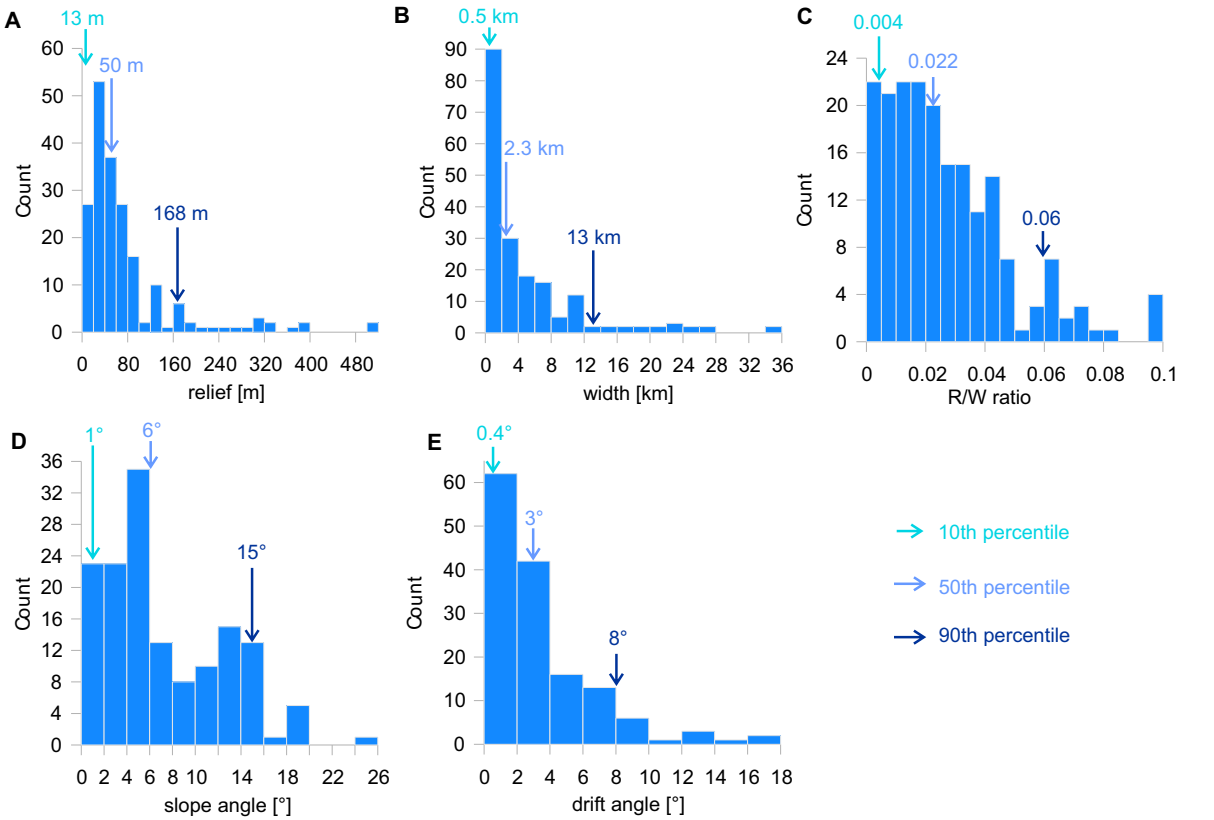

Figure 4.3: Histograms showing the range of (A) relief, (B) width, (C) relief-width ratio, (D) slope angle and (E) drift angle

of the slope on which the moats form varies between settings and in particular between open continental slopes and seamounts or other topographic obstacles. In this study, slopes with the highest angles of 25° from the Galicia Moat, located at a topographic obstacle, and 15° at the eastern slope of the Corsica Trough are included (Fig. 4.3; Table 4.2). Also, the contourite drift angles vary between settings (see methods for definition). It can be below 1°, for example at the Great Bahamas Bank Moat, but it can also be up to 11°, for example at the Galicia Moat or 10° at the Corsica Moat. However, 90% of the slope angles are below 15° and only 10% are below 1°. 90% of the drift angles are below 8° and only 10% are below 0.4. The median measured slope angle is 6° and the median drift angle is 3° (Fig. 4.3; Table 4.2).

4.4.2 Correlation between parameters of moat-drift systems

In this chapter, the hypothesized correlations between moat relief and width, as well as measured moat parameters and latitude, water depth, and steepness of the slope are tested. A comparison between relief and width shows a weak linear trend correlation coefficient (R) of 0.38 (Fig. 4.4A). The correlation is slightly higher for smaller systems (R=0.47). Some moat-drift systems, like the Great Bahamas Bank Moat, are up to 26 km wide but only have a maximum relief of 54 m, while others, like the Madagascar Moat,

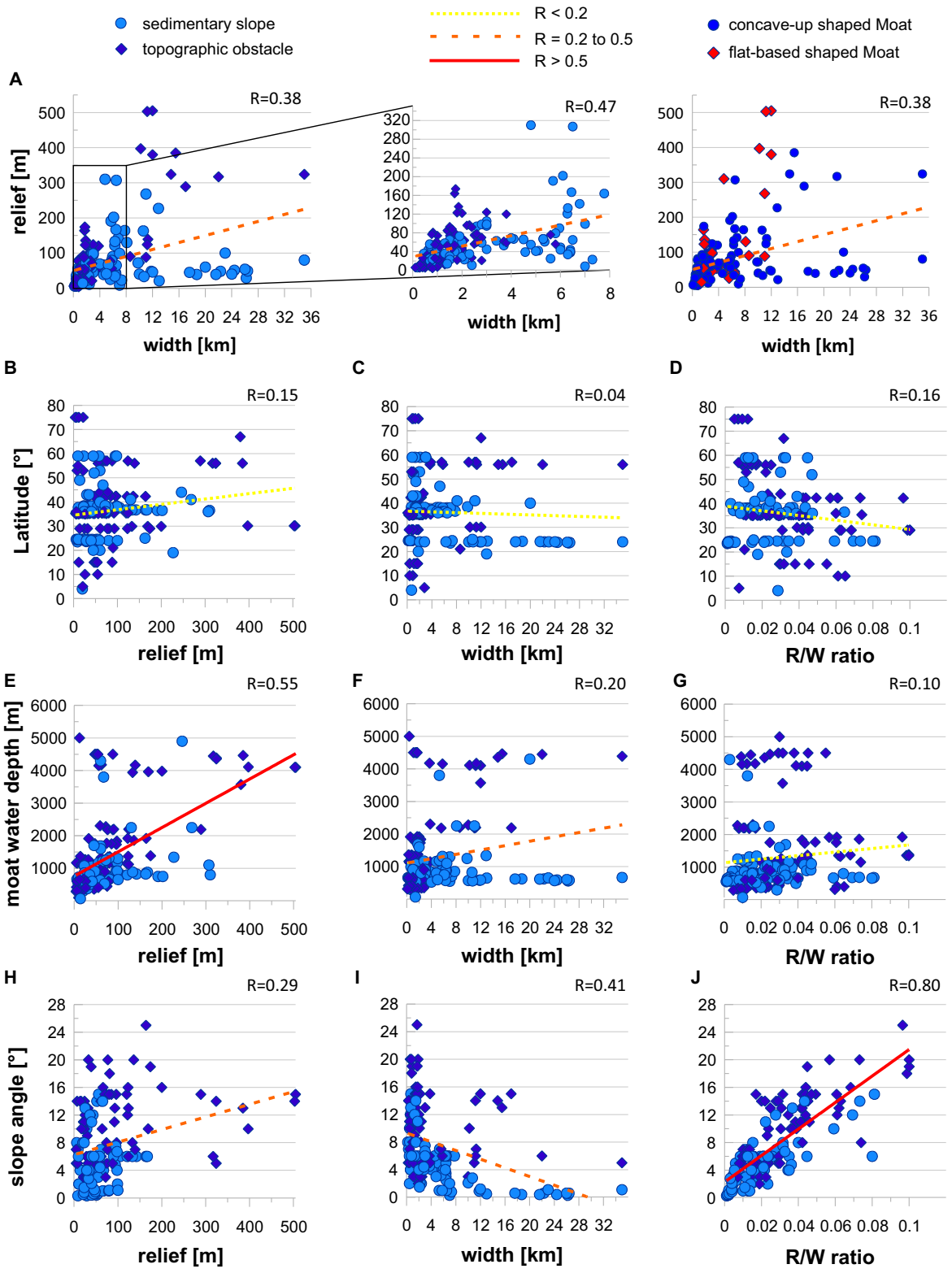

Figure 4.4: Diagrams showing correlations between (A) width and relief, (B) relief and latitude, (C) width and latitude, (D) relief-width ratio and latitude, (E) relief and moat water depth (F) width and moat water depth, (G) relief-width ratio and moat water depth, (H) relief and and slope angle, (I) width and slope angle and (J) relief-width ratio and slope angle for different latitudes.

have a relief of 505 m but are only 12 km wide. Neither relief, width or relief-width ratio show an apparent correlation with latitude (Fig. 4.4B-D). A linear fit for relief, width or relief-width ratio against latitude has in all cases a correlation coefficient below 0.16. Moats in deeper water mostly have a higher relief (Fig. 4.4B). A linear trend is recognized with R=0.55. However, it has to be noted that shallow moats have a low relief but deep moats can have both a low and a high relief. The width also increases with water depth but this linear trend is weaker with R=0.2 (Fig. 4.4F). As a consequence, two linear trends cancel each other out and the relief-width ratio shows no correlation with water depth (Fig. 4.4G).

The relief increases and the width decreases with a higher slope angle but the linear trend is only weak with R=0.29 and R=0.41 (Fig. 4.4H,I). As a consequence, there is a high linear correlation between slope angle and relief-width ratio with a correlation coefficient of R = 0.80 (Fig. 4.4J). Since this correlation is so significant it might overshadow the possibly small dependence of the moat aspect ratio on latitude. However, a slope angle-aspect ratio diagram with colour-coded latitudes also shows no apparent trend (Fig. 4.5A). The aspect ratio is influenced by the steepness of the drift angle. Accordingly, moat-drift systems that form at the foot of steep slopes often also have a high angle at the drift side. The angle of the slope side is usually 1.6 times higher than the angle of the drift side (calculated based on the linear fit in Fig. 4.5B).

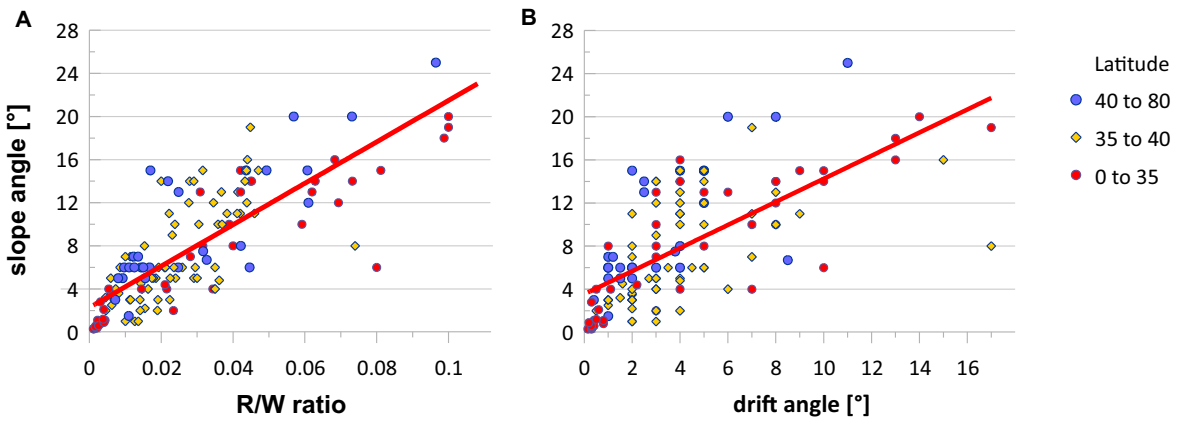

Figure 4.5: Diagrams showing correlations between (A) relief-width ratio and slope angle and (B) drift angle and slope angle at different latitudes.

4.4.3 Shape and stratigraphy of moat-drift systems

Some moats have a moat trough that is flat in cross-section with a very low slope gradient (0-0.5°) and the sides of the moat present a significant and abrupt increase of the slope gradient (2.5-25°). These shapes are here referred to as flat-base shaped e.g. the Beira Moat offshore Mozambique or the ET Moat 2 offshore Argentina (Fig. 4.6A,B).

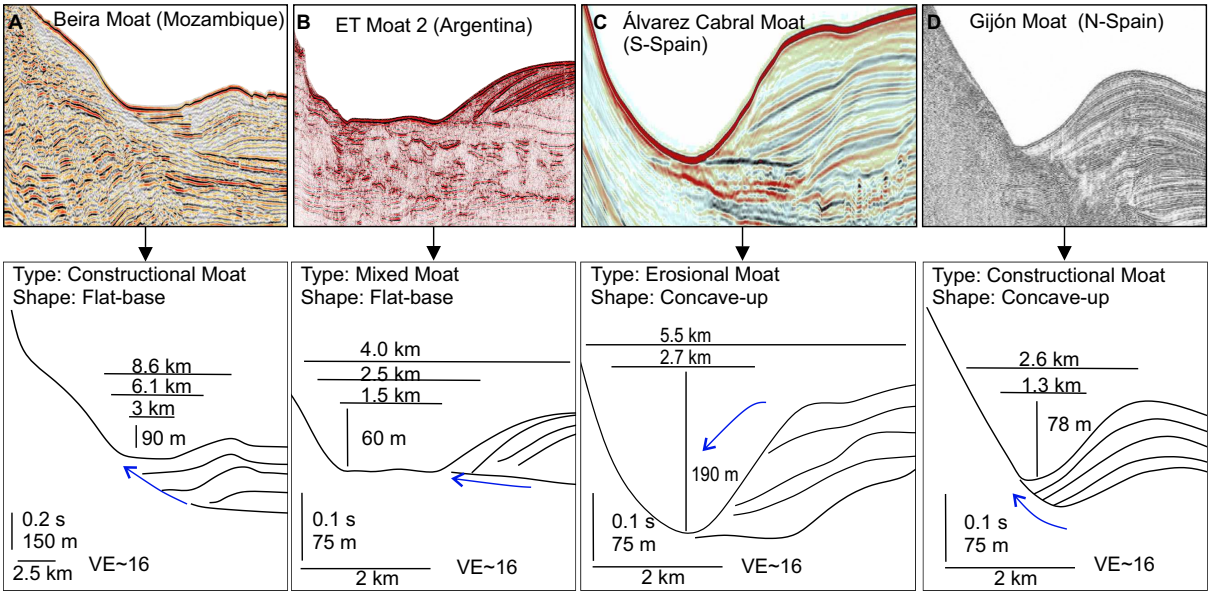

Figure 4.6: Stratigraphy with a Vertical Exaggeration (VE) of 16 of (A) the Beira Moat (adapted from Thiéblemont et al., 2019; Miramontes et al., 2021), (B) the ET Moat 2, (C) the Álvarez Cabral Moat (adapted from Hernández-Molina et al., 2016c) and (D) the Gijón Moat (adapted from Liu et al., 2020). The moats show examples of flat-base and concave-up shaped moats as well as three different stratigraphic types. The blue arrow indicates the migration direction of the moat.

In contrast, in other moats, the slope gradient continuously decreases until the deepest point of the moat and these moats do not present a flat thalweg in cross-sections (slope angle >0.5°). These shapes are here referred to as concave-up shaped. Concave-up shaped moats are for example the Álvarez Cabral Moat or the Gijón Moat offshore Spain (Fig. 4.6C,D). Of all measured moat cross-sections, 80% are concave-up shaped. The shape of the cross-section can change along a moat. For a more detailed comparison, we measured (in addition to the relief and the width at the top of the moat) also the width in the middle of the moat, and for flat-base shaped moats also the width at the bottom of the moat (Fig. 4.6). A comparison between flat-base and concave-up shaped moats indicates that the shape does not significantly depend on the width or relief of the moat (Fig. 4.6, 4.9A). The aspect ratio of flat-base shaped moats is on average 6% higher than from concave-up shaped moats.

The stratigraphy of analyzed moats differ in the way that (1) some reveal aggrading patterns, (2) some only migrate laterally and (3) some are more erosive. Examples of the first type showing an aggrading pattern are the Beira moat-drift system and the Gijón moat-drift system (Fig. 4.6A,B). The seismic reflections follow the moat morphology and onlap at the slope side. These are here defined as "Constructional Moats". An example of the second type with laterall migration is the ET moat-drift system 2 (Fig. 4.6B). Going from drift to moat, the slope angle of the seismic reflections increases and reflec-

tions downlap at the bottom of the moat. These are here defined as "Mixed Moats". An example of the third type that shows more erosion is the Álvarez Cabral moat-drift system (Fig. 4.6C). Here, seismic reflections are truncated at the drift side and show only a slight dip towards the moat. These are here defined as "Erosional Moats". It is possible that some cross-sections from the same moat show an Erosional Moat while others show a Constructional Moat. Additionally, moats may evolve with time from one type of moat to another. This is for example the case for the Álvarez Cabral Moat or the ET Moat 2. A comparison between different internal architectures of 40 classified moat cross-sections indicates that the stratigraphic differences do not depend on the width or relief of the moat. From all (40) classified moat cross-sections in this study 78% are Constructional Moats, 15% are Mixed Moats and only 8% are Erosional Moats.

4.4.4 Along-slope morphology and hydrodynamics of moat-drift systems

Bathymetry

Moats located in six different settings, covering a wide range of typical geological and hydrodynamic settings, are further analysed not only in across-slope direction, but also in along-slope direction (Figs. 4.7 and 4.8). Two moats are located in the Bahamas, two at the Argentine continental margin, one west of Corsica and one offshore Galicia. Two over 100-km long moats from the Santaren Channel in the Bahamas are chosen (Fig. 4.7B). Here, the current flows northward along the Great Bahamas Bank forming the Great Bahamas Bank Moat (GBB Moat) and southward along the Cay Sal Bank forming the Cay Sal Bank Moat (CSB Moat). The drift in the Santaren Channel (Bahamas) can be classified as a confined drift, due to the mounded drift morphology in the centre of the channel and the two moats on the flanks (Paulat et al., 2019). However, here the confined drift will simply be referred to as two separated mounded drifts that have grown into each other but are still associated to two moats (Fig. 4.7B). The eastern half of the confined drift, which is close to the GBB, is the drift that is associated with the GBB Moat, and the western half of the confined drift, is associated with the CSB Moat (Fig. 4.9). Two over 80-km long moats called Ewing Terrace Moat 1 (ET Moat 1) and Ewing Terrace Moat 2 (ET Moat 1) from the Argentine continental margin are found where the Malvinas current flows northward (Fig. 4.7C,D). The moat west of Corsica is, with only 2.8 km in length, much smaller than the other five moats and forms in a zone of northward current flow (Fig. 4.7E). The 17-km long moat offshore Galicia represents one example of a moat that formed at the foot of a topographical obstacle, where the current flows northward (Fig. 4.7E). For the six moats which were analysed in detail, the current main flow direction is known from previous studies (references listed in supplementary material Table 4.4). The moats are here always analysed in downstream direction (Fig. 4.8). Moat

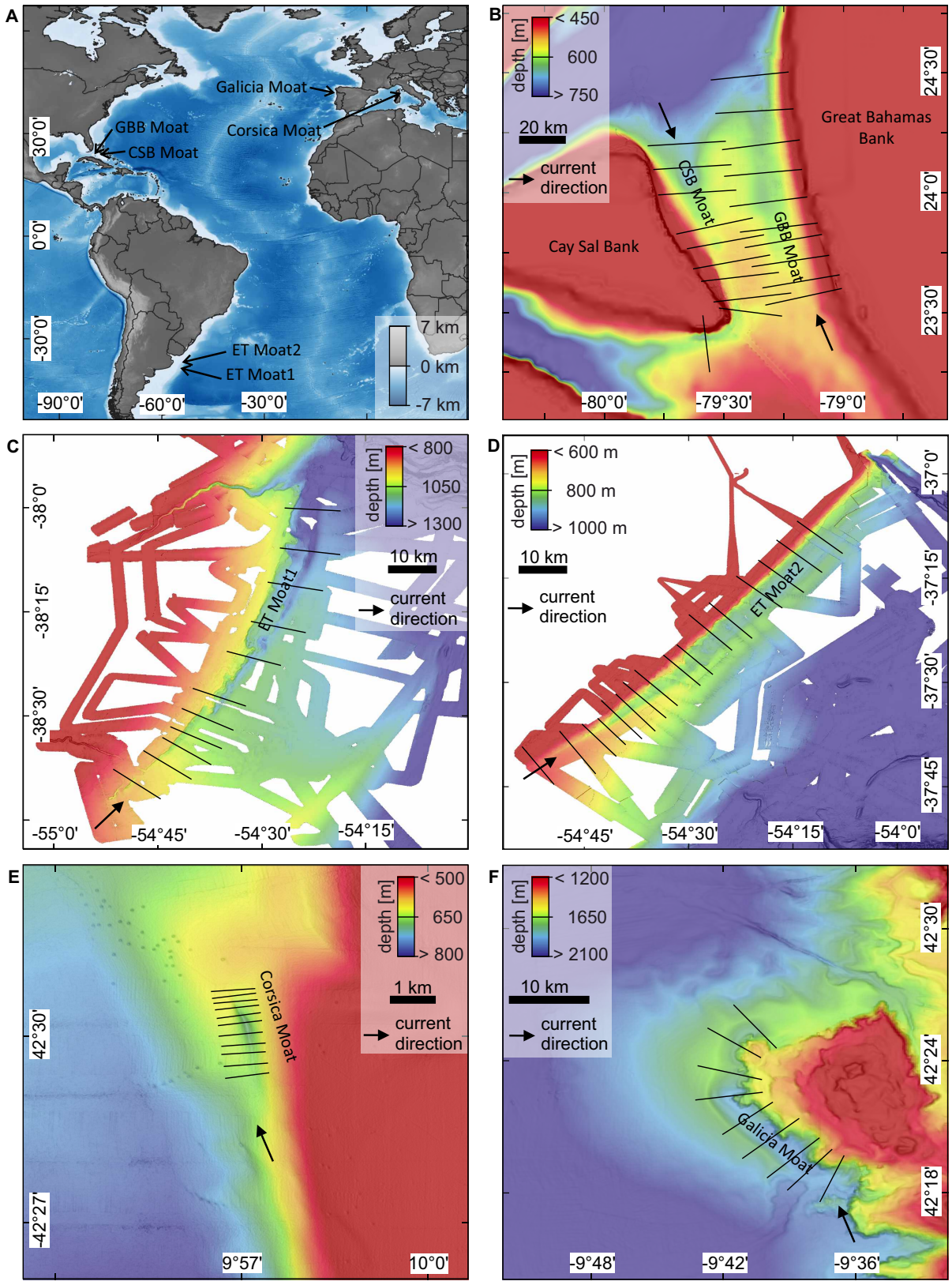

Figure 4.7: Bathymetry of six different moats. (A) Overview map showing location of moats. (B) Santaren Channel in the Bahamas with the GBB Moat (Great Bahamas Bank Moat) and the CSB Moat (Cay Sal Bank Moat). (C) ET Moat 1: Ewing Terrace Moat 1 and (D) ET Moat 2: Ewing Terrace Moat 2 offshore north Argentina. (E) Corsica Moat east of Corsica. (F) Galicia Moat at the foot of a topographic obstacle offshore Galicia. The black lines indicate the position of the measured topographic profiles.

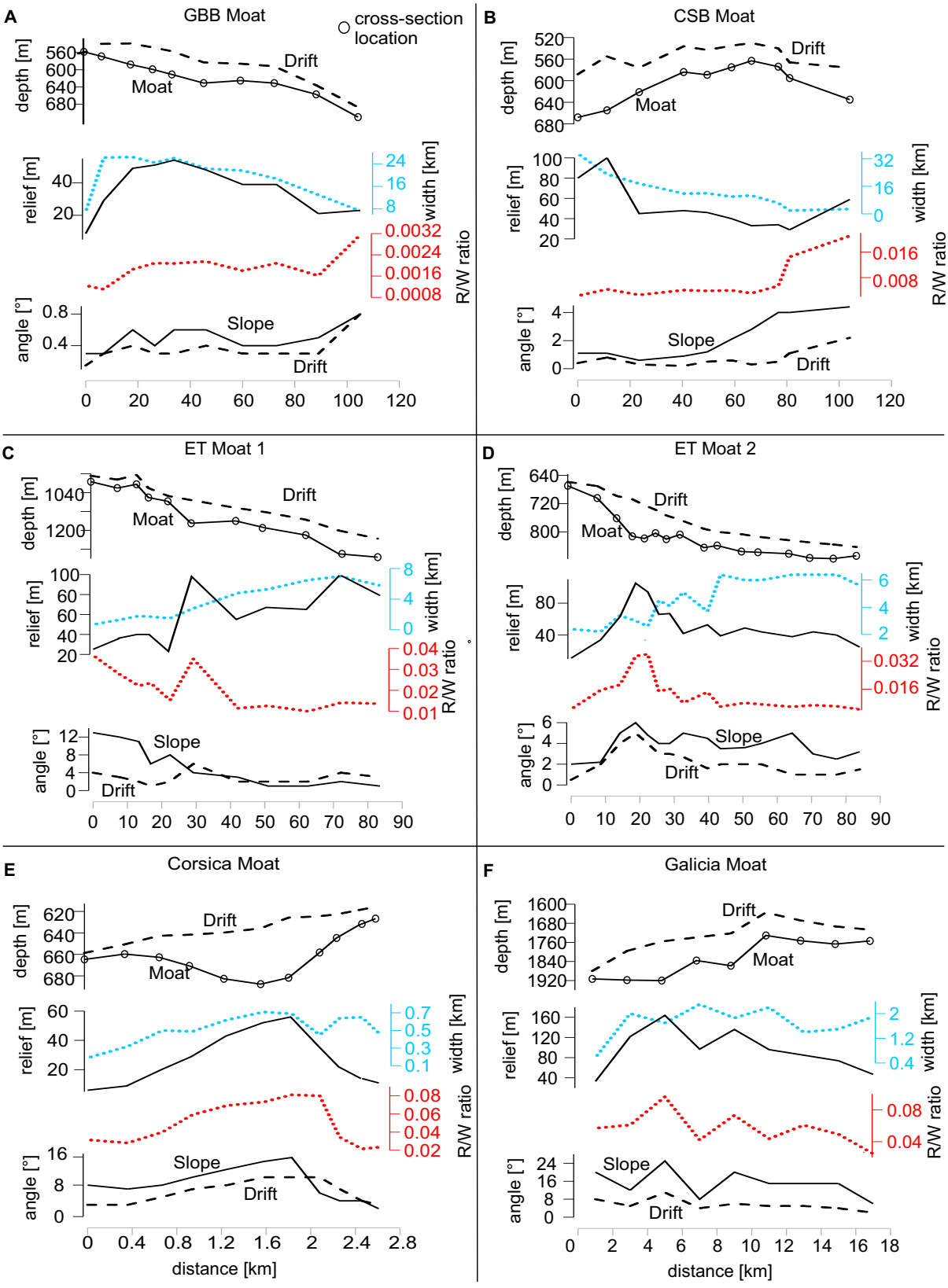

Figure 4.8: Along-slope measurements of six different moats. (A) GBB Moat: Great Bahamas Bank Moat, (B) CSB Moat: Cay Sal Bank Moat, (C) ET Moat 1: Ewing Terrace Moat 1, (D) ET Moat 2: Ewing Terrace Moat 2, (E) Corsica Moat, and (F) Galicia Moat. R/W ratio stands for relief-width ratio. For location of the measurements see Fig. 4.7.

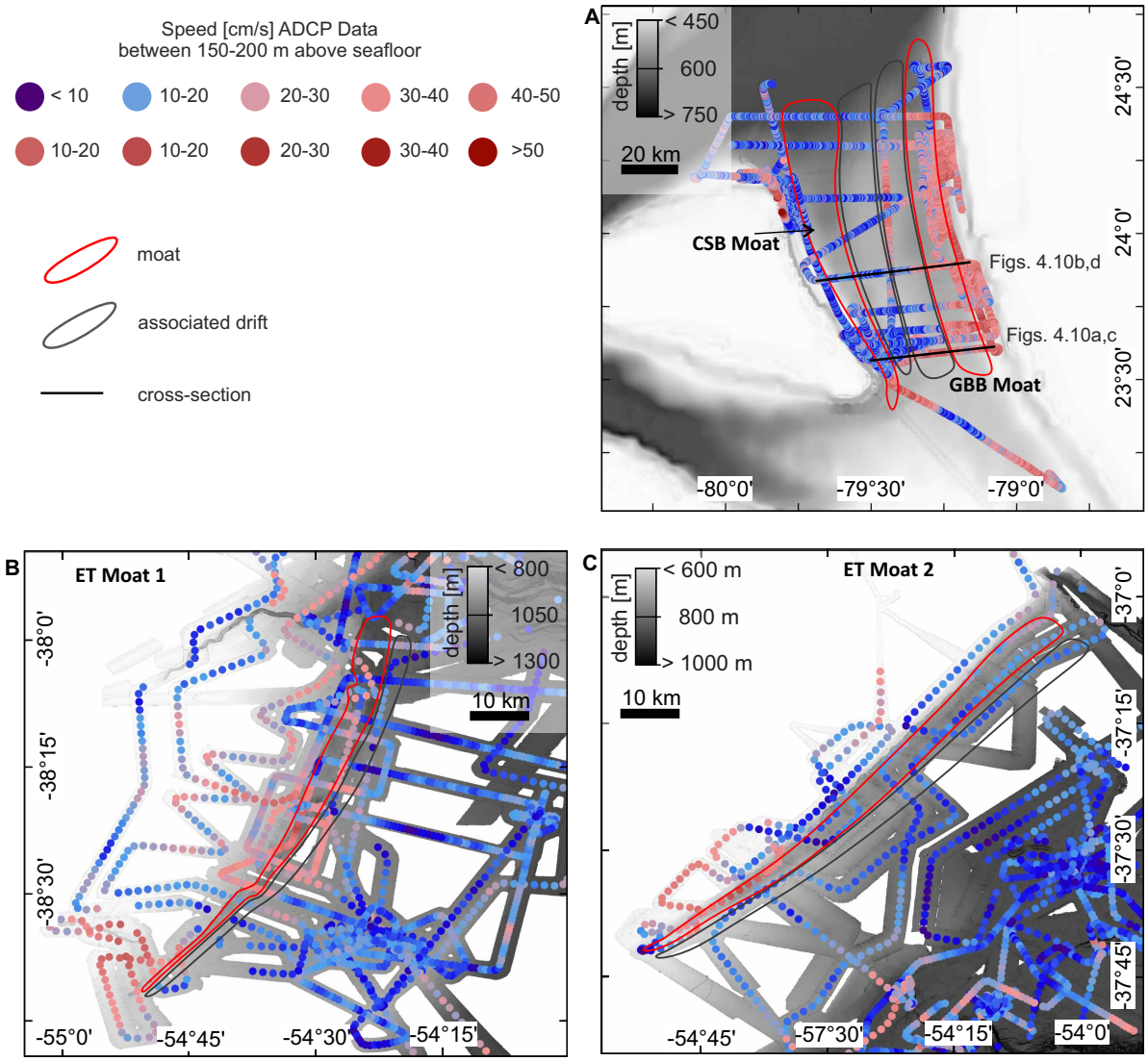

Figure 4.9: VM-ADCP data averaged between 150-200m above seafloor from (A) GBB Moat: Great Bahamas Bank Moat and CSB Moat: Cay Sal Bank Moat, (B) ET Moat 1: Ewing Terrace Moat 1, and (C) ET Moat 2: Ewing Terrace Moat 2.

and drift depth can become deeper (GBB Moat, ET Moats) or shallower (Corsica and Galicia Moats) in the downstream direction (Figs. 4.7 and 4.8). Comparing the moat depth with the drift crest depth shows that the relief is sometimes caused by a drastic deepening of the moat rather than the growing of a significant mounded drift. This is most significant for the Corsica Moat and is also observed in the ET Moat 2 at 10-20 km along-slope distance (Fig. 4.8D,E) demonstrating that the separated mounded drifts that is identified in the seismic cross-sections do not always show a pronounced mounded shape in the bathymetry in the along-slope direction. Only the GBB drift shows a slight mounded shape at the beginning at approximately 0-20 km distance (Fig. 4.8A). The straight moats at the open slope of the Argentine margin are widening in the downstream direction (Figs. 4.7c,d and 4.8c,d). However, the CSB Moat becomes narrower and the

GBB moat first widens and then gets narrower (Fig. 4.8A,B). The Galicia moat, located at the topographic obstacle, shows no clear trend regarding the width (Fig. 4.8f). The relief-width ratio curve always shows a similar trends as the relief curve. Generally, the relief-width ratio at the very gentle slopes of GBB Moat and CSB Moat is two orders of magnitude lower compared to the steeper slopes of the Corsica Moat or the Galicia Moat (Fig. 4.8). When the slope angle becomes steeper, the drift angle usually shows the same trend. At the Corsica Moat, where the slope angle smoothly but significantly increases from 8° to 15°, the drift is following the same trend but with slightly lower values (2° to 9°). While the slope angle starts decreasing again at a distance of 1.8 km, the drift angle only starts decreasing at 2.2 km distance (Fig. 4.8E).

Current measurements

The VM-ADCP data close to the seafloor generally shows stronger currents above the ET Moat 1, ET Moat 2, GBB Moat and CSB Moat compared to the speed above the associated separated mounded drift (Table 4.3). For the moats offshore Argentina (southern hemisphere; therefore the current is pushed towards the left by the Coriolis force), the difference in the mean near-bottom speed above the moat and above the drift is 9 cm/s (32%) for the ET Moat 1 and 14 cm/s (48%) for the ET Moat 2. For the GBB Moat, the near-bottom speed difference between moat and drift is slightly lower with 7 cm/s (20%) and for the CSB Moat the difference is small with only 1 cm/s (5%).

The ADCP data from the Bahamas (northern hemisphere; therefore the current is pushed towards the right by the Coriolis force) shows that the current flowing northward becomes more focused on the right boundary (the slope of the GBB) in downstream direction. At

Table 4.3: Mean speed at 150-200 m above the seafloor, as well as the standard deviation and maximal speed above the moats and above the associated drifts. ET Moat 1: Ewing Terrace Moat 1; ET Moat 2: Ewing Terrace Moat 2; GBB Moat: Great Bahamas Bank Moat; CSB Moat: Cay Sal Bank Moat.

	Moat speed [cm/s]			**Drift speed [cm/s]**			**Difference in mean speed between moat and drift [%]**
	Mean speed	Standard deviation	Max speed	Mean speed	Standard deviation	Max speed	
ET Moat 1	28	11	51	19	10	36	32
ET Moat 2	29	17	63	15	6	39	48
GBB Moat	35	13	87	28	14	72	20
CSB Moat	20	14	68	19	11	61	5

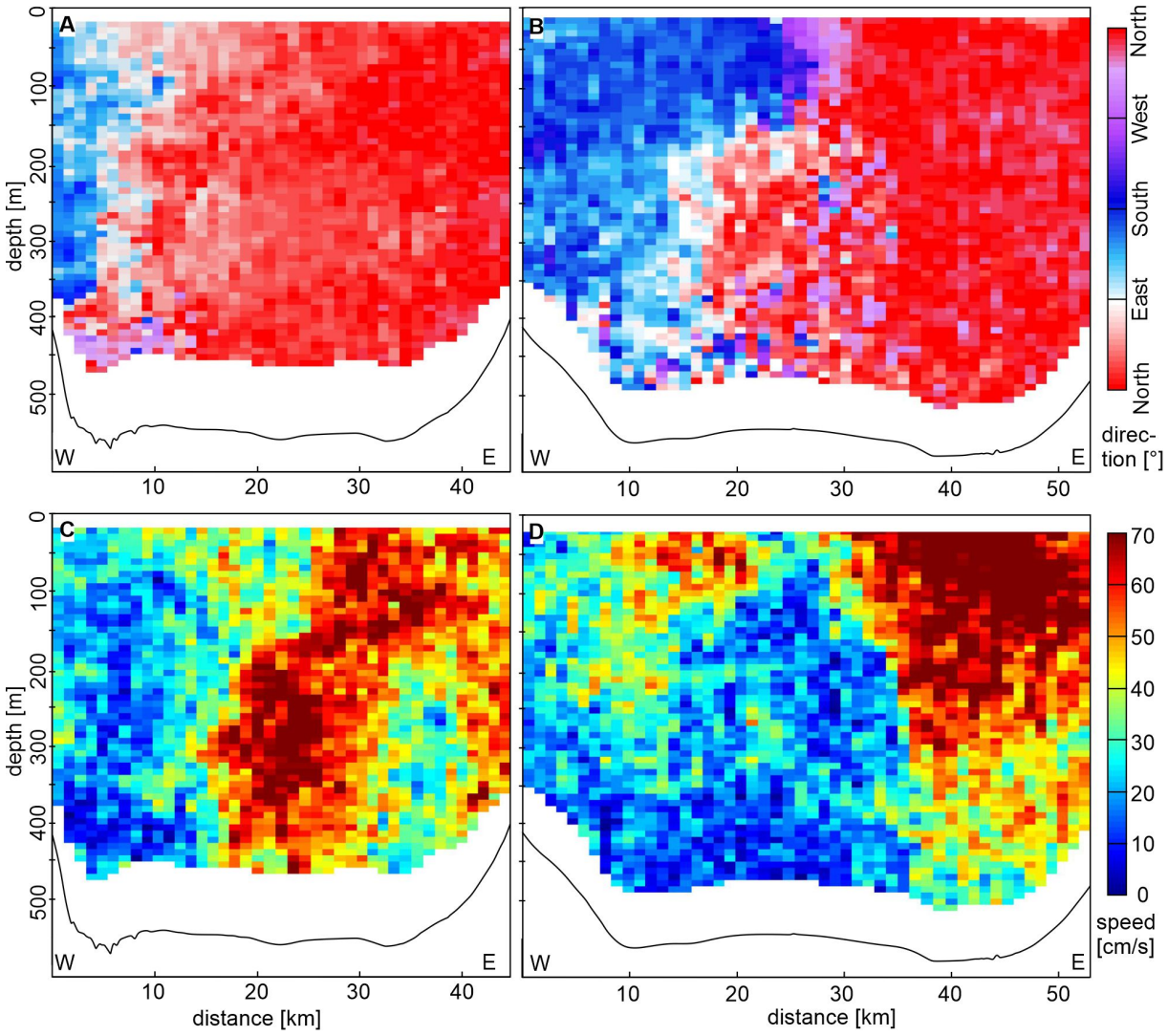

Figure 4.10: Cross-section of the Bahamas showing the measured flow direction at (A) southern part of the channel and (B) middle part of the channel and the measured flow speed at (C) southern part of the channel and (D) middle part of the channel. See Fig. 4.9 for location.

the first cross-section located at the southern side of the Santaren channel, the highest speed is situated in the middle of the channel and at the slope of the GBB (Fig. 4.10A,C). A second cross-section, located further to the north show higher speeds near the GBB (Fig. 4.10B,D).

4.5 Discusion

4.5.1 Classification of deep-sea elongated depressions

Different nomenclatures have been used for the elongated depressions that are formed by bottom currents. Faugères et al. (1999) introduced the terms 'moat channels' and 'drift levees'. Later the terms 'moat' and 'separated elongated mounded drift' were widely established (Rebesco, 2005; Rebesco et al., 2014). From our stratigraphic analysis, we suggest to subclassify 3 different main types of moats that can be distinguished based

on the termination location of the drift reflections. For the first moat stratigraphic type, reflections onlap at the slope side (Fig. 4.11A). They are classified as 'Constructional Moats' because they present an aggrading stacking pattern in the moat. This moat-drift system can also migrate up-slope. At this type of moat, the separated mounded drift has a pronounced drift crest (Betzler et al., 2014a; Zhao et al., 2015; Miramontes et al., 2016; Yin et al., 2019). However, the form of the drift crest is affected by the pre-existing morphology. For example, the drifts associated with a moat that form at a pre-existing slope will have a more pronounced drift crest (Miramontes et al., 2016) than the associated drifts that form on a flat surface, such as a terrace or the basin floor (Miramontes et al., 2019; Wilckens et al., 2021). For the second moat stratigraphic type, reflections downlap at the bottom of the moat (Fig. 4.4B). They are classified as 'Mixed depositional-erosional Moats' or in short 'Mixed Moats' because almost the same amount of sediment that is eroded is also deposited at the bottom of the moat (no erosion and no deposition occurs on average). Accumulation dominantly occurs at the drift alongside the moat. This moat-drift system mainly migrates laterally and does not show vertical aggradation at the moat trough. At the third moat stratigraphic type, reflections are truncated at the drift side (Fig. 4.11A). They are classified as 'Erosional Moats' because erosion is the dominant factor shaping the moat morphology. Here, no pronounced drift crest is present (Hernández-Molina et al., 2016c; Miramontes et al., 2021). It is possible that a moat transitions with time and/or in downstream direction into another moat type. Moats occur at erosive slopes (Hernández-Molina et al., 2016c; Wilckens et al., 2021) and non-erosive slopes (Wunsch et al., 2017).

Moats have often been described as erosive or non-depositional features (Hernández-Molina et al., 2006c; 2008; Ercilla et al., 2016; Yin et al., 2019; Miramontes et al., 2021; Chen et al., 2022). Miramontes et al. (2019) suggested that during energetic periods the sediment inside moats is eroded. During less energetic periods, the sediment can be deposited inside the moat. The balance between erosion and deposition determines the stratigraphy. This study shows that not all moats are erosive or non-depositional features. In fact, most moats (78%) considered in this study are Constructional Moats, which means that sediment is not only accumulated at the drift alongside the moat but also at the bottom of the moat. Based on these results it is hypothesised that on average most moats at present day are not erosive but rather formed by differential sedimentation; i.e. less sediment is deposited inside the moat compared to the separated elongated mounded drift alongside the moat.

Both moats and contourite channels are formed by contour currents. The elongated depression is defined as a moat when the drift reflections bend towards the deepest point of the moat (Fig. 4.11A-C). Alongside contourite channels no drift is formed and, thus,

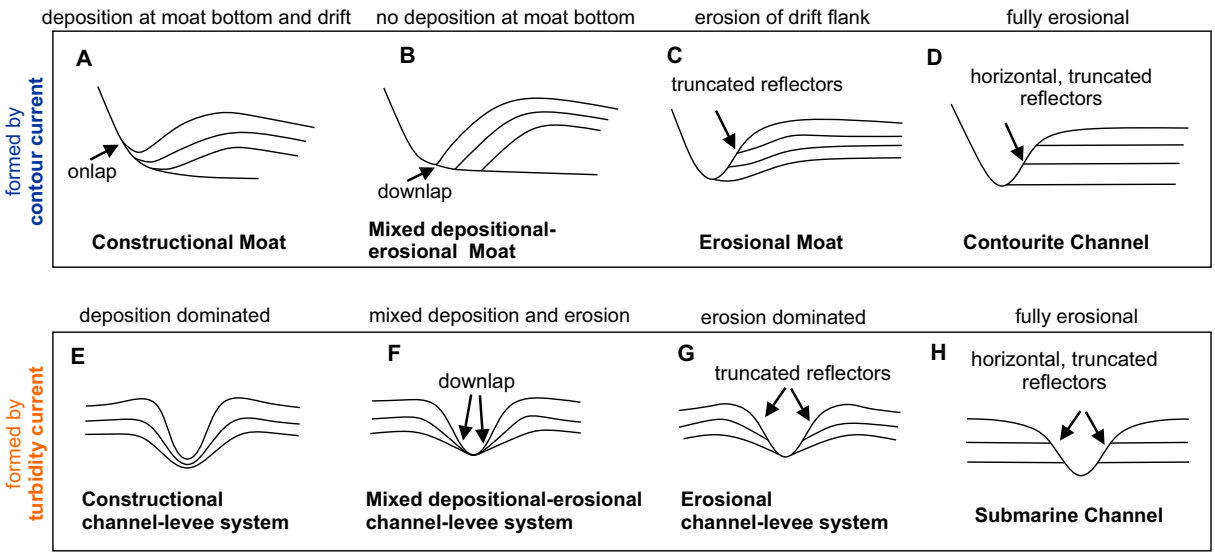

Figure 4.11: Nomenclature of elongated depressions in the deep sea based on seismic or sub-bottom profiler data. Three different stratigraphic types of moats: (A) Constructional Moat: Reflections onlap at the slope side; (B) Mixed Moat: reflections downlap at the bottom of the moat; (C) Erosional Moat: reflections are truncated at the drift side. (D) Similar to moats contourite channel are also formed due to contour currents, but they are more erosive and no pronounced drift crest is present. Three different stratigraphy types of leveed submarine channels (channel-levee systems) formed by gravity flows: (E) constructional channel-levee system, (F) mixed depositional-erosional channel-levee system, (G) erosional channel-levee system, (H) Submarine channel with no levees (adapted from Stow and Mayall, 2000 and Mulder, 2011).

no drift crest is present (Miramontes et al., 2021). Sometimes also other oceanic processes can form elongated depressions, this includes for example internal waves that propagate at density boundaries within the water column (Miramontes et al., 2020a); or several pockmarks that were formed by fluid seepage and then get eroded and thus elongated by bottom currents (Yu et al., 2021). These channels do not form alongside a slope break or an escarpment, but they occur on the slope without any topographic constraints. Similar to ocean driven currents, downslope flowing turbidity currents can also form elongated depressions that are called submarine channels and if sediment is overspilled at the channel walls, they form levees and are classified as channel-levee systems (Clark et al., 1992; Hiscott et al., 1997; Peakall et al., 2000; Deptuck and Sylverster, 2018). The channel forming a channel-levee system is here named submarine channel because it develops due to gravity driven flows (Clark et al., 1992; Hiscott et al., 1997; Peakall et al., 2000; Deptuck and Sylvester, 2018). They are subclassified in constructional (or depositional), mixed and erosional channel-levee systems based on the balance between deposition and erosion (Imran and Parker, 1998; Stow and Mayall, 2000; Mulder, 2011). Submarine channels that do not have associated leeves are fully erosive submarine channels (Fig. 4.11H) similar to contourite channels that do not have an an associated drift (Fig. 4.11D). Our suggested

nomenclature for the contour-current formed moats is adapted from the established subclassification for channel-levee systems and submarine channels (Stow and Mayall, 2000; Mulder, 2011) (Fig. 4.11E-H). The resembling nomenclature defines comparable stacking patterns observed in moats and submarine channels, despite the fact that the physical drivers behind the oceanographic and turbidity currents are different. In both cases, the current primarily transports sediment along the moat or channel and deposition rates are highest in the associated drift or levees.

4.5.2 Moat and contourite drift location

Moats are observed in many different settings distributed over the entire world's oceans and in lakes. However, regional studies show that moats are not observed at all slopes of contourite depositional systems (e.g. Miramontes et al., 2021; Wilckens et al., 2021). Thus, there must be additional factors that determine whether a moat can form at a specific location. One of these factors is the Coriolis force, which influences ocean circulation. On continental margins, moats can form where the Coriolis force is steering the current towards the slope (Faugères et al., 1999; Llave et al., 2001; Rebesco et al., 2014). Moats can be located in tectonically active areas like the Gulf of Cadiz (Llave et al., 2001; García et al., 2009), the Aegean Sea (Tripsanas et al., 2016) or offshore NW New Zealand (Steinbrick et al., 2020; Bailey et al., 2021). However, none of the moats analysed in this study are from a subduction zone (Fig. 4.1). One small moat is reported at the active area of the North Scotia Ridge (Nicholson et al., 2020). Active margins are shorter, steeper and contain 15% more canyons than passive margins and include shorter, steeper and more closely spaced submarine channels than passive margins (Harris and Whiteway, 2011). Furthermore, earthquakes that can trigger mass movements are common at active margins. Therefore, downslope processes occur more frequently at active margins and probably tend to overprint most moats. This might also be the case for Contourite Depositional Systems (CDSs) in general, which are predominant at passive margins (Rebesco et al., 2014). The failure that can be triggered by earthquakes and leads to a mass-wasting event is more likely to occur in contourites, particularly in plastered drifts, rather than hemipelagic sediment due to the convex geometry with steep slopes, but both types of sediments have similar mechanical properties (Miramontes et al., 2018). Nicholson et al. (2020) suggested that large drifts do also occur at active margins but are reshaped by downslope processes, which makes it difficult to identify them. In summary, only a few studies on contourites have been performed in active margins, but bottom currents also influence them. The resulting morphologies are often cannibalised by subduction processes, destroyed by tectonic processes, or removed or reworked by gravity-driven processes. This is likely the reason why along active margins a CDS cannot always be established, or current-related features are smaller because they are constrained to small-scale obstacles. More work is needed to understand the influence

of bottom currents on active margins and to determine the moat-drifts morphologies in these areas.

Moats are not only located along continental margins but also form around seamounts or other obstacles (e.g. cold-water coral mounds) in the ocean. Forcing from topographic barriers that can focus and intensify the current might also be involved in the moat formation. Examples are the Madagascar seamount moats (Miramontes et al., 2021) or a moat in the Mediterranean Sea (Llave et al., 2019). In the case of the Madagascar moat, the current is flowing through two seamounts (Miramontes et al., 2021) and in the case of the Mediterranean Sea moat, it is flowing through the Alboran Trough (Llave et al., 2019). These moats are often restricted to a relatively small area depending on the size of the topographic obstacle. At the Madagascar seamount, with a 20 km diameter, the moats are less than 25 km long. Around this large seamount two distinct moats form at each side, while around smaller seamounts (e.g. in the Gulf of Cadiz, with seamounts < 5 km in diameter), moats form all around the seamounts. The dimension of the seamount, the strength of the current and the latitude jointly influence sedimentation around seamount (Zhang et al., 2016). Additionally, moats that develop all around the seamounts might be linked to changes in current direction (e.g. driven by tides, mesoscale eddies). Without long-term current measurements or numerical modelling, it is difficult to conclude which process is dominant. At three seamounts in the Gulf of Cadiz, the moat closest to the shelf is wider and has a larger relief, while the moat that is on the side towards the basin is narrower and has a smaller relief. The uneven moat-drift system size might be related to more sediment being available on the landwards side of the seamount. Aspect ratio and drift angle are not affected by this. Previously, the uneven size of moats at seamounts was linked to the Coriolis force pushing the current towards one of the seamounts sides, which intensifies the current and leads to more erosion compared to the other side (Hernández-Molina et al., 2006c; Chen et al., 2022). However, both effects can explain all the here discussed examples and thus further data is needed to determine which process is dominant.

4.5.3 Factors influencing the moat and drift formation

Moats are formed by ocean currents, thus the information about the ocean current direction and speed that formed the moat and associated drift should be recorded in the morphology and stratigraphy. Untangling this information from other factors that affect moat development will only become possible after gaining a better understanding of what factors significantly influence moat development and how they affect them. The four moats considered in this study with ADCP data available show that the speed above the moats is higher compared to areas above the drift. This could mean that due to the higher transport capacity of strong currents more sediment is transported through

the moats compared to the surrounding area. This suggests that moats also play an important role in sediment transport. Our observations suggest that neither shape nor stratigraphic type depend only on the size of the moat. Furthermore, there is a wide range of aspect ratios for moats (Fig. 4.4A) and thus current speed alone cannot explain the development of moat-drift systems. Presumably, the development of moats is influenced by: 1. the steepness of the slope; 2. the geological and oceanographic setting; 3. the current velocity and velocity changes in time and space, and the Coriolis force and Rossby number; 4. sediment type and the amount of sediment that is transported by the currents. Furthermore, the influence of downslope transported sediment (Betzler et al., 2014a; Vandorpe et al., 2014) that can be deposited inside the moats like turbidites or mass transport deposits. An additional influence on moat shape can come from syn-sedimentary faults in the moat-drift system (Hernández-Molina et al., 2016c) or local eddies (Wilckens et al., 2021). Moats might also be influenced by internal waves propagating at density boundaries or by surface fronts in the ocean (Hernández-Molina et al., 2008; Nicholson and Stow, 2019). Furthermore, the statistical analyses of moat-drift systems confirm our hypothesis that moat morphology correlates with water depth. This might be because of the influence of sediment availability and limited accommodation space.

1. The statistical analyses indicate that the aspect ratio of moats correlates with the slope angle of the slope where the moat forms. More precisely, the steeper the slope, the larger the aspect ratio and the higher the drift angle. Thus, we suggest that the slope angle locally influences the along-slope current dynamics by affecting the across-slope velocity gradient and this controls the aspect ratio of moats. This correlation is not only shown by the analyses of 185 cross-sections, but also in the along-slope analyses of moats. Usually, when the slope angle changes in the downstream direction, the aspect ratio also changes. While the current flows along the slope, it needs time to adapt to changes in the slope. Thus, the adaptation in aspect ratio can only occur a couple of kilometres downstream (Fig. 4.7E). The amount of downslope transported sediment can affect the aspect ratio of moats but apparently this is usually not so significant that it overprints the effect of the slope angle on the moat development.

2. To further understand moat development, it is necessary to distinguish between 3 different environments: open slope, channel and topographic obstacle (Fig. 4.12). Moats can form at an open slope that is mainly affected by a current (e.g. Argentine margin). At the Argentine margin, the moats are widening in downstream direction. This might be also common at other open slopes but we currently do not have enough data to support and generalise this observation. Moats can form inside a channel with currents flowing in different directions (e.g. Santaren Channel). Here, the shape of the drift is possibly

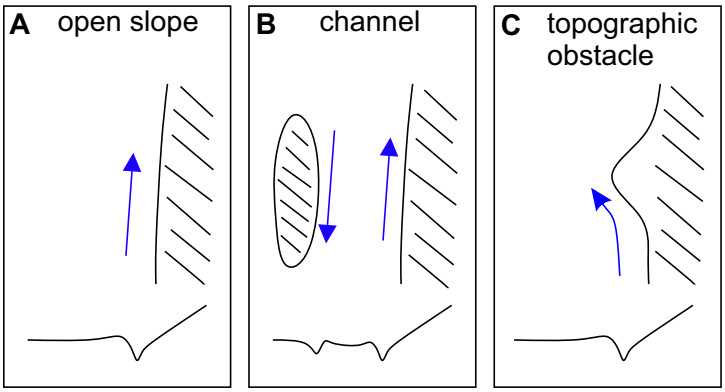

Figure 4.12: Sketches showing in plan view the main settings where moats form. Moats can form at an open slope that is affected by a current, they can form in a channel with currents flowing in different directions and they can form around topographic obstacles. Blue arrows indicate flow direction.

related to the strength difference of the two currents. In case of the Santaren Channel, the drift bends in the same way as the slope of the Great Bahamas Bank. This indicates that the northward flowing current that creates the Great Bahamas Bank moat is the strongest current and mainly responsible for the drift morphology. The VM-ADCP data also shows that the northward flowing current is stronger compared to the southward flowing current. At the southern side, the drift is very flat and not very mounded (Lüdmann et al., 2016). This indicates that the flow speed is higher here, which is also shown by the ADCP Data. Further downstream the current is adapting to the new hydrodynamic regime and morphological setting. Downstream, the current becomes more focused at the slope, and the drift gets more mounded (Fig. 4.10). The morphology can also be correlated with the discharge or volumetric flow rate of water depending on the speed of the current and the area of the cross-section through which the water can flow. As described by the continuity equation, this means that within one moat, the current velocity changes if the area of the cross-section changes. This link was shown for the moats in the Santaren Channel and the morphologic evolution could also be linked to the Gulf Stream that flows through the Florida Strait north of the study area (Paulat et al., 2019). Moats can also form around topographic obstacles. Here, the current has to adapt constantly to the changes in slope and thus is never in equilibrium with the morphology.

3. The importance of the Coriolis force in moat formation has been previously suggested (Faugères et al., 1999). Even though the Coriolis force strength depends on the latitude, there is no statistical correlation between latitude and size or aspect ratio of moat. Moats in very low latitudes ($<20°$) are in the presented analyses narrower and have a smaller relief than moats in higher latitudes ($>20°$). However, this is statistically not significant and should be further tested by numerical modelling. The Coriolis force also depends on the current speed, which is rarely known for moats and thus cannot be included in the

present analyses. The Rossby number (Ro=U/fL) is used to determine how important the Coriolis force is in a system (Davarpanah et al., 2020). The ADCP current speed measurements in this analysis show that the average speed above the moat is approximately $U = 0.25\,\mathrm{m/s}$ and the average moat width is 2300 m. Assuming that the average moat is at mid-latitudes (45° North or South) then the Coriolis frequency is $f = 0.0001\,\mathrm{rad/s}$ and together with the average moat width and average speed above moats, the Rossby number is 1. A small (<1) Rossby number indicates that the system is significantly influenced by the Coriolis force (Wells and Cossu, 2013). Contour currents that are in a geostrophic balance have by definition, a Rossby number of $Ro = 1$. Thus, the Coriolis force should play a role in moat development and moats should thus scale as $L \sim U \cdot f$. However, the data do not show a statistical dependence of moat parameters on the latitude, which indicates that other factors like the steepness of the slope at which the moat forms or current speed are so dominant that a small dependence on the Coriolis frequency cannot be recognized. New ADCP data can be used to properly scale the current flowing through the moat, similar to previous work about buoyant gravity currents (Lentz and Helfrich, 2002). As a next step, a multivariate analysis that includes current speed measurements inside and adjacent to moats is necessary to better understand how the Coriolis force affects moat development.

4. The slope angle only affects the aspect ratio, but the size and type of the moat is not constrained by the slope angle alone. Also, in the slope angle versus aspect ratio plot (Fig. 4.4J), we find some scattering of data points around a linear curve. Thus, other factors like current velocity and velocity gradient must be considered. We suggest that the size of the moat is controlled by the current speed and the horizontal velocity gradient (Fig. 4.13). Based on the ADCP current measurements, the bottom current is above 10 cm/s and below 1m/s, but the exact value cannot be given due to the limited current measurements above moats. For a moat to be formed, higher speeds must exist over the moat and lower speeds over the drift. One factor that influences this velocity gradient is the slope angle. Based on our combined results, we introduce a new moat formation concept that depends on current speed and slope angle. So far this is only a qualitative concept. We suggest that a current with low speeds at a gentle slope will not create a moat; while the same current at a steeper slope could create a moat. A fast current at a gentle slope can create a wide moat with a low aspect ratio (e.g. GBB moat); while the same current at a steeper slope would create a narrower moat with a higher aspect ratio. The slope angle is only one factor influencing the vertical speed gradient, another factor might be the interaction of two current with each other. One example is the interaction of the two currents in the Santaren Channel flowing in opposite direction.

5. Sediment supply and sediment type are most likely another important parameter influ-

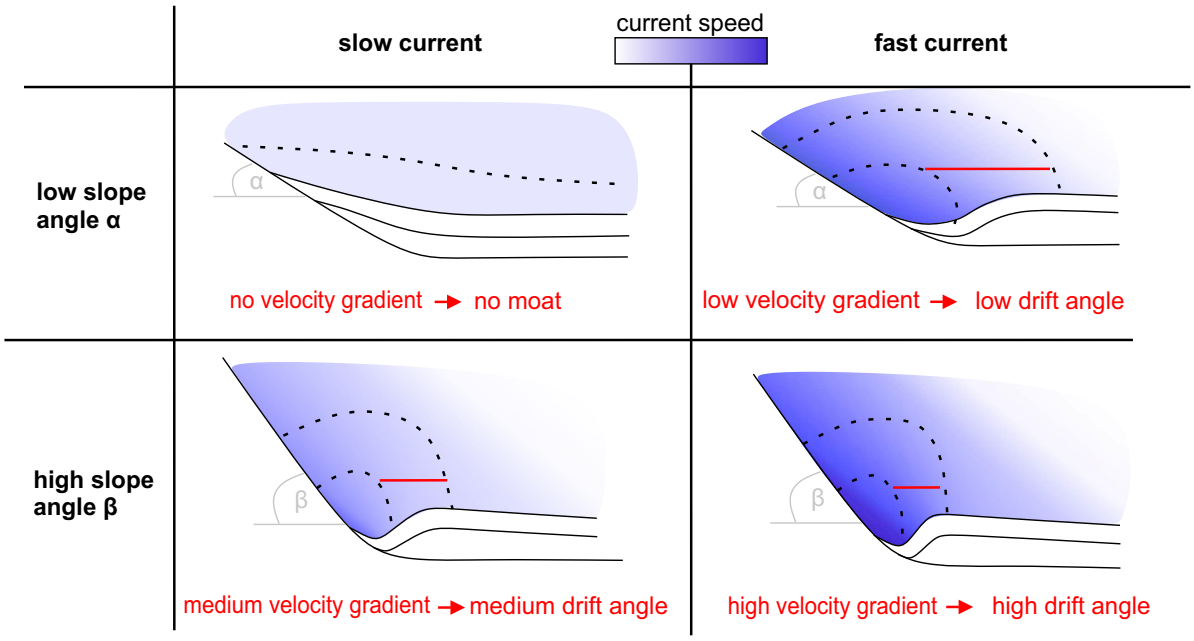

Figure 4.13: Conceptual model of how moats form under different slope angles and current velocities. Slope angles and current velocities together influence the current velocity gradient. The current velocity gradient then determines the drift angle and thus the shape of the moat.

encing the moat-drift system stratigraphy. The thickness of all constructional contouritic elements including Constructional Moats and the associated drift must depend on the sediment availability and current speed. Erosional features or non-depositional features must be connected to the absence of sediment availability and/or high bottom current speeds that allow only bypassing of the sediment. However, in this study, we could not quantify this effect. Possibly sediment consolidation and sediment composition can affect whether a moat becomes more flat-base or concave-up shaped. For future studies, we suggest using moorings with ADCPs and sediment traps to futher analyse the sediment transport and other possible oceanographic secondary processes such as internal waves, tides and vortices/eddies in moats.

4.6 Conclusions

This study provides a general comparison of 185 cross-sections from moat-drift systems distributed in 39 different parts of the oceans and lakes as well as a detailed analysis of six moat-drift systems that cover a wide range of typical geological and hydrodynamic settings. Additionally, measured current data from four moats were analysed to better understand the hydrodynamics. This allows us to propose a general conceptual model of moat-drift system morphology and stratigraphy and what parameters influence their development. The conclusions can be summarized as follows:

- Based on the measurements of 185 cross-sections, we determined the parameters that are common for moats. The median moat cross-section has a 50 m relief, 2.3

width, 0.022 relief-width ratio, 6° slope angle and 3° drift angle.

- Three main types of moats can be distinguished based on their stratigraphy. Constructional Moat where reflections onlap at the slope side; Mixed Moat where reflections downlap at the bottom of the moat and Erosional Moat where reflections are truncated at the drift side. We suggest that some moats are driven by sediment erosion while others primarily exist due to differential sedimentation, meaning, less sediment is deposited inside the moat compared to the separated elongated mounded drift alongside the moat. From this study (at present day), 78% of the moats are Constructional Moats and are thus formed due to uneven sedimentation without erosive features.
- The Coriolis force has a significant control over the general ocean circulation. Its strength is dependent on the latitudes and current speed. However, our statistical analyses show no statistically significant correlation between latitude and the shape and size of moats. Thus, a multivariate analysis that includes more current speed measurements is necessary to determine better how the Coriolis force affects moat development.
- Our measurements from moats show a correlation between slope angle (adjacent to the emplacement of the moat) and drift angle. We interpret that the current is locally focused and intensified due to the steepness of the adjacent slope. This agrees with the measured current data. We hypothesize that a steeper slope focuses the current, resulting in a higher velocity gradient across the moat, which then leads to a steeper drift. Thus, the slope angle indirectly controls the drift angle and thereby the moat morphology. This clearly shows how the pre-existing morphology affects the ocean currents and associated sedimentation patterns.

4.7 Data availability

The seismic data of this study from the ET Moat 2 offshore Argentina are available from the corresponding author upon reasonable request. The measured parameters from moat-drift systems for the statistical analyses are available on PANGAEA (Wilckens et al., 2023; `https://doi.org/10.1594/PANGAEA.955053`). For all other data, sharing is not applicable to this article as it was previously published, and references are listed in Table 4.4 of the supplementary material.

4.8 Acknowledgments

We thank the captains, crews and onboard scientific teams for their work during cruise SO260 on bord R/V SONNE 2018, cruise PAMELA-MOZ2 onbard R/V L'Atalante in 2014, cruise PRISME2 onbard the R/V L'Atalante and cruise PRISME3 onboard the R/V Pourquoi pas? in 2013, cruise M95 onboard the R/V Meteor in 2013, cruise M84/4

onboard the R/V Meteor in 2011, R/V Meteor cruise M78/3 in 2009, cruise CADIPOR 1+2 onboard the R/V Belgica in 2002 and 2005 and cruise M49/2 onboard the R/V Meteor in 2001. The PAMELA-MOZ2 cruise was co-funded by TOTAL and IFREMER as part of the PAMELA project. The PAMELA (Passive Margin Exploration Laboratories) project is a scientific project led by IFREMER and TOTAL in collaboration with Université de Bretagne Occidentale, Université Rennes 1, Université Pierre and Marie Curie, CNRS and IFPEN. This study was carried out in collaboration with "The Drifters" Research Group at Royal Holloway University of London (RHUL). We thank TGS for their permission in using the seismic profile fragment for the Álvarez-Cabral Moat in Figure 4.6c. We thank Ellen Unland (University Bremen) for processing the seismic data from the ET Moat 2 offshore Argentina. We thank the reviewers Uisdean Nicholson and Mathew Wells, Associate Editor Jeff Peakall and Chief Editor Piret Plink-Björklund for their constructive comments that greatly improved our manuscript.

4.9 Supplementary material

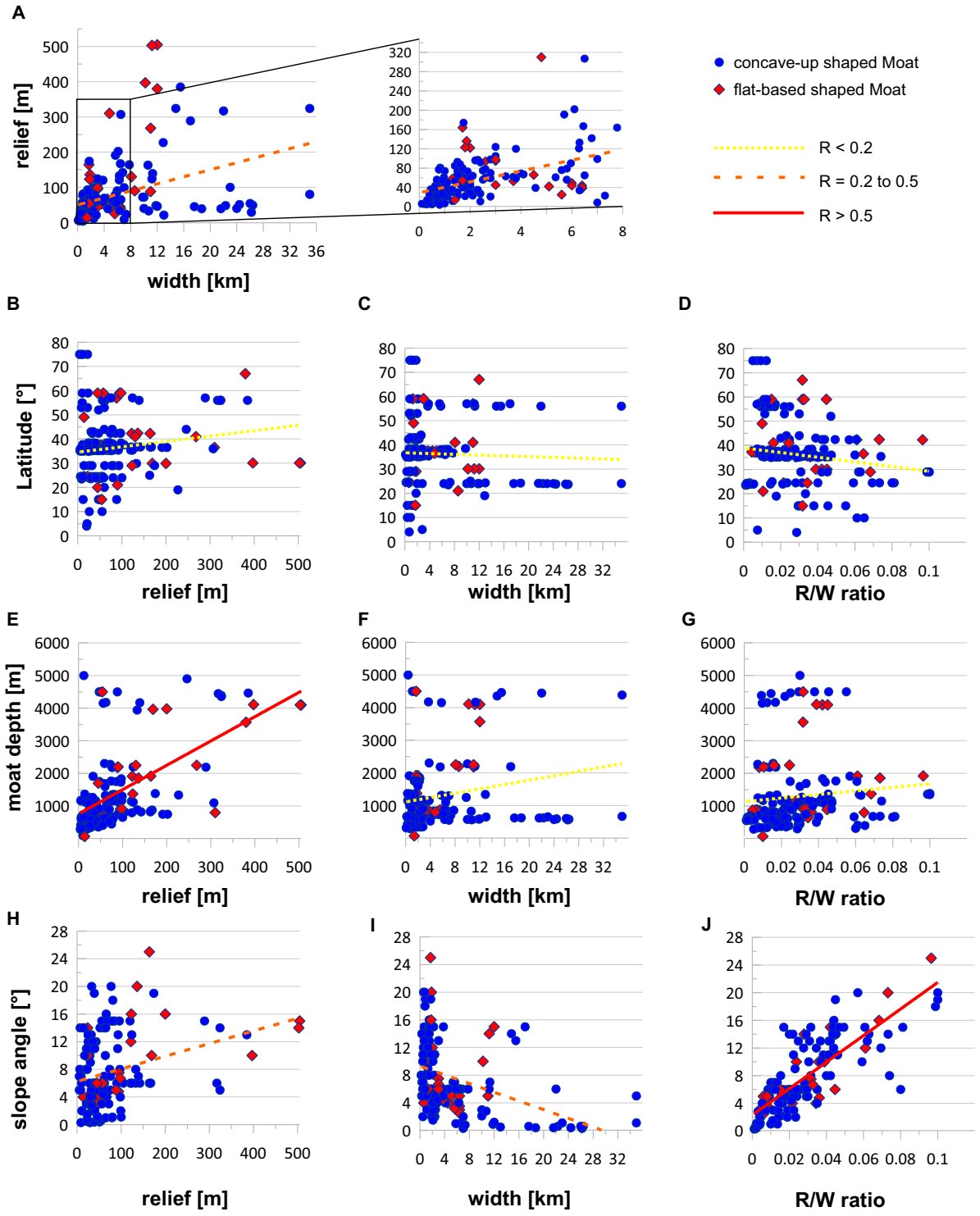

Figure 4.14: Diagrams showing correlations between (A) width and relief, (B) relief and latitude, (C) width and latitude, (D) relief-width ratio and latitude, (E) relief and moat water depth (F) width and moat water depth, (G) relief-width ratio and moat water depth, (H) relief and and slope angle, (I) width and slope angle and (J) relief-width ratio and and slope angle.

Table 4.4: Contourite moats reported in the literature from locations all over the world considered in this study (see Fig. 4.1) and key data used to quantify moat parameters.

NR	**Key reference**	**Location**	**Measured from**
1	Rebesco et al. 2016	NW Barents Sea	Figure
2	Masson et al. 2002	North Rockall Trough	Bathymetry EMODnet
3	Roberts 1974/Jones et al. 1994	Rockall Trough (Seamount)	Bathymetry EMODnet
4	Hebbeln et al. 2016	North Atlantic (Ireland)	Figure
5	Sivkov et al. 2002	Baltic Sea	Figure
6	Liu et al. 2020	Gulf of Biscay	Figure
7	Haberkern 2017/Hanebuth et al. 2015	North Atlantic (Galicia)	Bathymetry MBES
8	Hernández-Molina et al. 2016c	Gulf of Cadiz	Figure
9	García et al. 2009	Gulf of Cadiz	Figure
10	Vendorpe et al. 2014	Gulf of Cadiz	Bathymetry MBES
11	Vendorpe et al. 2014	Gulf of Cadiz	Figure
12	Verdicchio and Trincardi 2006	Mediterranean Sea (Adriatic Sea)	Figure
13	Martorelli et al. 2010	Mediterranean Sea (Adriatic Sea)	Figure
14	Miramontes et al. 2019	Mediterranean Sea (Balearic Sea)	Figure
15	Miramontes et al. 2016	Mediterranean Sea (Tyrrhenian Sea)	Bathymetry MBES
16	Ercilla et al. 2016/Llave et al. 2020	Mediterranean Sea (Alboran Sea)	Figure
17	Palomino et al. 2011	Mediterranean Sea (Alboran Sea)	Figure
18	Tripsanas et a. 2016	Mediterranean Sea (Aegean Sea)	Figure
19	Micallef et al. 2016	Mediterranean Sea (Strait of Sicily)	Figure
20	Acosta et al. 2005	Canary Islands, eastern Atlantic (Lanzarote)	Bathymetry EMODnet
21	Lüdmann et al. 2016	Santaren Channel (Bahamas)	Bathymetry MBES
22	Mulder et al. 2019	Santaren Channel (Bahamas)	Figure
23	Betzler et al. 2013	North Indian Ocean (Maldives)	Figure
24	Luedmann et al. 2013	North Indian Ocean (Maldives)	Figure
25	Yin et al. 2019	China Sea	Figure
26	Zhao et al. 2015	China Sea	Figure
27	Palamenghi et al. 2015	China Sea	Figure
28	Juan et al. 2018	Pacific Ocean (Clarion-Clipperton Zone)	Figure
29	Haberkern 2017	South Atlantic (Angola, Anna Ridge)	Figure
30	Miramontes et al. 2021	Mozambique Channel (Mozambique)	Figure
31	Miramontes et al. 2021	Mozambique Channel (Madagascar)	Bathymetry MBES
32	Wilckens et al. 2021	South Atlantic (Argentina)	Bathymetry MBES
33	Uenzelmann et al. 2017	South Atlantic (Argentina)	Figure
34	Gruetzner et al. 2016	South Atlantic (Argentina)	Figure
35	Nicholson et al. 2019	Drake Passage	Figure
36	GeoMapApp (V1807, RC1606, RC1503)	Drake Passage	Bathymetry GEBCO
37	Steinbrick et al. 2020	Pacific Ocean (New Zeeland)	Figure
38	GeoMapApp (ELT27)	Indian Ocean (Antarctica)	Figure
39	Gilli et al. 2004	Lago Cardiel (Lake in Argentina)	Figure

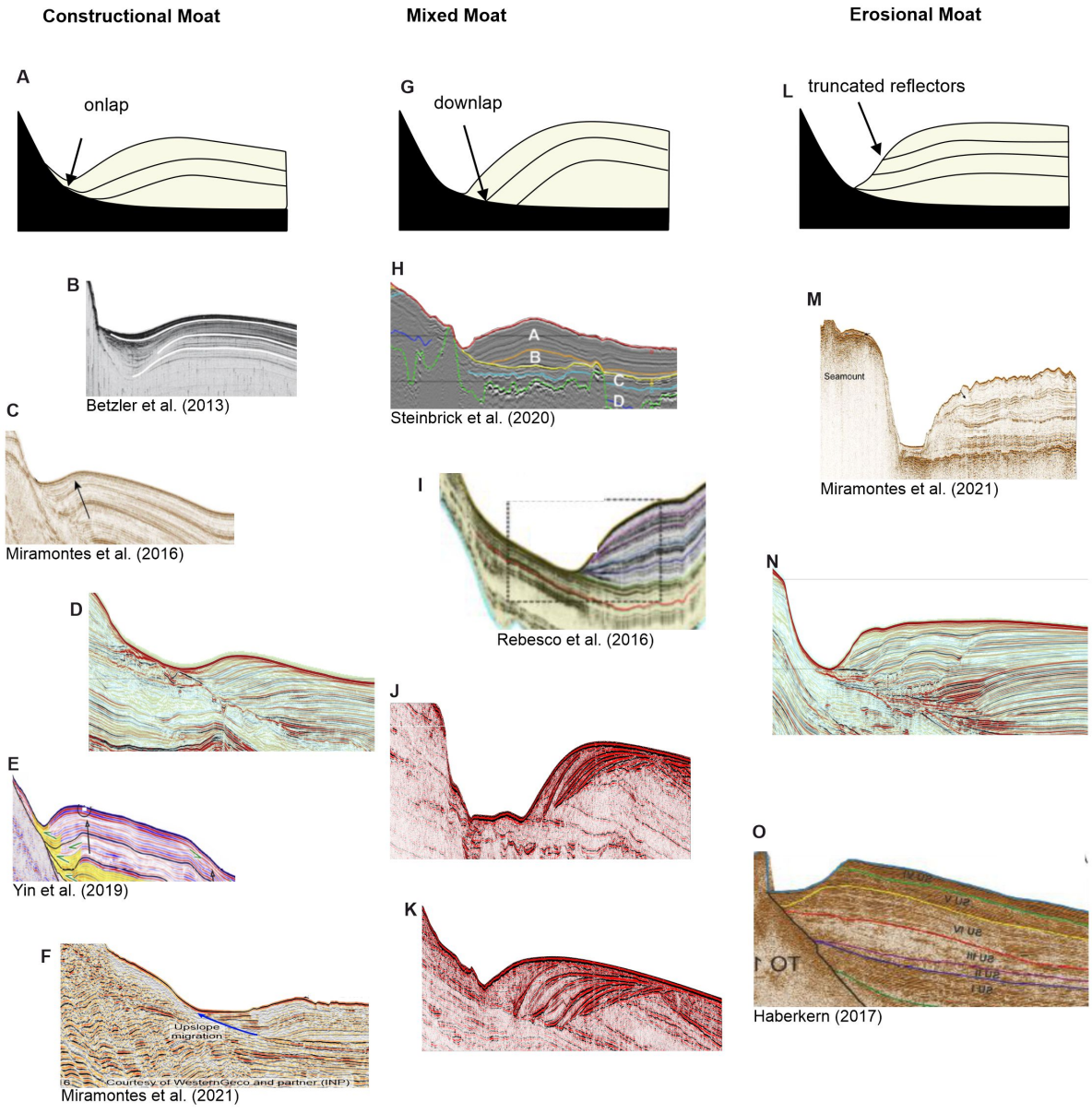

Figure 4.15: Classification of moat-drift systems. (A-F) Constructional Moats; (G-K) Mixed Moates; (L-O) Erosional Moats.

Chapter 5

First flume tank experiments with a self-emerging contourite system demonstrate conditions necessary to form moat-drift-systems

Submitted to Communications Earth & Environment, 23 January 2023 (under review)

Henriette Wilckens [a,b], Joris T. Eggenhuisen [c], Pelle H. Adema [c], F. Javier Hernández-Molina [d], Ricardo Silva Jacinto [e], Elda Miramontes [a,b]*

a Faculty of Geosciences, University of Bremen, Bremen, Germany.

b MARUM - Center for Marine Environmental Sciences, University of Bremen, Germany

c Faculty of Geosciences, Utrecht University, P.O. Box 80021, 3508 TA Utrecht, Netherlands

d Department of Earth Sciences, Royal Holloway University of London, Egham, Surrey, UK

e UMR 6538 GEO-OCEAN, Ifremer, Univ Brest, CNRS, Univ. Bretagne-Sud, France

* Corresponding author: Henriette Wilckens: cwilcken@uni-bremen.de

Keywords: Geomorphology; Contourite drift; Bottom current; Sedimentary processes; Sediment transport; Moats

5.1 Abstract

Ocean currents control seafloor morphology and the transport of sediments, organic carbon, nutrients, and pollutants in deepwater environments. A better connection between sedimentary deposits formed by bottom currents (contourites) and hydrodynamics is necessary to improve reconstructions of paleocurrent and sediment transport pathways. For the first time, the morphology and hydrodynamics of a self-emerging contourite system were analyzed in a three-dimensional flume tank. The sedimentary features that developed on a flat surface parallel to a slope are an elongated depression (moat) and an associated sediment accumulation (drift). The moat-drift system can only form in the presence of a secondary flow near the seafloor that transports sediment from the slope toward the drift. The secondary flow increases with higher speeds and steeper slopes, leading to steeper adjacent drifts. This study shows how bottom currents shape the morphology of the moat-drift system and highlights their potential to be used as paleo-velocimeter.

5.2 Introduction

Oceanic currents play an important role in climate and ecosystems and can strongly impact sedimentation and seafloor morphology in deepwater environments. These currents transport sediment, microplastics, and organic matter (Hebbeln et al., 2016; Kane et al., 2020). Establishing a conceptual model that integrates the current dynamics and the morphology of a contourite system can help to understand the sediment transport pathways and how that affects the ecosystem. Ocean currents will be modified under the present climate change (Voosen, 2020). Predicting how these currents evolve under different climatic situations could be improved by understanding how the ocean system changed in the past. Paleoreconstructions of ocean currents can be performed by analysing contourites, which are the sediment accumulations that have been substantially affected by currents flowing near the seafloor (i.e. bottom currents) (Rebesco et al., 2014). Paleocurrent information can be obtained from grain size analyses of sediment cores and of the internal sediment architecture using seismic data (Hernández-Molina et al., 2014; Uenzelmann-Neben et al., 2017; McCartney, 1982; McCave et al., 1995; McCave, 2017). However, our poor understanding of linking hydrodynamic processes with contourite features limits the integration of seismic data for quantitative paleoceanographic reconstructions (Miramontes et al., 2021). Thus, current speed reconstructions are mostly based on grain size of samples from sediment cores (McCave et al., 1995; McCave, 2017; Wu et al., 2021), or only provide rough estimates depending on the observed bedforms (Stow et al., 2009). Sediment cores only provide very local information and spacing between cores often exceeds the size of architectural elements within a contourite system. Combining core data with regional data sets, which can be obtained from bathymetric and seismic data, improves paleoceanographic interpretations (Stow and Smillie, 2020). Furthermore, velocity

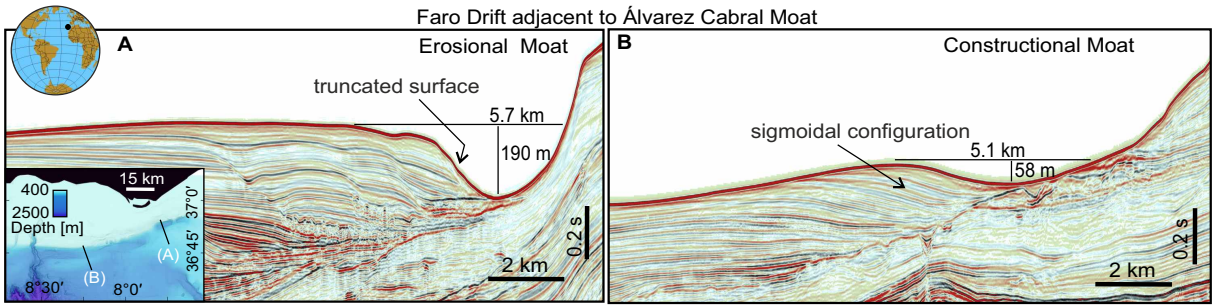

Figure 5.1: Moat-drift systems show a large variety in terms of morphology and seismic stratigraphy. The figure shows a seismic cross-section of the Álvarez Cabral Moat in the Gulf of Cadiz located (A) upstream and (B) downstream of the bottom current.

measurements from bottom currents in the deep sea are very scarce (de Lavergne et al., 2016), due to the depth limitations of vessel-mounted acoustic currentmeters (commonly upper ∼1000 m of the ocean) (Wilckens et al., 2021; Frey et al., 2021) and the logistics and economic costs of maintaining moorings in deep-water environments. In contrast, multibeam bathymetric data is much more frequently collected in the deep sea nowdays. Thus, a stronger understanding of the link between bathymetry and ocean currents would help to understand today's current dynamics and possibly help to suggest where focused measurements are needed to reveal the spatial variability of bottom currents.

In this study, we analyze the processes that control the development of a contourite depositional system that consists of an elongated depression parallel to a submarine slope, called a 'moat', and an associated sedimentary deposit named an 'elongated and separated mounded drift' that forms seaward and parallel to the moat (Rebesco et al., 2014; Miramontes et al., 2021). These systems show high variability in terms of width and depth as well as seismic stratigraphy (Fig. 5.1). Moat-drift systems provide a clear indication of the dominant bottom current direction, which is useful for reconstructing bottom currents (Surlyk and Lykke-Andersen, 2007; Betzler et al., 2013; Hernández-Molina et al., 2014). However, the characteristics of the current, in terms of strength and local hydrodynamics, can presently not be deduced from the moat and drift characteristics (Miramontes et al., 2021; Wilckens et al., 2021; Zhang et al., 2016; Hernández-Molina et al., 2008). Moats have been interpreted to have formed at the location of the velocity core of the current (Miramontes et al., 2020a; Wilckens et al., 2021). Several authors have hypothesized a helicoidal flow structure over the moat, but the suggested spin direction differs between authors (Gong et al., 2017; Rebesco et al., 2014; Hernández-Molina et al., 2008). The helicoidal concept has not been supported by measurements or theory yet, and it remains unclear whether such a structure is a necessary condition for the emergence of moats, or whether it forms as a result of hydrodynamic interaction between existing moats and active contour currents. Vessel-mounted acoustic doppler current profiler data could so

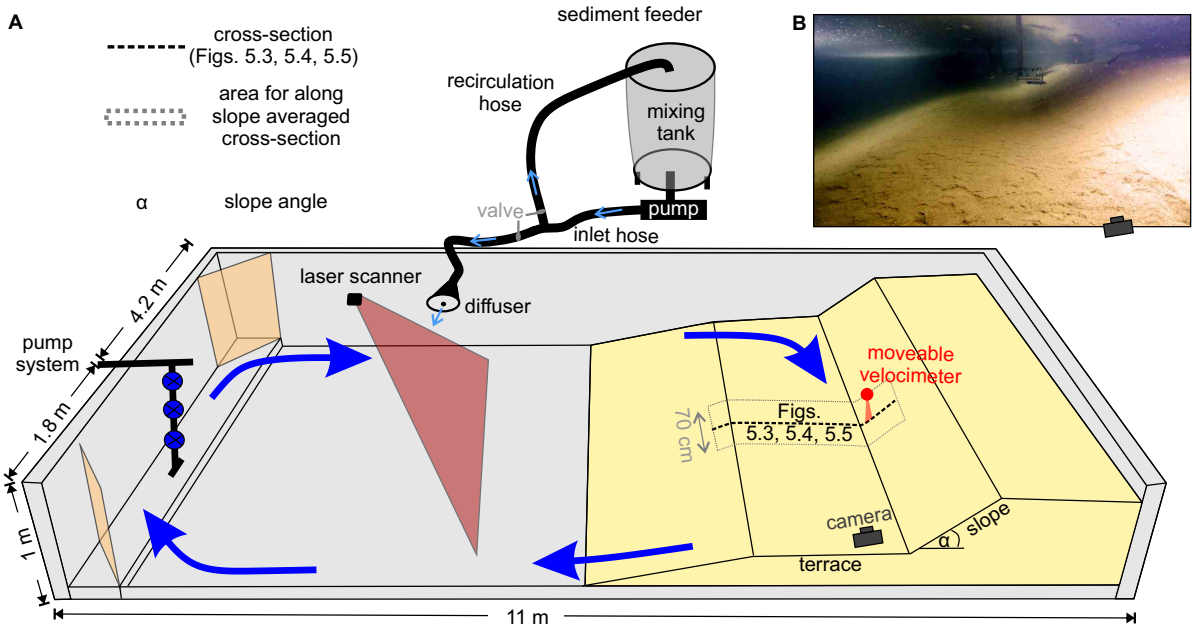

Figure 5.2: Experimental setup. (A) Schematic drawing of the experimental setup (modified from Miramontes et al., 2020b). (B) Underwater photo of the flume tank floor and the velocimeter.

far not confirm the existence of a helicoidal flow over moats, but this could be due to the poor resolution near the seafloor, and the rare collection of data over moats (Wilckens et al., 2021).

This study presents the first analysis of a contourite depositional system developed in a 3D flume tank (EUROTANK) at Utrecht University (Fig. 5.2). We focus on a contourite depositional system that consists of a moat and a separated mounded drift. A circulation system generates a current flowing parallel to the slope of the tank, as an analog for a contour current flowing parallel to a continental margin. For the analysis of the bathymetric evolution of the contourite system, we calculate the average along-slope elevation of a 70 cm wide swath in the middle of the tank (Fig. 5.3) and plot the data as one cross-section (Fig. 5.3). This procedure averages out the bathymetric perturbations of un-scaled ripples (Fig. 5.2B). The analyses of the contourite depositional system that develops in the flume tank test the following hypotheses: 1) moats and drifts migrate upslope with higher sediment availability; 2) the morphology of moats and drifts depends on current speed; and 3) there is a secondary across-slope flow in the moat-drift system that depends on the along-slope velocity and the steepness of the continental slope.

5.3 Materials and methods

The experiments are conducted in a 6*11*1 (width*length*depth) m flume tank. The floor morphology consists of a gentle lower slope (not part of the study area), a flat ter-

race, and an upper slope of 18° or 26°. The morphology is built out of sediment and then covered by artificial grass. The artificial grass stabilizes the morphology that forms the base of each experiment. The artificial grass is covered before the first experiments by a thin 1.5 cm layer of walnut shells and for experiments 2-6 by a 0.5 cm layer. Based on this starting morphology, we conduct different experiments. We removed all added walnut shells after each experiment.

During the experiments, 3 pumps created a current flowing clockwise in the tank and parallel to the slope at the study zone, which is an analog to a contour current flowing parallel to a continental margin (similar to Miramontes et al., 2020b). Since the Earth rotates, ocean currents are affected by the Coriolis force. In the lab, the size of the experiment is too small for the Coriolis force to have a significant effect. For gravity-driven currents a rotating flume tank has been used in previous studies (Wells and Cossu, 2013; Lentz and Helfrich, 2002). For contour currents, we use a current flowing in a circular motion. Run-up against the slope provides a barotropic pressure gradient that forces the radial acceleration of the circulation. We consider this a simplified analogue to the Coriolis effect in a natural system. A UDOP 4000 velocimeter measures the velocity during the experiments. One 1 MHz probe is the emitter, and three probes are used as receivers to record the velocity in 3D along a vertical line. The three velocity components (x,y,z direction) were measured simultaneously. The UDOP was positioned ∼15 cm above the bed at the beginning of the experiment. In the first 5 cm near the emitter, the data quality is poor and the data is not usable. The velocity measurements shown in Fig 5.4 were carried out within the first 20 minutes of the experiments, which is before the moat-drift system was established. For the across-slope profile, the velocity was measured for 2 min, and then the UDOP was moved horizontally by 5-10 cm. After the data was collected the measurements at each location of the cross-section were combined and interpolated in MATLAB. When the velocity was not measured, the instrument was located in the middle of the tank to ensure that it cannot influence the current- and morpho-dynamics of the study area.

In the experiments, two phases are distinguished. One is the sediment input phase where sediment is added and the other is the sediment reworking phase where no sediment is added. In the first experiment, the first sediment input phase is 3 h, the reworking phase is 8 h and the second input phase is 7 h. In experiments 2-6, the sediment input phase is 3 h, and the reworking phase is 4 h. During the beginning of the sediment input phase, a pump on the side of the flume tank pumped water mixed with 80 dm3 of crushed walnut shells of a volume concentration below 2% for 2 h in the flume tank. The particles are transported to the study site by the contour current and start to settle on the study site. The contour current reworks the previously deposited walnut shells. Contourite drifts are

often composed of fine-grained sediments (Rebesco et al., 2014; Miramontes et al., 2021). Previously walnut shells were used as an analog for mud in estuaries (Ganti et al., 2016). The experiments were conducted with crushed walnut shells with a grain size range of 200 - 450 μm and a density of 1350 kg/m^3. We use walnut shells as an analog for silt because similar current speeds transport the particles as bedload. The advantage of the coarse walnut shell over the fine silt is that the settling velocity is higher due to the larger diameter, which allows us to run the experiments in a smaller setup. The crushed walnut shells are then transported as bedload similar to silt because they are coarser but have a lower density. The particles start to settle on the study site, which consists of a slope and a flat terrace. A laser scanner measures the bathymetry in the flume tank, after draining the tank, every 2 mm with a swath width of 50 cm on pre-defined across-slope profiles. The data result in a bathymetric map with a grid cell size of 5 mm.

5.4 Results

5.4.1 Morphological evolution

All six experiments start with the same terrace and slope (with a slope gradient of 18° or 26°). In all experiments, we distinguish between two phases. In the sediment input phase of the experiments, 80 dm^3 of sediment is added with the sediment feeder. In the reworking phase, the sediment is reworked by the flow while no extra sediment is added to the flume tank.

Experiment 1 shows how the morphology evolves in response to changes in the sediment

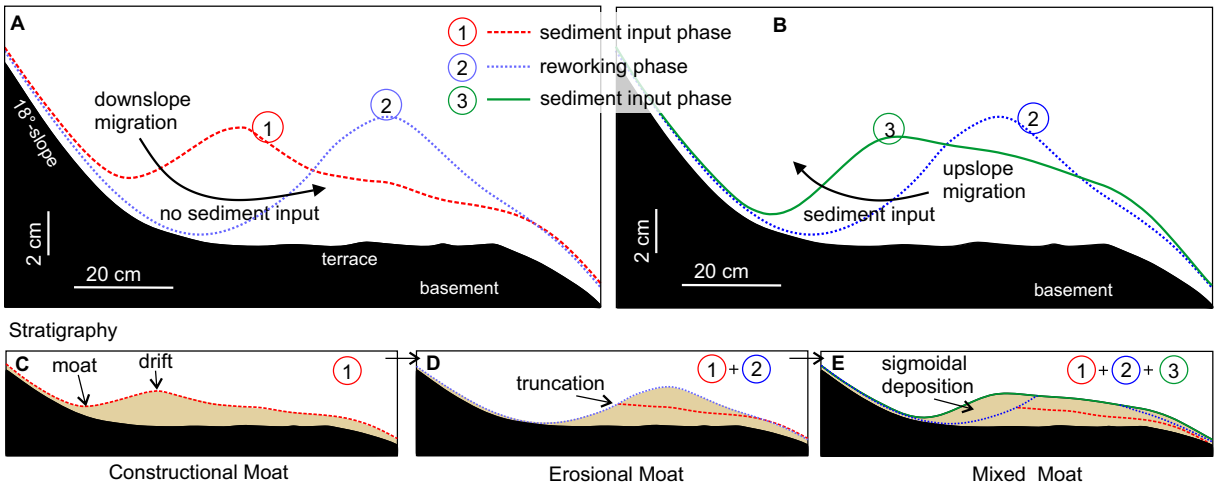

Figure 5.3: Comparison of moat-drift migration without and with sediment input. Measured cross-sections from moat-drift systems show that (A) a moat migrates downslope when no sediment is available and (B) a moat can migrate upslope when sediment is supplied. (C) The moat self-emerges after the sediment input phase. (D) Stratigraphy of a moat with no sediment input. (E) Stratigraphy of a moat with phases with and without sediment input. The stratigraphy is compiled from the measured bathymetry. The location of the cross-sections is shown in Fig. 5.2.

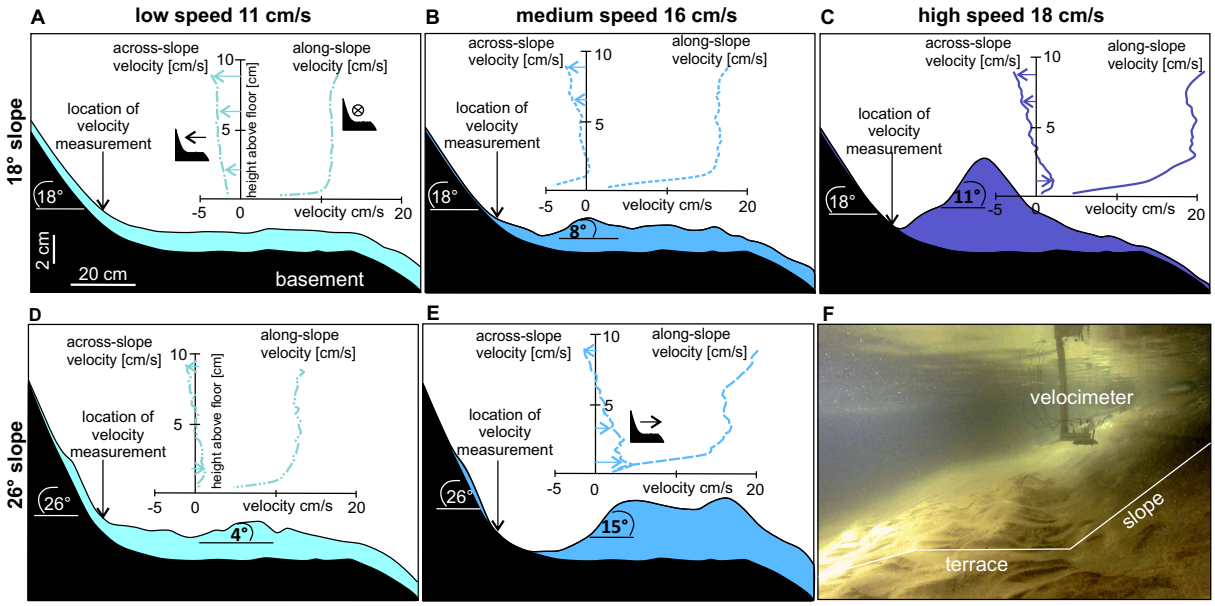

Figure 5.4: Comparison of moat-drift systems developed at a gentle and a steep slope with different velocities shows that steep slopes and faster currents lead to a steep drift. (A) Measured cross-sections showing aggradation. (B-E) Measured cross-sections from moat-drift systems show that the morphology depends on current speed and slope gradient. Additionally, the graph shows the along-slope and across-slope velocity measured at the lower slope. Positive across-slope velocities correspond to a current flowing away from the slope. (F) Underwater photo of the moat-drift system in the flume tank that developed with a current speed of 18 cm/s and a slope angle of 18°. The location of the cross-sections is shown in Fig. 5.2.

input (Fig. 5.3). In the first phase, sediment was added to the tank and transported to the study area by an 18 cm/s current. This leads to an elongated depression parallel to the 18° slope (a moat) and an adjacent elongated mounded drift basinward (Fig. 5.3A). The moat migrates downslope in the second phase of the experiment, during which no sediment was supplied (Fig. 5.3A). In the third phase, sediment was supplied again, and the moat migrated upslope due to formation of a sigmoidal deposit (Fig. 5.3B).

In experiments 2-4, the moat-drift system develops at an 18° slope with different current velocities. Three velocities were tested with the same slope-terrace setup. The experiments consist of one sediment input phase and a subsequent reworking phase. After a moat-drift system formed, we measured the width between the drift crest and the slope, relief (depth between moat trough and drift crest), and drift angle (slope angle of the drift on the side of the moat) (Table 5.1). In experiment 2, with a low speed of 11 cm/s, sediment drapes the slope and terrace, but no moat develops even after an extra 9 h of sediment reworking (Fig. 5.4A). In experiment 3, with a medium speed of 16 cm/s, a small moat develops with a drift angle of 8° (Fig. 5.4B). A faster current speed of 18 cm/s in experiment 4 creates a larger moat with a higher drift angle of 11° (Fig. 5.4C), compared to experiments 2 and 3, which have lower current speed.

Table 5.1: Summary of flume tank experiments

Fig. 5.4	Slope angle [°]	Velocity [cm/s]	Moat width [cm]	Moat relief [cm]	Moat aspect ratio	Drift angle [°]
A	18	11	-	-	-	-
B	18	16	28.5	1	0.04	8
C	18	18	42.5	3.8	0.09	11
D	26	11	44.0	1.1	0.02	4
E	26	16	47.0	3.6	0.08	15

Experiments 5 and 6 are similar to experiments 2-4 with input and reworking phases but the slope increased to 26°. Here, two different current speeds were tested (Table 5.1). In experiment 5, with a low current speed of 11 cm/s, a small moat with a drift angle of 4° develops (Fig. 5.4D). In experiment 6, the drift angle increases to 15° when running the experiment with a stronger current of 16 cm/s speed (Fig. 5.4E).

5.4.2 Current velocity measurements

The velocity was measured at the base of the slope at the lowest 10 cm above the bed (Fig. 5.4A-E). All velocity measurements presented in Fig. 5.4 were carried out at the beginning of the experiment meaning before the moat-drift system was established. For analysing the velocity in three dimensions, we look at the speed component in along, across and vertical directions. For all experiments, the velocity is strongest along slope (making this the primary flow). For the low current speed setting with the 18° slope, there is a small secondary flow towards the slope. For the other settings, with a stronger along-slope velocity or a steeper slope, the direction of the secondary flow depends on the distance above the bed. In the secondary flow (vertical plan across-slope), the velocity at ∼5 cm above the bed is directed towards the slope but in the lowest ∼5 cm above the bed, the bottom current is flowing away from the slope (Fig. 5.4 B-E).

Across-slope velocity measurements, carried out during the first hour of the experiment with the fastest current setting and a slope angle of 18°, show that the along-slope velocity is higher near the slope and decreases on the terrace (Fig. 5.5A). At the beginning of the experiments in the first 5 cm above the bed on the lower slope, the across-slope velocity is directed away from the slope and the current is flowing over the terrace towards the basin (Fig. 5.5B). At approximately 5-10 cm above the bed, the across-slope velocity is directed towards the slope (Fig. 5.5B). Furthermore, at the lower slope, the vertical velocity is directed downwards and at the basinward side of the terrace, it is directed upwards (Fig. 5.5C). After the moat-drift system self emerged, the velocity was measured again (Fig. 5.5D-E). The velocity increased over the area above the moat compared to the measurements before the moat formed. The velocity is higher over the moat and decreases over

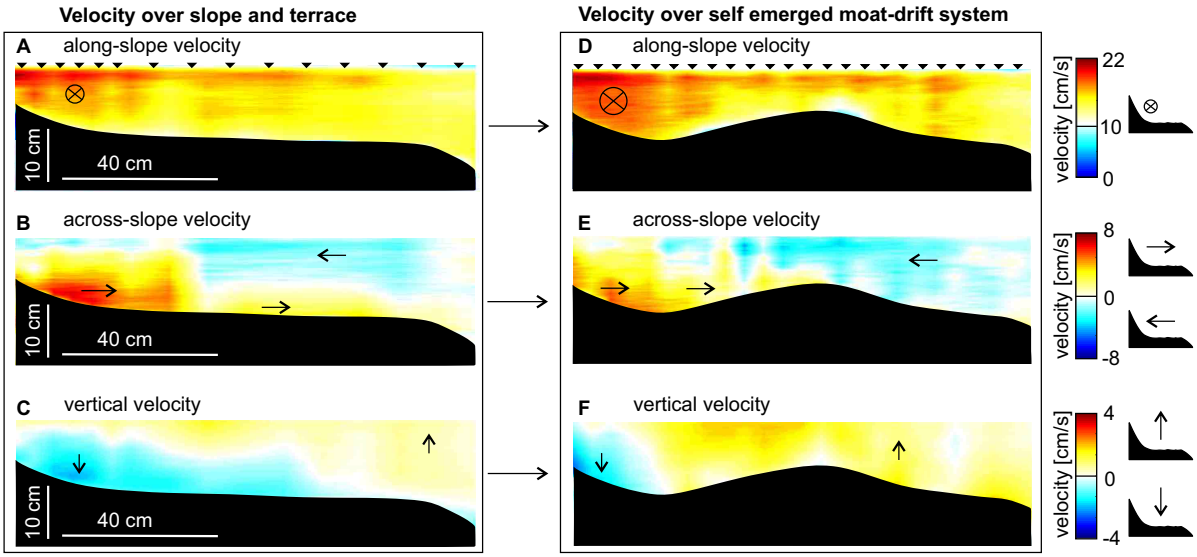

Figure 5.5: Velocity across-slope obtained with the fastest current setting. Velocity measurements at the beginning of the experiments in (A) Along-slope direction; (B) Across-slope direction; (C) Vertical direction. Velocity measurements after moat-drift system emerged in (D) Along-slope direction; (E) Across-slope direction; (F) Vertical direction. Note: the color scale variates between the plots. The velocimeter location is indicated by black triangles. The location of the cross-sections is shown in Fig. 5.2.

the drift (Fig. 5.5D). The across-slope velocity near the seafloor between the slope and drift crest is directed away from the slope, but between drift crest and basin, it is directed toward the slope (Fig. 5.5E). On the slope, the velocity is downwards, and everywhere else it is upwards (Fig. 5.5F).

5.5 Discussion

5.5.1 Comparison between experiments and natural systems

An open question in the study of marine natural systems is that the flow conditions that initially started to create a specific morphology, like a contourite drift, remain unknown because there are no oceanographic measurements from when the features started to form. Moreover, these sedimentary features take thousands to millions of years to form. To overcome this issue, we created a simple setup in a flume tank in which moat-drift systems can form, to allow us to investigate their evolution through time. The setup of the experiment consists of an upper slope and a terrace representing a continental margin that is, for example, analogous to the Argentine continental margin (Hernández-Molina et al., 2009). For the experiments, we chose a slope angle of 18° and 26°, which is steeper than the average slopes of continental margins, which are often below 10°(O'Grady et al., 2000). However, local steeper slopes are common in many environments, they can exist for instance around topographic obstacles, ridges or seamounts (Hanebuth et al., 2015; Miramontes et al., 2016). Measurements from 38 locations in the world ocean show that

typical values for moat-drift systems are a 50 m relief (between 4 m and 505 m), 2.3 km width (between 200 m and up to 35 km), 0.022 relief-width ratio (between 0.003 and 0.1), 6° slope angle (between 0.3° and 25°) and 3° drift angle (between 0.5° and 17°) (Wilckens et al., accepted). Similar to the deep sea, the drift angle from the moat in the flume tank (4°-15°) is lower than the slope angle. The moats in the flume tank are much smaller in terms of width and relief compared to natural systems, but the aspect ratio (0.02-0.9) is similar to moats in nature. The experiments demonstrate that the development of a contourite depositional system depends on sediment input. When sediment is added to the 18 cm/s strong contour current, the moat-drift system migrates upslope, similar to some moat-drift systems in deep-marine environments (Miramontes et al., 2016; 2021; Betzler et al., 2013; Liu et al., 2020; Uenzelmann-Neben et al., 2017). In the deep sea, moat-drift systems can also migrate downslope (Hernández-Molina et al., 2016c; Rebesco et al., 2016). In the experiments, the deposits differ between a current transporting sediments and the same current not transporting sediments. Similar to gravity-driven flows, currents with high velocity might be able to transport more sediment and thus have a higher transport capacity than slower-flowing currents. If the currents sediment transport capacity is reached, sediment is deposited. When the water is relatively clear it may pick up sediment to fulfill its transport capacity. As a result, the moat-drift system can migrate downslope by reworking the side of the drift at the moat under constant contour current speed when no sediment is added to the contour current. Due to the erosion, the moat becomes wider and the relief increases. Thus, the migration direction depends on both current speed and sediment supply. A current with no sediments can erode, while the same current with more sediments than its transport capacity will deposit sediment. If the current speed for the moat-drift system is known, this can be used to understand sediment availability and how it has changed over time. The internal stratigraphic architecture of the drift partly preserves the evolution of the morphological elements. The stacking pattern of the moat-drift systems that self-emerged in the flume tank is comparable to the recorded seismic reflection profiles from the deep sea (Fig. 5.8 of the supplementary material). Erosional periods are identified by truncated reflections and depositional periods show sigmoidal reflections. The constructional moat-drift system in the flume tank (Fig. 5.3C) is comparable to the downstream cross-section from the Álvarez Cabral Moat in the Gulf of Cadiz (Fig. 5.1B). Our results indicate that the sediment supply of the experiment is high for constructional moat-drift systems. The erosional moat-drift system (Fig. 5.3D) shows similar truncations at the drift side, to an upstream cross-section from the Álvarez Cabral Moat (Fig. 5.1A). In this part of the system, the current must be intense, and/or the sediment supply must be low. Erosional and depositional periods can vary over time because ocean current speed and sediment supply change. In our experiments, variations in sediment supply under constant current-forcing led to a mixed constructional-erosional moat-drift system (Fig. 5.3E) similar to the Ewing Terrace Moat 2 off north Argentine

(Wilckens et al., 2021).

5.5.2 Current dynamics and sediment transport pathways over slope and terrace

The hydrodynamics of the current when the moat-drift system initially started to form is so far unknown. Our experiments show that the current is flowing primarily parallel to the slope. The current speed is higher near the slope and decreases over the terrace, already before the formation of a moat-drift system. This is due to the circular current that has a higher speed away from the vortex center and becomes zero in the center of the vortex. Furthermore, the depth decreases above the slope and thus the centrifugated and thinned water mass needs to increase its velocity in order to preserve centrifugal vorticity. Thus, the centipedal pressure gradient depends on the slope angle and current speed. The velocity measurements in the flume tank show that a secondary basinward flow can occur before the moat-drift system is established (Fig. 5.5A). Because of the rotating current there is a superelevated surface and an inward directed pressure gradient. The centripetal force required for radial acceleration is caused by this inward directed pressure gradient. This centripetal pressure gradient is barotropic (constant in depth), but the velocity decreases towards the bed due to bed friction. Because of this, the slow moving particles near the bed are accelerated away from the slope, while the fast flowing particles higher up in the water column are flowing towards the slope, resulting in a secondary flow near the bottom. Conservation of volume is achieved by the downward and upward water exchanges between the lateral flows, which leads to the helix flow over the moat. This current is recorded by the across-slope velocity measurements and shows that the secondary flow directed downslope and across the terrace at the lowest $\sim$5 cm above the seafloor. Furthermore, when the current velocity is increased, both centrifugal and centripetal force become higher and the secondary flow increases (Fig. 5.4C). Similarly in nature, the bottom boundary Ekman transport also increases with higher current velocity (Wåhlin et al., 2012). Cross-shelf Ekman transport can occur in a rotating frame in the frictional boundary layer when a current flows over a sloping seabed (Ekman, 1905). It can transport dense water upslope or light water downslope, depending on the hemisphere and current direction (Ekman, 1905; Trowbridge and Lentz, 1991; Weatherly, 1975; Weatherly and Martin, 1978; Wåhlin et al., 2012). When the slope gradient is increased, also the horizontal pressure gradient increases, thereby enhancing the secondary flow (Salon et al., 2008). As a result, a steeper slope and a faster current lead to a stronger secondary flow. When the secondary flow becomes stronger, more sediment can possibly be transported from the slope towards the drift.

In all experiments where a secondary flow is recorded, a moat-drift system later self-emerges. But if no secondary flow is recorded, only aggradation occurs on the terrace and

no moat-drift system is established. This situation occurred at the combination of the lowest velocity and lowest slope in our experiments (Fig. 5.4A). In nature, this occurs for example at the La Plata terrace at the Argentine margin south of the Mar del Plata canyon (Preu et al., 2012). In summary, we suggest that a current with a velocity that is strong enough to transport particles together with a secondary flow near the seabed is necessary for a moat-drift system to develop. This means that there is a threshold below which no moat-drift system can form, which is in agreement with observations from many locations at continental margins where no moat-drift system forms. Some authors suggest that the moat formation, or contourite formation in general, could be also influenced by internal waves or other turbulence at density contrast between two water masses (Zhang et al., 2016; Miramontes et al., 2020a; Preu et al., 2013; Hernández-Molina et al., 2016a; Rebesco et al., 2014; Shanmugam, 2013; Hanebuth et al., 2015). Others suggest that they form in association with ocean current surface fronts (Nicholson and Stow, 2019; Hanebuth et al., 2015). Our experiments shows that moat-drift systems can form solely with alongslope currents if sediment is available to be transported and shaped into a drift deposit, without any of these additional oceanographic processes. However, the experiments do not disprove possible contributions of these other processes in natural systems, because the processes were not tested in the experiments.

5.5.3 Current dynamics and sediment transport pathways of moat-drift systems

Moats are hypothesized to be related to the highly energetic cores of the current (Yin et al., 2019; Wilckens et al., 2021; Thiéblemont et al., 2019; Llave et al., 2020; De Castro et al., 2021). Previous velocity measurements show an intensification in bottom current velocity over a moat and lower speeds over the drift and terrace offshore north Argentina (Wilckens et al., 2021). This is similar to the velocity measurements over the moat-drift system in the flume tank. It was speculated that the current velocity is increased over the moat due to the morphology of the moat, which could stabilize and focus the bottom current by limiting the variability in the cross-slope direction (Wilckens et al., 2021). This hypothesis is supported by the flume tank experiments. Several authors hypothesized that there is a secondary flow over moats, but the suggested direction differs between authors, and this interpretation has not been supported by measurements yet (Rebesco et al., 2014; Hernández-Molina et al., 2008; Gong et al., 2017). The experiments show that the vertical velocity is upwards along the drift-side of the moat, which closes the secondary circulation into the previously suspected helix-structure within the moat (Fig. 5.5E,F). The orientation of the helix within the moat is not switched around compared to the secondary circulation before moat-formation: the near-bottom flow is directed offshore, and the top of the helix is directed towards the slope. This observed spinning direction of the helix flow within the moat is in agreement with the previously hypothesized helix

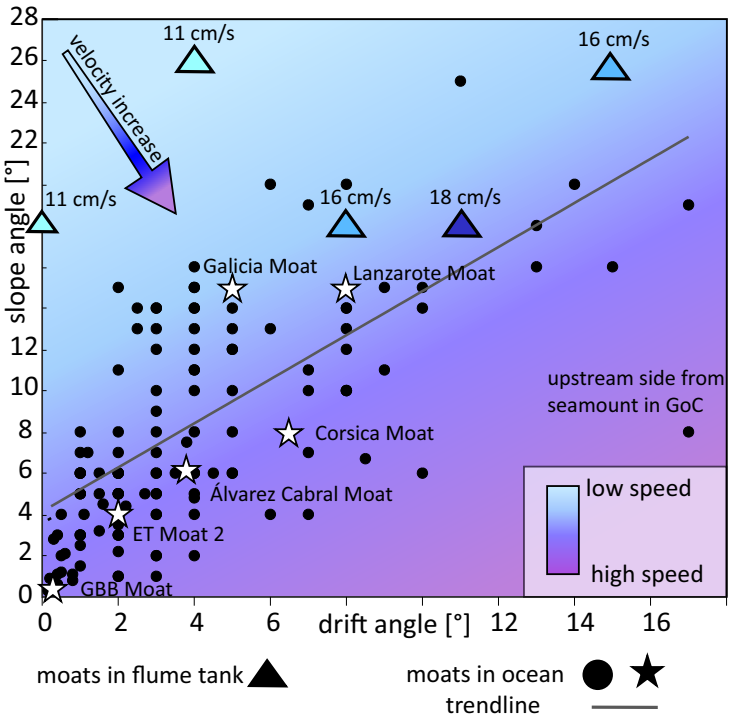

Figure 5.6: Diagram showing the link between current speed, slope angle and drift angle. GoC: Gulf of Cadiz, ET Moat 2: Ewing Terrace Moat 2 offshore Argentine, GBB Moat: Great Bahamas Bank Moat in the Bahamas.

flow of some authors (Rebesco et al., 2014). The secondary circulation is contained within the moat by the drift, and it does not continue flowing over the terrace (Fig. 5.5E). This enclosure of the helix within the moat coincides with an increase of the primary along-slope velocity component, which suggests that moat-drift formation provides a fundamental mechanism for contour-current strength enhancement.

5.5.4 Current speed reconstructions based on morphology

The experiments show that steeper slopes and faster currents lead to steeper drifts next to a moat (Figs. 5.4 and 5.6). The experiments that only lead to aggradation on the terrace when the velocity and/or the slope angle are too low for moat-drift formation (Fig. 5.4) indicate that for a specific current speed, it exists a minimum slope angle to allow moat-drift system formation.

Plotting the slope angle against the drift angle shows that data points clustering in the upper left corner (meaning high slope and low drift angle) are related to low current speeds. The experimental data exhibit a trend whereby the lowest velocities plot to the top left of the diagram (steep slope and low drift angle), and the faster velocities to the bottom right (lower slope and higher drift angle; Fig. 5.6). This trend is also observed for moat-drift systems in the deep sea but the trend is unclear due to the limited amount of data and the short velocity recording period. For example, velocity data shows an average

bottom current speed over the Great Bahamas Bank Moat of 36 cm/s and for the Ewing Terrace Moat 2 offshore north Argentine of 29 cm/s (Lüdmann et al., 2016; Wilckens et al., 2021). We use this structure to suggest interpretations of natural conditions from slope-moat-drift architectures. For example, the Galicia Moat (Hanebuth et al., 2015) and Lanzarote Moat (Acosta et al., 2005) have the same slope angle but different drift angles. Our results suggest that the drift angle from Lanzarote Moat is higher because the current speed is higher. Our results also suggest that Ewing Terrace Moat 2 (Wilckens et al., 2021), Álvarez Cabral Moat (García et al., 2009), and Corsica Moat (Miramontes et al., 2016) are probably formed with similar currents speeds and the difference in drift angle is likely due to differences in the slope angle.

Results from topographic obstacles seem to be less reliable for the current reconstruction because such environments are often strongly diverted from the trendline, e.g. at the upstream side of topographic obstacles in the Gulf of Cadiz (Fig. 5.6). This might be linked to a less constant current along the slope of seamounts that could be related to changes in the direction in which the current hits the slope of the seamount. Whether these systems mainly react to mean or peak velocity remains unknown. Numerically modelled bottom currents over moats show high variability in current speed in the Mozambique channel and at the north-west Spanish margin, which suggests that moats and drifts are not necessarily continuously formed but rather more episodic (Miramontes et al., 2021; Zhang et al., 2016). Future flume tank experiments can test the influence of velocity variability. The present results from the flume tank experiments are limited to one range of sediment grain size. Thus, future experiments can test the influence of different sediment compositions and grain sizes on contourite development.

5.6 Conclusions

In summary, this study presents the first experiments in which a contourite depositional system self-emerges in a three-dimensional flume tank, with no prior formation of any contourite feature. The experiments demonstrate the conditions necessary to form moat-drift systems. Taking into account the influence of current speed, slope and drift angle, together the with secondary flow measured in the flume tank, we suggest (Fig. 5.7):

- The moat-drift system is only able to form if there is a secondary flow near the seafloor that transports sediment from the slope toward the drift (basinward). The secondary flow increases with higher speeds and steeper slopes.
- After the moat is formed, the secondary flow is confined in the moat and decreases but the along-slope velocity becomes more focused and increases.
- Migration of the moat, and formation of internal stratigraphic architecture, is a function of current strength in combination with sediment availability. Low sediment

availability leads to migration away from the slope and truncation of reflectors. High sediment availability leads to migration towards the slope and formation of sigmoidal deposits on the terrace-side of the moat.

- Higher current speeds and steeper slopes lead to a steeper sediment drift. Thus, current speed reconstructions from seismic data or bathymetric data are possible but the slope angle has to be taken into account when the current speed is reconstructed. This shows that moat-drived sysemes can be used as a paleo velocety meter, which allows reconstructions of current spped and direction over past millions of years. This might be an important step forward for paleocurrent reconstructions.

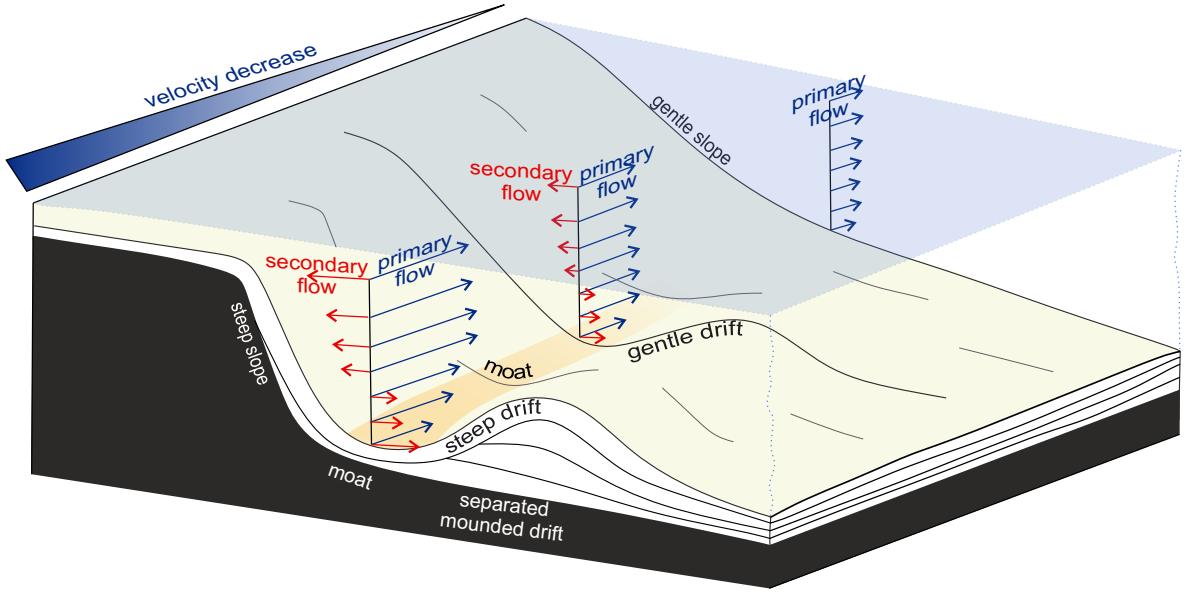

Figure 5.7: Conceptual model of how moats form under different slope angles and current velocities. Slope angles and current velocities together influence the current velocity gradient. The current velocity gradient then determines the drift angle and thus the shape of the moat.

5.7 Data availability

All data needed to evaluate the conclusions in the paper are present in the paper and will be made available on PANGAEA. Supplementary material for this article will be made available on YouTube for videos of the sediment input phase and the reworking phase.

5.8 Acknowledgments

We thank Han de Witte for technical support with the experiments. This work has been done in collaboration within the "The Drifters" Research Group at Royal Holloway University of London (RHUL). We thank TGS for their permission to use the seismic profile of the Álvarez Cabral Moat in Figure 5.1. H.W.'s research stay at the Utrecht University was supported by the BremenIDEA funding line from the University of Bremen.

5.9 Supplementary material

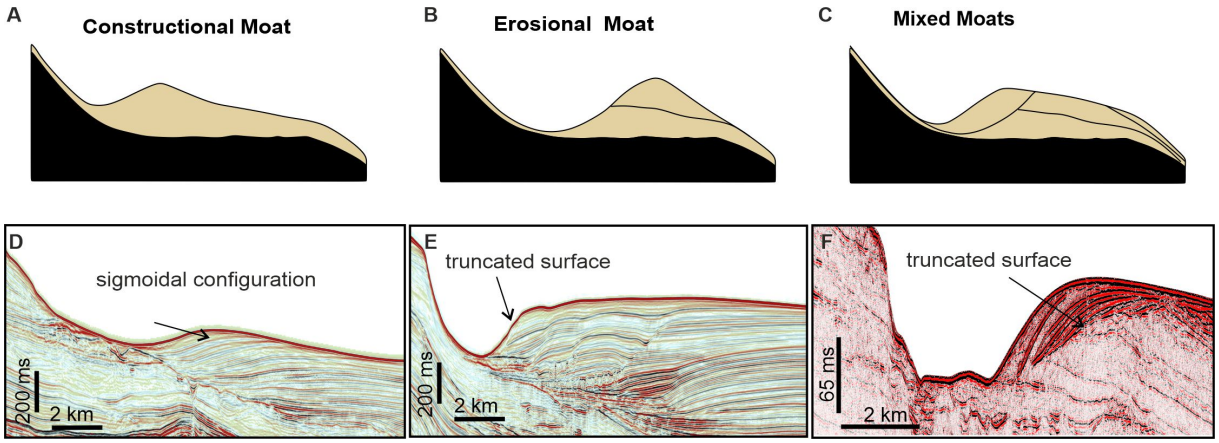

Figure 5.8: Comparison between moat-drift-systems in flume tank experiments and stratigraphy of moat-drift-systems in natural systems. (A) The moat self-emerges after the sediment input phase. (B) Stratigraphy of a moat with no sediment input. (C) Stratigraphy of a moat with phases with and without sediment input. The stratigraphy is compiled from the measured bathymetry. Seismic cross-section of the Álvarez Capral Moat in the Gulf of Cadiz located (D) upstream and (E) downstream of the bottom current. (F) Seismic cross-section of the Ewing Terrace Moat 2 offshore Argentine.

Chapter 6

Synthesis

6.1 Conclusions

This study provides new insights into the interactions between ocean currents and sedimentary structures, and how they affect the evolution of contourites. The combined data show the importance of currents related to the thermohaline circulation for the development of contourites as well as the role of other oceanographic processes (e.g. small eddies), and sediment supply to the water column. Mean modelled currents averaged over 25 years show that the current speed is higher over an abraded surface between the La Plata Terrace and Ewing Terrace than on the the terraces themselves. Furthermore, the mean modelled currents decrease northward, which explains the observed accumulation of finer sediment deposits north of the Mar del Plata (MdP) Canyon. Generally, the velocity over the large contourite terraces is low, suggesting that sediment deposition should occur in these areas. However, despite the contourite terraces being mainly a depositional environment, there are small patchy erosional surfaces. Current model and VM-ADCP measurements show cyclonic eddies in the lower part of the water column that do not reach the sea surface. These cyclonic eddies may lead to the patchy erosional surfaces on the terrace. The diverting isobaths on the Ewing Terrace, together with the sloping morphology, may trigger the eddies near the seafloor, suggesting that they occur because of the underlying morphology. Thus, near-seafloor eddies might also exist over large contourite terraces elsewhere.

The combined data indicate that sediment transport at the northern Argentine margin is associated with high-velocity along-slope near-bottom current jets. These might play an important role in sediment supply to the MdP Canyon head, similar to longshore currents feeding shelf-incised submarine canyons. This is an alternative sediment transport mechanism to a previously suggested nepheloid layer on the Ewing Terrace (Voigt et al., 2013; Warratz et al., 2019). Additionally, the samples of the surface sediment together with the measured and modelled current speeds suggest that the sediment would not be suspended in a nepheloid layer. The Ewing Terrace Moat 1 is possibly another pathway for sediment

transport to the MdP Canyon head. This might also be true in general, as moats are associated with the core of the current. Furthermore, moats occur all over the world's oceans, making them a perfect target to study and reconstruct past ocean current direction and speed based on their morphology and internal architecture, which can be observed in seismic data. So far, moats have been given little attention in measuring and comparing their average morphologic features and seismic reflection patterns. Therefore, I systematically compared 185 cross-sections of moat-drift systems distributed over 39 different locations worldwide. The median of all profiles across all moat-drift systems reveals a 50 m relief, a width of 2.3 km, a relief to width ratio of 0.022, a slope angle of 6°, a drift angle of 3° and a concave-up shaped morphology. Some moats, for example two of the moats from the Argentine margin as well as two moats in the Bahamas area, are over 100 km long. In the Bahamas area bathymetric data, together with current measurements, indicate that the current is not in equilibrium with the morphology at the upstream side. The current then adapts to the morphological changes while flowing along the slope. Moats at continental slopes are relatively straight, but moats around topographic obstacles can be more curved. In the latter case the current has to constantly adapt to the changes in slope and, consequently, is never in equilibrium with the morphology.

One of the initial hypotheses was that there is a correlation between the aspect ratio of the moat and the Coriolis force since the Coriolis frequency depends on the latitude, and the Coriolis force plays an essential role in moat formation. However, the statistical analyses show no relation between latitude and moat-drift morphology or stratigraphy. The results confirm that moat morphology correlates with water depth. This might be due to the influence of the amount of sediment supply to the water column and limited accommodation space. Furthermore, a linear correlation exists between the slope angle (adjacent to the emplacement of the moat) and the drift angle (at the side towards the moat). Most likely, the current is locally focused and intensified due to the steepness of the adjacent slope. The measured current speed from the Argentine margin, the Bahamas area, and the three-dimensional flume tank experiments show that the speed is higher over the moats and decreases by 5-48% over the associated drifts. The current speed and the horizontal velocity gradient are suggested to be important factors for the formation of a moat-drift system. A steeper slope might focus the current more, resulting in a higher horizontal velocity gradient across the moat and as a consequence to a steeper drift. Thus, the steepness of the slope where the moat forms indirectly controls the drift angle and, thereby, the moat morphology. Flume tank experiments also confirm that steeper slopes lead to steeper drifts.

Sediment availability plays a crucial role in the development of moat-drift systems. Flume tank experiments show that the migration direction of the moat-drift system, the mor-

phology, and the internal stratigraphic architecture is a function of current strength in combination with sediment availability. Higher current speeds lead to larger moats than low current speeds over the same period. A current with no suspended sediment can erode, while the same current carrying more sediment than its transport capacity will deposit sediment. Low sediment availability can force moat-drift systems to migrate onto the terrace and lead to the truncation of reflectors at the drift side. Whereas high sediment availability forces moat-drift systems to migrate onto the slope and leads to the formation of sigmoidal deposits on the terrace-side of the moat. The different types of more erosive or more depositional moat-drift systems have also been observed in seismic data from the deep sea and lakes. Three main types of moats can be distinguished based on their stratigraphy: (1) ''Constructional Moats" where reflections onlap at the slope side; (2) ''Mixed Moats" where reflections downlap at the bottom of the moat; and (3) ''Erosional Moats" where reflections are truncated at the drift side. From this study, 78% of the moats are Constructional Moats (at present day). The Ewing Terrace moat shows that, with time, moats can transition from one type to another. The stratigraphy of the Ewing Terrace moat-drift system suggests that this transition occurred rapidly (similar to the flume tank experiments), indicating that the ocean current regime abruptly changed from a strong current regime with little suspended sediment into a lower energetic current regime with higher sediment availability.

Three-dimensional flume tank experiments show under which conditions a moat-drift system can form. Some authors previously suggested that the moat formation, or contourite formation in general, could also be influenced by internal waves or other processes at the density contrast between two water masses (Zhang et al., 2016; Miramontes et al., 2020a; Preu et al., 2013; Hernández-Molina et al., 2016a; Rebesco et al., 2014; Shanmugam, 2013; Hanebuth et al., 2015). Others postulated that they form in association with ocean current surface fronts (Nicholson and Stow, 2019; Hanebuth et al., 2015). The flume tank experiments show that a moat-drift system can form on the flat surface parallel to a slope solely with along-slope currents. However, the experiments do not disprove possible contributions of other oceanographic processes in natural systems. In the flume tank experiments, the main current direction is along-slope and the speed is higher against the slope and decreases on the terrace basinwards. Current measurements in the flume tank show a basinwards secondary flow, which increases with higher speeds and steeper slopes, leading to a steeper adjacent drift. The correlation between current speed and the morphology of the moat-drift system suggests that the sediment architecture of moat-drift systems can be used as a paleo-velocimeter (Fig. 6.1). The presented results facilitate the qualitative reconstruction of the speed of the currents involved during the moat formation and development. However, the analyses of moats from natural environments cannot yet give absolute values for the current speed. Here, more in-situ

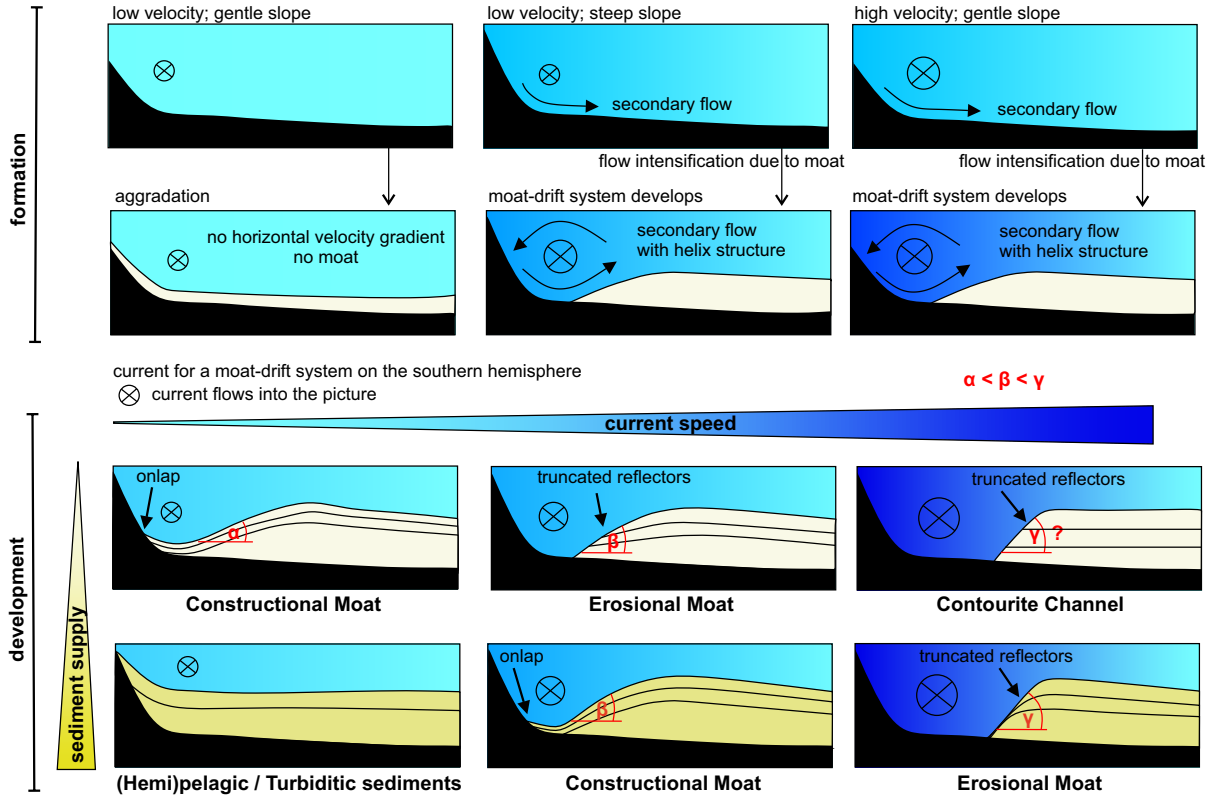

Figure 6.1: Conceptual model of moat formation and development. With a high enough current velocity and steep enough slope, a secondary flow flows basinwards. Then, a moat-drift system develops, which confines the secondary flow into a helix structure. During the development of the moat-drift system, the slope angle increases with higher current speeds, assuming a constant slope angle. The type of moat-drift system depends on the combination of sediment supply and current speed.

measurements are needed to scale the current speed to the moat morphology. The developed moat-drift systems in the flume tank show similar aspect ratios and drift angles as moats in natural marine environments. After the moat-drift system is formed, the secondary flow decreases. The drift confines the flow into a helix structure inside the moat. Thus, the experiments deliver clarity on a previous theoretical discussion about a helicoidal flow in the moat (Hernández-Molina et al., 2008; Rebesco et al., 2014). At the same time, the along-slope velocity becomes more focused, which is in line with the observed intensification of the current over the moat at the Ewing Terrace at the Argentine margin.

This study shows the importance of current strength, current variability (in time and space) and sediment supply/availability for the formation of contourite systems. It shows the limits of the knowledge we currently have about the role of oceanographic processes on sedimentary systems. Overall, this research identifies the need to collect more detailed information on the processes occurring a few meters above the seafloor as well as simultaneous observation and sampling of the surface sedimentary deposits in modern deep-water environments.

6.2 Outlook

Ideally, future research cruises will incorporate more ADCP measurements in their scientific programmes, which can further improve the reconstruction of ocean currents and sediment transport pathways. While in-situ measurements from mooring stations already exist for submarine channels, I suggest that similar measurements are carried out for moat-drift systems.

The flume tank experiments are, to the best of my knowledge, the first ones in which a contourite drift self-emerged. Now a number of follow-up experiments could be conducted involving the following analyses: (1) the effect of different sediment grain-sizes on the internal architecture of moat-drift systems; (2) the fluctuation of current speed in order to analyse if the moat-drift system mainly reacts to the mean, maximum, minimum speed or its variability range; (3) analysis of sediment transport pathways by colouring the sediment from different areas in different colours; (4) analyse the effect of the Coriolis force on moat-drift systems by using a rotating flume tank; (5) analyse the differences in carbonate versus siliciclastic moat-drift systems; (6) decrease the slope angle and try to generate the formation of a plastered drift. Some of these analyses can also be done by numerical modelling.

Besides along-slope currents, other processes have been suggested to affect the seafloor morphology. Zhang et al. (2014) showed that eddies can trap sediment and transport it elsewhere. Eddies are also suggested to erode sediment (Chene at al., 2019; Breitzke et al., 2017; Miramontes et al., 2021). The Zapiola drift in the Argentine Basin might also be explained by eddies (de Miranda et al., 1999). Thus, eddies can lead to sediment deposition as well as erosion. If erosion or deposition occurs and how well the sediment is trapped inside the eddy might be determined by upwelling or downwelling in eddies depending on their spinning direction and on which hemisphere they occur. Thus, I suggest to compare cyclonic and anti-cyclonic eddies in terms of the amount of sediment they trap and what sedimentological features they cause while monitoring their size and speed (Fig. 6.2).

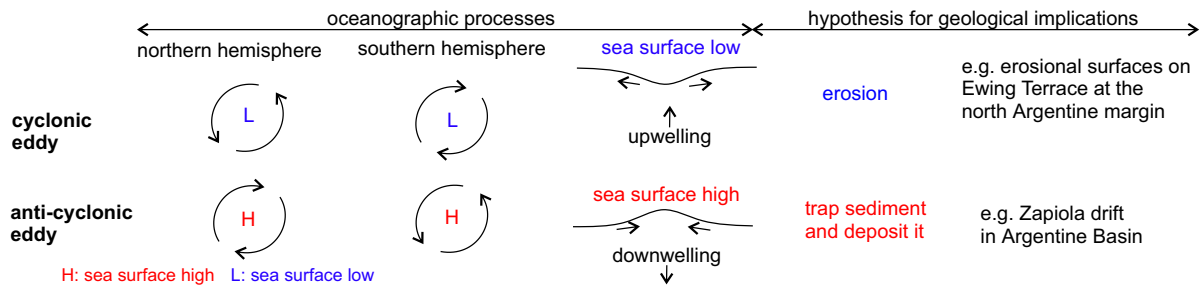

Figure 6.2: Hydrodynamics related to eddies and their hypothesized geological implications.

Acknowledgements

The time I spent pursuing my PhD has been great, and I very much enjoyed working on it. For that, I would like to thank several people. First, I would like to thank Elda Miramontes for the time she spent discussing new ideas with me, challenging me to think critically about scientific results and encouraging me to approach the project in my own way. Your constant support and guidance when I needed it allowed me to develop and follow my own research ideas. I could not have asked for a better supervisor. I would also like to thank my second supervisor Tilmann Schwenk for the helpful discussions and for making the data available to me as well as the tools to deal with them. You always asked critical questions that helped to improve the manuscripts. In the same way, I would like to thank Javier Hernández-Molina, Wenyan Zhang, Alice Lefebvre and Volkhard Spieß in their capacity as part of my thesis committee who always offered helpful advice and discussed the data with me. Many thanks to Michele Rebesco for agreeing to be the second reviewer of my dissertation.

I thank Joris Eggenhuisen for welcoming me to his research group and flume tank lab during my time at the University of Utrecht. Thank you for taking a chance and believing in my suggested experiments. Without your support, these flume tank experiments would not have happened. I thank Pelle Adema for welcoming me to Utrecht, introducing me to the people there, and helping set up the experiments. I thank Mateus Kroth and João Trabucho Alexandre for the interesting field trip in France. I would also like to acknowledge the additional funding I received from the BremenIDEA funding line from the University of Bremen for conducting the experiments in Utrecht.

I thank Ricardo Silva Jacinto for the great discussions we had about the hydrodynamic processes in the flume tank. I thank Camila Artana, Alberto R. Piola, Michele Baques and Christine Provost for the helpful Oceanographic discussions about the Argentine continental margin. Also, I would like to thank Thomas Lüdmann and Christian Betzler for discussing the bathymetry and ADCP data from the Bahamas with me, which greatly improved the second manuscript. I thank Meret Felgendreher for the grain size analyses from the sediment samples offshore Argentina, and Jiayue Chen for the discussion about the hydrodynamic processes above moats. I thank Sabine Kasten and Antonio Cattaneo

for allowing me to use their data, which facilitated the interdisciplinary context of the study. Finally, I thank my co-authors for their helpful comments, which significantly improved the manuscripts.

Many thanks also to my research group and Marcello Gugliott. We had good coffee breaks, group meetings, Christmas celebrations and dinners. Furthermore, I thank my colleagues at the University of Bremen from the Faculty of Geosciences and MARUM – Center for Marine Environmental Sciences for offering a relaxed and yet highly productive working atmosphere. Additionally, I want to thank the Graduate School GLOMAR for offering interesting coursework and the financial support I received for attending the International Conference on Seafloor Forms, Processes and Evolution. I would also like to acknowledge the platform Pixabay for providing nice, free-of-charge and licence-free images.

Finally, I would like to thank my family and friends for their support during the last three years and the entire time I have known them.

Bibliography

Acosta, J., Uchupi, E., Muñoz, A., Herranz, P., Palomo, C., Ballesteros, M., & ZEE Working Group. (2005). Salt diapirs, salt brine seeps, pockmarks and surficial sediment creep and slides in the Canary Channel off NW Africa. In Geophysics of the Canary Islands (pp. 41-57). Springer, Dordrecht.

Allen, C., Peakall, J., Hodgson, D., Bradbury, W., & Booth, A. (2022). Latitudinal changes in submarine channel-levee system evolution, architecture and flow processes. Frontiers in Earth Science.

Artana, C., Lellouche, J.M., Park, Y.H., Garric, G., Koenig, Z., Sennéchael, N., Ferrari, R., Piola, A.R., Saraceno, M., & Provost, C., (2018). Fronts of the malvinas current system: surface and subsurface expressions revealed by satellite altimetry, argo floats, and mercator operational model outputs. Journal of Geophysical Research: Oceans 123, 5261–5285.

Artana, C., Provost, C., Lellouche, J.M., Rio, M.H., Ferrari, R., & Sennéchael, N., (2019). The Malvinas current at the confluence with the Brazil current: inferences from 25 years of Mercator Ocean reanalysis. Journal of Geophysical Research: Oceans, 124 (10), 7178–7200.

Artana, C., Provost, C., Poli, L., Ferrari, R., & Lellouche, J.-M., (2021a). Revisiting the Malvinas Current upper circulation and water masses using a high-resolution ocean reanalysis. Journal of Geophysical Research: Oceans, 126 (6) e2021JC017271.

Artana, C., Ferrari, R., Bricaud, C., Lellouche, J.-M., Garric, G., Sennéchael, N., Lee, J.-H., Park, Y.-H., & Provost, C., (2021b). Twenty-five years of Mercator Ocean reanalysis GLORYS12 at Drake Passage: velocity assessment and total volume transport. Adv. Space Res. 68 (2), 447–466.

Bailey, W.S., McArthur, A.D., & McCaffrey, W.D. (2021). Distribution of contourite drifts on convergent margins: Examples from the Hikurangi subduction margin of New Zealand. Sedimentology, 68(1), 294-323.

Betzler, C., Lüdmann, T., Hübscher, C., & Fürstenau, J., (2013). Current and sea-level signals in periplatform ooze (Neogene, Maldives, Indian Ocean). Sediment. Geol. 290, 126–137.

Betzler, C., Lindhorst, S., Eberli, G.P., Lüdmann, T., Möbius, J., Ludwig, J., Schutter, I., Wunsch, M., Reijmer, J.J.G., & Hübscher, C. (2014a). Periplatform drift: The combined result of contour current and off-bank transport along carbonate platforms. Geology, 42(10), 871-874.

Betzler, C., Lindhorst, S., Lüdmann, T., von Borstel, F., Büld, M., Djamlan, E., Eberli, G., Eversheim, J., Jentzen, A., Keizer, F., Ludwig, J., Möbius, J., Paulat, M., Reiche, S., Reijmer, J., Reolid, J., Schiebel, L., Schutter, I., Ulferts, L., Winter, S., Wolf, D., Wunsch, M., Rentsch, H., & Raeke, A. (2014b). CICARB - Cruise No. M95 - March 29 - April 25, 2013 - Kingston (Jamaica) - Pointe à Pitre (Guadeloupe). In METEOR-Berichte (Vol. M95, pp. 1-36). DFG-Senatskommission für Ozeanographie. https://doi.org/10.2312/cr_m95

Bikonis, K., & Demkowicz, J. (2018). MEMS technology quality requirements as applied to multibeam echosounder. Polish Maritime Research.

Blumsack, S., & Weatherly, G., (1989). Observations of the nearby flow and a model for the growth of mudwaves. Deep Sea Res. A Oceanogr. Res. Pap. 36, 1327–1339.

Bozzano, G., Violante, R.A., & Cerredo, M.E., (2011). Middle slope contourite deposits and associated sedimentary facies off NE Argentina. Geo-Mar. Lett. 31, 495–507.

Bozzano, G., Cerredo, M.E., Remesal, M., Steinmann, L., Hanebuth, T.J.J., Schwenk, T., Baqués, M., Hebbeln, D., Spoltore, D., Silvestri, O., Acevedo, R.D., Spiess, V., Violante, R.A., & Kasten, S., (2021). Dropstones in the Mar del Plata Canyon Area (SW Atlantic): evidence for provenance, transport, distribution, and oceanographic implications. Geochem. Geophys. Geosyst. 22(1) e2020GC009333.

Brackenridge, R.E., Nicholson, U., Sapiie, B., Stow, D., & Tappin, D.R., (2020). Indonesian Throughflow as a preconditioning mechanism for submarine landslides in the Makassar Strait. Geol. Soc. Lond., Spec. Publ. 500, 195–217.

Breitzke, M., Wiles, E., Krocker, R., Watkeys, M. K., & Jokat, W. (2017). Seafloor morphology in the Mozambique Channel: evidence for long-term persistent bottom-current flow and deep-reaching eddy activity. Marine Geophysical Research, 38, 241-269.

Buiter, S.J.H., Funiciello, F., & Van Hunen, J. (2013). Introduction to the special issue on" Subduction Zones". Solid Earth, 4(1), 129.

Cacchione, D.A., Pratson, L.F., & Ogston, A.S. (2002). The shaping of continental slopes by internal tides. Science, 296(5568), 724-727.

Carranza, A., Recio, A.M., Kitahara, M., Scarabino, F., Ortega, L., López, G., Franco-Fraguas, P., De Mello, C., Acosta, J., & Fontan, A., (2012). Deep-water coral reefs from the Uruguayan outer shelf and slope. Marine Biodiversity. 42, 411–414.

Cattaneo Antonio (2013a) PRISME 2 cruise, RV L'Atalante, https://doi.org/10.17882/87317

Cattaneo Antonio (2013b) PRISME 3 cruise, RV Pourquoi pas ?, https://doi.org/10.17600/13030060

Cécile, R., & Laurence, D., (2014) PAMELA-MOZ02 cruise, RV L'Atalante, https://doi.org/10.17600/14001100

Chen, H., Zhang, W., Xie, X., & Ren, J., (2019). Sediment dynamics driven by contour currents and mesoscale eddies along continental slope: a case study of the northern South China Sea. Marine Geology, 409, 48–66.

Chen, H., Zhang, W., Xie, X., Gao, Y., Liu, S., Ren, J., Wang, D., & Su, M. (2022): Linking oceanographic processes to contourite features: Numerical modelling of currents influencing a contourite depositional system on the northern South China Sea margin. Marine Geology, 444, 106714.

Clark, J.D., Kenyon, N.H., & Pickering, K.T. (1992). Quantitative analysis of the geometry of submarine channels: implications for the classification of submarine fans. Geology, 20(7), 633-636.

Corney, R.K., Peakall, J., Parsons, D.R., Elliott, L., Amos, K.J., Best, J.L., Keevil, G.L., & Ingham, D.B. (2006). The orientation of helical flow in curved channels. Sedimentology, 53(2), 249-257.

Cossu, R., Wells, M.G., & Wåhlin, A.K. (2010). Influence of the Coriolis force on the velocity structure of gravity currents in straight submarine channel systems. Journal of Geophysical Research: Oceans, 115(C11).

Crutchley, G.J., Kopp, H. (2018). Reflection and Refraction Seismic Methods. In: Micallef, A., Krastel, S., Savini, A. (eds) Submarine Geomorphology. Springer Geology. Springer, Cham. https://doi.org/10.1007/978-3-319-57852-1_4

de Castro, S., Hernández-Molina, F.J., De Weger, W., Jiménez-Espejo, F.J., Rodríguez-Tovar, F.J., Mena, A., Llave, E., Sierro, F.J., (2021). Contourite characterization and its discrimination from other deep-water deposits in the Gulf of Cadiz contourite depositional system. Sedimentology 68, 987-1027.

de Miranda, A. P., Barnier, B., & Dewar, W. K. (1999). On the dynamics of the Zapiola Anticyclone. Journal of Geophysical Research: Oceans, 104(C9), 21137-21149.

de Lavergne, C., Madec, G., Capet, X., Maze, G., & Roquet, F., (2016). Getting to the bottom of the ocean. Nature Geoscience 9, 857-858.

de Souza, M.M., Mathis, M., & Pohlmann, T., (2019). Driving mechanisms of the variability and long-term trend of the Brazil–Malvinas confluence during the 21st century. Climate Dynamics 53 (9–10), 6453–6468.

Davarpanah Jazi, S., Wells, M.G., Peakall, J., Dorrell, R.M., Thomas, R.E., Keevil, G.M., Darby, S.E., Sommeria, J., Viboud, S., & Valran, T. (2020). Influence of Coriolis force upon bottom boundary layers in a large-scale gravity current experiment: Implications for evolution of sinuous deep-water channel systems. Journal of Geophysical Research: Oceans, 125(3), e2019JC015284.

Deptuck M.E., & Sylvester Z. (2018) Submarine Fans and Their Channels, Levees, and Lobes. In: Micallef A., Krastel S., Savini A. (eds) Submarine Geomorphology. Springer Geology. Springer, Cham. https://doi.org/10.1007/978-3-319-57852-1_15

Dondurur, D. (2018). Acquisition and processing of marine seismic data. Elsevier.

Droghei, R., Falcini, F., Casalbore, D., Martorelli, E., Mosetti, R., Sannino, G., Santoleri, R., & Chiocci, F., (2016). The role of Internal Solitary Waves on deep-water sedimentary processes: the case of up-slope migrating sediment waves off the Messina Strait. Sci. Rep. 6, 36376.

Ekman, V.W., (1905). On the influence of the earth's rotation on ocean-currents.

Ercilla, G., Juan, C., Hernández-Molina, F.J., Bruno, M., Estrada, F., Alonso, B., Casas, D., Farran, M., Llave, E., García, M., Vázquez, J.T., D'Acremont, E., Gorini,C., Palomino, D., Valencia, J., El Moumni, B., & Ammar, A. (2016). Significance of bottom currents in deep-sea morphodynamics: an example from the Alboran Sea. Marine Geology, 378, 157-170.

Ercilla, G., Schwenk, T., Bozzano, G., Spiess, V., Violante, R., Estrada, F., Iannicchéri, F., Spoltore, D.A. & Alonso, B. (2019). Cenozoic sedimentary history of the northern Argentine continental slope, off Bahia Blanca, the location of the Ewing Terrace: Palaeogeodynamic and palaeoceanographic implications. Marine Geology, 417, 106028.

Falcini, F., & Jerolmack, D.J., (2010). A potential vorticity theory for the formation of elongate channels in river deltas and lakes. J. Geophys. Res. Earth Surf. 115.

Faugères, J.C., Stow, D.A., Imbert, P., & Viana, A. (1999). Seismic features diagnostic of contourite drifts. Marine Geology, 162(1), 1-38.

Felgendreher, M., (2019). Analyse der Korngrößenverteilung auf dem Meeresboden des oberen Kontinentalhanges vor Argentinien und Uruguay. Bachelortheesis at University of Bremen

Flood, R.D., (1988). A lee wave model for deep-sea mudwave activity. Deep Sea Res. A Oceanogr. Res. Pap. 35, 973–983.

Franco, B.C., Defeo, O., Piola, A.R., Barreiro, M., Yang, H., Ortega, L., Gianelli, I., Castello, J.P., Vera, C.S., Buratti, C., Pájaro, M., Pezzi, L.P., Möller, O.O., (2020). Climate change impacts on fisheries in the southwest South Atlantic Ocean: a review. Clim. Chang. 1-19.

Franco-Fraguas, P., Burone, L., Mahiques, M., Ortega, L., Urien, C., Muñoz, A., López, G., Marin, Y., Carranza, A., & Lahuerta, N., (2014). Hydrodynamic and geomorphological controls on surface sedimentation at the subtropical shelf front/Brazil–Malvinas confluence transition off Uruguay (southwestern Atlantic continental margin). Marine Geology, 349, 24–36.

Franco-Fraguas, P., Burone, L., Mahiques, M., Ortega, L., & Carranza, A., (2016). Modern sedimentary dynamics in the Southwestern Atlantic Contouritic Depositional System: new insights from the Uruguayan margin based on a geochemical approach. Marine Geology, 376, 15–25.

Franke, D., Neben, S., Ladage, S., Schreckenberger, B., Hinz, K., (2007). Margin segmentation and volcano-tectonic architecture along the volcanic margin off Argentina/Uruguay, South Atlantic. Marine Geology, 244, 46–67.

Frenz, M., Höppner, R., Stuut, J.-B., Wagner, T., Henrich, R., (2003a). Surface sediment bulk geochemistry and grain-size composition related to the oceanic circulation along the South American continental margin in the Southwest Atlantic. In: The South Atlantic in the Late Quaternary. Springer, pp. 347–373.

Frenz, Michael, Höppner, René, Stuut, Jan-Berend W., Wagner, Thomas, Henrich, Rüdiger, (2003b). Terrigenous silt grain-size distributions in the SW Atlantic. PANGAEA. `https://doi.org/10.1594/PANGAEA.95396` [dataset] In supplement to: Frenz, M et al. (2003): Surface Sediment Bulk Geochemistry and Grain-Size Composition Related to the Oceanic Circulation along the South American Continental Margin in the Southwest Atlantic. In: Wefer, G; Mulitza, S & Ratmeyer, V (eds.), The South Atlantic in the Late Quaternary: Reconstruction of Material Budgets and Current Systems, Springer, Berlin, Heidelberg, New York, 347–373.

Frey, D., Piola, A., Krechik, V., Fofanov, D., Morozov, E., Silvestrova, K., Tarakanov, R.Y., & Gladyshev, S., (2021). Direct measurements of the Malvinas Current velocity structure. Journal of Geophysical Research: Oceans, 126, e2020JC016727.

Gaiero, D.M., Probst, J.-L., Depetris, P.J., Bidart, S.M., & Leleyter, L., (2003). Iron and other transition metals in Patagonian riverborne and windborne materials: geochemical control and transport to the southern South Atlantic Ocean. Geochim. Cosmochim. Acta 67, 3603–3623.

Gaiero, D.M., Brunet, F., Probst, J.-L., & Depetris, P.J., (2007). A uniform isotopic and chemical signature of dust exported from Patagonia: rock sources and occurrence in southern environments. Chem. Geol. 238, 107–120.

Ganti, V., Chadwick, A.J., Hassenruck-Gudipati, H.J., Fuller, B.M., Lamb, M.P., (2016). Experimental river delta size set by multiple floods and backwater hydrodynamics. Science advances 2, e1501768.

García, M., Hernández-Molina, F.J., Llave, E., Stow, D.A.V., León, R., Fernández-Puga, M.C., Diaz del Río, V., & Somoza, L. (2009). Contourite erosive features caused by the Mediterranean Outflow Water in the Gulf of Cadiz: Quaternary tectonic and oceanographic implications. Marine Geology, 257(1-4), 24-40.

GEBCO, Compilation-Group, (2020). GEBCO 2020 Grid.

Giberto, D., Bremec, C., Acha, E.M., & Mianzan, H., (2004). Large-scale spatial patterns of benthic assemblages in the SW Atlantic: the Rıo de la Plata estuary and adjacent shelf waters. Estuar. Coast. Shelf Sci. 61, 1–13.

Gilli, A., Anselmetti, F. S., Ariztegui, D., Beres, M., McKenzie, J. A., & Markgraf, V. (2005). Seismic stratigraphy, buried beach ridges and contourite drifts: the Late Quaternary history of the closed Lago Cardiel basin, Argentina (49 S). Sedimentology, 52(1), 1-23.

Gong, C., Peakall, J., Wang, Y., Wells, M.G., Xu, J., (2017). Flow processes and sedimentation in contourite channels on the northwestern South China Sea margin: A joint 3D seismic and oceanographic perspective. Marine Geology 393, 176-193.

Gordon, A.L., & Greengrove, C.L., (1986). Geostrophic circulation of the Brazil-Falkland confluence. Deep Sea Res. A Oceanogr. Res. Pap. 33, 573–585.

Grant, J., & Schreiber, R., (1990). Modern swathe sounding and sub-bottom profiling technology for research applications: the Atlas Hydrosweep and Parasound systems. In: Marine Geological Surveying and Sampling. Springer, pp. 9–19.

Gruetzner, J., Uenzelmann-Neben, G., & Franke, D. (2011). Variations in bottom water activity at the southern Argentine margin: indications from a seismic analysis of a continental slope terrace. Geo-Marine Letters, 31, 405-417.

Gruetzner, J., Uenzelmann-Neben, G., & Franke, D. (2016). Evolution of the northern Argentine margin during the Cenozoic controlled by bottom current dynamics and gravitational processes. Geochemistry, Geophysics, Geosystems, 17(8), 3131-3149.

Haberkern, J. (2017). Contouritic depositional systems influenced by complex seafloor topography: Late Cenozoic seismoacoustic reconstructions from the Galicia and Angola Continental Margins (Doctoral dissertation, Universität Bremen).

Hales, B., & Emerson, S. (1997). Calcite dissolution in sediments of the Ceara Rise: In situ measurements of porewater O2, pH, and CO2 (aq). Geochimica et Cosmochimica Acta, 61(3), 501-514.

Hand, B.M., (1974). Supercritical flow in density currents. J. Sediment. Res. 44, 637–648.

Hanebuth, T.J. & cruise participants. Report and preliminary results of RV METEOR Cruise M84/4, GALIOMAR III, Vigo – Vigo, 1st – 28th May, 2011. (2011) Berichte, Fachbereich Geowissenschaften, Universität Bremen, No. 283, 139 pages. Bremen

Hanebuth, T.J., Zhang, W., Hofmann, A.L., Löwemark, L.A., & Schwenk, T. (2015). Oceanic density fronts steering bottom-current induced sedimentation deduced from a 50 ka contourite-drift record and numerical modeling (off NW Spain). Quaternary Science Reviews, 112, 207-225.

Harris, P.T., & Whiteway, T. (2011). Global distribution of large submarine canyons: Geomorphic differences between active and passive continental margins. Marine Geology, 285(1-4), 69-86.

Hebbeln, D., Van Rooij, D., & Wienberg, C. (2016). Good neighbours shaped by vigorous currents: Cold-water coral mounds and contourites in the North Atlantic. Marine Geology, 378, 171-185.

Heezen, B.C., (1959). Dynamic processes of abyssal sedimentation: erosion, transportation, and redeposition on the deep-sea floor. Geophys. J. Int. 2, 142–163.

Heezen, B.C., & Hollister, C., (1964). Deep-sea current evidence from abyssal sediments. Marine Geology, 1, 141–174.

Hernández-Molina, F.J., Larter, R.D., Rebesco, M., & Maldonado, A. (2006). Miocene reversal of bottom water flow along the Pacific Margin of the Antarctic Peninsula: stratigraphic evidence from a contourite sedimentary tail. Marine Geology, 228(1-4), 93-116.

Hernández-Molina, F.J., Llave, E., & Stow, D.A.V. (2008). Continental slope contourites. Developments in sedimentology, 60, 379-408.

Hernández-Molina, F.J., Paterlini, M., Violante, R., Marshall, P., de Isasi, M., Somoza, L., & Rebesco, M., (2009). Contourite depositional system on the Argentine Slope: an exceptional record of the influence of Antarctic water masses. Geology 37, 507–510.

Hernández-Molina, F.J., Stow, D.A.V., Alvarez-Zarikian, C.A., Acton, G., Bahr, A., Balestra, B., Ducassou, E., Flood, R., Flores, J.A., Furota, S., Grunert, P., Hodell, D., Jimenez-Espejo, F., Kim, J.K., Krissek, L., Kuroda, J., Li,B., Llave, E., Lofi, J., Lourens, L., Miller, M., Nanayama, F., Nishida, N., Richter, C., Roque, C., Pereira, H., Sanchez Goni, M.F., Sierro, F.J., Singh, A.D., Sloss, C.R., Takashimizu, Y., Tzanova, A., Voelker, A., Williams, T. & Xuan, C.(2014) Onset of Mediterranean outflow in to the North Atlantic. Science, 344, 1244–1250.

Hernández-Molina, F.J., Wåhlin, A., Bruno, M., Ercilla, G., Llave, E., Serra, N., Rosón, G., Puig, P., Rebesco, M., & Van Rooij, D., (2016a). Oceanographic processes and morphosedimentary products along the Iberian margins: a new multidisciplinary approach. Marine Geology, 378, 127–156.

Hernández-Molina, F.J., Soto, M., Piola, A.R., Tomasini, J., Preu, B., Thompson, P., Badalini, G., Creaser, A., Violante, R.A., Morales, E., Paterlini, M., & De Santa Anab, H., (2016b). A contourite depositional system along the Uruguayan continental margin: sedimentary, oceanographic and paleoceanographic implications. Marine Geology, 378, 333–349.

Hernández-Molina, F.J., Sierro, F.J., Llave, E., Roque, E., Stow, D.A.W., William, T., Lofi, J., Vand der Schee, M., Arnáiz, A., Ledesma, S., Rosales, C., Rodriquez-Tovar, F.J., Pardo-Igúzquiza, E., & Brackenridge, R.E. (2016c). Evolution of the gulf of Cadiz margin and southwest Portugal contourite depositional system: Tectonic, sedimentary and paleoceanographic implications from IODP expedition 339. Marine Geology, 377, 7-39.

Hernández-Molina, F.J., Campbell, S., Badalini, G., Thompson, P., Walker, R., Soto, M., Conti, B., Preu, B., Thieblemont, A., & Hyslop, L., (2018). Large bedforms on contourite terraces: Sedimentary and conceptual implications. Geology 46, 27–30.

Hinz, K., Neben, S., Schreckenberger, B., Roeser, H., Block, M., De Souza, K.G., Meyer, H., (1999). The Argentine continental margin north of 48 S: sedimentary successions, volcanic activity during breakup. Marine and Petroleum Geology, 16, 1–25.

Hiscott, R.N., Hall, F.R., Pirmez, C., Flood, R.D., Piper, D.J.W., Klaus, A., & Peterson, L.C. (1997). Turbidity-current overspill from the Amazon Channel: texture of the silt/sand load, paleoflow from anisotropy of magnetic susceptibility, and implications for flow processes. In Proceedings-Ocean Drilling Program Scientific Results (pp. 53-78). NATIONAL SCIENCE FOUNDATION.

Hopfauf, V., & Spieß, V., (2001). A three-dimensional theory for the development and migration of deep sea sedimentary waves. Deep-Sea Res. I Oceanogr. Res. Pap. 48, 2497–2519.

Hughes Clarke, J.E. (2018). Multibeam Echosounders. In: Micallef, A., Krastel, S., Savini, A. (eds) Submarine Geomorphology. Springer Geology. Springer, Cham. https://doi.org/10.1007/978-3-319-57852-1_3

Imran, J., Parker, G., & Katopodes, N. (1998). A numerical model of channel inception on submarine fans. Journal of Geophysical Research: Oceans, 103(C1), 1219-1238.

Inman, D.L., (1949). Sorting of sediments in the light of fluid mechanics. J. Sediment. Res. 19, 51–70.

Jackson, C.R., Da Silva, J.C., Jeans, G., (2012). The generation of nonlinear internal waves. Oceanography 25, 108–123.

Jones, E.J.W., Siddall, R., Thirlwall, M.F., Chroston, P.N., & Lloyd, A.J. (1995). Anton Dohrn Seamount and the evolution of the Rockall Trough. Oceanographic Literature Review, 5(42), 352.

Juan, C., Van Rooij, D., & De Bruycker, W. (2018). An assessment of bottom current controlled sedimentation in Pacific Ocean abyssal environments. Marine Geology, 403, 20-33.

Kane, I.A., Clare, M.A., Miramontes, E., Wogelius, R., Rothwell, J.J., Garreau, P., & Pohl, F., (2020). Seafloor microplastic hotspots controlled by deep-sea circulation. Science 368, 1140–1145.

Kasten, S., Schwenk, T., Aromokeye, D.A., Baques, M., Baumann, K.-H., Bergenthal, M., Bösche, J., Bozzano, G., Brune, R., Bülten, J., Chiessi, C.M., Coffinet, S., Crivellari, S., Garcia Chapori, N., Gonzalez, L., Hanebuth, T.J.J., Hilgenfeldt, C., Hüttich, D., Jones, C.K., Klann, M., Klar, S., Klein, T., Kockisch, B., Köster, M., Lantzsch, H., Linowski, E., Long, J.H., Melcher, A.-C., Ogunleye, O.J., Pereyra, N., Rehage, R., Riedinger, N., Rosiak, U., Schmidt, W., Schnakenberg, A., Spieß, V., Steinmann, L., Thieblemont, A., Volz, J., Warnke, F., Warratz, G., Wenau, S., & Zonneveld, K.A.F., (2019). Dynamics of sedimentation processes and their impact on biogeochemical reactions on the continental slope off Argentina and Uruguay (MARUM). In: Cruise No. SO260/Leg 1 & Leg 2, Leg 1: January 12-January 30, 2018, Buenos Aires (Argentina)-Montevideo (Uruguay), Leg 2: February 2-February, 14, 2018, Montevideo (Uruguay)-Buenos Aires (Argentina), DosProBio, Sonne-Berichte.

Krastel, S., Wefer, G., Hanebuth, T.J., Antobreh, A.A., Freudenthal, T., Preu, B., Schwenk, T., Strasser, M., Violante, R., & Winkelmann, D., (2011). Sediment dynamics and geohazards off Uruguay and the de la Plata River region (northern Argentina and Uruguay). Geo-Mar. Lett. 31, 271–283.

Keevil, G.M., Peakall, J., Best, J.L., & Amos, K.J. (2006). Flow structure in sinuous submarine channels: Velocity and turbulence structure of an experimental submarine channel. Marine Geology, 229(3-4), 241-257.

Krastel, S., & Wefer, G., (2012). Report and preliminary results of RV METEOR Cruise M78/ 3. In: Sediment Transport off Uruguay and Argentina: From the Shelf to the Deep Sea; 19.05. 2009–06.07, 2009, Montevideo (Uruguay)–Montevideo (Uruguay). Meteor-Berichte.

Laberg, J.S., Dahlgren, T., Vorren, T.O., Haflidason, H., & Bryn, P. (2001). Seismic analyses of Cenozoic contourite drift development in the Northern Norwegian Sea. Marine Geophysical Researches, 22(5), 401-416.

Lellouche, J.-M., Greiner, E., Le Galloudec, O., Garric, G., Regnier, C., Drevillon, M., Benkiran, M., Testut, C.-E., Bourdalle-Badie, R., Gasparin, F., Hernandez, O., Levier, B., Drillet, Y., Remy, E., & Le Traon, P.-Y., (2018). Recent updates on the Copernicus Marine Service global ocean monitoring and forecasting real-time 1/12◦ high resolution system. Ocean Sci. Discuss. 14, 1093–1126.

Lentz, S.J., &Helfrich, K.R., (2002). Buoyant gravity currents along a sloping bottom in a rotating fluid. Journal of Fluid Mechanics 464, 251-278.

Li, L., Liu, Z., Zhu, C., He, C., & Otto-Bliesner, B. (2021). Shallowing Glacial Antarctic Intermediate Water by Changes in Sea Ice and Hydrological Cycle. Geophysical Research Letters, 48(16), e2021GL094317.

Liu, S., Hernández-Molina, F.J., Ercilla, G., & Van Rooij, D. (2020). Sedimentary evolution of the Le Danois contourite drift systems (southern Bay of Biscay, NE Atlantic): A reconstruction of the Atlantic Mediterranean Water circulation since the Pliocene. Marine Geology, 427, 106217.

Llave, E., Hernández-Molina, F.J., Somoza, L., Díaz-del-Río, V., Stow, D.A.V., Maestro, A., & Alveirinho Dias, J.M. (2001). Seismic stacking pattern of the Faro-Albufeira contourite system (Gulf of Cadiz): a Quaternary record of paleoceanographic and tectonic influences. Marine Geophysical Researches, 22(5), 487-508.

Llave, E., Hernández-Molina, F.J., García, M., Ercilla, G., Roque, C., Juan, C., van Rooij, D., Rebesco, M., Brackenridge, R., Jané, G., Gómez-Ballesteros, M., & Stow, D. (2020). Contourites along the Iberian continental margins: conceptual and economic implications. Geological Society, London, Special Publications, 476(1), 403-436.

Lüdmann, T., Kalvelage, C., Betzler, C., Fürstenau, J., & Hübscher, C. (2013). The Maldives, a giant isolated carbonate platform dominated by bottom currents. Marine and Petroleum Geology, 43, 326-340.

Lüdmann, T., Paulat, M., Betzler, C., Möbius, J., Lindhorst, S., Wunsch, M., & Eberli, G.P. (2016). Carbonate mounds in the Santaren Channel, Bahamas: a current-dominated periplatform depositional regime. Marine Geology, 376, 69-85.

Lumpkin, R., Garzoli, S., 2011. Interannual to decadal changes in the western South Atlantic's surface circulation. Journal of Geophysical Research: Oceans, 116.

Maamaatuaiahutapu, K., Garçon, V.C., Provost, C., Boulahdid, M., & Bianchi, A.A., (1994). Spring and winter water mass composition in the Brazil-Malvinas Confluence. J. Mar. Res. 52, 397–426.

Magalhaes, J., & da Silva, J., (2017). Close Internal waves along the Malvinas Current: evidence of transcritical generation in satellite imagery. Oceanography 30, 110–119.

Marchitto, T. M., & Broecker, W. S. (2006). Deep water mass geometry in the glacial Atlantic Ocean: A review of constraints from the paleonutrient proxy Cd/Ca. Geochemistry, Geophysics, Geosystems, 7(12).

Martorelli, E., Falcini, F., Salusti, E., & Chiocci, F.L. (2010). Analysis and modeling of contourite drifts and contour currents off promontories in the Italian Seas (Mediterranean Sea). Marine Geology, 278(1-4), 19-30.

Masson, D.G., Howe, J.A., & Stoker, M. S. (2002). Bottom-current sediment waves, sediment drifts and contourites in the northern Rockall Trough. Marine Geology, 192(1-3), 215-237.

Mazières, A., Gillet, H., Castelle, B., Mulder, T., Guyot, C., Garlan, T., & Mallet, C., (2014). High-resolution morphobathymetric analysis and evolution of Capbreton submarine canyon head (Southeast Bay of Biscay—French Atlantic Coast) over the last decade using descriptive and numerical modeling. Marine Geology, 351, 1–12.

McCartney, M.S., (1982). The subtropical recirculation of mode waters. J. Mar. Res 40, 64.

McCave, I.N., & Tucholke, B.E. (1986). Deep current-controlled sedimentation in the western North Atlantic. https://doi.org/10.1130/DNAG-GNA-M.451

McCave, I.N., Manighetti, B., & Robinson, S.G. (1995). Sortable silt and fine sediment size/composition slicing: parameters for palaeocurrent speed and palaeoceanography. Paleoceanography, 10(3), 593-610.

McCave, I.N., Thornalley, D.J.R., & Hall, I.R. (2017). Relation of sortable silt grain-size to deep-sea current speeds: Calibration of the 'Mud Current Meter'. Deep Sea Research Part I: Oceanographic Research Papers, 127, 1-12.

McCave, I.N., (2017). Formation of sediment waves by turbidity currents and geostrophic flows: A discussion. Marine Geology, 390, 89-93.

Micallef, A., Georgiopoulou, A., Mountjoy, J., Huvenne, V.A., Iacono, C.L., Le Bas, T., Del Carlo, P., & Otero, D.C. (2016). Outer shelf seafloor geomorphology along a carbonate escarpment: The eastern Malta Plateau, Mediterranean Sea. Continental Shelf Research, 131, 12-27.

Miramontes, E., Cattaneo, A., Jouet, G., Thereau, E., Thomas, Y., Rovere, M., Cauquil, E., & Trincardi, F., (2016). The Pianosa contourite depositional system (northern Tyrrhenian Sea): drift morphology and Plio-Quaternary stratigraphic evolution. Marine Geology, 378, 20–42.

Miramontes, E., Garziglia, S., Sultan, N., Jouet, G., & Cattaneo, A., (2018). Morphological control of slope instability in contourites: a geotechnical approach. Landslides 15, 1085–1095.

Miramontes, E., Garreau, P., Caillaud, M., Jouet, G., Pellen, R., Hernández-Molina, F. J., Clare, M.A., & Cattaneo, A. (2019). Contourite distribution and bottom currents in the NW Mediterranean Sea: Coupling seafloor geomorphology and hydrodynamic modelling. Geomorphology, 333, 43-60.

Miramontes, E., Jouet, G., Thereau, E., Bruno, M., Penven, P., Guerin, C., Le Roy, P., Droz, L., Jorry, S.J., Hernández-Molina, F.J., Thiéblemont, A., Jacinto, R.S., & Cattaneo, A. (2020a). The impact of internal waves on upper continental slopes: insights

from the Mozambican margin (southwest Indian Ocean). Earth Surface Processes and Landforms, 45(6), 1469-1482.

Miramontes, E., Eggenhuisen, J.T., Jacinto, R.S., Poneti, G., Pohl, F., Normandeau, A., Campbell, D.C., & Hernández-Molina, F.J., (2020b). Channel-levee evolution in combined contour current–turbidity current flows from flume-tank experiments. Geology 48, 353-357.

Miramontes, E., Thiéblemont, A., Babonneau, N., Penven, P., Raisson, F., Droz, L., Jorry, S.J., Fierens, R., Counts, J.W., Wilckens, H., Cattaneo, A., & Jouet, G. (2021). Contourite and mixed turbidite-contourite systems in the Mozambique Channel (SW Indian Ocean): link between geometry, sediment characteristics and modelled bottom currents. Marine Geology, 437, 106502.

Mulder, T. (2011). Gravity processes and deposits on continental slope, rise and abyssal plains. In Developments in Sedimentology, Vol. 63, pp. 25-148. Elsevier.

Müller, D.S., Wagner, C.R., Rehmel, M.S., Oberg, K.A., & Rainville, F. (2009). Measuring discharge with acoustic Doppler current profilers from a moving boat (p. 72). Reston, Virginia (EUA): US Department of the Interior, US Geological Survey

Muñoz, A., Cristobo, J., Rios, P., Druet, M., Polonio, V., Uchupi, E., Acosta, J., & Group, A, (2012). Sediment drifts and cold-water coral reefs in the Patagonian upper and middle continental slope. Marine and Petroleum Geology, 36(1), 70-82.

Nicholson, U., & Stow, D. (2019). Erosion and deposition beneath the Subantarctic Front since the Early Oligocene. Scientific reports, 9(1), 1-9.

Nicholson, U., Libby, S., Tappin, D. R., & McCarthy, D. (2020). The Subantarctic Front as a sedimentary conveyor belt for tsunamigenic submarine landslides. Marine Geology, 424, 106161.

O'Grady, D.B., Syvitski, J.P., Pratson, L.F., & Sarg, J., (2000). Categorizing the morphologic variability of siliciclastic passive continental margins. Geology 28, 207-210.

Pahnke, K., & Zahn, R. (2005). Southern Hemisphere water mass conversion linked with North Atlantic climate variability. Science, 307(5716), 1741-1746.

Palamenghi, L., Keil, H., & Spiess, V. (2015). Sequence stratigraphic framework of a mixed turbidite-contourite depositional system along the NW slope of the South China Sea. Geo-Marine Letters, 35(1), 1-21.

Palomino, D., Vázquez, J. T., Ercilla, G., Alonso, B., López-González, N., & Díaz-del-Río, V. (2011). Interaction between seabed morphology and water masses around the seamounts on the Motril Marginal Plateau (Alboran Sea, Western Mediterranean). Geo-Marine Letters, 31(5), 465-479.

Paulat M., Lüdmann T., Betzler C., & Eberli G.P., (2019). Neogene palaeoceanographic changes recorded in a carbonate contourite drift (Santaren Channel, Bahamas). Sedimentology, 66, 4, S. 1361-1385 25 S. DOI: 10.1111/sed.12573

Paull, C.K., Mitts, P., Ussler III, W., Keaten, R., & Greene, H.G., (2005). Trail of sand in upper Monterey Canyon: offshore California. Geological Society of America Bulletin, 117(9-10), 1134-1145.

Peakall, J., McCaffrey, B., & Kneller, B. (2000). A process model for the evolution, morphology, and architecture of sinuous submarine channels. Journal of Sedimentary Research, 70(3), 434-448.

Piola, A.R., Franco, B.C., Palma, E.D., & Saraceno, M., (2013). Multiple jets in the Malvinas Current. Journal of Geophysical Research: Oceans, 118(4), 2107-2117.

Piola, A.R., Palma, E.D., Bianchi, A.A., Castro, B.M., Dottori, M., Guerrero, R.A., Marrari, M., Matano, R.P., Möller, O.O., & Saraceno, M., (2018). Physical oceanography of the SW Atlantic Shelf: a review. In: Plankton Ecology of the Southwestern Atlantic. Springer, pp. 37–56.

Piola, A.R., & Matano, R.P., (2019). Ocean currents: Atlantic Western Boundary – Brazil Current/Falkland (Malvinas) Current. In: Cochran, J.K., Bokuniewicz, H., Yager, P. (Eds.), Encyclopedia of Ocean Sciences, 3rd ed.

Preu, B., Hernández-Molina, F.J., Violante, R., Piola, A.R., Paterlini, C.M., Schwenk, T., Voigt, I., Krastel, S., & Spiess, V., (2013). Morphosedimentary and hydrographic features of the northern Argentine margin: The interplay between erosive, depositional and gravitational processes and its conceptual implications. Deep Sea Research Part I: Oceanographic Research Papers 75, 157-174.

Preu, B., Schwenk, T., Hernández-Molina, F.J., Violante, R., Paterlini, M., Krastel, S., Tomasini, J., & Spieß, V., (2012). Sedimentary growth pattern on the northern Argentine slope: The impact of North Atlantic Deep Water on southern hemisphere slope architecture. Marine Geology, 329-331, 113-125.

Provost, C., Gana, S., Garçon, V., Maamaatuaiahutapu, K., England, M., 1995. Hydrographic conditions in the Brazil-Malvinas Confluence during austral summer 1990. Journal of Geophysical Research: Oceans, 100(C6), 10655-10678.

Razik, S., Chiessi, C. M., Romero, O. E., & Von Dobeneck, T. (2013). Interaction of the South American monsoon system and the southern westerly wind belt during the last 14 kyr. Palaeogeography, Palaeoclimatology, Palaeoecology, 374, 28-40.

Razik, S., Govin, A., Chiessi, C.M., & von Dobeneck, T., (2015a). Depositional provinces, dispersal, and origin of terrigenous sediments along the SE South American continental margin. Marine Geology, 363, 261–272.

Razik, Sebastian, Govin, Aline, Chiessi, Cristiano Mazur, von Dobeneck, Tilo, (2015b). (Fig. 3) Grain-size distributions of the terrigenous sediment fraction from surface sediment samples along the continental margin between East Brazil and Patagonia. PANGAEA. https://doi.org/10.1594/PANGAEA.843433 [dataset] In supplement to: Razik, S et al. (2015): Depositional provinces, dispersal, and origin of terrigenous sediments along the SE South American continental margin. Marine Geology, 363, 261–272, doi:10.1016/j.margeo.2015.03.001.

Rebesco, M., (2005). Contourites R.C. Selley, L.R.M. Cocks, I.R. Plimer (Eds.), Encyclopedia of Geology, Elsevier, Oxford, pp. 513-527.

Rebesco, M., & Camerlenghi, A., (2008). Contourites. Elsevier.

Rebesco, M., Hernández-Molina, F.J., Van Rooij, D., & Wåhlin, A., (2014). Contourites and associated sediments controlled by deep-water circulation processes: State-of-the-art and future considerations. Marine Geology, 352, 111-154.

Rebesco, M., Özmaral, A., Urgeles, R., Accettella, D., Lucchi, R.G., Rüther, D., Winsborrow, M., Llopart, J., Caburlotto, A., & Lantzsch, H., (2016). Evolution of a high-latitude sediment drift inside a glacially-carved trough based on high-resolution seismic stratigraphy (Kveithola, NW Barents Sea). Quaternary Science Reviews 147, 178-193.

Rebesco, M., Camerlenghi, A., Munari, V., Mosetti, R., Ford, J., Micallef, A., & Facchin, L. (2021). Bottom current-controlled Quaternary sedimentation at the foot of the Malta Escarpment (Ionian Basin, Mediterranean). Marine Geology, 441, 106596.

Reeder, D.B., Ma, B.B., & Yang, Y.J., (2011). Very large subaqueous sand dunes on the upper continental slope in the South China Sea generated by episodic, shoaling deep-water internal solitary waves. Marine Geology, 279, 12–18.

Reiche, S., Hübscher, C., Brenner, S., Betzler, C., & Hall, J.K., (2018). The role of internal waves in the late Quaternary evolution of the Israeli continental slope. Marine Geology, 406, 177–192.

Reid, J.L., Nowlin, W.D., & Patzert, W.C., 1977. On the characteristics and circulation of the southwestern Atlantic Ocean. Ocean. Journal of Physical Oceanography, 7(1), 62-91.

Renard, V., & Allenou, J.P. (1979). Sea Beam, Multi-Beam Echo-Sounding in" Jean Charcot"-Description, Evaluation and First Results. The International Hydrographic Review.

Ribó, M., Puig, P., Muñoz, A., Iacono, C.L., Masqué, P., Palanques, A., Acosta, J., Guillén, J., & Ballesteros, M.G., (2016). Morphobathymetric analysis of the large fine-grained sediment waves over the Gulf of Valencia continental slope (NW Mediterranean). Geomorphology 253, 22–37.

Roberts, D.G., Hogg, N.G., Bishop, D.G., & Flewellen, C.G. (1974). Sediment distribution around moated seamounts in the Rockall Trough. In Deep Sea Research and Oceanographic Abstracts, Elsevier 21(3), 175-184.

Roberts, J.M., Wheeler, A.J., & Freiwald, A., (2006). Reefs of the deep: the biology and geology of cold-water coral ecosystems. Science 312, 543–547.

Robin, C., Droz, L., 2014. PAMELA-MOZ02 Cruise, RV L'Atalante. `https://doi.org/10.17600/14001100`.

Roden, G.I. (1987). Effect of seamounts and seamount chains on ocean circulation and thermohaline structure. Seamounts, islands, and atolls, 43, 335-354. `https://doi.org/10.1029/GM043p0335`

Ronge, T. A., Steph, S., Tiedemann, R., Prange, M., Merkel, U., Nürnberg, D., & Kuhn, G. (2015). Pushing the boundaries: Glacial/interglacial variability of intermediate and deep waters in the southwest Pacific over the last 350,000 years. Paleoceanography, 30(2), 23-38.

Sachs, S.D., & Ellwood, B.B., (1988). Controls on magnetic grain-size variations and concentration in the Argentine Basin, South Atlantic Ocean. Oceanograph. Res. Paper. 35 (6), 929–942.

Salon, S., Crise, A., & Van Loon, A., (2008). Dynamics of the bottom boundary layer. Developments in sedimentology 60, 83-97.

Schlichting, H., (1962). Boundary Layer Theory, 6th ed. McGraw-Hill, New York. 744 pp.

Schlichting, H., Gersten, K., (2016). Boundary-Layer Theory. Springer.

Shanmugam, G., (2013). Modern internal waves and internal tides along oceanic pycnoclines: Challenges and implications for ancient deep-marine baroclinic sandsInternal Waves, Internal Tides, and Baroclinic Sands. AAPG Bulletin 97, 799-843.

Simpson, M.R. (2001). Discharge measurements using a broad-band acoustic Doppler current profiler p. 123. Reston, CA, USA: US Department of the Interior, US Geological Survey.

Sivkov, V., Gorbatskiy, V., Kuleshov, A., & Zhurov, Y. (2002). Muddy contourites in the Baltic Sea: an example of a shallow-water contourite system. MEMOIRS-GEOLOGICAL SOCIETY OF LONDON, 22, 121-136.

Soulsby, R., & Whitehouse, R., (1997). Threshold of sediment motion in coastal environments, Pacific Coasts and Ports' 97: Proceedings of the 13th Australasian Coastal and Ocean Engineering Conference and the 6th Australasian Port and Harbour Conference; Volume 1. Centre for Advanced Engineering, University of Canterbury, p. 145.

Spieß, V., Albrecht, N., Bickert, T., Breitzke, M., Brüning, M., Dreyzehner, A., Groß, U., Krüger, D., von Lom-Keil, H., & Möller, H., (2002). ODP Südatlantik 2001 Part 2. Meteor-Berichte 2, 1.

Steinbrink, L., Gohl, K., Riefstahl, F., Davy, B., & Carter, L. (2020). Late Cretaceous to recent ocean-bottom currents in the SW Pacific Gateway, southeastern Chatham Rise, New Zealand. Palaeogeography, Palaeoclimatology, Palaeoecology, 546, 109633.

Steinmann, L., Baques, M., Wenau, S., Schwenk, T., Spiess, V., Piola, A.R., Bozzano, G., Violante, R., & Kasten, S., (2020). Discovery of a giant cold-water coral mound province along the northern Argentine margin and its link to the regional Contourite Depositional System and oceanographic setting. Marine Geology, 427, 106223.

Stow, D.A., & Mayall, M. (2000). Deep-water sedimentary systems: new models for the 21st century. Marine and Petroleum Geology, 17(2), 125-135.

Stow, D.A., Faugères, J.C., Howe, J.A., Pudsey, C.J., & Viana, A.R., (2002). Bottom currents, contourites and deep-sea sediment drifts: current state-of-the-art. Geological Society, London, Memoirs, 22(1), 7-20.

Stow, D.A., Hernández-Molina, F.J., Llave, E., Sayago-Gil, M., Díaz del Río, V., & Branson, A., (2009). Bedform-velocity matrix: the estimation of bottom current velocity from bedform observations. Geology 37, 327–330.

Stow, D.A., & Smillie, Z., (2020). Distinguishing between deep-water sediment facies: Turbidites, contourites and hemipelagites. Geosciences 10, 68

Sumer, B.M., and Fredsøe, J. (2002). The mechanics of scour in the marine environment, World Scientific, Singapore.

Sumner, E.J., Peakall, J., Dorrell, R.M., Parsons, D.R., Darby, S.E., Wynn, R.B., McPhail, S.D., Perrett, J., Webb, A., & White, D. (2014). Driven around the bend: Spatial evolution and controls on the orientation of helical bend flow in a natural submarine gravity current. Journal of Geophysical Research: Oceans, 119(2), 898-913.

Surlyk, F., & Lykke-Andersen, H., (2007). Contourite drifts, moats and channels in the Upper Cretaceous chalk of the Danish Basin. Sedimentology 54, 405–422.

Tavouktsoglou, N. S., Harris, J. M., Simons, R. R., & Whitehouse, R. J. S. (2017). Equilibrium scour-depth prediction around cylindrical structures. Journal of Waterway, Port, Coastal, and Ocean Engineering, 143(5), 04017017.

Thiéblemont, A., Hernández-Molina, F.J., Miramontes, E., Raisson, F., & Penven, P. (2019). Contourite depositional systems along the Mozambique channel: The interplay between bottom currents and sedimentary processes. Deep Sea Research Part I: Oceanographic Research Papers, 147, 79-99.

Thran, A.C., Dutkiewicz, A., Spence, P., Müller, R.D., 2018. Controls on the global distribution of contourite drifts: insights from an eddy-resolving ocean model. Earth Planet. Sci. Lett. 489, 228–240.

Tripsanas, E.K., Panagiotopoulos, I.P., Lykousis, V., Morfis, I., Karageorgis, A.P., Anastasakis, G., & Kontogonis, G. (2016). Late quaternary bottom-current activity in the south Aegean Sea reflecting climate-driven dense-water production. Marine Geology, 375, 99-119.

Trowbridge, J., & Lentz, S., (1991). Asymmetric behavior of an oceanic boundary layer above a sloping bottom. Journal of Physical Oceanography 21, 1171-1185.

Uenzelmann-Neben, G., Weber, T., Grützner, J., & Thomas, M. (2017). Transition from the Cretaceous ocean to Cenozoic circulation in the western South Atlantic—A twofold reconstruction. Tectonophysics, 716, 225-240.

Urien, C.M., & Ewing, M., (1974). Recent sediments and environment of southern Brazil, Uruguay, Buenos Aires, and Rio Negro continental shelf. In: The Geology of Continental Margins. Springer, pp. 157–177.

Valla, D., Piola, A.R., Meinen, C.S., & Campos, E., (2018). Strong mixing and recirculation in the northwestern Argentine Basin. Journal of Geophysical Research: Oceans, 123(7), 4624-4648.

Van Haren, H., & Gostiaux, L., (2011). Large internal waves advection in very weakly stratified deep Mediterranean waters. Geophysical Research Letters, 38(22).

Van Keken, P.E., Hacker, B.R., Syracuse, E.M., & Abers, G.A. (2011). Subduction factory: 4. Depth-dependent flux of H2O from subducting slabs worldwide. Journal of Geophysical Research: Solid Earth, 116(B1)

Van Rensbergen, P., Depreiter, D., Pannemans, B., Moerkerke, G., Van Rooij, D., Marsset, B., Akhmanov, G., Blinova, V., Ivanov, M., Rachidi, M., Magalhães, V., Pinheiro, L.M., Cunha, M., & Henriet, J.P. (2005). The El Arraiche mud volcano field at the Moroccan Atlantic slope, Gulf of Cadiz. Marine Geology, 219(1), 1-17.

Van Rooij, D., Iglesias, J., Hernández-Molina, F.J., Ercilla, G., Gomez-Ballesteros, M., Casas, D., Llave, E., De Hauwere, A., Garcia-Gil, S., Acosta, J., & Henriet, J.P. (2010). The Le Danois Contourite Depositional System: interactions between the Mediterranean outflow water and the upper Cantabrian slope (North Iberian margin). Marine Geology, 274(1-4), 1-20.

Vandorpe, T., Van Rooij, D., & De Haas, H. (2014). Stratigraphy and paleoceanography of a topography-controlled contourite drift in the Pen Duick area, southern Gulf of Cádiz. Marine Geology, 349, 136-151.

Verdicchio, G., & Trincardi, F. (2006). Short-distance variability in slope bed-forms along the Southwestern Adriatic Margin (Central Mediterranean). Marine Geology, 234(1-4), 271-292.

Vivier, F., & Provost, C., (1999). Direct velocity measurements in the Malvinas Current. Journal of Geophysical Research: Oceans, 104(C9), 21083-21103.

Voigt, I., Chiessi, C.M., Piola, A.R., & Henrich, R., (2016). Holocene changes in Antarctic Intermediate Water flow strength in the Southwest Atlantic. Palaeogeogr. Palaeoclimatol. Palaeoecol. 463, 60–67.

Voigt, I., Henrich, R., Preu, B., Piola, A.R., Hanebuth, T.J., Schwenk, T., & Chiessi, C.M., (2013). A submarine canyon as a climate archive—interaction of the Antarctic Intermediate Water with the Mar del Plata Canyon (Southwest Atlantic). Marine Geology, 341, 46–57.

Volbers, A. N., & Henrich, R. (2004). Calcium carbonate corrosiveness in the South Atlantic during the Last Glacial Maximum as inferred from changes in the preservation of Globigerina bulloides: A proxy to determine deep-water circulation patterns?. Marine Geology, 204(1-2), 43-57.

Voosen, P., (2020). Climate change spurs global speedup of ocean currents. Science 367, 612–613.

Wåhlin, A., Muench, R., Arneborg, L., Björk, G., Ha, H., Lee, S., & Alsén, H., (2012). Some implications of Ekman layer dynamics for cross-shelf exchange in the Amundsen Sea. Journal of Physical Oceanography 42, 1461-1474.

Warratz, G., Henrich, R., Voigt, I., Chiessi, C.M., Kuhn, G., & Lantzsch, H., (2017). Deglacial changes in the strength of deep southern component water and sediment supply at the Argentine continental margin. Paleoceanography 32, 796–812.

Warratz, G., Schwenk, T., Voigt, I., Bozzano, G., Henrich, R., Violante, R., & Lantzsch, H., (2019). Interaction of a deep-sea current with a blind submarine canyon (Mar del Plata Canyon, Argentina). Marine Geology, 417, 106002.

Weatherall, P., Marks, K.M., Jakobsson, M., Schmitt, T., Tani, S., Arndt, J.E., Rovere, M., Chayes, D., Ferrini, V., & Wigley, R. (2015). A new digital bathymetric model of the world's oceans. Earth and space Science, 2(8), 331-345.

Weatherly, G.L., (1975). A numerical study of time-dependent turbulent Ekman layers over horizontal and sloping bottoms. Journal of Physical Oceanography 5, 288-299.

Weatherly, G.L., & Martin, P.J., (1978). On the structure and dynamics of the oceanic bottom boundary layer. Journal of Physical Oceanography 8, 557-570.

Wells, M., & Cossu, R. (2013). The possible role of Coriolis forces in structuring large-scale sinuous patterns of submarine channel–levee systems. Philosophical Transactions of the Royal Society A: Mathematical, Physical and Engineering Sciences, 371(2004), 20120366.

Wilckens, H., Miramontes, E., Schwenk, T., Artana, C., Zhang, W., Piola, A.R., Baques, M., Provost, C., Hernández-Molina, F.J., Felgendreher, M., Spieß, V., & Kasten, S., (2021). The erosive power of the Malvinas Current: Influence of bottom currents on morpho-sedimentary features along the northern Argentine margin (SW Atlantic Ocean). Marine Geology, 439, 106539.

Wilckens, H., Miramontes, E., Schwenk, T., Artana, C., Zhang, W., Piola, A.R., Baques, M., Provost, C., Hernández-Molina, F.J., Felgendreher, M., Spieß, V., & Kasten, S., (2021). Acoustic Data (Vessel-Mounted ADCP, Parasound and Multi-Channel Seismic Reflection Profiles) and Grain-Size Analyses of Surface Sediment Samples from off Northern Argentina and Uruguay. PANGAEA `https://doi.org/10.1594/PANGAEA.931130`. [dataset] In supplement to: Wilckens, H., Miramontes, E., Schwenk, T., Artana, C., Zhang, W., Piola, A.R., Baques, M., Provost, C., Hernández-Molina, F.J., Felgendreher, M., Spieß, V., & Kasten, S., (2021). The erosive power of the Malvinas Current: Influence of bottom currents on morpho-sedimentary features along the northern Argentine margin (SW Atlantic Ocean). Marine Geology, 439, 106539.

Wilckens, H., Schwenk, T., Lüdmann, T., Betzler, C., Zhang, W., Chen, W., Hernández-Molina, F.J., Lefebvre, A., Cattaneo, A., Spiess, V., & Miramontes, E., (accepted). Factors controlling the morphology and internal sediment architecture of moats and their associated contourite drifts. Sedimentology.

Wu, S., Lembke-Jene, L., Lamy, F., Arz, H.W., Nowaczyk, N., Xiao, W., Zhang, X., Hass, H.C., Titschack J., & Kuhn, G. (2021). Orbital-and millennial-scale Antarctic Circumpolar Current variability in Drake Passage over the past 140,000 years. Nature Communications, 12(1), 1-9.

Wynn, R.B., & Stow, D.A. (2002). Classification and characterisation of deep-water sediment waves. Marine Geology, 192(1-3), 7-22.

Wynn, R.B., & Masson, D.G. (2008). Sediment waves and bedforms. Developments in sedimentology, 60, 289-300.

Wunsch, M., Betzler, C., Lindhorst, S., Lüdmann, T., & Eberli, G. P. (2017). Sedimentary dynamics along carbonate slopes (Bahamas archipelago). Sedimentology, 64(3), 631-657.

Yin, S., Hernández-Molina, F.J., Zhang, W., Li, J., Wang, L., Ding, W., & Ding, W. (2019). The influence of oceanographic processes on contourite features: A multidisciplinary study of the northern South China Sea. Marine Geology, 415, 105967.

Yin, S., Hernández-Molina, F.J., Lin, L., Chen, J., Ding, W., & Li, J. (2021). Isolation of the South China Sea from the North Pacific Subtropical Gyre since the latest Miocene due to formation of the Luzon Strait. Scientific reports, 11(1), 1-9.

Yu, K., Miramontes, E., Alves, T.M., Li, W., Liang, L., Li, S., Zhan, W., & Wu, S. (2021). Incision of submarine channels over pockmark trains in the South China Sea. Geophysical Research Letters, 48(24), e2021GL092861.

Zárate, M., & Blasi, A., (1993). Late Pleistocene-Holocene eolian deposits of the southern Buenos Aires Province, Argentina: a preliminary model. Quat. Int. 17, 15–20.

Zhang, W., Hanebuth, T.J., & Stöber, U., (2016). Short-term sediment dynamics on a meso-scale contourite drift (off NW Iberia): impacts of multi-scale oceanographic processes deduced from the analysis of mooring data and numerical modelling. Marine Geology, 378, 81–100.

Zhang, Y., Liu, Z., Zhao, Y., Wang, W., Li, J., & Xu, J. (2014). Mesoscale eddies transport deep-sea sediments. Scientific reports, 4(1), 5937.

Zhao, Y., Liu, Z., Zhang, Y., Li, J., Wang, M., Wang, W., & Xu, J. (2015). In situ observation of contour currents in the northern South China Sea: Applications for deepwater sediment transport. Earth and Planetary Science Letters, 430, 477-485.